University of Iowa

Iowa Research Online

Theses and Dissertations

Spring 2013

Interaction of polymeric particles with surfactant interfaces

Amir Mohammad Farnoud
University of Iowa

Recommended Citation

INTERACTION OF POLYMERIC PARTICLES WITH SURFACTANT INTERFACES

by

Amir Mohammad Farnoud

<u>An Abstract</u>

Of a thesis submitted in partial fulfillment
of the requirements for the Doctor of
Philosophy degree in Chemical and Biochemical Engineering
in the Graduate College of
The University of Iowa

May 2013

Thesis Supervisor: Assistant Professor Jennifer Fiegel

ABSTRACT

Films of phospholipids and biologically relevant surfactants at the air-water interface provide a well-defined medium to study molecular alignment, phase behavior and interactions of biomembranes and lung surfactant with exogenous materials. Interactions between lung surfactant interfaces and solid particles are of particular interest due to the increased use of nanomaterials in industrial applications and the promise of polymeric particles in pulmonary drug delivery. Understanding such interactions is necessary to avoid potential adverse effects on surfactant function after exposure to particles.

In this thesis, the mechanisms of surfactant inhibition after exposure to submicron particles via different routes were investigated. The effects of carboxyl-modified polystyrene particles (200 nm) on films of dipalmitoyl phosphatidylcholine (DPPC) and Infasurf (calf lung surfactant extract) were studied. Surfactants were exposed to different concentrations of particles in a Langmuir trough with symmetric surface compression and expansion. Surface tension, potential, microstructure and topology were examined to monitor particle effects on surfactant function. Several methods of surfactant exposure to particles were studied: particle injection into the subphase after spreading surfactant monolayers (subphase injection), mixing the particles with the subphase and spreading the surfactant on top (monolayer addition) and particle aerosolization onto surfactant films.

Studies with DPPC monolayers revealed that particle-surfactant interactions are dependent on the particle introduction method. In the subphase injection method, particles did not penetrate the monolayer and no inhibitory effects on surfactant function were observed. However, in the monolayer addition method, particles caused a premature monolayer collapse and hindered surfactant respreading likely by penetrating into the DPPC monolayer. Finally, particle aerosolization on surfactant was performed to mimic

the physiologically relevant route of surfactant exposure to particles. Particle aerosolization on DPPC monolayers significantly inhibited surfactant function in the lung-relevant surface tension range. When aerosolized on Infasurf, particles caused inhibitory effects as a function of time suggesting adsorption of surfactant components on particle surfaces as the main mechanism of interaction. This research will enhance understanding of the mechanisms of particle-induced surfactant dysfunction, thereby providing information for the safe design of polymeric particles for drug delivery and for developing guidelines for particles used in occupational settings.

Abstract Approved: _____

                    Thesis Supervisor

           _____

                    Title and Department

           _____

                    Date

INTERACTION OF POLYMERIC PARTICLES WITH SURFACTANT INTERFACES

by

Amir Mohammad Farnoud

A thesis submitted in partial fulfillment
of the requirements for the Doctor of Philosophy degree in
Chemical and Biochemical Engineering
in the Graduate College of
The University of Iowa

May 2013

Thesis Supervisor: Assistant Professor Jennifer Fiegel

Graduate College
The University of Iowa
Iowa City, Iowa

CERTIFICATE OF APPROVAL

_____

PH.D. THESIS

_____

This is to certify that the Ph.D. thesis of

Amir Mohammad Farnoud

has been approved by the Examining Committee
for the thesis requirement for the Doctor of Philosophy
degree in Chemical and Biochemical Engineering at the May 2013 graduation.

Thesis Committee: _____
                  Jennifer Fiegel, Thesis Supervisor
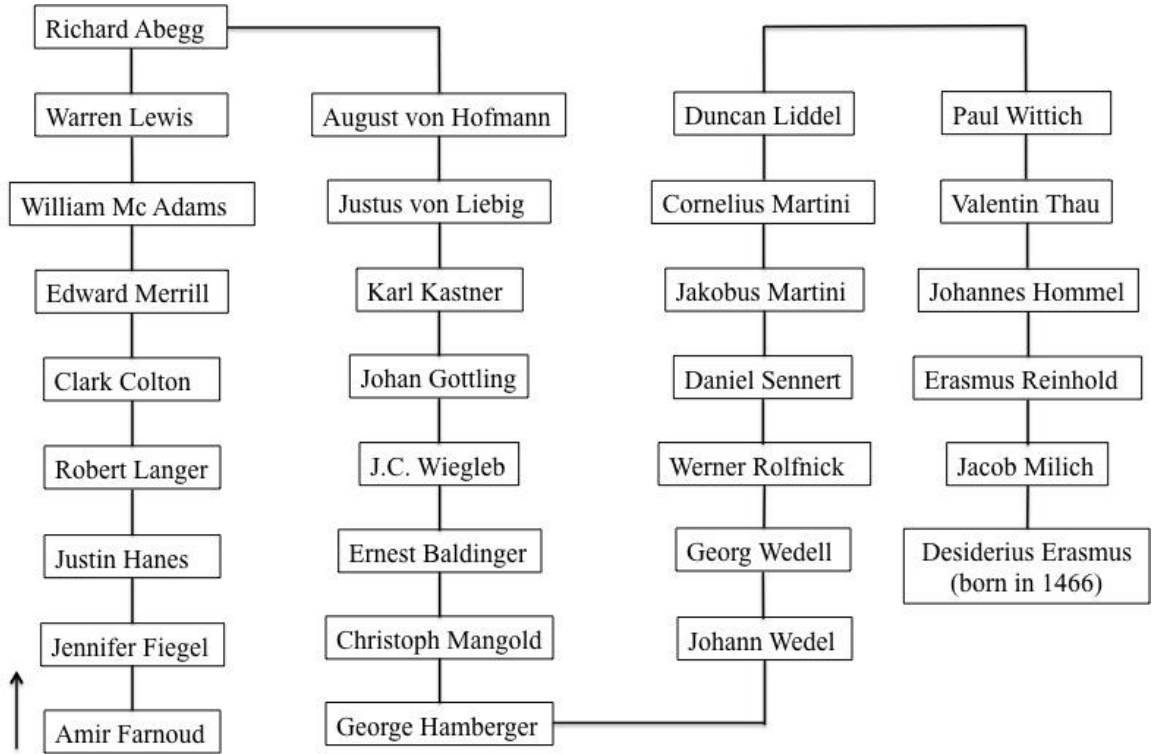
                _____
                  Vicki Grassian

                _____
                  Julie Jessop

                _____
                  Eric Nuxoll

                _____
                  Thomas Peters

To those who believe in the power of dreams

Amir M. Farnoud's Scientific Family Tree

Richard Abegg			
Warren Lewis	August von Hofmann	Duncan Liddel	Paul Wittich
William Mc Adams	Justus von Liebig	Cornelius Martini	Valentin Thau
Edward Merrill	Karl Kastner	Jakobus Martini	Johannes Hommel
Clark Colton	Johan Gottling	Daniel Sennert	Erasmus Reinhold
Robert Langer	J.C. Wiegleb	Werner Rolfnick	Jacob Milich
Justin Hanes	Ernest Baldinger	Georg Wedell	Desiderius Erasmus (born in 1466)
Jennifer Fiegel	Christoph Mangold	Johann Wedel	
Amir Farnoud	George Hamberger		

ACKNOWLEDGMENTS

There are no words to explain my gratitude towards my parents Adin and Reza. Everything I have achieved in life is because of them, they created my most beautiful moments and stood by me in the most difficult ones. The only way I know to thank them is to make them proud by being the best I can be as a human being and as a professional and I will do my best to achieve that. My brother Ali has been my mentor and motivator in everything in life. He was the reason I went to graduate school, he and his wife Stephanie were always there, ready to listen, cheer me up and be supportive with whatever means possible. Finally, I wish to thank my girlfriend Golnaz, who was unbelievably patient and supportive. Through listening to my complaints about data, wrong experiments and surface pressure isotherms, she is totally capable of understanding and interpreting each and every graph presented in this thesis!

Finally, I would like to dedicate this work to those who believe in the power of their dreams. I was not a good undergraduate student by any means, but I always had a vision of myself being a researcher and changing the world through my research. It was perhaps the power of my dream that allowed me to keep pushing and not be discouraged by bad grades or wrong experiments, and finally go from a below average undergraduate student to a Ph.D. in chemical engineering. I will turn thirty a few days before my graduation and I can't be anything but happy and thankful to God when I look back to the past decade. In the past 10 years, I have received three degrees, survived cancer, lost 70 pounds of weight, won the state of Iowa chess championship and found the best relationship of my life. There is not much more one can ask from a decade of life, I will continue to believe in the power of dreams.

ABSTRACT

Films of phospholipids and biologically relevant surfactants at the air-water interface provide a well-defined medium to study molecular alignment, phase behavior and interactions of biomembranes and lung surfactant with exogenous materials. Interactions between lung surfactant interfaces and solid particles are of particular interest due to the increased use of nanomaterials in industrial applications and the promise of polymeric particles in pulmonary drug delivery. Understanding such interactions is necessary to avoid potential adverse effects on surfactant function after exposure to particles.

In this thesis, the mechanisms of surfactant inhibition after exposure to submicron particles via different routes were investigated. The effects of carboxyl-modified polystyrene particles (200 nm) on films of dipalmitoyl phosphatidylcholine (DPPC) and Infasurf (calf lung surfactant extract) were studied. Surfactants were exposed to different concentrations of particles in a Langmuir trough with symmetric surface compression and expansion. Surface tension, potential, microstructure and topology were examined to monitor particle effects on surfactant function. Several methods of surfactant exposure to particles were studied: particle injection into the subphase after spreading surfactant monolayers (subphase injection), mixing the particles with the subphase and spreading the surfactant on top (monolayer addition) and particle aerosolization onto surfactant films.

Studies with DPPC monolayers revealed that particle-surfactant interactions are dependent on the particle introduction method. In the subphase injection method, particles did not penetrate the monolayer and no inhibitory effects on surfactant function were observed. However, in the monolayer addition method, particles caused a premature monolayer collapse and hindered surfactant respreading likely by penetrating into the DPPC monolayer. Finally, particle aerosolization on surfactant was performed to mimic

the physiologically relevant route of surfactant exposure to particles. Particle aerosolization on DPPC monolayers significantly inhibited surfactant function in the lung-relevant surface tension range. When aerosolized on Infasurf, particles caused inhibitory effects as a function of time suggesting adsorption of surfactant components on particle surfaces as the main mechanism of interaction. This research will enhance understanding of the mechanisms of particle-induced surfactant dysfunction, thereby providing information for the safe design of polymeric particles for drug delivery and for developing guidelines for particles used in occupational settings.

TABLE OF CONTENTS

x

LIST OF TABLES

LIST OF FIGURES

xv

CHAPTER 1

INTRODUCTION

1.1 Lung Function and Structure

The respiratory system is responsible for providing a continuous supply of oxygen to the body of air breathing animals. The lungs are an essential part of the respiratory system and are the sites of gas exchange within the body. With each breath, fresh air containing oxygen is inspired into the lungs through the conducting airways. At the same time, blood with high carbon dioxide and low oxygen content is pumped into the lungs. In lung capillaries, carbon dioxide is exchanged with oxygen resulting in a high oxygen and low carbon dioxide content in the blood that leaves the lungs and is distributed to the tissues.

The delicate structure of the lungs allows for efficient gas exchange in the body by providing a large surface area. Upon inspiration, the inhaled air is conditioned to the physiological environment in the nose, pharynx and larynx and enters the trachea. The trachea directs the inhaled air to the lungs as it branches into smaller divisions. This branching continues as the trachea is divided into bronchus, bronchiolus, alveolar ducts and alveolar sacs (Figure 1-1). With each division, the diameter of the units decreases, while the number of units increases. Branching of trachea starts from two bronchi with a diameter of about 1.2 cm and ends with about 480 million alveolar sacs with an average diameter of about 200 μm.[1] The large number of alveolar sacs leads to a surface area of more than 100 m^2 in the alveolar region which is the site of gas exchange.[2, 3]

Each lung is covered by pleura, which is a membrane connecting the lung to the chest wall. The cavity inside this membrane is known as pleural cavity. The pressure difference between the alveoli and this cavity (commonly known as transpulmonary pressure) plays a major role in the initiation of air flow to the lungs. Inspiration occurs by the contraction of the diaphragm and expansion of the chest wall causing a negative
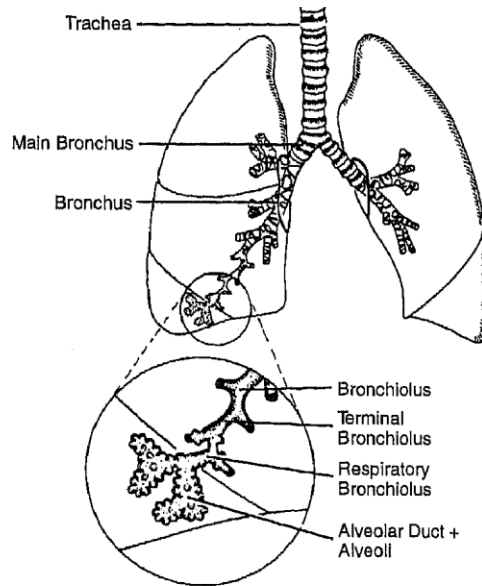
Figure 1-1. The trachea branches into smaller units as it conducts air into the lungs with the alveoli being the smallest of these units. Modified with permission.[4]

pressure in the pleural cavity and increasing the transpulmonary pressure (Figure 1-2).

This results in passive enlargement of the alveoli and establishes a pressure gradient
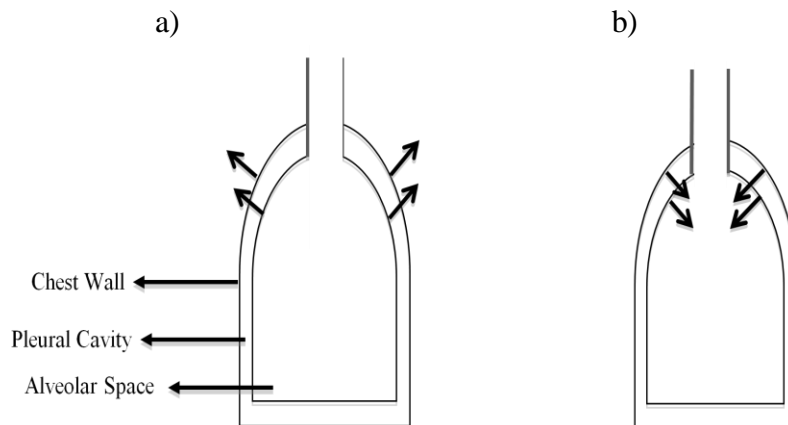
Figure 1-2. Mechanics of breathings: (a) expansion of the chest wall during inspiration leads to a positive transpulmonary pressure, expansion of the alveoli and air entrance into the lungs, (b) relaxation of chest wall during expiration results in ejection of air from the alveoli.

between the alveoli and the air outside the body causing the air flow to the lungs. Once the inhaled air reaches the alveoli, gas exchange between the air and blood occurs by diffusion which is facilitated by the large surface area of the alveolar region and the large number of capillaries in each alveolus (about 1000 capillaries per alveolus).[5]

1.2 Pulmonary Surfactant Composition and Function

The surface of all alveoli is covered with a complex surface-active fluid known as the pulmonary surfactant. Pulmonary surfactant is synthesized by type II epithelial cells and secreted into alveolar subphase via exocytosis. This secreted surfactant is in the form of closely packed bilayers known as the lamellar bodies. In the presence of calcium these structures change their formation to cylindrical tubes of lipids and proteins called tubular myelin.[6, 7] Surfactant components adsorb to the surface of the alveoli from tubular myelin forming a film on the surface of the alveolar fluid.[8]

Surfactant film on the surface of the alveolar fluid is subject to continuous compression and expansion cycles as a result of lung inflation and deflation during breathing. Upon cycling, part of surfactant molecules detach from the alveolar surface. The majority of detached molecules are taken up by type II epithelial cells and are reincorporated into lamellar bodies and secreted again, or degraded and utilized for synthesis of new surfactant material.[9-11] Part of the detached surfactant molecules are taken up by alveolar macrophages and degraded.[12] A small portion of surfactant molecules at the alveolar surface are oxidized or flow to trachea and are eventually swallowed.[11, 13] The loss of surfactant molecules is balanced by secretion of surfactant that is stored in lamellar bodies and adsorbed to the alveolar surface to keep the surfactant pool constant.[14] Although the factors controlling surfactant clearance from the alveolar surface are not as well characterized as those that control surfactant secretion,[11] the importance of maintaining a balance between clearance and secretion and retaining a constant surfactant concentration at the alveolar surface is well established.[15]

The composition of pulmonary surfactant is similar between mammalian species[16] and is composed of approximately 90% lipids and 10% proteins by weight.[17] The composition of bovine pulmonary surfactant reported by Yu and colleagues[18] is generally used as a representative for all mammalian species. According to this study, about 36% of the pulmonary surfactant is composed of dipalmitoyl phosphatidylcholine (DPPC), 33% unsaturated phosphatidyl choline (PC), 10% is made of phosphatidyl glycerol (PG) while small amounts of phosphatidyl ethanolamine, diacyl glycerol and other unsaturated lipids.[18] Four surfactant proteins are associated with the lung surfactant (named surfactant proteins A, B, C and D). Surfactant proteins A and D are hydrophilic proteins and play a major role in protecting the lungs against bacteria and viruses.[19] Surfactant proteins B and C are hydrophobic proteins and are involved in adsorption and re-spreading of surfactant phospholipids at the alveolar surface.[20]

Pulmonary surfactant plays an important role in a variety of lung functions. The surfactant is known to have bactericidal properties against a number of bacteria, thus protecting the lungs against bacterial infection. Rat lung surfactant has been shown to kill staphylococci.[21] Also, surfactant proteins A and D have been shown to inhibit the growth of *E.coli* by increasing membrane permeability.[22] Pulmonary surfactant is also believed to protect the pulmonary epithelial cells against physical damage caused by sudden thrusts of air into the alveoli. Bilek and colleagues have shown that exposure of epithelial cells covered with a layer of phosphate buffer solution to fast moving air bubbles leads to cell damage, this damage did not occur when a layer of surfactant was spread on the buffer solution.[23] However, the most important function of the pulmonary surfactant is to reduce the surface tension of the alveolar fluid.

Surface tension is defined as the energy required to increase the surface area of a liquid by a unit area. Thus, by lowering the surface tension, the pulmonary surfactant reduces the energy required to inflate the lungs during inspiration meaning a modest transpulmonary pressure is enough to inflate the lungs.[17] If the surfactant is

dysfunctional, the volume of air entering the lungs upon inspiration at a fixed transpulmonary pressure will decrease leading to lower levels of oxygen in the lungs and inadequate gas exchange. For example, it has been shown that upon mechanical ventilation at a fixed pressure, the volume of air in normal rat lungs was three times that of rat lungs with dysfunctional surfactant.[24]

Surfactant also plays an important role in the lungs during expiration by maintaining the same recoil pressure in all alveoli. Upon expiration, the inflated alveoli recoil inward. According to Laplace's law, the recoil pressure (p) in spherical elastic bodies is directly related to surface tension (γ) and inversely related to the diameter of the sphere (r) according to Equation 1-1.

$$P = (2\gamma)/r \tag{1-1}$$

By reducing the surface tension upon compression, the surfactant retains the same recoil pressure in all alveoli during expiration preventing the collapse of smaller alveoli into the larger ones due to pressure difference.[17, 25] As depicted in Figure 1-3, when the surfactant is not present in the alveoli (Figure 1-3-a), the recoil pressure in the smaller alveolus will be larger than the pressure of the larger alveolus. As a result, the smaller alveolus will deflate and 'collapse' leading to a reduction in the functional surface area of the lung. However, in the presence of surfactant, the smaller alveoli will have a lower surface tension resulting in the same recoil pressure in the alveoli regardless of their size (Figure 1-3-b).

a)   b)

Without Surfactant   With Surfactant

Large alveolus: $P = \dfrac{2 \times 50 \; mN/m}{0.0005 \; m} = 200$ Pa   Large alveolus: $P = \dfrac{2 \times 50 \; mN/m}{0.0005 \; m} = 200$ Pa

Small alveolus: $P = \dfrac{2 \times 50 \; mN/m}{0.00025 \; m} = 400$ Pa   Small alveolus: $P = \dfrac{2 \times 25 \; mN/m}{0.00025 \; m} = 200$ Pa
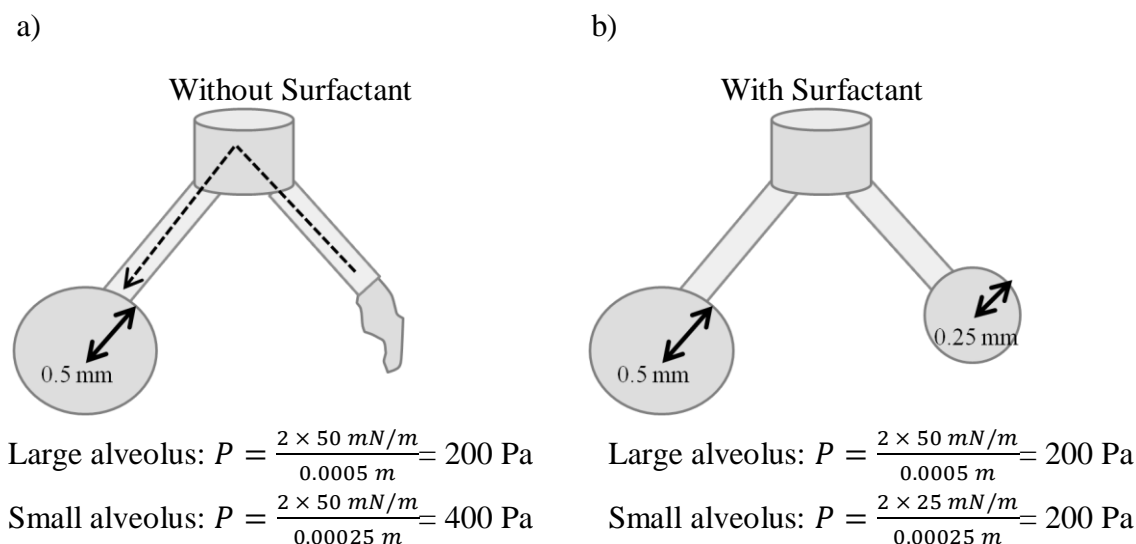
Figure 1-3. The presence of surfactant avoids alveolar collapse, in the absence of surfactant (a) the smaller alveolus has higher recoil pressure (assuming a surface tension of 50 mN/m) and will lose its air content to the larger alveolus with lower recoil pressure (collapse). Dashed arrow shows the direction of air. In the presence of surfactant (b), the lower surface tension in the smaller alveolus will retain the same recoil pressure in both alveoli avoiding alveolar collapse. Figure adapted from Rhoades and Bell[26] with permission.

1.3 Surfactant Dysfunction

A number of factors can cause surfactant dysfunction in the lungs, some of these (as listed by Griese[8]) include a reduction in the overall phospholipid content, altered proportion of surfactant components, increased amounts of less-surface active phospholipids, lipolytic or proteolytic degradation, changes in surfactant after secretion and presence of inhibitory compounds (e.g. albumin[27]). Also, mutations in the genes encoding surfactant proteins can also lead to surfactant dysfunction.[28] Pulmonary surfactant deficiency leads to higher surface tension in the alveolar region. Elevated surface tension values in the alveoli have been reported with a number of diseases such as asthma,[29] pneumonia[30] and respiratory distress syndrome[31] and results in increased work of breathing, impaired gas exchange and alveolar collapse followed by a reduction in the available surface area.[31] Considering the serious implications of surfactant dysfunction,

the function of the pulmonary surfactant in disease states and upon exposure to impurities has been frequently studied.[32-35] These studies have focused on the interactions between the pulmonary surfactant and foreign molecules such as drugs, proteins and solid particles.

1.3.1 *In vitro* Studies of Pulmonary Surfactant Function

Pulmonary surfactant is a mixture of various lipids and proteins making it a challenging task to mimic its composition and perform mechanistic studies *in vitro*. Thus, *in vitro* studies have often used simpler models to study surfactant biophysical behavior. Such models can be divided into three categories: 1. Models that have used a single molecule to mimic surfactant function (monomolecular models), 2. Models that have used two or more surfactant molecules but have not included all the components known to be in natural surfactant (multi-molecular models) and 3. Models that have used natural surfactant extracts or synthesized complex surfactant models.

Studies with monomolecular models have almost exclusively used DPPC (the component with the highest concentration in the pulmonary surfactant[18]) as surfactant model. When spread and compressed on an air-water interface, DPPC molecules reach near zero surface tension values upon compression.[36-38] The interfacial behavior of these molecules is also very well studied in the literature making DPPC an appropriate, simplistic model to study surfactant behavior. Studies of multi-molecular surfactant models have used combinations of DPPC and other surfactant molecules to provide a more physiologically relevant model. Examples of these models include mixtures of DPPC and phosphatidyl glycerol,[39, 40] DPPC, palmitoyl-oleoyl-phosphatidylglycerol (POPG) and surfactant protein B,[41] DPPC and DPPG[42] and DPPC and palmitic acid.[43] Multi-molecular surfactant models are closer mimics of lung surfactant composition; however, performing mechanistic studies with these models is complicated due to the presence of multiple molecules. Also, the likelihood of confounding effects from the

surfactant components not included in these model needs to be considered in mechanistic studies. Finally, a number of studies have used synthetic or natural pulmonary surfactant models to study surfactant behavior. Examples of such models include Infasurf (calf lung lavage)[44-47], Curosurf (porcine lung mince),[47, 48] Survanta (bovine lung mince)[47, 48], Exosurf (synthetic preparation)[41] and BLES (bovine lung lavage)[47]. These models closely mimic pulmonary surfactant composition and function; however, performing mechanistic studies with such models is a challenging task due to the number of molecules present in the surfactant which increase the likelihood of potential parallel mechanisms.

Surfactant function *in vitro* is studied by changing the area between surfactant molecules and monitoring surface tension. Three main methods have been used to perform the changes in the area between surfactant molecules and measuring the surface tension. One method is using a Langmuir-Wilhelmy balance, in this method a trough is filled with an aqueous subphase and DPPC or other surfactant molecules are spread on top. DPPC is an amphiphilic molecule (i.e. contains both hydrophilic and hydrophobic moieties) that is insoluble in water. When spread on an air-water interface, the hydrophilic moiety comes in contact with water whereas the hydrophobic moiety orients toward air. This conformation leads to the formation of a one molecule thick monolayer commonly known as Langmuir monolayers.[49] These monolayers at the surface are compressed and expanded using barriers for surface compression and the surface tension is measured using a Wilhelmy plate balance. This is the most commonly used method for characterizing surfactant models due to its relative simplicity and the ability to give the surface tension over a wide range of mean molecular areas.

A few studies have used a captive bubble tensiometer (CBT) to reduce the area between surfactant molecules and measure the surface tension.[36, 50, 51] In this method surfactant molecules are spread inside an air bubble that is confined within a cuvette sealed with agarose gel. Reducing the air inside the bubble with a syringe results in compression of its surface and a consequent reduction in the area between surfactant

molecules and surface tension. Reduction in surface tension changes the bubble morphology from spherical to flat allowing to relate surface tension to bubble morphology.[51] The use of this instrument has been limited due to the likelihood of penetration of surface-active material into the agarose gel and the challenges of removing the organic solvent in which the surfactant is dissolved from the system.[36]

Finally, the pulsating bubble surfactometer (PBS) has been used as an effort to mimic the alveoli.[52] In this method, a chamber is filled with subphase and an air bubble connected to ambient air via a capillary is used to mimic an alveolus. The motion of a piston produces a negative pressure in the chamber and the pressure difference is measured using a pressure sensor. The changes in pressure along with bubble diameter are recorded and the surface tension is estimated using the Laplace equation (Equation 1-1). The advantages of this method are the ability to simulate breathing dynamics and the ability to adjust pulsation rates to breathing rates. However, it is difficult to use this method at low surface tension values as the bubble becomes flat and Laplace equation needs to be modified. Also, studying the surface pressure values throughout bubble compression and expansion requires recording bubble diameter at all times which can be challenging especially at high pulsation rates. Finally, at low surface tension values some of the surfactant film might be extruded into the capillary thus affecting surface tension measurements.[53]

The above-mentioned methods all work based on changing the area between surfactant molecules and monitoring the changes in surface tension. Information on changes in surface tension with surface area reduction (or expansion) serves as the main metric to characterize the function of surfactant models in health or disease or following exposure to contaminants.

1.4 Particle-Surfactant Interactions

Inhalable airborne particles are a major source of contaminants that might affect surfactant function. Particles larger than 10 micron do not reach the alveolar region. However, depending on particle size, up to 50% of inhaled particles less than 10 micron in diameter can deposit in the alveolar region.[54] Particles that deposit in the alveoli come into direct contact with the pulmonary surfactant. This has raised concerns about the interactions of nanomaterials and surfactant function, especially since the availability of nano-based products has increased the chance of human exposure to nanoparticles.[55] Given that lungs are the main portal of entry for the airborne particles, studies of particle interactions with pulmonary surfactant is of utmost importance to the field of environmental and occupational health.

1.4.1 A Review of Previous Studies on Particle-Surfactant Interactions

The potential negative effects of particles on pulmonary surfactant function have been shown in several studies. For example, exposure to environmental nanoparticles has been reported to alter the interfacial properties of model surfactants *in vitro*. Gold nanoparticles (15 nm) were reported to increase the surface tension of a model pulmonary surfactant (DPPC/ palmitoyl-oleoyl-phosphatidylglycerol (POPG)/Surfactant protein B, 70:30:1 wt%) by more than 20 mN/m when added at low concentrations.[41] Kanishtha and colleagues[39] have shown that deposition of nanoparticles generated from combustion of dried cow dung and wood increases the surface tension of a DPPC monolayer up to 15 mN/m depending on composition and concentration of particles. The problem with the deposition of particles becomes more evident considering that surface tension of the alveolar region during normal breathing ranges approximately between 3 mN/m and 22 mN/m and the difference between the minimum surface tension of the pulmonary surfactant of a normal adult and a premature infant is about 15 mN/m.[56]

Although reports exist on the negative effects of nanoparticles on surfactant function, the mechanisms controlling such effects are not exactly known. Some of the proposed mechanisms for surfactant inhibition by solid particles are particle penetration into the monolayer and adsorption to the air-water interface disrupting the integrity of the rigid surfactant film upon compression,[39] [57] adsorption of surfactant lipids and proteins on particle surfaces[41, 44, 45, 58, 59] and a combination of the two.[42] Finally, electrostatic interactions between charged particles and surfactant components have also been suggested to affect the orientation of surfactant molecules and alter their interfacial behavior.[60, 61] Although several mechanisms have been proposed for particle-induced surfactant inhibition, it is important to understand how these mechanisms relate to the structure of nanoparticles and predict the effects of particle properties on pulmonary surfactant function.

A summary of the previous studies of particle-surfactant interactions is presented in Table 1-1. As seen in this table, various particles and surfactant models have been used in previous studies. Although exposure of a certain surfactant to particle with different physicochemical properties can generate mechanistic information on particle-surfactant interactions, the use of different surfactant models, particle concentrations and routes of surfactant exposure to particles have limited our knowledge of such interactions.

In spite of the limitations mentioned above, changes in the physicochemical properties of nanoparticles such as size (or size distribution), charge, surface groups and wetting behavior have been successfully applied to explain the mechanisms of surfactant interactions with engineered particles. The role of particle size in particle-surfactant interactions has been shown in several previous studies. It has been shown that polystyrene and TiO_2 particles will not affect the function of Curosurf (a natural porcine surfactant) when added as micron-sized particles, but significantly increase the minimum surface tension when added as nano-sized particles.[58] Also, the effect of plain polystyrene nanoparticles on minimum achievable surface tension of a complex surfactant model has

been shown to be size dependent with pronounced effects observed with 20 nm particles and no effect with 130 nm particles.[61, 62] It has been suggested that the increased effect of smaller particles is a result of their ability to penetrate through the closely packed surfactant monolayer at high surface pressures.[61]

The effect of wetting behavior of particles on their interaction with surfactant has also been shown in several studies. Guzman and colleagues[63] have reported that hydrophilic silica nanoparticles do not significantly affect surfactant function whereas hydrophobic carbon black particles inhibit surfactant function at high concentrations. This is in agreement with the previous studies with surfactant monolayers hydrophobic molecules,[34] and the suggested mechanism that hydrophobic compounds adsorb to the air-water interface causing surfactant inhibition.[39, 57] However, a conflicting result has been reported by Al-Hallak and colleagues,[64] who reported improvement in surfactant function with hydrophobic polybutylcyanoacrylate nanoparticles and inhibition in surfactant function with the same particles coated with hydrophilic polysorbate-80. These reports suggest that relative hydrophobicity affects the interaction of particles and surfactants although inconsistent results show the lack of understanding about the mechanism of effect.

Particle charge and surface group is another important factor in particle-surfactant interactions. To date, there have been only two published studies on the effect of positively charged particles on surfactant function both of which report that particles did not induce inhibitory effects on surfactant function. Beck-Broichsitter and colleagues[59] exposed Alveofact (a commercially available bovine surfactant) to positively charged poly(butyl methacrylate-co-(2-dimethylaminoethyl) methacrylate-co- methyl methacrylate) 1:2:1 (Eudragit E100) particles and observed no surfactant inhibition even at very high particle concentrations. Peetla and Labhasetwar[61] reported improvement in the surface pressure isotherm (i.e. higher surface pressure values at fixed surface areas) of an endothelial model cell membrane after exposure to positively charged amine-modified

Table 1-1. A summary of previous studies on nanoparticle-pulmonary surfactant model interactions ordered by publication year.

Reference	Particle Type	Surfactant	Route of Exposure	Particle Concentration (g/L)
Sosonowski et al.[45]	Soot	Infasurf	Mixing	1
Kanishtha et al.[39]	Biofuel combustion emission	DPPC/Exosurf	Mixing/Monolayer Addition	N/A*
Stuart et al.[65]	Gelatin	DPPC	Mixing/Monolayer Addition	0.1
Bakshi et al.[41]	Gold	DPPC/POPG/SP-B	Mixing	0.002
Ku et al.[66]	Gelatin	DPPC	Monolayer Addition	1
Peetla and Lahasetwar[61]	Polystyrene	Endothelial model cell membrane	Subphase Injection	0.01
Peetla and Lahasetwar[62]	Surfactant-coated polystyrene	Endothelial model cell membrane	Subphase Injection	0.01
Schleh et al.[58]	Titanium dioxide and Polystyrene	Curosurf	Mixing	0.5
Kondej and Sosonowski[67]	Dust with high metal conc.	Infasurf	Mixing	0.864
Al-Hallak et al.[64]	PCBA	DPPC	Monolayer Addition	1
Beck-Broichsitter et al.[59]	Polystyrene, PLGA, Eudagrit-E 100	Alveofact	Mixing	2
Fan et al.[44]	Hydroxyapatite	Infasurf	Mixing	0.05

Table 1-1. Continued

Guzman et al.[43]	Silica	DPPC/DOPC	Monolayer Addition	10
Santini et al.[68]	Silica	Palmitic acid	Monolayer Addition	10
Tatur and Badia[69]	Alkylated gold	DPPC and Survanta	Mixing	N/A*
Guzman et al.[60]	Silica	DPPC/palmitic acid	Monolayer Addition	10
Guzman et al.[63]	Silica and carbon black	DPPC	Monolayer Addition	10
Guzman et al.[70]	Silica	DPPC/cholesterol	Monolayer Addition	10

* N/A: Not applicable, particle concentrations not stated in the study.

polystyrene particles. The mechanism of this improvement has been suggested as electrostatic interaction between amine groups on the particles and phosphate groups of the surfactant leading to an artificial compression of surfactant molecules at the surface.

The effect of negatively charged particles on surfactant function is not well understood and several conflicting reports have been published on this subject. The knowledge gained from studies of the interactions between subphase ionic species and DPPC monolayers suggest that adsorption of negative ions to the monolayers can improve surfactant function likely by electrostatic screening of surfactant dipoles. Accordingly, it was suggested that the negative ions have screening effects on DPPC dipoles, thereby reducing electrostatic repulsion between DPPC molecules bringing them closer to each other.[71] The study by Guzman and colleagues[60] with negatively charged

silica nanoparticles and DPPC monolayers agreed with this hypothesis. However, in contrast to these studies, Peetla and Labhasetwar[61] reported no significant change in the surface pressure isotherm of an endothelial model cell membrane after exposure to negatively charged carboxyl-modified polystyrene particles. Moreover, Schleh and colleagues[58] reported surfactant inhibition after exposure to negatively charged polystyrene nanoparticles. Such conflicting reports underscore the lack of understanding in particle-surfactant interactions, such understanding is very useful especially even for simple, non-degradable particle systems.

Adsorption of surfactant components on nanoparticle surfaces has been suggested to be another mechanism of effect of nanoparticles on surfactants. Binding of phospholipids to fine urban particles[72] and surfactant proteins to carbon nanotubes[73] have been previously shown after incubating nanoparticles with the bronchoalveolar lavage fluid. In studies of nanoparticle interactions with surfactant, Bakhshi and colleagues[41] have suggested that gold nanoparticles can sequester POPG and surfactant protein B on their surfaces and hinder surfactant function. Binding of surfactant proteins or phospholipids on nanoparticle surfaces has also been suggested with hydroxyapatite[44], titanium dioxide[58] and polystyrene, poly(lactide co glycolide) (PLGA) and poly(butyl methacrylate-co-(2-dimethylaminoethyl) methacrylate-co-methyl methacrylate) 1:2:1 (Eudragit E100) nanoparticles.[59] This mechanism has been reported only with complex surfactant models where many components might bind to particle surfaces and not with surfactant models based on single phospholipids such as DPPC monolayers.

1.4.2 Limitations of Existing Studies

Although various reports have investigating surfactant interfacial behavior after exposure to nano- and sub-micorn particles, there are still gaps within the existing body of literature that need to be addressed. A major limitation in previous studies is using a number of different routes of surfactant exposure to nanoparticles.

Three different exposure routes have been used in the literature to study the interactions between particles and surfactants (Figure 1-4). One method is to mix the particle and surfactant beforehand and then spread this mixture in the tensiometric instrument. This method is referred to as "mixing" in Table 1-1. Although mixing has been used by several research groups, it seems to be the least relevant for mimicking inhalation where particles come into contact with a surfactant film that is already spread. Mixing also provides ample time for adsorption of surfactant components onto particle surfaces even before tensiometric experiments. Interestingly, most of the studies that have used mixing as a method of exposure have reported adsorption of surfactant components on particles as the mechanism of surfactant inhibition.[41, 45, 59, 67] Other methods of surfactant exposure to particles include spreading the surfactant on top of a subphase in which the particles are already dispersed (monolayer addition) or injecting the particles in a subphase upon which surfactant is already spread (subphase injection) (Figure 1-4). The latter methods both seem to have some physiological relevance; however, it is not known if and how the route of exposure affects particle-surfactant interactions and therefore the conclusion on whether or not a certain particle inhibits surfactant function.

Another major limitation comes from the fact that none of the previously used exposure routes mimic inhalation. Although mixing the particles with surfactant or adding the particles to the subphase can be quite useful for studies of nanoparticle-biomembrane interactions, none of these routes mimic inhalation. To the best of our knowledge, a realistic route of surfactant exposure to particles (i.e. aerosolization of particles on top of surfactant) has not been studied before. This has hampered researchers' ability to provide realistic predictions on the effect of a certain particle type on pulmonary surfactant function.

Finally, realistic particle concentrations have rarely been used in previous studies and estimations on physiologically relevant concentrations have not been published. A
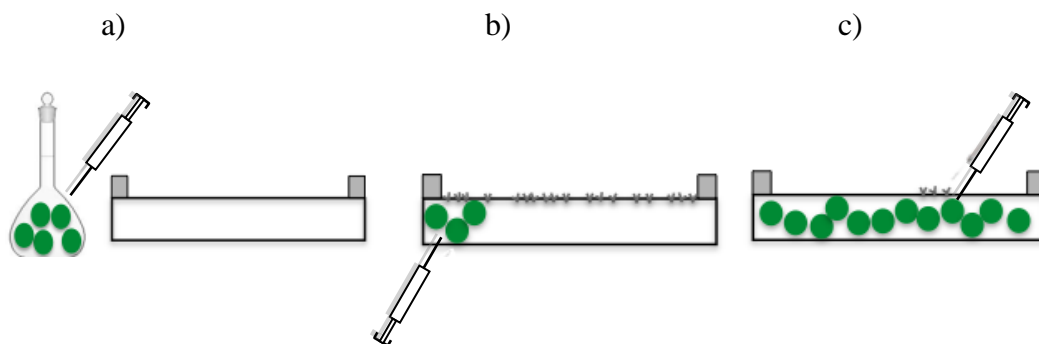
Figure 1-4. Different methods of surfactant exposure to particles: a) mixing the particles with the surfactant solution and spreading the mixture on the surface of Langmuir trough, b) spreading the surfactant on the surface and injecting the particles in the subphase (subphase injection) and c) spreading the surfactant on top of a subphase in which already the particles are already dispersed.

range of particle concentrations from 0.002 g/L to 10 g/L[60] have been studied in the literature pointing to a lack of knowledge on physiologically relevant particle concentrations.[41, 43] Moreover, realistic surfactants have also been rarely tried with previous studies being mostly focused on using DPPC or mixtures phospholipids as surfactant model. Although a lot of valuable mechanistic information can be drawn from studies with simple surfactant models, such studies need to be linked to the studies with physiologically relevant surfactant models to provide information on particle-surfactant interactions upon inhalation.

Given the limitations of the previous studies and the complexity of the system, it is hard to conclude which particle properties have led to certain surface behavior and consequently the mechanisms of interaction are poorly understood. These limitations are best shown by the fact that even for a commonly used nanoparticle model such as polystyrene, two different mechanisms of interaction with surfactant have been proposed in the literature.[58, 61] A comprehensive study on different routes of exposure and well-characterized surfactants and particles is still lacking making it difficult to predict the effect of particles on the loss of surfactant function. Such studies can be beneficial for the

design of nanoparticles for pulmonary drug delivery and for setting new health and safety standards regarding exposure to nanomaterials.

1.5 Objectives

A major improvement in our current state of knowledge of particle-surfactant interactions can be made by understanding how these interactions are affected by different routes of exposure. Therefore, the research presented in this thesis aims to elucidate the interactions between negatively charged polymeric particles (which have shown promise as drug delivery vehicles[74]) and pulmonary surfactant using various exposure routes. We hypothesize that the route of exposure to particles alters the mechanisms of particle-surfactant interaction. The objectives and specific aims of this research are explained as follows:

Objective 1: Determine the interactions between sub-micron particles and a simple model of pulmonary surfactant after particle addition using the subphase injection route.

Specific Aim 1.1: Characterize the physicochemical properties of polystyrene particles and the interfacial behavior of DPPC.

Specific Aim 1.2: Investigate the effects of exposure to particles on the interfacial behavior of surfactant.

Specific Aim 1.3: Investigate the effects of exposure to particles on surfactant microstructure and topology.

Objective 2: Determine the interactions between particles and DPPC when the particles are added using the monolayer addition route.

Specific Aim 2.1: Study the effects of particles on surfactant interfacial properties after particles are added using the monolayer addition route.

Specific Aim 2.2: Study the effects of particles on the alignment and orientation of surfactant molecules.

Objective 3: Determine the effect of a realistic route of surfactant exposure to particles (i.e. aerosolization) on the interactions between particles and pulmonary surfactant function.

Specific Aim 3.1: Develop a method for particle aerosolization onto surfactant films.

Specific Aim 3.2: Characterize the interfacial properties of a calf lung surfactant extract (Infasurf) as a realistic surfactant model.

Specific Aim 3.3: Investigate the effects of particles on the interfacial behavior of DPPC and Infasurf.

CHAPTER 2

SURFACTANT CHARACTERIZATION USING THE LANGMUIR

TROUGH

2.1 Introduction

In vitro studies of surfactant function have mainly relied on tensiometers to evaluate surfactant functionality. Three main tensiometers have been used to characterize pulmonary surfactant models *in vitro*: pulsating bubble surfactometer (PBS)[58], captive bubble tensiometer (CBT)[36, 41] and the Langmuir-Wilhelmy balance [42, 57, 61, 62, 64-66, 75] (see section 1.3.1 for a brief review of each technique). Of these instruments, the Langmuir-Wilhelmy balance has been the most popular method for characterizing pulmonary surfactant models and other surface-active monolayers. Although this instrument does not mimic the geometry of alveoli, Langmuir trough can be used for studies at very low surface tension values (a problem with PBS), does not risk the penetration of the sealing surface-active material such as agarose (a problem with CBT) and provides a well-defined medium to study monolayers as molecular orientation, packing and surface tension of the monolayer can be easily controlled merely by compression and expansion of the surface. Moreover, the Langmuir trough setup allows for mounting of additional instrument such as microscopes or surface potentiometers facilitating additional analysis of surfactant behavior.

Introduced and used by Langmuir in 1917,[76] the Langmuir-Wilhelmy balance has undergone little changes over time. The instrument consists of a long narrow trough confined on the sides with two barriers. The trough is filled with an aqueous subphase upon which droplets of surfactant are spread. The barriers are then used to compress the surface and reduce the surface area between the molecules of the surface-active agent while a Wilhelmy plate balance is used to measure the surface tension. The earlier models of the Langmuir trough generally used Teflon barriers;[77] however, these barriers

were later replaced with Delrin which is more hydrophilic and has been shown to reduce the chance of surfactant leakage from the trough.[78]

Although a large body of literature has developed on characterization of the interfacial properties of pulmonary surfactant models using the Langmuir trough, the reported surface tension behavior is not always similar between different studies. Such differences are observed even for simple surfactant models such as pure DPPC (see Duncan and Larson[79] for a discussion on differences in the literature). The main reasons for differences in literature are believed to be the use of different organic solvents, aqueous subphases, surface compression rates and temperatures.[79] Thus, in studies of Langmuir monolayers each of these variables need to be carefully chosen and the generated results need to be compared with studies that have used similar variables to provide a fair comparison to previous studies.

This chapter focuses on tensiometric experiments on the pulmonary surfactant models used in this work (DPPC and Infasurf). To provide a basis for the remainder of this work, a brief review of each surfactant model and their interfacial behavior at the air-water interface is provided, followed by introduction of the metrics used to characterize surfactant films in previous studies. Then, experiments performed to calibrate the Langmuir-Wilhelmy balance and characterize the interfacial behavior of each surfactant will be described.

2.1.1 Surfactant Models: DPPC and Infasurf

Two surfactant models were used in this research to mimic the surface-active properties of the pulmonary surfactant; DPPC and Infasurf. DPPC provided a simple, single molecule model of the pulmonary surfactant, whereas Infasurf provided a more complex and physiologically relevant model.

DPPC is a zwitterionic phospholipid and is the component with the highest concentration in the pulmonary surfactant. The composition of the pulmonary surfactant

between mammals is very similar[16] and the composition given for bovine pulmonary surfactant can be used as a representative for most mammals. DPPC accounts for 36% by weight of bovine pulmonary surfactant.[17, 18] DPPC is composed of a phosphatidyl choline (hydrophilic headgroup) connected to two palmitic acids with 16 carbon atoms (hydrophobic tails) (Figure 2-1). When spread on an air-water interface, DPPC forms a monolayer at the interface with the hydrophilic headgroup remaining hydrated and the hydrophobic tails remaining out of the water phase.
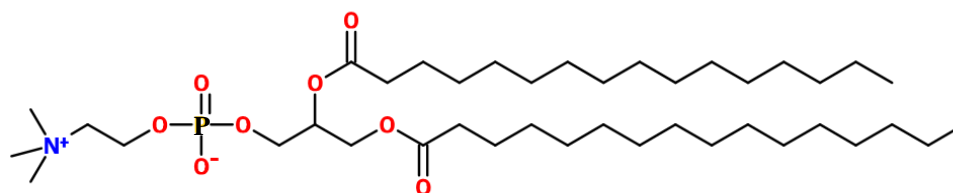
Figure 2-1. Molecular structure of DPPC, a zwitterionic surfactant with a hydrophilic headgroup and two hydrophobic tails.

DPPC reduces the surface tension of water to near zero values upon compression.[38] Due to its efficiency in reducing the surface tension and its high concentration in pulmonary surfactant composition, DPPC has been used as a model pulmonary surfactant in many studies.[32, 34, 36, 37, 39] DPPC is also present in the cell membrane and therefore has been used in cellular membranes studies.[80-82] Consequently, there are many reports available in literature on the surface pressure-surface area isotherms of DPPC. The significant body of literature on DPPC and the fact that it is a simple surfactant model make it a favorable model for mechanistic studies of pulmonary surfactant.

Infasurf is an extract from bovine lung lavage used for surfactant replacement therapy.[83] Infasurf is composed of various lipids and proteins. A milliliter of Infasurf contains about 35 mg of lipids and 0.65 mg of surfactant proteins B and C.[84] The study of Notter and colleagues[85] has provided more information of the composition of Infasurf. According to this study, phosphatidyl cholines are the dominants species in Infasurf accounting for more than 84% of Infasurf lipids followed by phosphatidylglycerol (4.8%), phosphatidylinositol (4.3%) and phosphatidylethanolamine (3%). These values are very similar to bovine lung surfactant composition reported in Chapter 1. The surfactant proteins are present in Infasurf in almost equal concentrations. However, there is some inconsistency in the values reported in the literature with one study[85] reporting that surfactant protein B accounts for more than 50% of the protein content of Infasurf and another study[86] reporting that surfactant protein C is the protein with the highest concentration. Differences are likely due to sample extraction from calves and concentration differences between the subjects. Due to its complexity, there are a limited number of reports in the literature on the surface pressure-surface area isotherms of Infasurf.[44, 46, 86, 87]

2.1.2 Evaluating The Surface Pressure Isotherms of DPPC and Infasurf

In vitro studies of DPPC and Infasurf commonly measure surface pressure as a function of mean molecular area or surface area isotherms to determine surfactant functionality. Analysis of surface pressure isotherms requires a number of metrics so that various isotherms can be compared. The most commonly used metrics for analyzing a surface pressure isotherm include surfactant phase behavior, collapse surface pressure and surface area, compression modulus and hysteresis area. These metrics are discussed below.

2.1.2.1 Surfactant Phase Behavior

Both DPPC and Infasurf show distinct phase behavior upon compression. Phase behavior provides information about the organization of surfactant molecules at the air-water interface. Surface compression reduces the surface area available to surfactant molecules and changes their orientation. The changes in molecular assembly at the interface for both surfactants are shown schematically in Figure 2-2. In this figure, the changes in surface pressure of DPPC has been reported as a function of mean molecular area, whereas for Infasurf surface pressure changes have been reported as a function of trough surface area. This is due to the presence of multiple lipids and proteins in Infasurf that do not allow for estimation of mean molecular area.
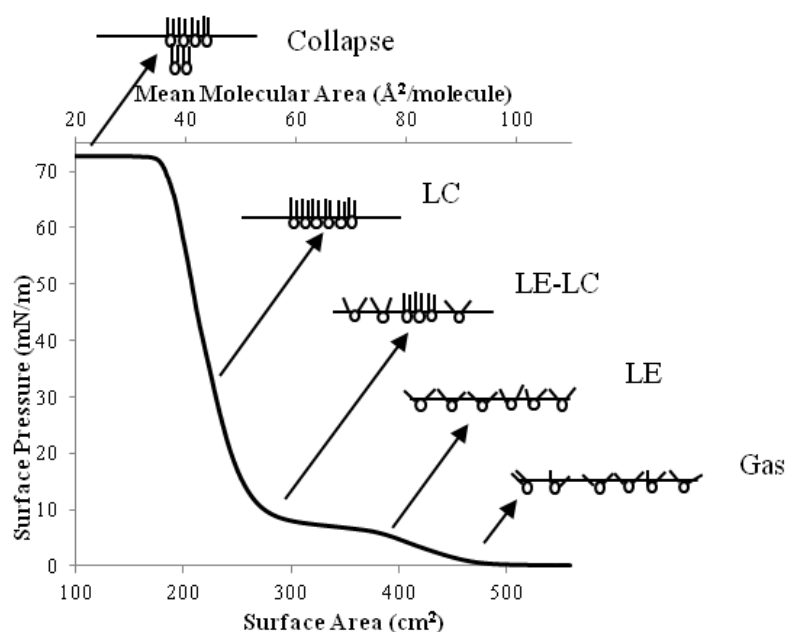
Figure 2-2. The surface pressure vs. surface area isotherm of DPPC after compressing the surface from an initial area of 558 cm^2 to a final area of 100 cm^2 on a subphase of 0.15 M NaCl and 1.5 mM CaCl$_2$ at a pH of 7 room temperature. Monolayers show distinct phase behavior including gas, liquid expanded (LE), liquid expanded-liquid condensed (LE-LC) and liquid condensed (LC) phases. A final collapse phase is observed when the monolayer changes its structure to a multilayer.

Reduction of mean molecular area between DPPC molecules alters their arrangement from a highly expanded state known as the gas phase, to a liquid expanded (LE) state where surfactant molecules start affecting the surface pressure. Further compression results in the appearance of gel-like lipid clusters in which the surfactant molecules are tightly packed and ordered at the air-water interface. These clusters are known as lipid rafts or domains and coexist with the liquid expanded state forming the liquid expanded-liquid condensed (LE-LC) phase where a plateau in the surface pressure is observed. Further compression results in the liquid condensed (LC) phase where the lipid domains dominate the surface and compression results in rapid increase of surface pressure. Further reduction of surface area results in molecules entering the subphase as a result of the limited surface area, a process known as collapse.[88]

The LE-LC phase of the monolayers has been of particular interest to researchers due to the coexistence of liquid expanded phase and lipid domains. Lipid domains in this phase can be visualized using an appropriate fluorescent probe which segregates into only one phase.[89, 90] The ratio of these domains to the entire surface gives an estimate of surface fluidity and the arrangement of molecules at the surface. The presence of the lipid domains has also been shown to significantly affect surfactant rheological properties.[91]

Unlike DPPC, there have been very few studies on the phase behavior of Infasurf films at the air-water interface. Infasurf forms monolayers at the air-water interface up until a surface pressure of ~40 mN/m where a plateau in surface pressure is observed. When studied using atomic force microscopy (AFM) three phases can be observed in Infasurf films at surface pressure values below 40 mN/m. These include a liquid expanded (LE) phase similar to DPPC, a liquid ordered (LO) phase that is rich in cholesterol and in terms of lipid packing is between liquid expanded and condensed phases[47] and a tilted condensed (TC) phase in the middle of the LO phases (Figure 2-3, AFM image at 40 mN/m). Note that the terminology for these phases are different from that used for DPPC and are based on the suggestions of Kaganer and colleagues.[92] The

tilted condensed phase refers to ordered lipid molecules where the hydrophobic tails are ordered but tilted with an angle, these domains consist of disaturated lipids (mostly DPPC) as shown by time of flight secondary ion mass spectrometry experiments.[93] Further compression during the plateau region results in collapse of LE and LO phases. At the end of the plateau region, these phases form multilayers about 4 nm high at the air water interface, thus the TC domains (about 1.5 nm high) appear as holes in between the multilayers (Figure 2-3, AFM image at 50 mN/m).[46, 87] Further compression to 60 mN/m increases the width of the multilayers without affecting their height (Figure 2-3, AFM image at 60 mN/m); however, during Infasurf collapse multilayers as high as 10 nm can be observed.[47] As the TC domains are mainly consisted of DPPC, the process of changing from monolayers to multilayers is suggested to be a refining process enriching the surface with DPPC by squeezing out the non-DPPC components.[46]
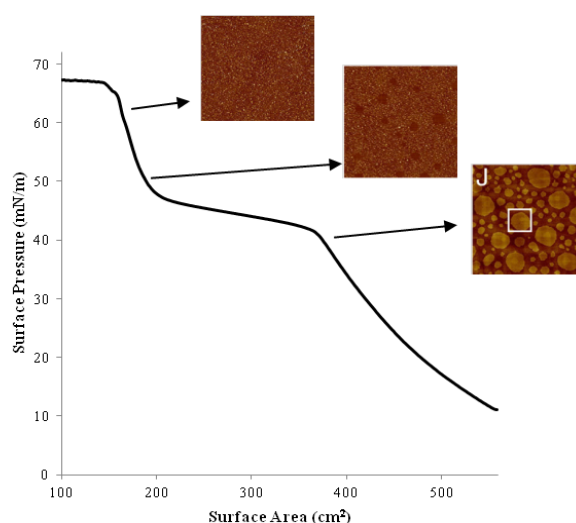
Figure 2-3. The surface pressure vs. surface area isotherm of Infasurf after compressing the surface from an initial area of 558 cm^2 to a final area of 100 cm^2 on a subphase of 0.15 M NaCl and 1.5 mM CaCl$_2$ at a pH of 7. Surface compression of Infasurf leads to ordered lipid phases (rectangular box) with higher height compared to disordered phases when examined under atomic force microscopy (AFM). The AFM scan area is 50 μm×50 μm and AFM images are reproduced from Zhang and colleagues with permission.[47]

2.1.2.2 Monolayer Collapse Surface Pressure and Surface Area

When DPPC molecules are compressed beyond their limiting cross-sectional area further compression results in molecules entering the subphase which destabilizes the 2D structure of the monolayer and results in a 3D structure.[94] The mechanism of collapse is dependent on the compression rate[95] and temperature.[96] However, it is known that lipid monolayers collapse by buckling and forming vesicles in the water subphase.[88]

The surface area of collapse provides an estimate of the limiting molecular area for pure monolayers. Also, the kinetics of readsorption of the squeezed out molecules is a major determinant of the surface pressure at fixed surface areas obtained in the following cycles. For example, monolayers consisting only of DPPC have slow readsorption kinetics,[97] but it has been shown that surfactant proteins and unsaturated lipids improve the readsorption kinetics of squeezed molecules.[98]

The collapse mechanism for Infasurf films is more complicated and less studied compared to DPPC. As mentioned in the previous section, it is known that after the plateau region between 40 mN/m to 50 mN/m, Infasurf films contain monolayers of the DPPC-rich TC phase and multilayers of other surfactant components.[46] As the Infasurf films are compressed beyond the plateau region, the multilayers increase in height but not in width.[46] During collapse, the height of these multilayers can be as much as 10 nm higher than the TC phases as shown by atomic force microscopy studies.[47] No sign of buckling is observed in Infasurf during collapse which is evidence of a different collapse mechanism compared to DPPC.[47]

2.1.2.3 Compression Modulus

Compression modulus or dilational elasticity is a measure of the elastic energy stored in the monolayer upon compressive deformation of the surface.[99] This metric is better defined by first understanding Gibbs elasticity. When a surface with an insoluble

monolayer is stretched, the dilation will cause a local thinning or reduction in concentration of the molecules of the monolayer, this will then result in a gradient in surface tension which resists the dilation giving the monolayer elastic properties known as Gibbs elasticity.[100] On the other hand, if the surface is compressed, as happens during dynamic experiments in a Langmuir trough, there will be a local decrease in surface tension and the surface forces tend to redilate the surface causing a resistance toward surface compression known as compression modulus or dilational elasticity. During constant surface compression, this redilation is limited by the time scale of area variations. Thus, the compression modulus will be directly related to the local changes in surface tension and conversely related to changes in surface area (speed of compression) as seen in Equation 2-1, where C_s^{-1} is the compression modulus, π is the surface pressure (mN/m) and A is the surface area (cm^2).

$$C_s^{-1} = -A\left(\frac{d\pi}{dA}\right) \tag{2-1}$$

Based on the above definition, the compression modulus is in fact a measure of the resistance of the monolayer to compression or monolayer rigidity. Higher values of dilatational elasticity denote a more rigid monolayer, it has been suggested that rigid monolayers can be characterized with compression moduli higher than 50 mN/m; whereas fluid monolayers have compression moduli of less than 50 mN/m.[99] Values of less than 10 mN/m are reported for monolayers in the gas or liquid expanded phase, whereas values in the range of 250 mN/m to 300 mN/m are reported for the more crystalline films in the liquid condensed phase where the monolayer is more rigid.[60, 80, 101] Values of compression moduli have been used to estimate the incorporation of exogenous particles in the monolayer and the changes in the cohesive forces between the molecules of the monolayer.[63]

Compression modulus is a metric for pure monolayers and thus has not been widely used for Infasurf. There is only one published study on the compression modulus of Infasurf. Using compressibility (i.e. the inverse of compression modulus), Zhang and colleages[46] have shown Infasurf films compressed beyond 50 mN/m show the same compressibility profile as pure DPPC further confirming that Infasurf films are enriched in DPPC at high surface pressure values.

2.1.2.4 Hysteresis Area

Hysteresis area is the area between the compression and expansion cycles in a surface pressure isotherm. Surface compression changes the structure of surfactant to a crystalline state and may lead to the squeeze out of molecules to the subphase. Readsorption of these molecules to the surface is a timely process resulting in a hysteresis area between compression and expansion. This area has been used as a measure of surfactant respreadability on the surface upon consecutive cycling. However, as a metric of surfactant function, hysteresis area is not very well understood. A large hysteresis area has been referred to both as a sign of surfactant functionality[45, 67, 97, 102] and dysfunction.[103] From a thermodynamic viewpoint, a small hysteresis is preferable as it denotes the squeeze-out of only a small portion of molecules from the air-water interface at the end of compression. However, a large hysteresis area appears to play a role in proper lung function as shown by comparing the hysteresis area of the lung surfactant extracts from healthy adults and patients with respiratory distress syndrome.[56, 104]

2.2 Materials and Methods

2.2.1 Materials

DPPC was purchased from Genzyme Pharmaceuticals (Cambridge, MA). This molecule was R oriented and did not include any racemates as it is fully synthetic.

Purchased DPPC was in form of a powder, DPPC solutions were made by dissolving 61 mg of DPPC in 50 mL of HPLC-grade chloroform (Sigma-Aldrich, St. Louis, MO) at a concentration of 1.22 g/L. Infasurf was a gift from ONY Inc. (Amherst, NY). Infasurf was received in 6 mL vials of surfactant in saline solution. The concentration of phospholipids in the received vials was 35 g/L. Infasurf solutions were made by dissolving 174 μL of the surfactant in 5 mL of chloroform/methanol (2/1 volume ratio) to obtain a final phospholipid concentration of 1.22 g/L, equal to the concentration of phospholipids in DPPC solutions. Methanol used in these solutions was purchased from Research Product International, Mount Prospect, IL. Sodium chloride and calcium chloride were purchased from Sigma-Aldrich and were dissolved in purified water for subphase preparation. All water used in experiments was obtained from a Barnstead NANOpure II system from Barnstead International (Dubuque, IA) and had a resistivity of 18.2 MΩ·cm.

2.2.2 Langmuir Trough Setup

The Langmuir trough used in these studies was a Minitrough System 4 purchased from KSV Instruments Ltd. (now KSV-NIMA, Finland). The length, width and the depth of the trough were 782 mm, 75 mm and 5 mm, respectively. This trough was also equipped with two Helmholtz coils which could be used for interfacial stress rheometry, but were not used in the current research. This setup was placed in an enclosure to reduce the deposition of dust and other environmental contaminants. A view of the Langmuir trough setup is presented in Figure 2-4.

A Wilhelmy plate was used to measure the surface tension in real-time. The Wilhelmy plate is a thin platinum plate connected to a sensitive force transducer that provides accurate measurements of surface tension. When the plate is in contact with the liquid, the wetting of the plate results in a downward pull as the surface forces minimize the surface area of the liquid. The downward force on the plate is measured (usually in
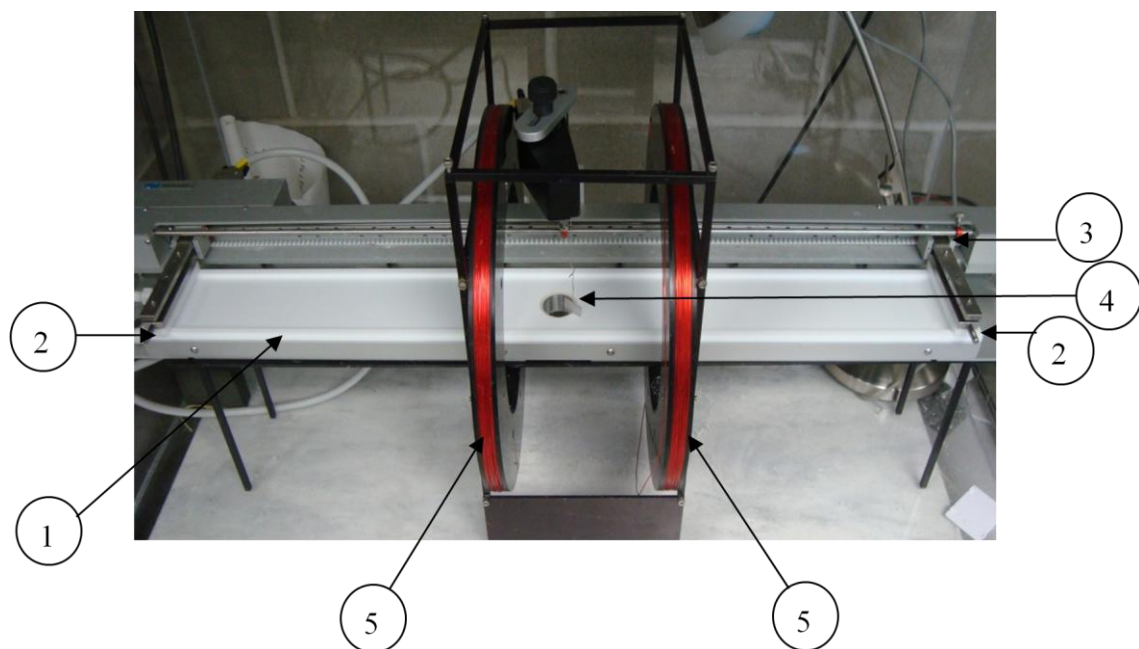
Figure 2-4. The Langmuir trough instrument used in this study. Key components of the instrument are labeled: 1. The Langmuir trough, 2. Barriers, 3. Computer controlled barrier drive, 4. Wilhelmy plate and 5. Helmholtz coils for interfacial stress rheometry.

mN or dyne) and is divided by the wetted perimeter (usually in m or cm) to provide surface tension measurements in mN/m or dyne/cm (Equation 2-2). The Wilhelmy plates are made very thin, so the role of thickness on the wetted surface of the plate can be considered negligible and the perimeter is considered two times the length of the plate.

$$\gamma = \frac{F}{2L \cdot Cos\theta}$$ (2-2)

where γ is the surface tension at the air-water interface, F is the force exerted on the plate by the liquid, L is the length of the plate and θ is the contact angle between the plate and the liquid surface. The contact angle is reduced to zero (i.e. complete wetting of the plate) by cleaning the plate by burning it in a flame before each experiment. Also, the Wilhelmy plates are usually roughened by sandblasting with very small grain sand to increase wetting characteristics of their surfaces and ensure a contact angle of zero.[105] The

Wilhelmy plate used with the setup is shown in Figure 2-5, this plate had a perimeter of 39.24 mm with a width of 19.62 mm and height of 10 mm (KSV-NIMA, Finland).
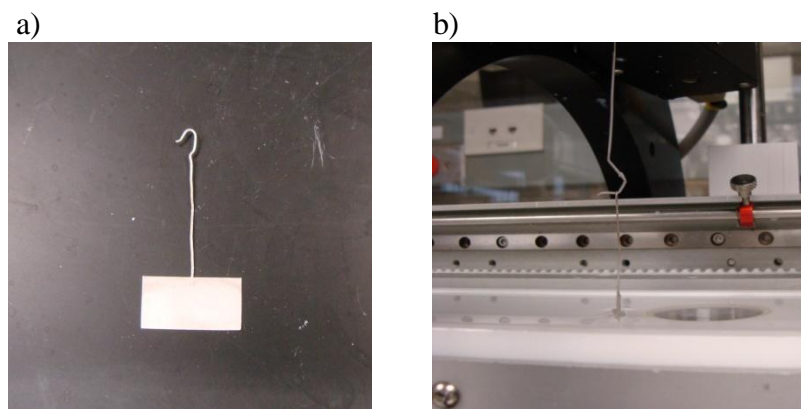
Figure 2-5. The Wilhelmy plate used with the setup (a). The hook above the plate was used to connect it to the tensiometer in the Langmuir-Wilhelmy setup. The thickness of the plate is negligible compared to other dimensions as shown in the side view (b).

2.2.3 Subphase Preparation

For tensiometric experiments the trough was filled with a subphase on which the surfactants were spread. In these studies, subphase composition of 150 mM NaCl, 1.5 mM $CaCl_2$ dissolved in purified water was used. This subphase was adjusted to the pH of 7 using droplets of 0.1 M NaOH. This subphase mimics the ionic composition of the alveolar subphase.[106] It has been shown that DPPC added on this subphase can reduce the surface tension to a constant value in a matter of seconds.[107]

2.2.4 Tensiometric Experiments

Tensiometric experiments were started by carefully cleaning the surface of the trough. To this aim, the surface of the trough and the barriers were brushed with ethanol (Figure 2-6) and then washed with copious amounts of purified water to ensure cleaning.
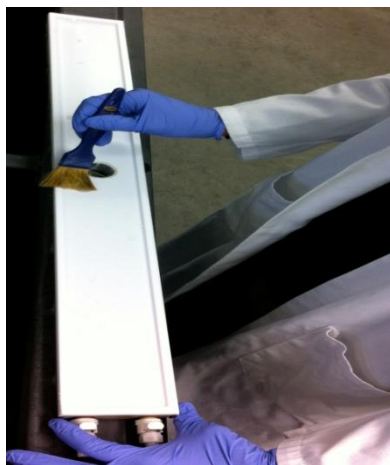
Figure 2-6. Surface of the trough and the barriers were brushed with ethanol to ensure cleaning.

Following the cleaning, the trough and the barriers were connected to the computer-controlled barrier drive. Then, the Wilhelmy plate was cleaned by placing it on a flame from a Bunsen burner and attached on a hook on top of the trough. The force transducer was zeroed and the trough was filled with 250 mL of freshly made subphase solution. The trough can contain up to 290 mL of liquid; however, it is not recommended to fill the trough with more than 250 mL of liquid as higher volumes will cause a convex surface which will increase the chance of surfactant leakage.

This subphase was allowed to equilibrate to room temperature (23.3 ± 0.6 °C) or 37 °C for 30 min. A water bath was connected to the trough to regulate the temperature during the 37 °C experiments. Then, the surface was aspirated while the barriers were compressed to remove any surface impurity. Changes in surface tension during this initial compression were monitored and a change of higher than 0.5 mN/m was considered a sign of surface impurities and the need for repetition of the experiments. The surface tension of pure subphase was measured before each experiment to confirm a surface tension close to that of pure water (72.3 mN/m at room temperature and 70.1 mN/m at 37 °C). Then, the surface tension was zeroed to allow for measurement of surface pressure.

Surface pressure is the measure of changes in surface tension and is obtained by subtracting the surface tension of pure subphase from the surface tension of the subphase in the presence of surfactant.

Surfactant monolayers were obtained by adding droplets of surfactant solutions on top of the subphase using a Hamilton microsyringe and allowing 20 min for solvent evaporation. For control experiments with the subphase and organic solvent, droplets of chloroform with no surfactant were added on top of the subphase. An initial amount of 50 μL out of 1.22 g/L solutions of DPPC in chloroform was used for all DPPC experiments. This amount resulted in a calculated mean molecular area of 111.6 Å^2/molecule which is higher than 100 Å^2/molecule where DPPC molecules induce changes in surface tension.[79] This area is calculated by dividing the surface area of the trough by the number of molecules of DPPC added on the surface (Equations 2-3 and 2-4).

$$\frac{50\mu L \times 1.22 g/L \times 6.02 \times 10^{23} \, ^\#/_{mol}}{734 g \, DPPC/mol} = 5.00 \times 10^{16} \text{ molecules} \qquad (2\text{-}3)$$

$$\frac{558 \text{ cm}^2 \times \frac{10^{16} \text{angstrom}^2}{1 \text{ cm}^2}}{5.00 \times 10^{16}} = 111.6 \, \text{Å}^2/_{molecule} \qquad (2\text{-}4)$$

Surface compression and expansion in the trough was performed with two different barrier speeds. Slow compression experiments were performed with a speed of 10 mm/min (1.5 Å^2/molecule·min). This was the lowest speed possible on the instrument and allowed for studying the system close to its equilibrium state, avoiding the complications that can arise by fast compression complicating mechanistic studies. A fast compression speed of 150 mm/min (22.5 Å^2/molecule·min) was used when DPPC and Infasurf were compared for dynamics of surfactant respreading and readsorption of surfactant molecules to the air-water interface. Barrier speed of 150 mm/min was the fastest speed on the instrument and was chosen to mimic the fast, physiologically relevant breathing rates.

A single compression cycle was performed for monolayer collapse experiments, whereas three compression and expansion cycles were performed for hysteresis experiments where the dynamic behavior of surfactant was studied. Surface tension data were acquired approximately every second and were recorded using the LayerBuilder software. The area between the compression and expansion curves (hysteresis area) was determined by subtracting the area under the curve for expansion from the area under the curve for compression. KaleidaGraph software v. 3.6 was used to calculate area under the curve for each case. Finally, the compression modulus of the isotherm was calculated using Equation 2-1. The surface pressure and surface area values needed for this equation were recorded using the LayerBuilder software and plotted in Microsoft Excel.

Initial experiments with Infasurf films were performed by adding an initial amount of 50 μL out of a solution with a final phospholipid concentration of 1.22 g/L. However, Infasurf films require a large surface area reduction to reach high surface pressure values of ~40 mN/m (Figure 2-7). Also, at this surface pressure, these films show a long plateau region making it difficult to obtain the complete surface pressure isotherm of Infasurf in one experiment when starting from a surface pressure of zero. Therefore, an initial amount of 70 μL out of a solution with a final phospholipid concentration of 1.22 g/L was used for Infasurf experiments. This amount resulted in an initial surface pressure of 10.9 ± 0.6 mN/m allowing for observing all different phases of Infasurf isotherm in one compression cycle. Similar to DPPC experiments, the surface of the trough was compressed and expanded with a barrier speed of 10 mm/min (1.5 $\mathring{A}^2$/molecule·min) for low-speed compression experiments and a barrier speed of 150 mm/min (22.5 $\mathring{A}^2$/molecule·min) for high-speed compression experiments.
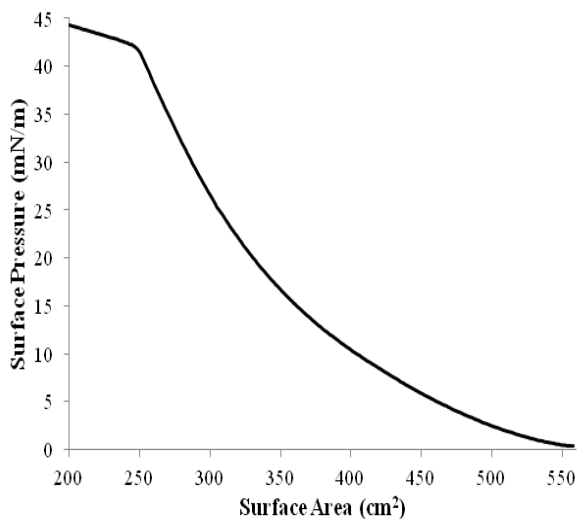
Figure 2-7. Infasurf surface pressure vs. surface area isotherm initiated after the addition of 50 µL of a solution with a final phospholipid concentration of 1.22 g/L. The films require a large surface area reduction to reach high (above 50 mN/m) surface pressure values.

2.3 Results and Discussion

2.3.1 Collapse Studies on DPPC Monolayers and

Comparison to Literature

Although DPPC monolayers have been studied for a long time, many differences are reported in the surface pressure-surface area isotherms at room temperature (Figure 2-8). As shown by Duncan and Larson[79] in their comparison of DPPC isotherms reported in literature, these differences are most likely the result of the different temperatures, different subphase compositions, different organic solvents and different compression speeds. Thus, the effect of these components on the surface pressure isotherm of DPPC was examined.

Control experiments were performed to ensure that the subphase components were not surface active and that the organic solvent evaporated. For these experiments, chloroform was added to the surface of the subphase and the surface was compressed

(Figure 2-9).The surface pressure after addition of chloroform to the surface showed a slight negative change of less than 0.05 mN/m, potentially due to impurities in solvent or surface perturbations caused by addition of chloroform. Upon surface compression from the initial area of 558 cm^2 to 150 cm^2 the surface pressure changed by less than 0.2 mN/m, confirming that the subphase and the organic solvent do not affect the surface pressure isotherms of the subphase.
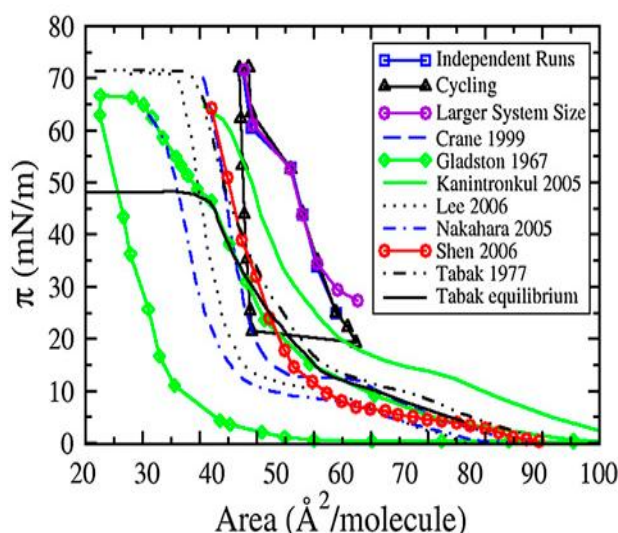
Figure 2-8. The surface pressure vs. surface area isotherms of DPPC reported by various studies at 20 °C. There is no consensus on the shape of the surface pressure vs. surface area isotherms. The parallelogram shapes in the middle of the graph represent the simulation data performed by Duncan and Larson.[79] Reprinted with permission.

Many different values have been reported for compression speed in the previous studies of DPPC surface pressure isotherm, values such as 0.6,[108] 7.8[109] and 38[110] Å^2/molecule·min have been previously used with little or no rationale for the choice. Slower compression rates are a better mimic for equilibrium conditions and help with generating mechanistic information; however, faster compression speeds are a closer

mimic to lung-relevant conditions. Since this study was focused on mechanistic information, the lowest compression speed available on the Langmuir-Wilhelmy apparatus (10 mm/min or 1.5 Å^2/molecule·min) was used for most experiments with surfactant and solid particles. The highest compression speed available on the instrument (150 mm/min or 22.5 Å^2/molecule·min) was used for experiments where the primary goal was to study surfactant behavior and spreading efficiency during fast cycling to mimic physiologically relevant conditions.
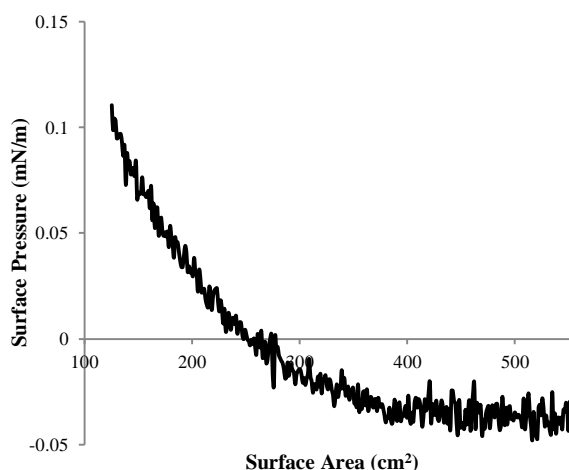
Figure 2-9. Surface pressure versus surface area isotherm of the subphase solution (150 mM NaCl, 1.5 mM CaCl$_2$, pH=7) after addition of 50 μL of pure chloroform to the subphase and allowing 20 minutes for chloroform evaporation. Surface compression performed between surface areas of 558 cm^2 and 150 cm^2.

Experiments with both fast and slow compression rates proved that compression rate did not affect the surface pressure isotherm of DPPC at room temperature (Figure 2-10). These results are in good agreement with the study of Jyoti and colleagues[111] who have shown no significant effect on the surface pressure isotherm of DPPC by changing the barrier speed between 3.8 Å^2/molecule·min and 31.6 Å^2/molecule·min.

The experiments with DPPC were performed in two different modes: monolayer collapse and hysteresis experiments. In monolayer collapse experiments, the monolayer was compressed beyond the cross-sectional area of DPPC molecules (39 Å^2/molecule according to Hauser and colleagues[112]). These experiments helped determine the maximum attainable surface pressure (π_{max}), the different phases of the surface pressure isotherm and the area of the monolayer collapse. The hysteresis experiments were performed to study the dynamic behavior of the surfactant monolayer upon multiple compression and expansion.
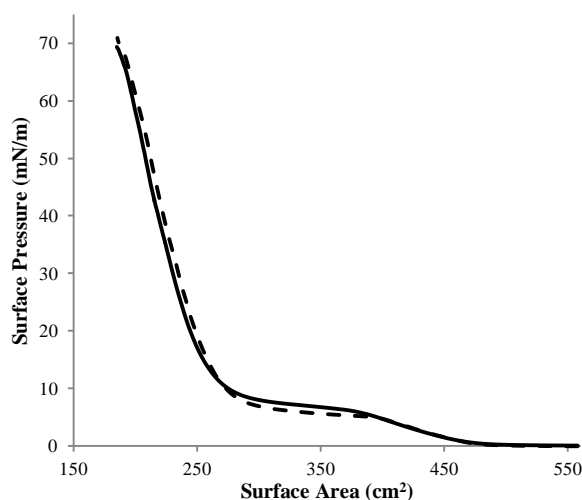
Figure 2-10. Average of three surface pressure vs. surface area isotherm of DPPC at room temperature acquired with compression rates of 10 mm/min (1.5 Å^2/molecule·min) (solid line) and 150 mm/min (22.5 Å^2/molecule·min) (dashed line). Changes in compression speed do not significantly affect the DPPC surface pressure isotherm.

Monolayer collapse experiments were performed with a compression rate of 10 mm/min by compressing DPPC monolayer from an initial trough area of 558 cm^2 (111.5 Å^2/molecule) to a final area of 100 cm^2 (20 Å^2/molecule). This range of mean molecular areas was chosen so that the entire spectrum of surface pressure change from the surface

tension of pure subphase to near zero surface tensions can be observed in one monolayer compression experiment. The majority of studies on DPPC surface pressure isotherm have shown that DPPC monolayers do not affect the surface pressure at room temperature when the area between molecules is above 100 $Å^2$/molecule (i.e. the isotherm is in the gas phase).[32, 36, 90, 111, 113] Also, the maximum surface pressure obtained by DPPC monolayers should theoretically occur at the cross sectional area of DPPC molecules is 39 $Å^2$/molecule[112] although it has been suggested that DPPC molecules should be compressed to 70% of their cross sectional area (27 $Å^2$/molecule) to reach maximum surface pressure.[37] Therefore, a range of 111.5 $Å^2$/molecule to 20 $Å^2$/molecule allowed for observing the complete range of changes in the surface pressure isotherm (Figure 2-11-a). Also, in comparison of the generated isotherm with previous studies only the studies that did not report changes in surface pressure at mean molecular areas of higher than 100 $Å^2$ and had a collapse surface pressure above 27 $Å^2$/molecule were considered. The shape and the phases of the pure DPPC surface pressure isotherm were in good agreement with previously reported results (Figure 2-11-b).[37, 114, 115]

The four different phases of DPPC surface pressure isotherm mentioned in section 2.1.2.1 could be observed in monolayer collapse experiments at room temperature. The gas phase started at from the initial mean molecular area (111.6 $Å^2$) and continued to a mean molecular area of 100 $Å^2$. The LE phase spanned a mean molecular area range from ~100 $Å^2$ to 80 $Å^2$. The LE-LC coexistence phase covered a mean molecular area range of 80 $Å^2$ and 65 $Å^2$ whereas the LC phase occurred at mean molecular areas of less than 65 $Å^2$. Finally, the monolayer collapse was observed at a mean molecular area of 35 ± 0.40 $Å^2$). Interestingly, this value was lower than the limiting area of 39 $Å^2$ reported for DPPC molecules.[112] Collapse mean molecular areas of less than 39 $Å^2$ have been reported commonly and in multiple other studies.[114, 116] This may be caused by the leakage of the monolayer from the edges of the Langmuir trough at very low surface tensions[37] or by the presence of trace amounts of chloroform in the monolayer which would be ejected upon

surface compression and might result in the ejection of some DPPC molecules as well.[117] An alternate explanation is the theory of Wustneck and colleagues[37] suggesting that DPPC monolayers need to be "over-compressed" to reach near zero surface tension values which is supported by the large number of studies that have reported collapse mean molecular areas of less 39 Å^2. If in fact, this phenomenon is caused by monolayer leakage the use of ribbon barriers might be a way to minimize leakage.[118] In cases where Langmuir monolayers in the presence of impurities are studied, leakage and chloroform ejection are likely to be present both in pure DPPC experiments and experiments with impurities and thus are likely to have an insignificant effect on the resulting isotherms.

a)   b)
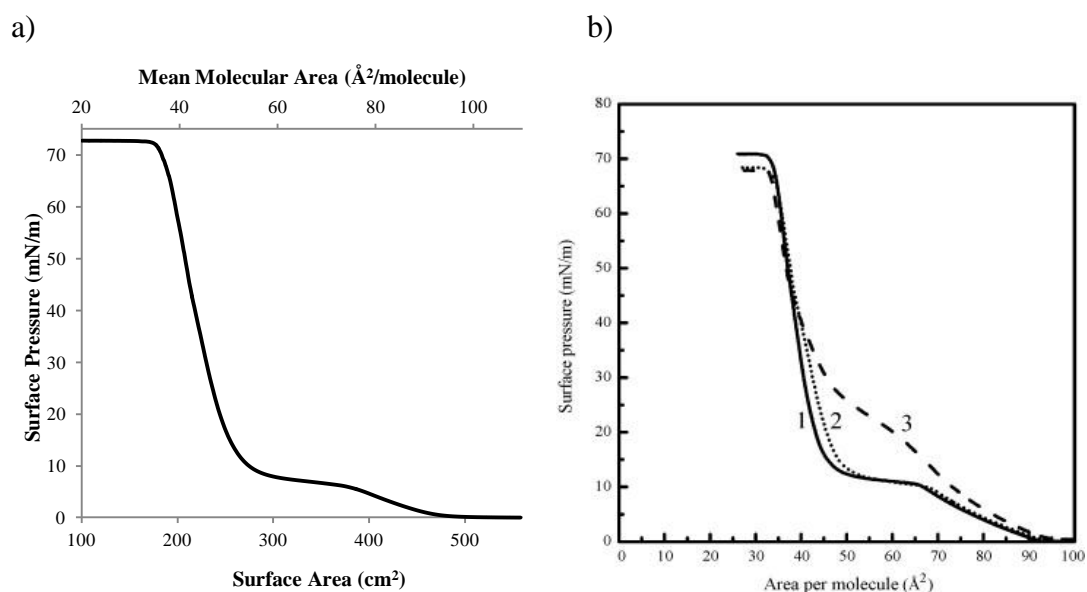
Figure 2-11. Surface pressure vs. surface area isotherm of DPPC at room temperature compressed until 100 cm^2 (20 Å^2/molecule) to achieve monolayer collapse (a) showed a similar shape to those previously reported in literature (b). Literature data reprinted from Hsiao and colleagues[114] with permission. Curve number 1 presents the isotherm for pure DPPC at 25 °C. Curves number 2 and 3 represent the DPPC surface pressure isotherm after the addition of HAuCl$_4$ ions to the subphase.

Since each surface pressure isotherm at low speed consists of more than 1700 data points, showing standard deviations on each data point is not practical and is not common practice. To provide an estimate for the reproducibility of these experiments, six independent surface pressure isotherms performed at 10 mm/min are overlayed in Figure 2-12. Comparison of the overlaid surface pressure isotherms shows that the obtained isotherms are very reproducible. The average and standard deviations for surface pressures at fixed mean molecular areas for the experiments plotted in Figure 2-12 are presented in Table 2-1, the low standard deviations of surface pressures at fixed mean molecular areas confirm the reproducibility of the surface pressure isotherms.
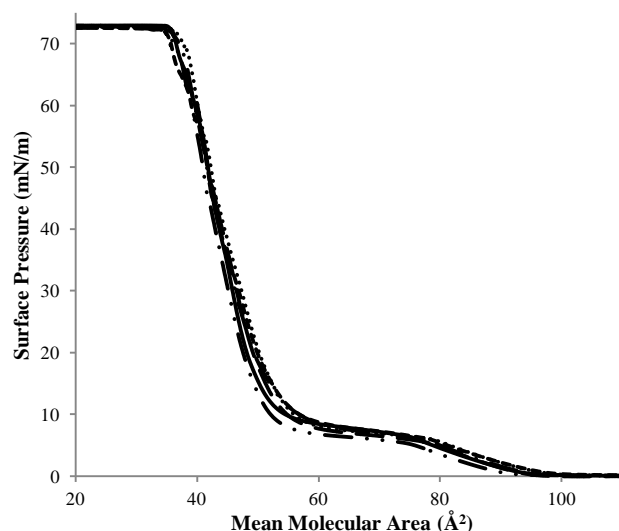
Figure 2-12. An overlay of the surface pressure vs. surface area isotherms of DPPC from six independent monolayer collapse experiments conducted at room temperature with a compression speed of 10 mm/min.

The compression modulus of the DPPC monolayers was compared to previously reported values in the literature to further ensure the similarity of the isotherms generated in this study compared to those in literature. The plots of compression modulus vs. mean molecular area of DPPC monolayers were biphasic with two maxima at mean molecular

Table 2-1. Average and standard deviations of surface pressure at fixed mean molecular
areas for DPPC monolayer collapse studies plotted in Figure 2-12.

Mean Molecular Area (Å^2)	Average Surface Pressure (mN/m)	Standard Deviation
110	0.0	0.0
100	0.1	0.1
90	1.5	0.6
80	4.8	0.7
70	6.8	0.5
60	8.0	0.7
50	17.5	2.8
40	58.1	2.0
30	72.6	0.2
20	72.7	0.1

areas of 87.3 ± 4.2 Å^2 (437 ± 21 cm^2) and 40.7 ± 0.8 Å^2 (214 ± 4 cm^2) referring to the LE

and the LC phase (Figure 2-13-a) relating to the maximum elasticity of the monolayer in

each phase. The shapes of these plots were in good agreement with those previously

reported in the literature[101] (Figure 2-13-b). Interestingly, there has been no consensus on

the maximum value of compression modulus in the literature. The maximum value of

compression modulus in this study was 239.6 ± 39.1 mN/m which was in reasonable

agreement with the previously reported values of ~260 mN/m and 269.6 ± 20 mN/m.[80, 101]

Higher values of 281 mN/m[99] and ~290 mN/m[60] have also been reported; however, these

studies did not report the error in their measurements making it difficult to compare their

values with those obtained in this study. The maximum compression modulus values tend

to have high standard deviations as they occur in the LC region of the isotherm where a

sharp increase in the slope of the surface pressure isotherm is observed. A small shift in

the slope of the isotherm can cause large deviations in compression modulus, this may

explain the wide range of maximum compression modulus values reported to date. The

average and standard deviations for compression moduli at fixed mean molecular areas

for the experiments presented in Figure 2-13-a are presented in Table 2-2. While large

values of standard deviation are observed in the LC phase (mean molecular areas of 50

Å^2 and 40 Å^2) the other standard deviation values are lower than 10 mN/m. The

comparisons of phase behavior, surface pressure at collapse, the mean molecular area of

monolayer collapse and the compression modulus ensured the similarity of the isotherms

generated in this study with those in the literature during monolayer collapse experiments

during one compression cycle.

a)   b)
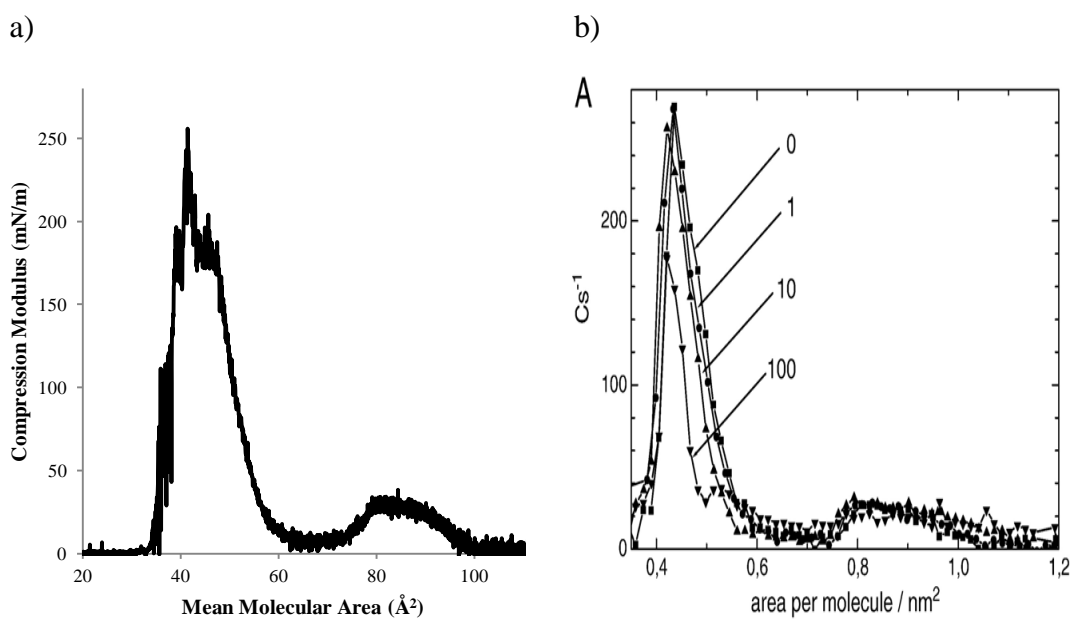
Figure 2-13. Compression modulus vs. mean molecular area of DPPC obtained in this
study (a) were biphasic with two maxima at mean molecular areas of 87.3 ±
4.2 Å^2 and 40.7 ± 0.8 Å^2. These results were in good agreement with those
reported in the literature (b). Literature data from Jablonowska and
colleagues[70] reprinted with permission. The plot labeled as zero represents the
compression modulus for pure DPPC monolayers, other plots represent the
compression moduli of DPPC monolayers exposed to various concentrations
of ibuprofen.

Table 2-2. The average and standard deviations of compression moduli at fixed mean
molecular areas in DPPC monolayer collapse experiments presented in Figure
2-13-a.

Surface Area (cm^2)	Average Compression Modulus (mN/m)	Standard Deviation
110	2.0	5.6
100	3.4	9.6
90	22.3	6.0
80	26.4	7.8
70	9.6	3.2
60	14.1	5.0
50	115.7	19.4
40	182.0	57.9
30	-0.1	2.3
20	-0.4	2.0

2.3.2 Hysteresis Experiments on DPPC Monolayers and

Comparison to Literature

Dynamic behavior of the surfactant was studied by compressing DPPC
monolayers to 200 cm^2 and back to 558 cm^2 for three cycles with a barrier speed of 10
mm/min. The target surface area of 200 cm^2 (40 $Å^2$) was chosen to be above the limiting
mean molecular area of DPPC molecules so that monolayer collapse did not occur.
Hysteresis experiments resulted in a similar isotherm to monolayer collapse experiments
(Figure 2-14). However, the surface pressure of the isotherm was generally lower in the
second and third compression cycle compared to the first. This was due to ejection of
some DPPC molecules from the air-water interface at the end of each cycle likely due to
surfactant leakage[21] or ejection of trace amounts of solvent from the monolayer as
mentioned above.[68] The isotherms generated in this study closely matched those reported
by Notter and colleagues both in terms of the shape of the isotherms and surface pressure

values during surface expansion.[60] Similar to the monolayer collapse experiments an
overlay of seven independent hysteresis experiments are presented in Figure 2-15 to
provide an estimate for the reproducibility of these experiments. Although variations in
the hysteresis curves were observed, all curves show similar trends with the deviations
being about 15% of the average.
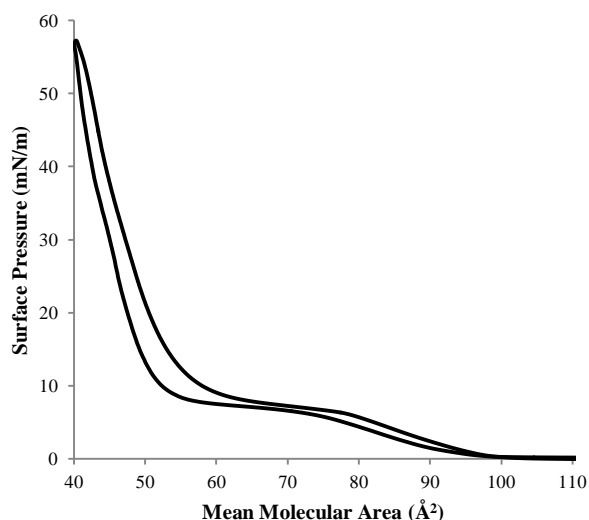
Figure 2-14. Surface pressure vs. mean molecular area of DPPC monolayer obtained after
one compression and expansion cycle between surface areas of 558 cm^2 and
200 cm^2 at room temperature.

A hysteresis area of 750.2 ± 118.7 mN/m•cm^2 was observed at the end of the first
compression-expansion cycle. This area decreased to 539.8 ± 195.8 mN/m•cm^2 and
remained almost the same at 543.2 ± 214.8 mN/m•cm^2 in the third cycle. As mentioned
above, this hysteresis is dependent on the kinetics of the readsorption of ejected DPPC
molecules to the air-water interface. DPPC forms a crystalline surface at the end of
compression which does not allow for fast readsorption of ejected molecules resulting in
hysteresis areas and maximum surface pressure values as the cycles continue.

It should be noted that the high standard deviations in the hysteresis area were mainly caused by changes in the Wilhelmy plate. It was observed that when the plates
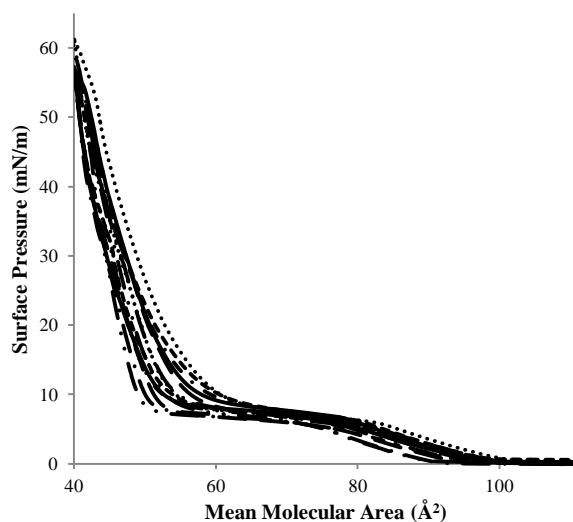
Figure 2-15. An overlay of seven independent DPPC surface pressure isotherms after one compression and expansion cycle performed at room temperature with a compression rate of 10 mm/min.

were used for about 8 months, a larger reduction in hysteresis areas, especially those of the second and third cycles, could be observed. This was likely due to sticking of some lipids to the plate at the end of the compression cycles which affected the surface pressure during surface expansion and reduced the generated hysteresis area. Coating the plate with carbon when cleaning with flame could be another source of this inaccuracy but was unlikely to be the case here. Coating should be at least partially solved by soaking the plate in acid; however, in this case cleaning the plate in acid bath only aggravated the problem. When these reductions in hysteresis area were observed, a new Wilhelmy plate was used which eliminated the problem. The controls shown in Figure 2-15 have been performed over a period of a few months and show this variation in hysteresis areas.

2.3.3 Effects of Temperature on DPPC Surface Pressure

Isotherm

The surface pressure isotherm of DPPC at physiological temperature (37°C) was studied and the surface pressure isotherms were found to be temperature-dependent. DPPC surface pressure isotherms generated at 37°C showed a good agreement with the previously published isotherms[119] (Figure 2-16). The surface pressure isotherm at 37°C showed higher surface pressure values in the LE-LC region compared to the isotherm at room temperature. A higher surface pressure of about 10 mN/m could be observed between the mean molecular areas of 70 $Å^2$/molecule and 60 $Å^2$/molecule. DPPC surface pressure isotherm at 37°C also had a reduced maximum surface pressure of 68.8 $\pm$ 2.0 mN/m compared to the isotherm obtained at room temperature (72.7 $\pm$ 0.1 mN/m). The reduction in the maximum surface pressure is due to the reduction in surface pressure of pure subphase at 37°C. The effect of temperature on the surface pressure of the LE-LC region is likely due to delayed formation of crystalline phases at higher temperatures which results in a linear increase (characteristic of liquid-expanded phase) until about 30 mN/m.

At 37°C, changes in surface compression rate had a significant effect on the surface pressure of monolayer collapse in contrast to the observations at room temperature. At the fast compression speed of 150 mm/min (22.5 $Å^2$/molecule.min) monolayer collapse occurred at a surface pressure of 69.2 $\pm$ 0.9 mN/m, whereas at the low barrier speed of 10 mm/min (1.5 $Å^2$/molecule.min) the monolayer collapse plateau was observed at surface pressure values below 55 mN/m (Figure 17). The lowest compression speed at which a collapse surface pressure comparable to that 150 mm/min could be achieved was 46 mm/min (6.9 $Å^2$/molecule.min). This effect is an indication that at 37°C the organization of DPPC molecules at the interface is dependent on compression speed. To the best of our knowledge, this effect of barrier speed on the surface pressure isotherm of DPPC at 37°C has not been reported.

(a)

(b)
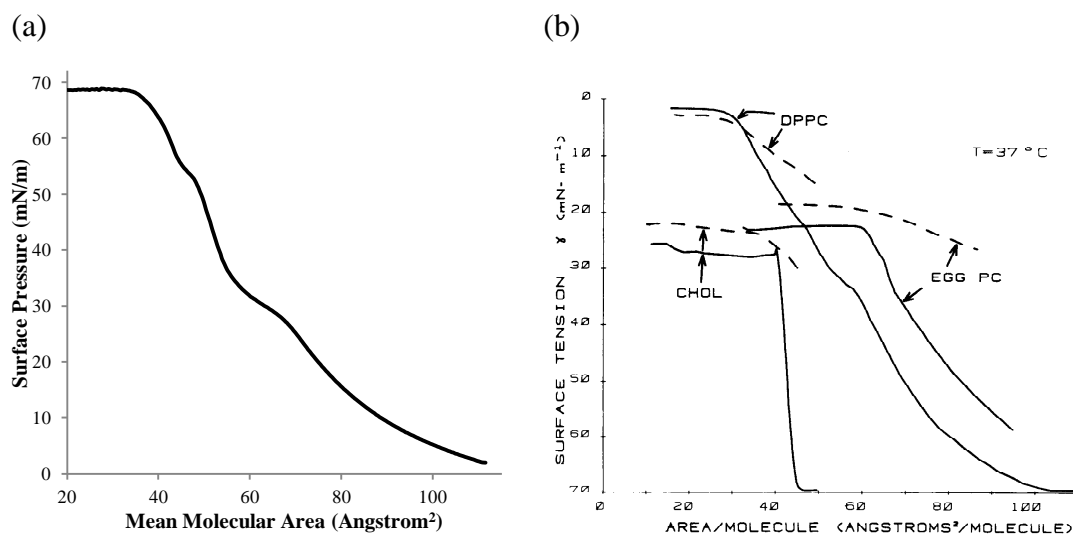
Figure 2-16. Surface pressure vs. mean molecular area isotherm of DPPC at 37°C after compression from mean molecular area of 111.6 Å^2 to of 20 Å^2. The generated isotherm was in good agreement with literature data for DPPC from Hildebran and colleagues[119] (in surface tension). Solid lines in (b) denote surface tension isotherms whereas dashed lines show the surface potential curves. Chol stands for cholesterol and PC stands for phosphatidylcholine. Figure reprinted with permission.
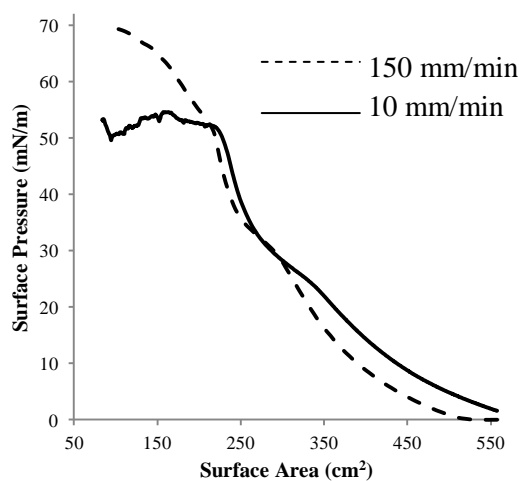
Figure 2-17. Changes in compression rate changed the maximum achievable surface pressure at 37°C. A low compression rate of 10 mm/min (solid line) resulted in monolayer collapse at surface pressure values below 55 mN/m (a), whereas a barrier speed of 150 mm/min (dashed line) resulted in monolayer collapse surface pressure of 69.2 ± 0.9 mN/m.

2.3.4 Studies of Infasurf and Comparison to Literature

DPPC serves as a simplistic model of pulmonary surfactant. However, a surfactant model consisting of just one molecule cannot completely mimic the complex behavior of lung surfactant. Thus, Infasurf was used as a more realistic model of the pulmonary surfactant. Unlike DPPC, only a few published reports exist on the surface pressure isotherm of Infasurf with most of them being very recent.[44, 46, 47, 86, 87]

First attempts in generating surface pressure isotherms of Infasurf were focused on reproducing the data reported in the literature. To avoid potential complications from the differences in compression speed, attempts were made to keep the barrier consistent with those in the reported studies. Since the trough surface areas were different, the division of barrier speed over trough area was used to provide a benchmark for barrier speed. This value was kept constant at 0.08/min for three studies of the available studies.[44, 46, 47, 86, 87] This value is equivalent to a barrier speed of 60 mm/min on the
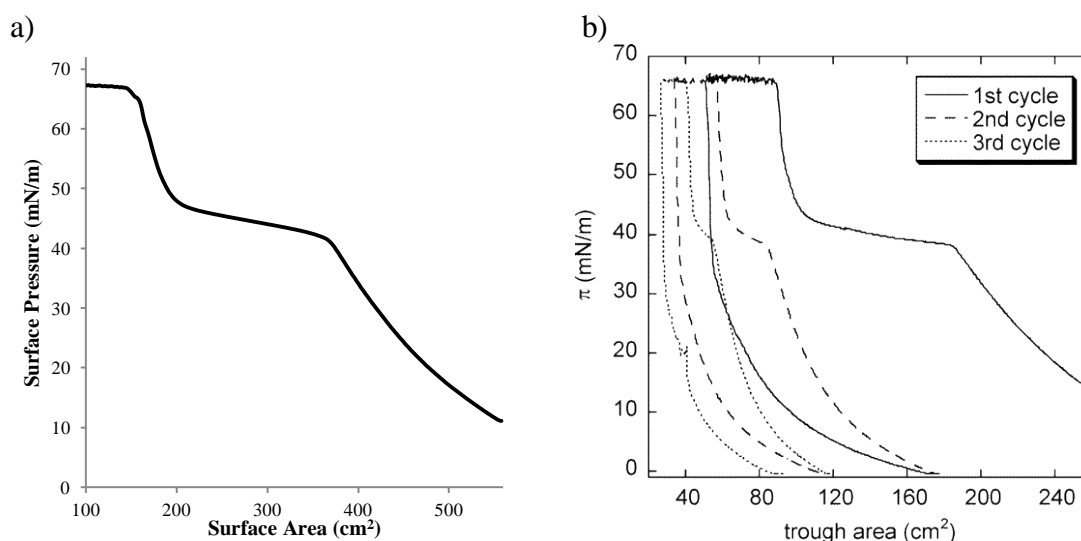
Figure 2-18. The surface pressure vs. surface area isotherm of Infasurf generated with a barrier speed of 60 mm/min at room temperature (a) was in good agreement with the previously reported results reported by Alonso and colleagues[86] (b). Figure reprinted with permission.

 Langmuir trough used in this study and was used for the initial experiments. The surface

pressure isotherms of Infasurf generated using this barrier speed were in good agreement

with those previously reported in the literature (Figure 2-18).

Table 2-3. A comparison between the surface pressure-surface area isotherm of Infasurf
films generated in this study and previous reports in the literature, the surface
pressure at the start of film collapse ($\pi_{collapse}$) and plateau ($\pi_{plateau}$) closely
matched those reported previous studies.

Study	$\pi_{collapse}$ (mN/m)	$\pi_{plateau}$ (mN/m)	Barrier Speed (cm^2/min)/Trough area (cm^2)
Alonso et al.[86]	68	~40	Not mentioned
Wang et al.[87]	~70	~42	0.08/min
Zhang et al.[47]	~70	~42	0.08/min
Fan et al.[44]	~70	~42	0.08/min
This Study	67.6 ± 0.5	40.6 ± 0.3	0.08/min

As demonstrated in Figure 2-18, the surface pressure isotherm for Infasurf is

similar to the isotherms previously reported in the literature and the same features such a

long plateau at about 40 mN/m and a monolayer collapse surface pressure approximately

at 68 mN/m can be observed. In comparing the graphs in Figure 2-18 it should be noted

that the difference in trough surface areas between the studies has resulted in difference

in x-axes. However, the percent of area reduction required to reach the collapse surface

pressure from an initial surface pressure of ~14 mN/m was about 70% in both studies

confirming that the surface pressure isotherm of Infasurf was similar between the studies.

To ensure the accuracy of the generated results, Infasurf surface pressure isotherm

obtained in this study was compared to isotherms reported in previous studies in terms of

the maximum surface pressure and surface pressure of plateau (Table 2-3). The results in Table 2-3 further confirm that the Infasurf surface pressure isotherms are similar to those previously reported in the literature as the surface pressure values matched those of the previous studies. The slight changes between various studies can be a result of different batches of Infasurf and different barrier speeds. Since a compression speed of 10 mm/min was used for DPPC surface pressure isotherms, it was desirable to use the same compression speed for Infasurf studies as well. Thus, the effect of a lower compression speed on the surface pressure isotherm of Infasurf was also examined and was shown to have little effect on the surface pressure isotherm of Infasurf. An overlay of three Infasurf experiments at a barrier speed of 10 mm/min is presented in Figure 2-19 and confirming that the isotherms showed very good reproducibility. The values for average and standard deviations of surface pressure at fixed surface areas in the surface pressure isotherms plotted in Figure 2-18 are presented in Table 2-4. The low standard deviations in surface pressure further confirm the reproducibility of the Infasurf surface pressure isotherm.
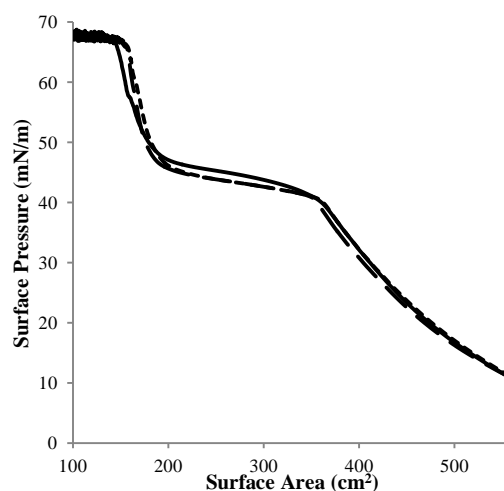
Figure 2-19. An overlay of three surface pressure isotherms of Infasurf at low compression speed (10 mm/min). All the isotherms had similar shapes and showed good reproducibility.

Although the surface pressure isotherm of Infasurf was almost similar at 10 mm/min and 60 mm/min, the barrier speed affected the shape of the isotherm when increased significantly. When the surface was compressed with a barrier speed of 150 mm/min, the isotherm showed higher surface pressure values compared to the isotherm

Table 2-4. The average and standard deviations of surface pressure at fixed surface areas in Infasurf surface pressure isotherms presented in Figure 2-19.

Surface Area (cm^2)	Average Surface Pressure (mN/m)	Standard Deviation
550	11.7	0.2
500	16.6	0.4
450	23.2	0.6
400	31.7	0.8
350	41.0	0.1
300	43.0	0.6
250	44.3	0.8
200	46.3	0.7
150	65.9	1.9
100	68.1	0.3

with a barrier speed of 10 mm/min (Figure 2-20). Also, the sharp monolayer collapse point observed at 10 mm/min was replaced with a more gradual collapse at 150 mm/min. This latter effect might be an artifact of the data collection speed. The software records surface pressure data each second and at a barrier speed of 150 mm/min the rate of changes in surface pressure might be faster than the rate of data collection. The few published studies on the surface pressure isotherm of Infasurf have not examined the effect of the changes in barrier speed on the shape of the surface pressure isotherm. This

phenomenon merits further investigation and can help clarify the *in vivo* behavior of the pulmonary surfactant.
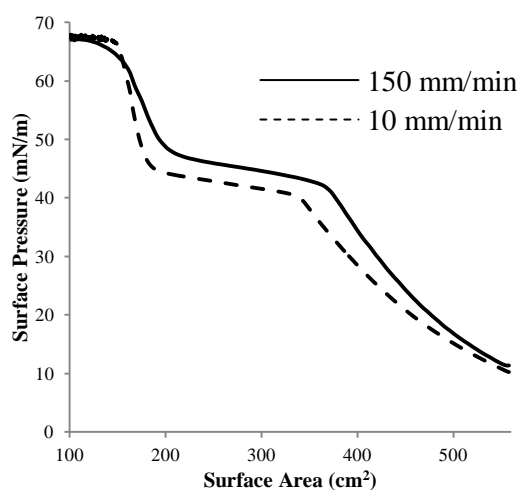
Figure 2-20. Infasurf surface pressure isotherm presented with a barrier speed of 150 mm/min (solid line) showed higher surface pressure values compared to the isotherm at generated with a barrier speed of 10 mm/min (dashed line).

It should be noted that although it was possible to reproduce literature results for Infasurf isotherms, a large variability in the isotherms was observed by changing the batches of Infasurf vials. The data presented in Figures 2-16 and 2-17 were generated using the lot number (89512070). Using a different lot (74209265) resulted in surface pressure isotherms that looked slightly different (Figure 2-21). As shown in Figure 2-21, the use of a different lot number resulted in an unstable collapse surface pressure and a longer plateau region compared to the previous lot. Considering that Infasurf is extracted from bovine lung lavage such differences between different lots can be expected. However, one should keep in mind such differences when comparing Infasurf isotherms between different studies.
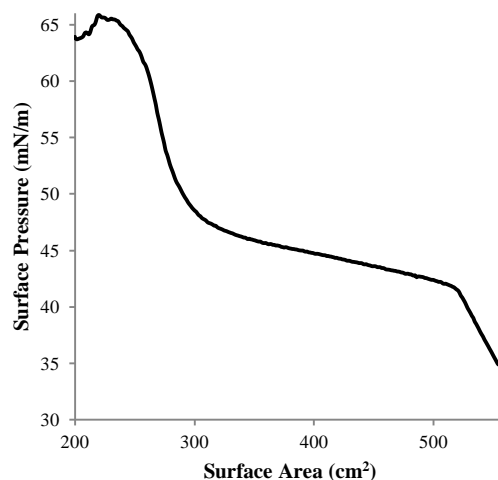
Figure 2-21. A representative surface pressure isotherm generated with Infasurf (lot 74209265). The isotherm is distinctly different from the isotherm generated from lot 89512070 (Figure 2-19).

2.3.5 The Origins and Importance of Hysteresis Area in
The Lungs and The Role of The Pulmonary Surfactant

As discussed in Section 2.1.2.3, a number of metrics have been used to assess the functionality of amphiphilic monolayer and pulmonary surfactant models. However, the importance of hysteresis area has been mostly overlooked in *in vitro* evaluations of surfactant behavior. Monolayers of DPPC, Infasurf and other pulmonary surfactant models increase the surface pressure more rapidly upon compression than expansion. This path-dependence leads to significant hysteresis in each compression and expansion cycle. Surfactant compression and expansion occurs in each breathing cycle; thus, it is important to study surfactant hysteresis alongside other measures of surfactant functionality to give a complete view of the dynamic surfactant behavior.

When the transpulmonary pressure (air pressure in alveoli subtracted by air pressure in the pleural cavity) vs. volume graphs of the lungs of animals and humans are plotted during normal breathing cycles, a hysteretic behavior similar to that of the pulmonary surfactant is observed.[120, 121] However, the exact role of the pulmonary

surfactant in lung hysteresis is not very well understood. In this section, the origins of lung hysteresis, the use of hysteresis area as a measure of surfactant functionality, the effect of surfactant components and the role of hysteresis in lung function will be discussed and DPPC and Infasurf will be compared in terms of their hysteresis behavior.

<u>2.3.5.1 The Origins of Lung Hysteresis</u>

To study lung hysteresis one needs to have a good understanding of the mechanism of breathing. Inspiration requires an increase in transpulmonary pressure which is produced by contraction of diaphragm or expansion of chest wall. These moves create a negative interpleural pressure. Since the pressure of alveoli is equal to atmospheric pressure, a negative interpleural pressure causes passive enlargement of alveoli and the entrance of air. During exhalation the chest or the diaphragm relaxes, lowering the transpulmonary pressure and causing the compression of alveoli and passive exit of air from the alveoli. Interestingly, during this process a lower transpulmonary pressure is needed to maintain a certain lung volume during expiration compared to inspiration causing a significant hysteresis to show in P-V curves of the lungs (Figure 2-22). In other words, a higher amount of energy is needed to expand the lung than it is needed to compress it. Three main sources cause this energy dissipation in the lungs: 1. lung tissue inelasticity, 2. alveolar recruitment and derecruitment in each respiratory cycle and 3. the pulmonary surfactant, each of these will be discussed in more detail.

Lung tissue inelasticity is a minor contributor to lung hysteresis. Parenchymal connective tissue of the lung is made of a network of collagen and elastin.[61-63] Unlike single fibers, these networks are not perfectly elastic. During breathing cycles, fibers undergo extension and show hysteretic behavior as fibers reorient, stretch and slip over other fibers (a feature named as "nylon stocking" extensibility). [64, 65] This phenomenon contributes to the total hysteresis of the lung. If the connective tissue was a perfectly elastic body, no work of hysteresis would be observed.
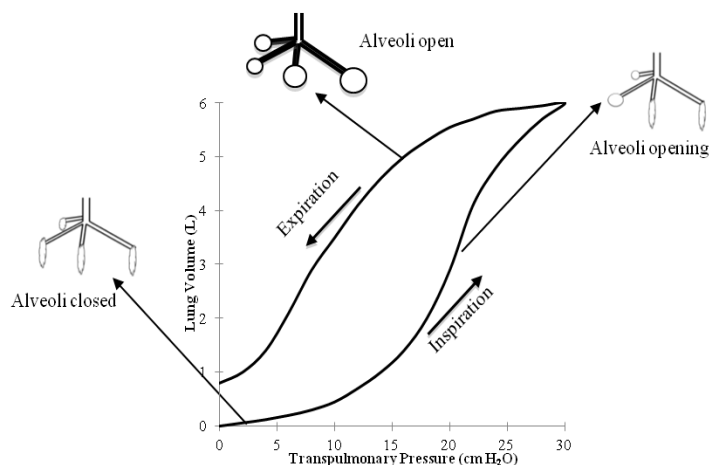
Figure 2-22. The resulting P-V curves during inspiration and expiration are not the same and a hysteresis is observed. The schematics show opening and closure of alveoli during breathing cycles as suggested by Frazer and colleagues.[60]

Recruitment and derecruitment of alveoli in each breathing cycle also contributes to lung hysteresis. Previous studies have shown that changes in alveolar surface area is a function of volume to the power of two third at volumes above 50% of total lung capacity (TLC)[66] and a function of volume to the power of one at less than 50% of TLC [67] leading to the conclusion that alveoli do not expand uniformly at low lung volumes. Gil and Weibel [67] showed the presence of many collapsed alveoli at low lung volumes and proposed that a large number of alveolar sacs are closed upon expiration (derecruitment) and opened again during inspiration (recruitment). Based on these studies, Frazer et al.[60] proposed a model to explain the alveolar recruitment during breathing cycles (Figure 2-22). Based on this model, the alveoli remain open during expiration and start getting closed at a transpulmonary pressure of 4 cm H_2O. Significant pressure is then needed to reopen these closed alveoli. As a result, if the lungs are inflated and deflated above 4 cm H_2O lower hysteresis will be observed. However, if lungs are inflated from lower transpulmonary pressures, an additional energy is needed to open the closed alveoli

resulting in higher hysteresis. This has been proved by experiments on the lungs of dogs[122] and lambs.[69]

Mead and colleagues[121] were the first group to show that the pulmonary surfactant is the main contributor to the lung hysteresis. In their study on the excised dog lungs a significantly lower hysteresis area was observed with saline-filled lungs (i.e. air-liquid interface eliminated) compared to the lungs filled with air (Figure 2-23). Filling the lungs with saline will not affect lung elastic properties or alveolar recruitment, but will eliminate the air liquid interface. This comparison demonstrated that the hysteresis caused by the pulmonary surfactant accounts for most of the hysteresis in the lung. These results were confirmed by the same method for human,[56] rat,[56] cat[123] and rabbit lungs.[124]
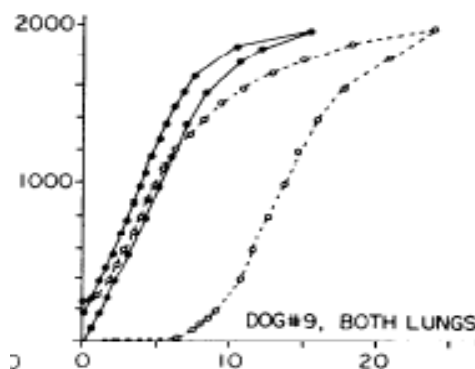
Figure 2-23. Saline filled dog lungs (curve on the left) show remarkably lower hysteresis compared to normal lungs. Figure from Mead and colleagues reprinted with permission.[121]

The role of pulmonary surfactant in lung hysteresis becomes clearer considering that surfactant films show considerable hysteresis when compressed and expanded *in vitro* (Figure 2-14). The extent of this hysteresis is related to the maximum surface pressure to which a surfactant is compressed. At 37°C, pure DPPC monolayers showed very little hysteresis when compressed to low (~10 mN/m) surface pressure values

(Figure 2-24-a). However, when compressed to surface pressures close to monolayer collapse a remarkable hysteresis was observed (Figure 2-24-b). This hysteresis can be quantified using normalized hysteresis area (i.e. hysteresis area divided by the change in mean molecular area). As mentioned in the discussion of surfactant phases, compression changes the structure of surfactant to a crystalline state and might result in the collapse of the monolayer and squeeze out of molecules to the subphase. Readsorption of the squeezed out molecules after surface area expansion is a timely diffusion process. Therefore, the start of expansion is accompanied by a sharp reduction in surface pressure and a large hysteresis area between compression and expansion.
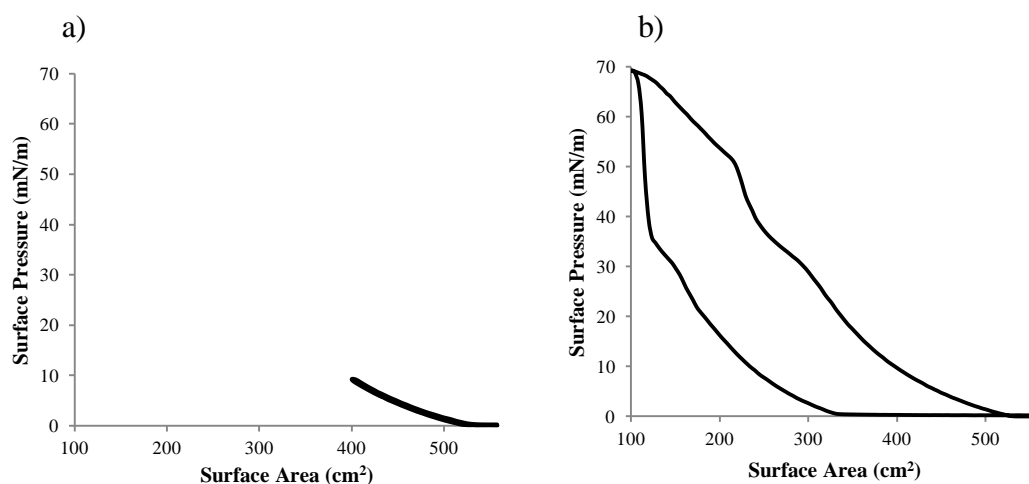
Figure 2-24. Hysteresis area of DPPC monolayers is dependent on the surface pressure to which the monolayer is compressed, (a) at low surface pressure values (~10 mN/m) DPPC monolayers generate low hysteresis (normalized hysteresis area= -0.4 ± 0.1 mN/m), (b) same monolayers generate large hysteresis when compressed to high (~70 mN/m) surface pressure values (normalized hysteresis area= 17.5 ± 0.1 mN/m).

2.3.5.2 Physiological Significance of Hysteresis

Although the first studies on lung hysteresis and the role of pulmonary surfactant were published in 1950s, the potential physiological significance of hysteresis is still not

very well understood. However, some evidence about the importance of hysteresis in normal lung function is provided by the study of Pison and colleagues.[104] Comparing the hysteresis in the films of the bronchoalveolar lavage of patients diagnosed with adult respiratory distress syndrome (ARDS) and normal adults, it was observed that the bronchoalveolar lavage of ARDS patients show a significantly lower hysteresis area compared to healthy adults. There was also a direct relationship between the reduction in hysteresis area and the severity of ARDS in those patients. Interestingly, the same samples did not show a significant difference in their surface tension values, leading to the conclusion that hysteresis area in itself is important for normal lung function. Clements and colleagues[56] provided further evidence about the importance of hysteresis for lung function. Comparing surfactant functionality between premature infants and normal adults, they reported that extracts from the lungs of infants who suffered respiratory distress showed much lower hysteresis compared to normal adults.

The examples mentioned above show the importance of hysteresis for the normal function of the lung. Notter et al.[125] have proposed a model to explain the role of hysteresis in lung function. According to this model hysteresis plays an important role in the expansion of new alveoli at the end of expiration. The surface tension of alveoli is at a minimum at the end of expiration. However, the presence of hysteresis means that this surface tension increases rapidly in a very short time at the start of inspiration. According to Laplace law, assuming the alveoli are spherical, the pressure in an alveolus is linearly related to its surface tension and inversely related to its diameter. Thus, the abrupt increase in the surface tension of alveoli results in a larger energy barrier to further open an already expanded alveolus. As a result, unexpanded or smaller alveoli with lower surface tension values can be opened with the same energy and become part of the active surface area of the lung (recruitment). Notter and colleagues[125] suggest that these alveoli could have been left unexpanded if it was not for the sharp increase in surface tension

which leads to a large hysteresis area. It should be noted that this idea of alveolar recruitment is in agreement with the model proposed by Frazer et al.[126] mentioned earlier.

Based on their model, Notter and colleagues[125] defined a new variable to quantify the effect of hysteresis on the expansion of new alveoli. This variable known as the Recruitment Index (RI) was defined as:

$$RI = \frac{\gamma_{min} + (\Delta\gamma)_{IE}}{\gamma_{min}} \tag{2-5}$$

where $(\Delta\gamma)_{IE}$ is the increase in surface tension (drop in surface pressure) following the initial expansion of surface area where there is a significant drop in surface pressure (e.g. surface areas between 100 and 125 cm^2 in Figure 24-b). Notter et al.[125] used the first 10% to 20% of surface area upon expansion to determine the changes in surface tension for calculation of $(\Delta\gamma)_{IE}$. A high RI for an alveolus means that its surface tension increases rapidly with a very small change in alveolar surface area, a high transpulmonary pressure is needed to further inflate this alveoli and it will be energetically more favorable to expand new alveoli. In other words, higher RI means more stability for the lung as more alveoli are expanded. Based on the data of Clements an colleagues[56] a RI of 6.5 was calculated for normal adult and a RI of 1.2 for premature infants. According to LaPlace law, with an RI of 6.5 alveoli that have the same surface tension as γ_{min} but their radii is 6.5 times lower than the radius of the already expanded alveoli can be expanded with the same transpulmonary pressure. The radius range of this newly expanded alveoli is only 1.2 for premature infants causing a non-uniform expansion in their lungs. In using RI for making comparisons between infants and adults lungs, one should consider that infants have a much faster breathing rate compared to adults and might not compress their alveoli to the same level as adults.[127]

2.3.5.3 The Effect of Surfactant Components on Hysteresis

For proper lung function, the pulmonary surfactant should retain functionality over an extended period of time. Although surfactant components are replenished over time, the estimated turnover time for different surfactant components are between 4 to 11 hours.[128] Thus, a functional surfactant should maintain a large hysteresis and RI over many cycles. Also, the cycling in the lung is very fast with each breathing cycle taking about 4 seconds, providing little time for the ejected surfactant molecules to adsorb to the air-water interface. Since DPPC is generally used as a simple pulmonary surfactant model, its ability to maintain a large and reproducible hysteresis over time was investigated by fast cycling (150 mm/min) for 10 cycles at 37°C (Figure 2-25).
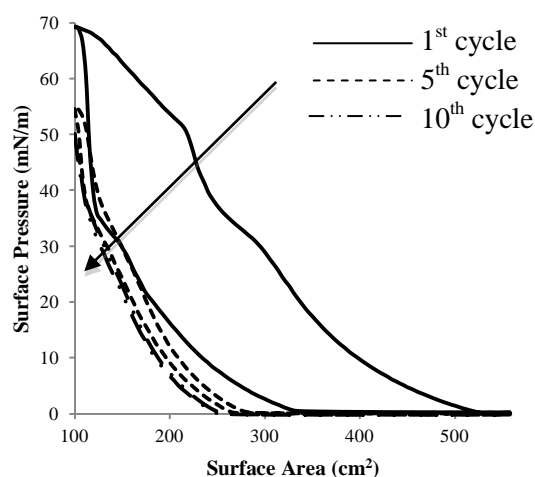
Figure 2-25. Films of pure DPPC show a reduction in hysteresis area and increment in maximum surface pressure when compressed and expanded for multiple cycles with a fast cycling rate (150 mm/min). Arrow shows the direction of cycling.

Fast cycling of DPPC monolayers soon led to a decrease in hysteresis area and RI and an increase in γ_{min}, all of which are signs of surfactant dysfunction (Table 2-5). An irreversible loss of DPPC molecules to the subphase was observed as confirmed by the

increase of γ_{min} from 69.2 ± 0.8 mN/m in the first cycle to 51.5 ± 1.9 mN/m in the 10th cycle. Normalized hysteresis area and RI were also reduced from 17.5 ± 0.1 mN/m and 9.7 ± 4.4 in the first cycle to 0.3 ± 0.1 mN/m and 3.8 ± 0.1 in the 10th cycle.

The results in Figure 2-25 and Table 2-5 prove that DPPC by itself is not a complete model for mimicking the pulmonary surfactant. This is not a surprising as the pulmonary surfactant is known to be composed of many other lipids and proteins.[17, 18] However, this puts forth a challenging question: what is the role of other lipids and proteins of a functional pulmonary surfactant in maintaining hysteresis and γ_{min}? A number of studies have tried to answer this question by examining binary and tertiary mixtures of DPPC and other surfactant components. A brief summary of the binary and tertiary studies with DPPC and cholesterol and DPPC and surfactant proteins is given below. These components are the most extensively studied species in combination with DPPC and are both present in Infasurf, another surfactant model used in this study.

Table 2-5. Fast cycling of pure DPPC films between surface areas of 558 cm^2 and 100 cm^2 at 37 °C for 10 cycles resulted in a reduction in hysteresis area and RI and an increase in the maximum surface pressure.

# Cycle	γ_{min} (mN/m)	HA$_n$ (mN/m)	RI
1st Cycle	69.2 ± 0.8	17.5 ± 0.1	9.7 ± 4.4
5th Cycle	56.1 ± 2.3	1.6 ± 0.1	4.1 ± 0.1
10th Cycle	51.5 ± 1.9	0.3 ± 0.1	3.8 ± 0.1

2.3.5.3.1 Binary studies of DPPC and Cholesterol

Cholesterol makes up about 90% of neutral lipids of the pulmonary surfactant[17, 18] and is the most widely studied molecule in binary studies with DPPC. It has been reported in multiple studies that cholesterol improves the respreadability of DPPC films as defined by maintaining a large hysteresis and a low surface tension. Studies on binary mixtures of cholesterol and DPPC at room[129] and body temperature[97] have reported that DPPC films show higher respreadability when mixed with cholesterol. Pure cholesterol films show complete respreadability and maintain the same hysteresis area after several cycles even when compressed past collapse[97] Thus, collapse seems to be a reversible process in the presence of cholesterol unlike pure DPPC films where it is an irreversible process.[129]

The ability of cholesterol to provide consistent hysteresis is likely due to its effect on surface fluidity. Cholesterol has been shown to increase the mean molecular area of DPPC and increase surface fluidity in DPPC monolayers compressed to low surface tensions.[78] Fluidity of DPPC and other lipids in the presence of cholesterol has been confirmed using differential scanning calorimetry to study the effect of cholesterol on chain melting temperature (T_m) of DPPC. Above T_m, molecules change from ordered crystalline phase to the liquid crystalline phase.[130] Ladbrooke et al.[131] reported that addition of 20% mole of cholesterol in mixtures of DPPC, cholesterol and water significantly reduces the T_m of DPPC and the heat flow needed for melting, resulting in a more fluid surface. These results were later confirmed in several other studies.[129, 132, 133] Respreadibility of highly compressed films is dependent on the kinetics of surface adsorption of molecules that have been ejected to the subphase with faster adsorption resulting in higher respreadability. A fluidized surface provides less resistance for molecules to readsorb compared to a crystalline surface. As a result, fewer molecules are left in the subphase after each cycle improving surfactant respreadability.

The effect of cholesterol on improved surface fluidity comes at the expense of increased minimum surface tension. Cholesterol molecules cannot be squeezed out from the mixed monolayer at the end of compression resulting in a minimum surface tension between that of pure DPPC and pure cholesterol.[134, 135] This effect has been reported even at physiological concentrations of cholesterol.[40, 135-137] As a result, cholesterol is currently not being used in synthetic clinical pulmonary surfactants such as Survanta[85] and BLES[138] although physiological amounts of cholesterol (5% to 10% of phospholipids by mass) do not affect the γ_{min} of BLES.[138, 139] However, cholesterol is found in Infasurf[140] meaning that it is present in normal calf lungs. These results imply that more studies are still needed to determine whether cholesterol is needed in clinical pulmonary surfactants.

2.3.5.3.2 Binary studies of DPPC and Surfactant Proteins

It has been shown that the presence of these proteins results in more reproducible hysteresis cycles and helps with maintaining a low surface tension beyond the first compression cycle. Taneva and colleagues[141] reported that addition of less than 10% (by weight) of SP-B and SP-C significantly increased the hysteresis area of DPPC and increased the number of DPPC molecules remaining on the surface after the first cycle. Reproducible hysteresis after the addition of surfactant proteins has also been reported with mixed monolayer of DPPC and other lipids.[142]

The dominant mechanism for the improved respreadability and hysteresis induced by surfactant proteins is likely specific interaction between the palmitate groups of proteins with the acyl groups of DPPC.[20, 142] This interaction keeps the ejected molecules close to the air-water interface facilitating their readsorption upon surface expansion.[20, 142] However, it has been shown that even depalmitoylated SP-C can improve the adsorption of DPPC molecules to the interface[142] suggesting the presence of another mechanism. Surface fluidization might also be in effect with surfactant proteins although to lower extents compared to cholesterol. Surfactant proteins do not reduce the T_m of

DPPC but slightly reduce the enthalpy of chain melting implying a slight surface fluidization.[136, 137] Fluorescent imaging of binary mixtures of DPPC and very high concentration of surfactant proteins (10% to 20% by weight) has confirmed increased fluidity in the presence of proteins.[110] At physiologically relevant protein concentrations of 1 to 2% by mass the extent of surface fluidity is likely to decrease significantly; however it can still occur. Both surface fluidization and specific interaction provide a partially reversible collapse and a consistently large hysteresis area.

2.3.5.4 Finding The Physiologically Relevant Surface Tension Range

Finding the range of physiologically relevant surface tensions in the lung is important for a variety of reasons. Surfactant cycling within this range allows for a realistic comparison of different surfactants in terms of their hysteretic behavior and functionality. Surfactant cycling in this range is also important for studies of surfactant exposure to sub-micron particles as it provides a more realistic view of the potential adverse effects of particles *in vivo*. Several previous studies have embarked on the challenge of finding the physiologically relevant surface tension values; however, no review of the previous literature in this field has been published and there is no consensus on the range of surface tension values during normal breathing.

One of the first attempts on finding the physiologically relevant surface tension values was performed by Horie and colleagues.[143] Using excised cat lungs and performing gas inflation and deflation, these researchers generated P-V curves (Figure 2-26-a) which were converted to γ-V curves using the relationship between transpulmonary pressure, volume and surface tension proposed by Bachofen et al.[123] The problem of converting P-V curves to γ-V curves was approached differently by Smith and Stamenovic.[144] In this work, excised rabbit lungs were fixed at constant surface tension values using test liquids and inflated and deflated. An index of P-V curves at different

surface tension values were generated using this method. Then the P-V curves of excised lungs with no test liquids were generated and the intersection of these P-V curves with the curves from the index gave an estimate of the surface tension at each point during inflation and deflation (Figure 2-26-b).

An improvement to the previous methods was made by Schurch and colleagues[145] who invented the microdroplet method. In this method, the alveoli of excised rabbit lungs were punctured and a drop of a test liquid was placed on its surface. This drop was then examined under a microscope as the lungs were compressed and expanded. Changes in the surface tension of the alveolar fluid caused changes in the shape of the drop which were used to determine the surface tension of the lung during inflation and deflation. At surface tensions above 20 mN/m the drop was spherical and the equations for relating the shape of sessile drops to surface tension were used to measure the surface tension.[146] At surface tensions below 20 mN/m, the drop was flat and an equation relating the surface tension to bubble height for flat drops was used. Using this method surface tension-lung volume curves were generated at different temperatures (Figure 2-26-c). The same method was followed by Bachofen and colleagues[147] for excised rabbit lungs and led to very similar results (Figure 2-26-d) denoting the reproducibility of this method. The graphs in Figure 2-26 show the changes in surface tension upon changes in lung volume from near zero to total lung capacity (TLC). However, such drastic changes in lung volume do not happen in each breath. In fact, a very small amount of air enters and exits the lungs during normal breathing. A lung capacity of 6 L, a resting volume of 3 L and a tidal volume (the volume of air entering the lungs in each breath) of 0.5 L have been suggested as typical values for human lungs.[5] Using these values, it can be estimated that the lungs are compressed and expanded between 50% and 58% of TLC in each normal breath. Since graphs of surface tension vs. lung volume between 50% and 58% TLC are not available, the surface tensions at 58% TLC during inflation and 50% TLC during

deflation from the graphs in Figure 2-26 was used to determine the physiologically relevant surface tensions.

a)

b)

c)

d)
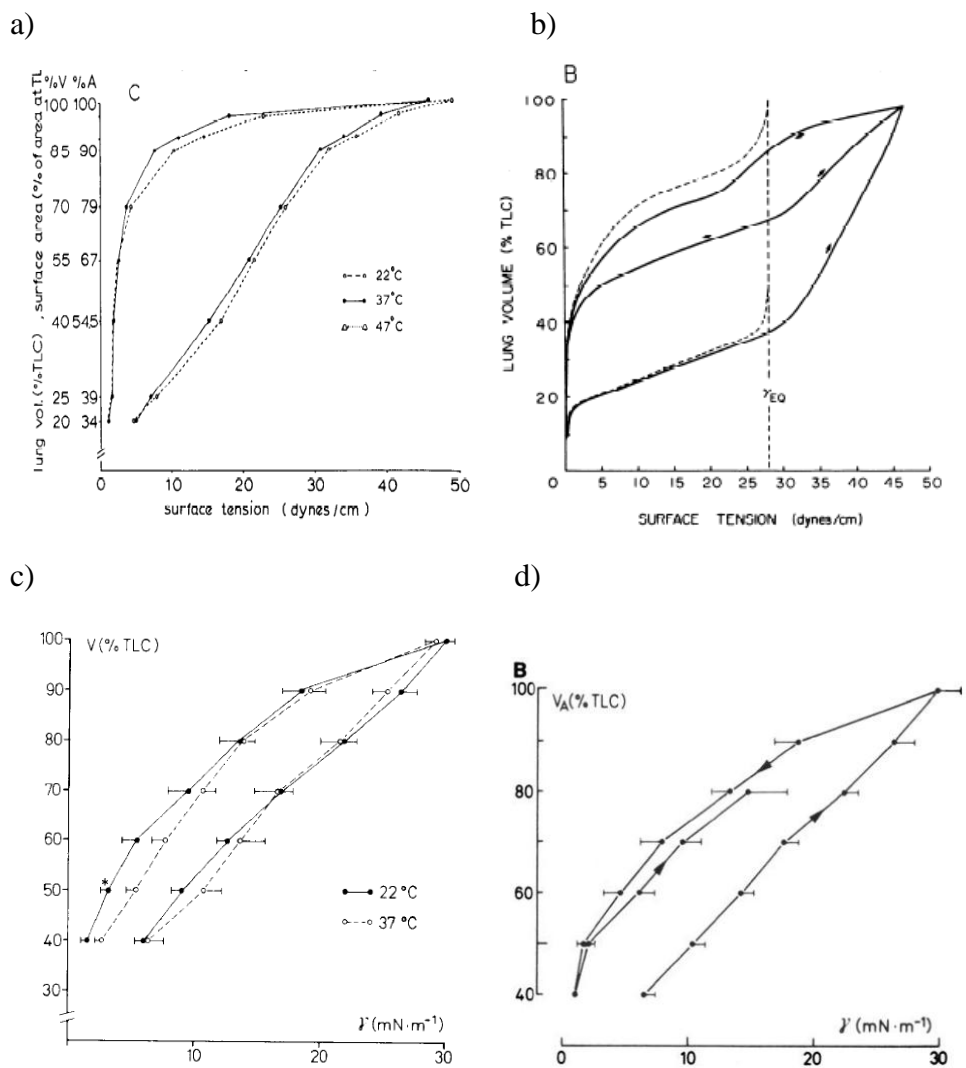
Figure 2-26. A summary of the surface tension ranges of excised animal lungs studied in literature: a) Horie et al.[143] reported for excised cat lungs, b) Smith and Stamenovic[144] reported for excised cat lungs, c) Schurch et al.[145] reported for excised rabbit lungs and d) Bachofen et al.[147] reported for excised rabbit lungs. The x-axes in all figures denote surface tension. All figures were reprinted with permission.

Using the range of 50% to 58% of TLC results in a surface tension range that is much narrower than complete inflation and deflation. Using this range, the following values were estimated for lung-relevant surface tensions: 3-24 mN/m (from Horie et al.[143]) , 5-14 mN/m (from Smith and Stamenovic[144]), 3-18 mN/m (from Schurch et al.[145]) and 3-15 mN/m (from Bachofen et al.[147]). Since the values are very close, the range of 3 mN/m to 24 mN/m (surface pressures of 67 mN/m to 46 mN/m at 37 ºC) can be estimated as the physiologically relevant surface tension range in the lungs. All the surface tension values estimated from the above mentioned studies fall within this range, providing a cautious estimate for the surface tension of the lungs in each breath.

2.3.5.5 Comparing Hysteresis Between DPPC and Infasurf

Several studies have used hysteresis area as a measure of surfactant functionality in the past.[45, 67] However, different pulmonary surfactant models have rarely been compared based on their hysteretic behavior. Considering the significant difference in the hysteresis area of normal and diseased lungs,[104] such comparison is important in choosing a potent surfactant model both for surfactant replacement therapy and as a model for *in vitro* studies. To our knowledge only one study has focused on comparing pulmonary surfactants based on their hysteresis area.[102] However, the evaluations in that study have been made based on one compression and expansion cycle where the films have been compressed from the surface tension of pure water at room temperature to near zero values and a realistic comparison of hysteretic behavior in the physiologically relevant surface tension range has not been performed.

Using the surface pressure range of 46 mN/m to 67 mN/m determined from Figure 2-26, monolayers of DPPC and Infasurf were compared for their hysteretic behavior and functionality over multiple cycles. Such studies help understand the role of additional components of lung surfactant in maintaining its functionality and the differences between a simplistic and realistic model of lung surfactants in terms of their

hysteretic behavior. For more realistic mimicking of physiologically relevant conditions, monolayers of DPPC and Infasurf were compressed at high speed (150 mm/min) for 10 compression and expansion cycles (Figure 2-27).

In Figure 2-27, the surface areas were chosen so that the first compression cycle was as close as possible to the physiologically relevant surface pressure range of 46 mN/m and 67 mN/m. Within the chosen surface areas the surface pressure in the first compression cycle ranged between 44.8 ± 0.9 mN/m and 65.7 ± 1.0 mN/m for DPPC and 45.6 ± 0.2 mN/m and 60.9 ± 1.8 mN/m for Infasurf. Although the values for DPPC were in the desirable range of surface pressures, the maximum surface pressure achievable for Infasurf in the Langmuir trough at 37 ºC was about 62 mN/m, thus a value slightly lower than the target was obtained. Hysteresis areas were normalized by dividing them by the compressed surface area (i.e. 59 cm^2 for DPPC and 153 cm^2 for Infasurf) to compensate
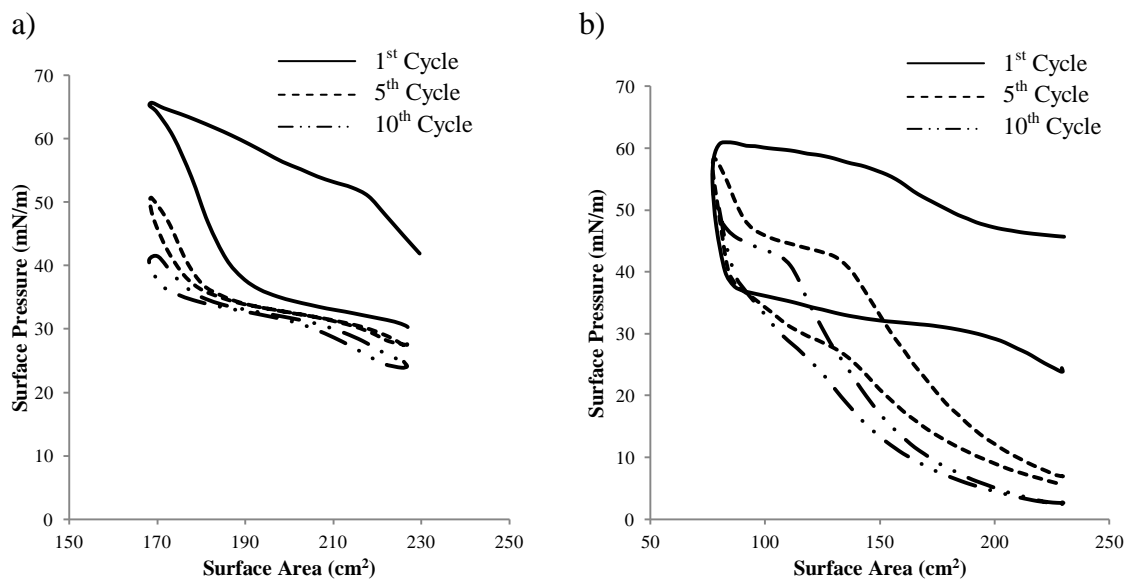
Figure 2-27. Surface compression and expansion of surfactants at a compression rate of 150 mm/min at physiological temperature with the surface pressure of the first compression cycle being at the lung-relevant surface tension range, a) DPPC and b) Infasurf.

for the differences in surface area reduction required for achieving the desired surface pressure values. Comparison of normalized hysteresis areas between the two surfactants showed that Infasurf produced larger hysteresis compared to DPPC in all cycles (Table 2-6). Higher recruitment indices were generally observed with Infasurf compared to DPPC which were significant in some of the cycles (e.g. 3.1 ± 0.6 for Infasurf vs. 1.7 ± 0.1 for DPPC in the fifth cycle).

Table 2-6. A comparison between DPPC and Infasurf surface pressure isotherms upon multiple cycling in the lung-relevant surface tension range.

# Cycle	DPPC				Infasurf			
	π_{max} (mN/m)	HA_n (mN/m)	$RI_{15\%}$ *	$\pi_{max}-\pi_{max.1st cycle}$ (mN/m) **	π_{max} (mN/m)	HA_n (mN/m)	$RI_{15\%}$	$\pi_{max}-\pi_{max.1st cycle}$ (mN/m)
1st Cycle	65.7 ± 1.0	18.7 ± 0.6	3.8 ± 0.8	0	60.9 ± 1.8	20.9 ± 1.1	3.8 ± 0.8	0
5th Cycle	50.7 ± 1.1	2.6 ± 0.9	1.7 ± 0.1	15.0 ± 1.8	58.4 ± 1.6	8.2 ± 0.5	3.1 ± 0.6	2.5 ± 0.7
10th Cycle	41.4 ± 1.8	1.1 ± 0.8	1.7 ± 0.2	24.2 ± 2.8	52.7 ± 2.3	4.8 ± 0.2	2.3 ± 0.4	8.2 ± 2.3

* Denotes the recruitment index calculated using Equation 2-5 and the difference in surface pressure in the first 15% of surface area expansion.
** The difference between π_{max} of each cycle and π_{max} of the first cycle.

Comparison of the maximum surface pressures between the two surfactants revealed an interesting phenomenon. Although a higher surface pressure at the end of the first compression cycle was observed with DPPC, Infasurf generated higher surface

pressure values as the cycles proceeded. After the 10th cycle a surface pressure of 52.7 ± 2.3 mN/m was observed with Infasurf compared to a value of 41.4 ± 1.8 mN/m with DPPC. The decrease in maximum surface pressure during cycling was expected and confirmed that both surfactants have lost some molecules from the air-water interface. However, the two surfactants showed a significant difference when the changes in maximum surface pressure between the first and the last cycles were compared. The difference in maximum surface pressure between the first and the last cycle for DPPC was 24.3 mN/m whereas for Infasurf this values was only 8.2 mN/m. This phenomenon confirms that the extra lipids and proteins in Infasurf are responsible for bringing some of the lost surfactant molecules back to the air-water interface.

In comparing two surfactants or evaluating the function of a certain surfactant, it is customary to use the maximum surface pressure for one cycle and the hysteretic and respreading behavior of surfactants or their maximum surface pressures over multiple cycles are rarely used. As shown in the comparison of DPPC and Infasurf (Table 2-6) if the maximum surface pressure alone had been used for comparison, pure DPPC would have been known as the better surfactant. However, when hysteresis and the maximum surface pressure over multiple cycles (respreading) were used Infasurf showed better surfactant qualities. This shows that hysteresis and maximum surface pressure over multiple cycles both need to be taken into consideration when comparing two surfactants.

2.4 Conclusions

Surface pressure vs. surface area isotherms were successfully generated for both DPPC and Infasurf. The generated isotherms closely matched those previously reported in the literature in terms of their phase behavior, collapse surface pressure and hysteresis areas. The effect of temperature and barrier speed was studied on the surface pressure isotherms of both surfactants. Increasing the temperature changed the phase behavior of DPPC surface pressure isotherm but induced little effect on the isotherm of Infasurf.

Changing the barrier speed did not affect Infasurf surface pressure isotherm but significantly reduced the maximum surface pressure achieved by DPPC. A discussion on the origins of lung hysteresis, the role of pulmonary surfactant and the importance of using hysteresis area as a measure of surfactant function was provided. Finally, the range of physiologically relevant surface tension values during normal breathing was estimated as 3 mN/m to 24 mN/m and Infasurf and DPPC were compared for their ability to reduce the surface tension and maintain a large and reproducible hysteresis area in this range. Infasurf produced lower surface tension values as the cycles proceeded and maintained a larger hysteresis area compared to DPPC confirming its superiority in matching the properties of the pulmonary surfactant.

CHAPTER 3

PARTICLE-SURFACTANT INTERACTIONS FOLLOWING

SUBPHASE INJECTION OF PARTICLES[*]

3.1 Introduction

Langmuir monolayers are insoluble films of amphiphilic molecules spread on an air-water interface. Amphiphilic molecule contain both hydrophilic and hydrophobic moieties. At an air-water interface, the hydrophilic moiety comes in contact with water and the hydrophobic moiety orients toward air leading to monomolecular films at the surface. Langmuir monolayers of phospholipids have been widely used to mimic biological phenomena at interfaces. These monolayers are a mimic for the surfactant layer that lines the alveolar region of the lungs and have been widely used to examine the interfacial behavior of lung surfactant.[43, 60, 63, 86, 148] Also, since biological membranes are made of two coupled monolayers, Langmuir monolayers of phospholipids have also had a wide use in the studies of biomembranes.[82, 101, 149] The well-defined, two-dimensional structure of these monolayers allows for easy manipulation of molecular behavior making these monolayers advantageous for mechanistic studies of molecular interactions. For example, interactions between drug molecules and Langmuir monolayers of phospholipids have been studied to provide information on the effects of drugs on cell membranes and lung surfactants.[87, 101, 149-151] A recent area of interest in the studies of Langmuir monolayers, is interactions between these Langmuir monolayers of surfactants

---

[*] Parts of this chapter have been reprinted from Farnoud, A.M.; Fiegel, J. Low concentrations of negatively charged sub-micron particles alter the microstructure of DPPC at the air-water interface. *Colloids and Surfaces A: Physicochemical and Engineering Aspects* **2012**, 415, 320-327. with permission from Elsevier.

and nano- and sub-micron particles. Information provided from such studies are important for various fields such as drug delivery and occupational health. In addition, mechanistic studies of particle-surfactant systems have applications in food [148,152], cosmetics[153] and even mining[154] industries.

A review of the previous studies of particle interactions with surfactant monolayers, reveals that there has been no consensus on the exposure method of surfactants to particles. As explained in Chapter 1, various methods have been used to expose surfactant monolayers to solid particles in previous studies.[60, 61, 65] Out of these methods, injecting the particles underneath an already spread monolayer (subphase injection method) has received little attention,[61, 62] but seems to have important physiological relevance. In exposure of healthy biological membranes and lung surfactants to solid particles, particles frequently come in contact with an already formed monolayer at the interface. Subphase injection of particles mimics this situation and allows for undisturbed adsorption of the monolayer at the air-water interface before interactions with particles.

There have only been two previous studies on the interactions between solid particles and surfactant monolayers using the subphase injection method. Using carboxyl modified, amine modified and plain polystyrene particles (20 and 60 nm in diameter), Peetla and Labhasetwar[61] investigated the role of particle surface properties on the monolayers of an endothelial cell membrane (ECM) model consisting of various lipids with DPPC being the major component. In this study, plain polystyrene particles caused a significant inhibition in surfactant function. This inhibition was suggested to be a result of the penetration of these particles into the monolayer, adsorption of hydrophobic chains

of phospholipids onto the particles and their displacement to the subphase. The penetration of hydrophobic particles into the lipid monolayer was later confirmed by atomic force microscopy (AFM) studies by the same investigators.[62] The amine modified particles caused an increase in the surface pressure values of the surface pressure vs. surface area isotherms of the ECM model. This was suggested to be a result of electrostatic interaction between the positively charged particles and the phosphate groups of surfactant molecules causing condensation of surfactant molecules at the surface and increasing the surface pressure. Finally, carboxyl modified particles showed no significant change in the surface pressure isotherm of the ECM surfactant model. The authors suggested that the carboxyl modified particles were squeezed out from the air-water interface into the subphase leaving the surface pressure isotherm intact. However, no further evidence was provided for the suggested mechanism.

Although valuable information on particle-surfactant interactions was gained by the previous studies of Peetla and Labhasetwar[61, 62] with the subphase injection method, there are still a few questions that remain unanswered. The role of the subphase injected particles on the surfactant microstructure and molecular packing remains unclear. However, the packing of molecules in biomembranes is very important in their biological functions. It has been shown that the presence of more fluid (i.e. liquid expanded) phases in cell membranes can lead to defective and leaky cell membranes.[155] Furthermore, the role of particles in surfactant respreading behavior upon cycling, an important factor in lung surfactant functionality, is not studied. Finally, the observation that carboxyl modified particles do not affect the interfacial behavior of the monolayer is in contrast with the observation of Beck-Broichsitter and colleagues[59] and Schleh and colleagues[58]

that negatively charged polystyrene particles can inhibit the function of model pulmonary surfactants. These contradicting results even for a common particle model such as negatively charged polystyrene emphasize the need for more fundamental mechanistic studies on particle-surfactant interactions.

The objective of the present study was to investigate the interactions between carboxyl modified polystyrene particles (200 nm) and DPPC. Polystyrene particles were chosen as the particle system because of their monodispersity, well-defined size and charge and the promise of negatively charged polymeric particles for drug delivery applications.[74] DPPC provides a simple lung surfactant and biomembrane model due to the presence of large amounts of phosphatidylcholines both in the alveolar lining layer[18] and cellular membranes.[156] The interactions between particles and DPPC monolayers were studied using tensiometric experiments during dynamic compression-expansion cycles or monolayer collapse, fluorescent, confocal and atomic force microscopy.

3.2 Materials and Methods

3.2.1 Materials

Dipalmitoyl phosphatidylcholine (DPPC) was purchased from Genzyme Pharmaceuticals (Cambridge, MA) and used without further purification. The glycerol stereocenter of the purchased DPPC was R oriented and did not include any racemates as the molecule is fully synthetic. Texas Red-dihexadecyl phosphatidyl ethanolamine (Texas Red-DHPE) was purchased from Molecular Probes (Eugene, OR). Sodium chloride, calcium chloride and HPLC-grade chloroform were purchased from Sigma-Aldrich (Sigma-Aldrich, St. Louis, MO). All water used in experiments was obtained from a Barnstead NANOpure II system from Barnstead International (Dubuque, IA) and had a resistivity of 18.2 MΩ·cm. White and fluorescent carboxyl modified polystyrene particles

were purchased as suspensions from Invitrogen (Carlsbad, CA). Particles had a nominal size of 200 nm and a carboxyl group content of $2x10^5$ groups per particle. Fluorescent particles were yellow-green with excitation and emission maxima of 505 nm and 515 nm, respectively.

3.2.2 Particle Washing

Particle washing was performed to separate the particles from any potential surfactants added in the particle suspensions by the manufacturer. For washing, particles were added to microcentrifuge tubes and centrifuged at 12000 g for 30 minutes in a microcentrifuge (model 5424, Eppendorf, Hauppauge, NY) resulting in a clear supernatant confirming that the majority of particles settled. The supernatant was carefully replaced with purified water. The microcentrifuge tubes were then vortexed for 90 seconds and sonicated for 10 minutes three times to redisperse the particles. Another round of centrifugation at 12000 g for 30 minutes was performed on the redispersed particles to ensure that any remaining surfactant molecule was separated in the supernatant. Then the supernatant was separated and the remaining particle pellets were frozen in liquid nitrogen for 10 minutes for lyophilization. Lyophilization was performed using a Labconco FreeZone 4.5 liter freeze dry system (chamber pressure of less than 0.02 mbar and collector temperature of less than -50°C). Particles were lyophilized overnight and the dried powders were collected and used to make particle suspensions. Suspensions were made by adding desired amounts of particles to a solution of 150 mM NaCl and 1.5 mM $CaCl_2$, which was adjusted to a pH of 7 with NaOH (henceforth referred to as the subphase solution) and performing three times of vortex and sonication for 90 seconds and 10 minutes, respectively.

3.2.3 Zetapotential and Size Distribution

The size distribution of particle suspensions in a solution of 150 mM NaCl and 1.5 mM $CaCl_2$ dissolved in purified water and adjusted to a pH of 7 using NaOH (i.e. the

subphase solution used in tensiometric studies) was determined by dynamic light scattering (DLS) and particle zeta potential was determined by laser Doppler anemometry using a Zetasizer Nano ZS (Malvern Instruments, Worcestershire, UK). Particles were vortexed for 90 seconds and sonicated for 10 minutes by bath sonication three times and diluted to approximately 0.01 g/L for the measurements. One mL of the suspension was loaded into clear disposable folded capillary cells (DTS 1060C cuvettes, Malvern Instruments) for characterization of size and zeta potential.

3.2.4 Transmission Electron Microscopy (TEM)

The nominal diameter of particles was verified using TEM. TEM imaging was performed using 400-mesh copper TEM grid. The grids were Formvar and carbon coated prior to imaging. For Formvar coating a clean microscope slide was dipped in a 0.5% solution of Formvar in ethylene chloride. The slide was then dried and a razor blade was used to scrape the edge of the slide to help remove the Formvar film. Then a container with a large surface was filled with water and the slide was brought in contact with the water surface vertically and slowly until the Formvar film was totally transferred from the slide to the water surface. The grids were then placed on the Formvar film using fine tweezers. A clean sheet of Parafilm was used to collect the Formvar film with the grids from the water surface so that the grids were in between the Parafilm and Formvar. Carbon coating of the Formvar surface was performed using a BOC Edwards Auto 306 vacuum coating system (BOC Edwards, Sanborn, NY) where a low tension voltage (30 V) was applied to carbon rods to uniformly deposit carbon on the Formvar surface. TEM grids were collected prior to imaging by carefully cutting the Formvar film using fine tweezers.

TEM samples were prepared by suspending washed and lyophilized particles in methanol to form a clear suspension. One drop of this suspension was placed onto a Formvar and carbon coated TEM grids using a Pasteur pipette. Imaging was performed

after the evaporation of methanol using a JEOL JEM-1230 with a Gatan UltraScan 1000 camera (Peabody, MA). Images were analyzed using the ImageJ software.[157] The diameters of at least 100 particles were measured to determine the average particle size.

3.2.5 Specific Surface Area

The surface area of the particles was measured using the Brunauer, Emmett, Teller (BET) adsorption method. Surface area was determined by nitrogen adsorption at 77.4 °K using an automated surface area analyzer with measurable surface area ≥0.01 m^2/g (Quantachrome BET Nova 4200e, Boynton Beach, FL). For each experiment approximately 100 mg of washed and lyophilized particles were degassed overnight under vacuum at 60°C to ensure the removal of adsorbed molecules from particle surfaces. The degassed samples were placed under liquid nitrogen and were exposed to nitrogen. The amount of adsorbed gas on particle surfaces was measured by monitoring the pressure in the sample chamber. The BET equation was used to determine the monolayer adsorbed nitrogen quantity:

$$\frac{P}{n(P_0\text{-}P)} = \frac{1}{cn_m} + \frac{c\text{-}1}{cn_m}\frac{P}{P_0} \tag{3-1}$$

where P is the equilibrium nitrogen pressure, P_0 is the saturation nitrogen pressure, n is the moles of gas adsorbed, n_m is the monolayer adsorbed gas quantity and c is the BET constant. The BET constant and the monolayer adsorbed gas quantity were estimated plotting the BET equation and the surface area per unit mass was calculated using equation (3-2).

$$S = N_A n_m \sigma \tag{3-2}$$

where N_A is Avogadro's number, σ is the area occupied by one nitrogen molecule (16.2 Å^2) and S is the surface area per unit mass.

3.2.6 Surface Chemical Composition

The surface chemical composition of washed and lyophilized particles was determined using X-ray photoelectron spectroscopy (XPS). This method is a 'photons in-electrons out' method, where the sample is irradiated with X-rays with the energy of hυ, photoelectrons are emitted from the sample and the kinetic energy (KE) is measured. The binding energy (BE) of the ejected electrons is calculated using Equation 3-3:

BE (eV)=hυ-KE-ϕ   (3-3)

where ϕ is the electron spectrometer and sample work function which is instrument dependent and determined during calibration.[158] The binding energy of the electrons can be determined after measuring the kinetic energy when ϕ, hυ are known.

A Kratos XPS Ultra-Axis instrument was used for measurements in this research. Lyophilized particles were pressed on indium foil and mounted on a copper stub. A monochromatic aluminum Al Kα (1486.6 eV) was used to eject the electrons from the sample and a hemispherical sector analyzer was used to determine the kinetic energy of electrons. XPS experiments were conducted at ultra high vacuum (~ 10^{-9} Torr) to minimize the scattering of photoelectrons by gas molecules inside the chamber. Survey scans were performed in the range of -5 eV to 1200 eV with a step size of 1 eV and high resolution scans were performed at regions of interest with a step size of 0.1 eV. CasaXPS software was used for XPS data analysis and spectra were calibrated using the carbon C 1s peak at 285 eV.

3.2.7 Tensiometric Experiments

Tensiometric experiments were performed in the Langmuir Wilhelmy setup as explained in Chapter 2. A subphase of 150 mM NaCl, 1.5 mM $CaCl_2$ dissolved in purified water, adjusted to a pH of 7 using 0.1 M NaOH, was used for all studies. Before each experiment the surface of the trough and the barriers were carefully brushed with ethanol and rinsed with copious amounts of purified water. Then, the Wilhelmy plate was

cleaned by placing it on a flame from a Bunsen burner and attached on a hook on top of the trough. The force transducer was zeroed and the trough was filled with 250 mL of freshly made subphase solution. The subphase was allowed to equilibrate to room temperature (23.3 ± 0.6 °C) for 30 min. Then, the surface was aspirated while the barriers were compressed to remove any surface impurity. If the changes in surface tension during this initial compression were less than 0.5 mN/m the surface was considered clean and the experiment was continued by recording the surface tension of pure subphase then zeroing it to allow for measurement of surface pressure. DPPC monolayers were obtained by spreading 50 μL of a 1.22 g/L DPPC solution in chloroform on top of the subphase (initial mean molecular area of 111.6 $Å^2$/molecule) using a Hamilton microsyringe and allowing 20 min for chloroform evaporation. Before each experiment 50 μL of the subphase solution was injected in the subphase and 30 minutes was allowed before barrier compression was initiated with a compression rate of 10 mm/min (1.5 $Å^2$/molecule·min).

Particle concentrations of 10^{-5} g/L to 10^{-3} g/L were chosen for the experiments with carboxyl modified polystyrene particles. These particle concentrations were taken from deposition fractions of sub-micron particles in the alveolar region reported by Lippmann.[54] The maximum deposition fraction of sub-micron sized particles in the alveolar region is about 47%. Taking an extreme case of exposure to 1 gram of particles as the highest exposure limit (exposure to 300 mg of particles is shown to cause coughing in subjects,[159, 160] the maximum deposition of particles in the alveolar region would be around 0.47 g. This corresponds to 2.57×10^{-4} g of particles in the trough when the surface area of the alveolar region (102 m^2 from Stone and colleagues[3]) and the trough (0.0558 m^2) are compared. The subphase volume in tensiometric experiments is 250 mL meaning the concentration of nanoparticles will be 10^{-3} g/L. Thus, particle concentrations of 10^{-5} g/L to 10^{-3} g/L were studied to observe concentration effects. Particle introduction was performed after adding the DPPC solution and allowing 20 minutes for chloroform

evaporation. Various amounts of a vortexed and sonicated 0.488 g/L particle suspension were injected into the subphase solution to obtain the desired particle concentration. Thirty minutes of adsorption time was allowed before the barrier compression was initiated. Control tensiometric experiments with the particles were performed by compressing the surface after injecting the highest particle concentration (10^{-3} g/L) into the subphase with no DPPC.

A single compression cycle was performed for monolayer collapse experiments, whereas three compression and expansion cycles were performed for hysteresis experiments where the dynamic behavior of surfactant was studied. Surface tension data were acquired and recorded using the LayerBuilder software and the hysteresis area was determined by subtracting the area under the curve for expansion from the area under the curve for compression. KaleidaGraph software v. 3.6 was used to calculate area under the curve for each case. The compression modulus (C_s^{-1}) of the isotherm was calculated using Equation 2-1, the surface pressure and surface area values needed for this equation were recorded using the LayerBuilder software and plotted in Microsoft Excel.

3.2.8 Fluorescent Imaging

Fluorescence and confocal microscopy experiments were performed to visualize surfactant microstructure and particle placement at different compression ratios. For these experiments, the fluorescent probe Texas-Red-1,2-dihexadecanoyl-*sn*-glycero-3-phosphoethanolamine, triethylammonium salt (Texas-Red-DHPE) to the DPPC solution at about 1 mol%. Texas-Red DHPE preferentially partitions into the fluid phases at the surface allowing for studies of structure of lipid domains which appear as black dots on a red background in the LE-LC phase of the surface pressure isotherm.[161, 162] Control tensiometric experiments were performed by adding 50 μL of a 1.22 g/L DPPC solution doped with Texas-Red-DHPE to ensure that the fluorescent probe did not alter the surface pressure isotherm.

Since the Langmuir trough used for tensiometric experiments was too heavy for a microscope stage, a small poly (methylmethacrylate) (PMMA) minitrough (7.5 cm x 12 cm x 0.6 cm) was used for microscopy experiments. The surface of this minitrough was washed similar to the Langmuir trough for microscopy experiments, then the trough was filled with 60 mL of subphase and mounted on the microscope stage. Eight microliters of a 1.22 g/L DPPC solution doped with Texas-Red-DHPE was added on top of the subphase for imaging providing an initial mean molecular area of 111.6 $Å^2$/molecule similar to tensiometric experiments. The surface of this trough was compressed manually using Delrin barriers and images of the microstructure were acquired at each surface pressure.

Since it was not possible to measure the surface pressure values on the microscope stage, off-line surface pressure measurement had to be performed. To this aim, the surface pressure values caused by the reduction in surface area were measured on the Wilhelmy plate setup (Figure 3-1). The surface areas at which the desired surface pressure values were reached were marked on the side of the trough. These marks were used as guides for barrier compression on the microscope stage. To ensure that hand compression did not affect the interfacial behavior of DPPC monolayers, a complete surface pressure isotherm was generated by hand compression using the Langmuir trough on the Langmuir-Wilhelmy setup.

Fluorescence microscopy experiments were performed using an Olympus BX-51 microscope (Olympus, Center Valley, PA) to image and video of the lipid microstructure upon compression. Confocal microscopy experiments were performed using a Bio-Rad MRC-1024 confocal microscope (Bio-Rad Labs, Hercules, CA) with depth of field of 4 μm focused at the air water interface to image microstructure and localization of fluorescent particles. Filters with emission ranges of 510-560 nm and 573-648 nm were used to enable visualization of the fluorescently labeled particles and the Texas-Red

probe, respectively. To reduce the movement of lipid domains due to air currents a cardboard shield was placed on top of the microscope for all imaging experiments.

Figure 3-1. The area of the PMMA trough was reduced using Delrin barriers and the surface pressure at each surface area reduction was measured using the Wilhelmy plate setup.

The "Analyze Particles" feature of the ImageJ software[157] was used to determine the area of condensed domains. The erosion and dilation functions were each used once on each image to minimize noise before the analysis was performed. These functions improve the edge definition of domains by removing (erosion) and adding (dilation) dark pixels at domain edge. During this process, the features that are just one pixel are eliminated by erosion and will not be reconstructed by dilation thus reducing the noise of the image. Images at each surface pressure were analyzed and the areas of all single domains were recorded. Histograms were generated by creating bins that were 10 μm^2 in size and counting the total number of condensed domain areas within a certain bin size.

3.2.9 Atomic Force Microscopy (AFM)

AFM experiments were performed to investigate the potential penetration of polystyrene particles into the DPPC monolayer. A Langmuir-Blodgett trough (Nima

Technology, model 610) with a volume of 150 mL was used for these experiments. The surface of this trough was washed and DPPC monolayers spread on top of the subphase. Polystyrene particles were injected into the subphase at a concentration of 10^{-3} g/L and given 30 minutes of adsorption time. Monolayers were transferred onto hydrophilic mica substrates by vertical dipping at a surface pressure of 10 mN/m and with an upstroke rate of 5 mm/min. Images were acquired with a Dimension 3100 scanning probe microscope and Nanoscope IV controller (Veeco Metrology, LLC, Santa Barbara, CA). Imaging was performed in tapping mode using silicon TESP7 AFM tips (Veeco Metrology, LLC, Santa Barbara, CA) with a spring constant of 70 Nm^{-1} and a resonance frequency of 280 kHz.

3.3. Results and Discussion

3.3.1 Particle Characterization

Carboxyl modified polystyrene particles with a nominal diameter of 200 nm (referred to as 0.2 μm CML from this point) were characterized to determine their average size and size distribution, zeta potential, surface area and surface functional groups. TEM images confirmed that particles were spherical and monodispersed (Figure 3-2). The diameter of 100 particles was measured in ImageJ resulting in a mean diameter of 218 ± 16 nm for white particles and a mean diameter of 195 ± 21 nm for fluorescent particles. Both values were very close to those reported by the manufacturer which was 200 ± 7 nm for white and 210 ± 10 nm for fluorescent particles.

The diameter and the charge of the particles in suspension was also measured. White particles exhibited a hydrodynamic diameter of 236 ± 5 nm and fluorescent particles exhibited a diameter of 257 ± 1 nm as measured by dynamic light scattering. The hydrodynamic diameter is the diameter of hydrated particles and depends on particle surface structure and the type and concentration of ions in solution. It typically measures
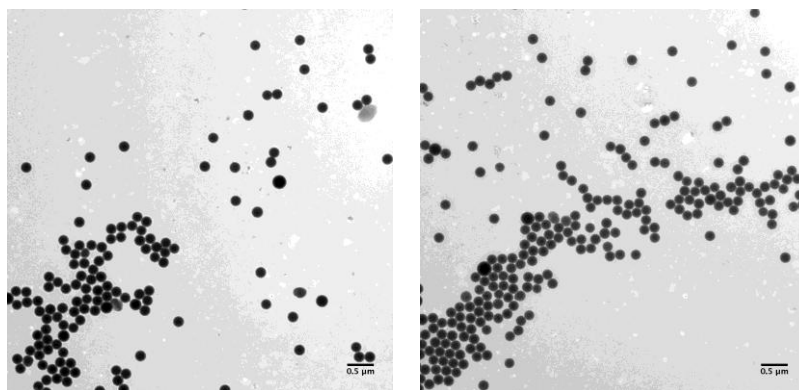
Figure 3-2. Representative TEM images of 0.2 µm CML particles suspended in methanol and dried on a Formvar coated TEM grid, scale bar = 0.5 µm.

a value larger than that measured in dry state, as with TEM measurement.[163] Particles were negatively charged, with a zeta potential of -28.4 ± 2.9 mV for white and -32.6 ± 2.3 for fluorescent particles in the subphase solution. As a result of their high zeta potential, particles were stable in the subphase, showing no signs of aggregation.

The surface area of the white particles was measured to be 27 ± 3 m^2/g via the BET adsorption method. This value was very close to theoretical size of spherical particles with a diameter of 200 nm (28.9 m^2/g), implying that particle surfaces were smooth and there was little or no aggregation. Finally, XPS analysis of the white particles confirmed the presence of a strong peak at 285.04 eV, indicating the saturated carbon bond, and the pi-pi* bond at 291.59 eV, both signature peaks of the polystyrene core (Figure 3-3).[164, 165] The peak at 289.48 eV confirmed the presence of 5.45% carboxyl group at the particle surface, while the peak at 286.50 eV shows the presence of C-OH bond which is likely the alcohol terminated end group on polystyrene. A summary of particle surface properties is presented in Table 3-1.

Name	Pos.	Area	At%
C-C	285.043	43197.14	83.61
C-OH	286.5	2838.29	5.494
COOR	289.48	2814.44	5.448
pi-pi	291.59	2812.25	5.444
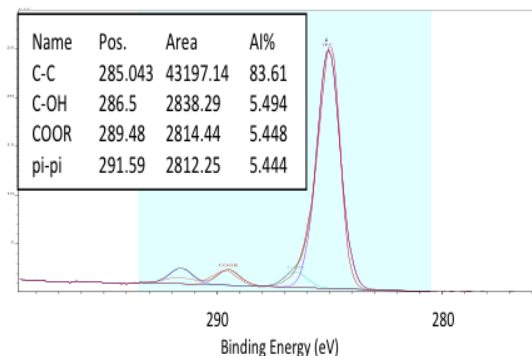
Figure 3-3. XPS spectra of 0.2 µm CML particles. The peaks confirm the presence of C-C and C-H bonds (285.04 eV), C-OH group (286.50 eV), COOR group (289.48 eV) and pi-pi bonds (291.59 eV) from the antibonding orbitals of the aromatic group in polystyrene.

Table 3-1. Particle characterization of 0.2 µm white and fluorescent CML particles.

Particle Property	White Particles	Fluorescent Particles
Average diameter in dry state[a]	218 ± 18 nm	195 ± 21 nm
Average diameter in solution[b]	236 ± 5 nm	210 ± 10 nm
Zeta potential[c]	-28.4 ± 2.9 mV	-32.6 ± 2.3 mV
Surface area[d]	27 ± 3 m^2/g	Not determined
Surface chemistry[e]	285.04 eV, C-C bond (83.61%) 286.50 C-OH bond (5.49%) 289.48 eV, COOR bond (5.45%) 291.59 eV, Pi-Pi* bond (5.44%)	Not determined

[a] Average size of > 100 particles measured by transmission electron microscopy.
[b] Average size in subphase measured by dynamic light scattering.
[c] Measurement in subphase by laser Doppler anemometry.
[d] Measurement of approximately 100 mg of particles by BET adsorption.
[e] Binding energy of specified bond (percent of area under the curve) measured by XPS.

3.3.2 Particle Effects on Surface Pressure Isotherms During

Compression to Collapse

Particles were examined for their surface activity in tensiometric experiments. A particle concentration of 10^{-3} g/L (the maximum concentration used with DPPC monolayers) in the subphase induced no significant effect on the surface pressure vs. surface area isotherm (Figure 3-4). The surface pressure remained below 0.2 mN/m after compressing the surface in the presence of particles from an initial area of 558 cm^2 to a final area of 200 cm^2 confirming that the particles are thoroughly washed and no surface-active component is present in particle suspensions.
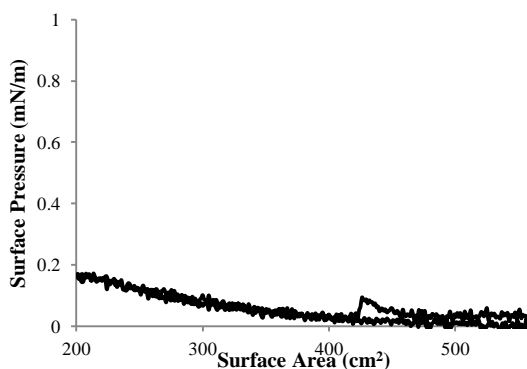
Figure 3-4. The surface pressure vs. surface area isotherm after the subphase injection of 10^{-3} g/L of 0.2 µm CML particles after one compression and expansion between the surface areas of 558 cm^2 and 200 cm^2 with no DPPC added on the surface.

The surface pressure vs. surface area isotherm of pure DPPC monolayers is presented in Figure 3-5-a. This isotherm showed a shape and phase behavior similar to those previously reported in the literature.[37, 113] The maximum surface pressure achievable was 72.3 ± 0.4 mN/m, demonstrating a near zero surface tension at collapse as expected for pure DPPC monolayers.[37, 39, 113] The addition of 0.2 µm CML particles at different concentrations to the subphase did not significantly affect the surface pressure

isotherm of DPPC (Figure 3-5-b to d). The surface pressure isotherms after the injection

of particles showed a similar shape to pure DPPC. The collapse surface pressure

remained close to 72 mN/m and no significant shifts were observed at the surface area at

which the monolayer collapse occurred (Table 3-2). At the highest particle concentration,

a slight but insignificant shift during the LC region of the surface pressure isotherm was

observed (Figure 3-5-d).
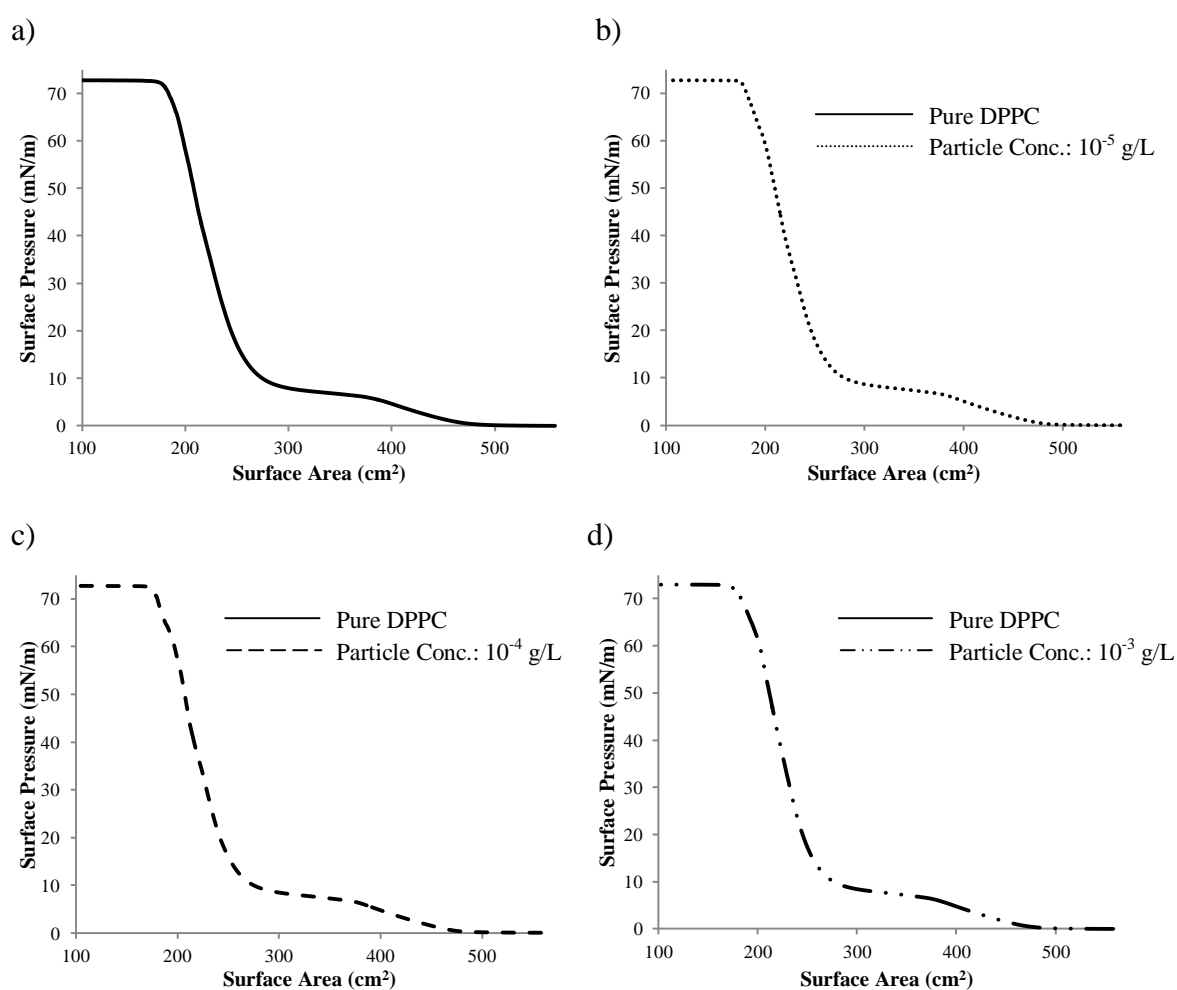
Figure 3-5. Surface pressure vs. surface area isotherms of (a) pure DPPC and DPPC after subphase injection of (b) 10^{-5} g/L, (c) 10^{-4} g/L and (d) 10^{-3} g/L of 0.2 µm CML particles. DPPC monolayers were compressed from an initial surface area of 558 cm^2 to a target area of 100 cm^2 in all experiments.

Table 3-2. Collapse surface pressure and surface area determined from surface pressure vs. surface area isotherms after compressing pure DPPC monolayers and the monolayers after subphase injection of 0.2 μm CML particles at concentrations of 10^{-5}, 10^{-4} and 10^{-3} g/L.

Particle Concentration (g/L)	Collapse Surface Pressure (mN/m) (± standard deviation)	Collapse Surface Area (cm^2) (± standard deviation)
Pure DPPC	72.3 ± 0.4	174 ± 2
10^{-5}	72.5 ± 0.0	176 ± 1
10^{-4}	72.7 ± 0.1	173 ± 4
10^{-3}	72.7 ± 0.1	175 ± 5

A similar result to the surface pressure isotherms observed in this study has been recently reported with silica nanoparticles (20 nm) and DPPC monolayers by Guzman and colleagues.[60, 63] In those studies, silica nanoparticles were shown to shift the surface pressure isotherm of DPPC during the LE-LC and LC region of the isotherm; however, the particles did not affect the maximum surface pressure obtained by DPPC monolayers. These results suggest that the particles remain in the subphase and do not penetrate the surfactant monolayer which is expected given their hydrophilic nature. Particle penetration into the monolayer has been previously reported for hydrophobic carbon black particles where a premature monolayer collapse and a reduction in the surface pressure of monolayer collapse was observed.[41, 63]

Similar to surface pressure isotherms, the presence of particles showed little effect on the dilational elasticity of DPPC monolayers. Dilational elasticity is a rheological quantity related to the monolayer rigidity and a measure of the elastic energy stored in the monolayer upon compressive deformation of the surface.[99] Subphase injection of the particles at the highest concentration of 10^{-3} g/L did not affect the dilational elasticity of DPPC monolayers. The shape of the dilational elasticity plot after the subphase injection

of particles remained very similar to that of pure DPPC monolayers with two maxima corresponding to LE and LC phases (Figure 3-6). The maximum value of dilational elasticity in the presence of particles was 236.9 ± 39.9 mN/m very similar to the maximum value of 239.6 ± 39.1 mN/m for pure DPPC monolayers. It has been shown that molecules and particles that can penetrate Langmuir monolayers show significant effects on the dilational elasticity of the monolayer.[57, 101] Thus, these results are further evidence that the hydrophilic particles used in these studies remain in the subphase and do not penetrate the air-water interface. This is in agreement with the tensiometric experiments where no significant effect on the surface pressure isotherm of DPPC was observed.
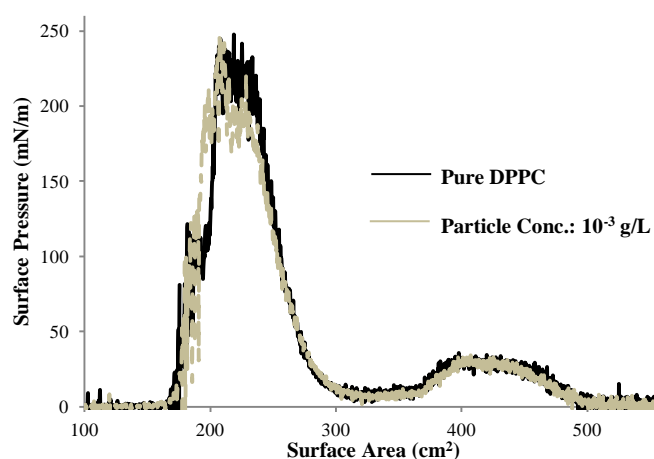
Figure 3-6. Dilational elasticity of DPPC monolayers with (grey) and without (black) the addition of 10^{-3} g/L of 0.2 μm CML particles in the subphase. Dilational elasticity values are calculated using Eq. 2-1 and the surface pressure isotherms presented in Figure 3-5.

3.3.3 Particle Effects on Surface Pressure Isotherms During Compression-Expansion Cycles

When expelled from the interface during compression, DPPC is slowly readsorbed to the surface. This lag in readsorption of ejected molecules results in a hysteresis area between the compression and expansion cycles of the monolayer. The effects of particles on the readsorption behavior of DPPC were studied by monitoring their effects on hysteresis area of DPPC monolayers upon multiple compression and expansion cycles. For hysteresis experiments, DPPC monolayers were compressed to 200 cm^2 (mean molecular area of 40 Å^2) and re-expanded three times. This mean molecular area is just above the theoretical limiting cross sectional area of DPPC molecules (39 Å^2 according to Hauser and colleagues[112]) to avoid complete monolayer collapse.

The hysteresis behavior of DPPC monolayers has been described in Section 2-3-6 and was in agreement with previously reported results.[125] The hysteresis behavior of DPPC monolayers with different particle concentrations is presented in Figure 3-7. Although no significant change in the hysteresis area of the first cycles was observed in the presence of particles, larger hysteresis areas were observed for the second and third compression-expansion cycles at the highest particle concentration (~800 mN/m·cm^2 for 10^{-3} g/L versus ~650 mN/m·cm^2 for control) (Table 3-3).

The increased hysteresis area in the presence of particles was primarily due to a shift in the surface pressure isotherm on compression in the LE-LC and LC region and the surface pressure during expansion looked nearly identical with or without the particles (Figure 3-7-e). Similar changes in the surface pressure isotherm of DPPC during the LE-LC and LC phase has been reported upon addition of ionic species to the subphase. In one study, increasing the concentration of chloroauric acid in the subphase significantly improved the surface active properties of DPPC in the LE-LC and the beginning of LC phase.[114] This effect was attributed to preferential adsorption of negatively charged auric chloride ions to zwitterionic DPPC headgroups. The same effect
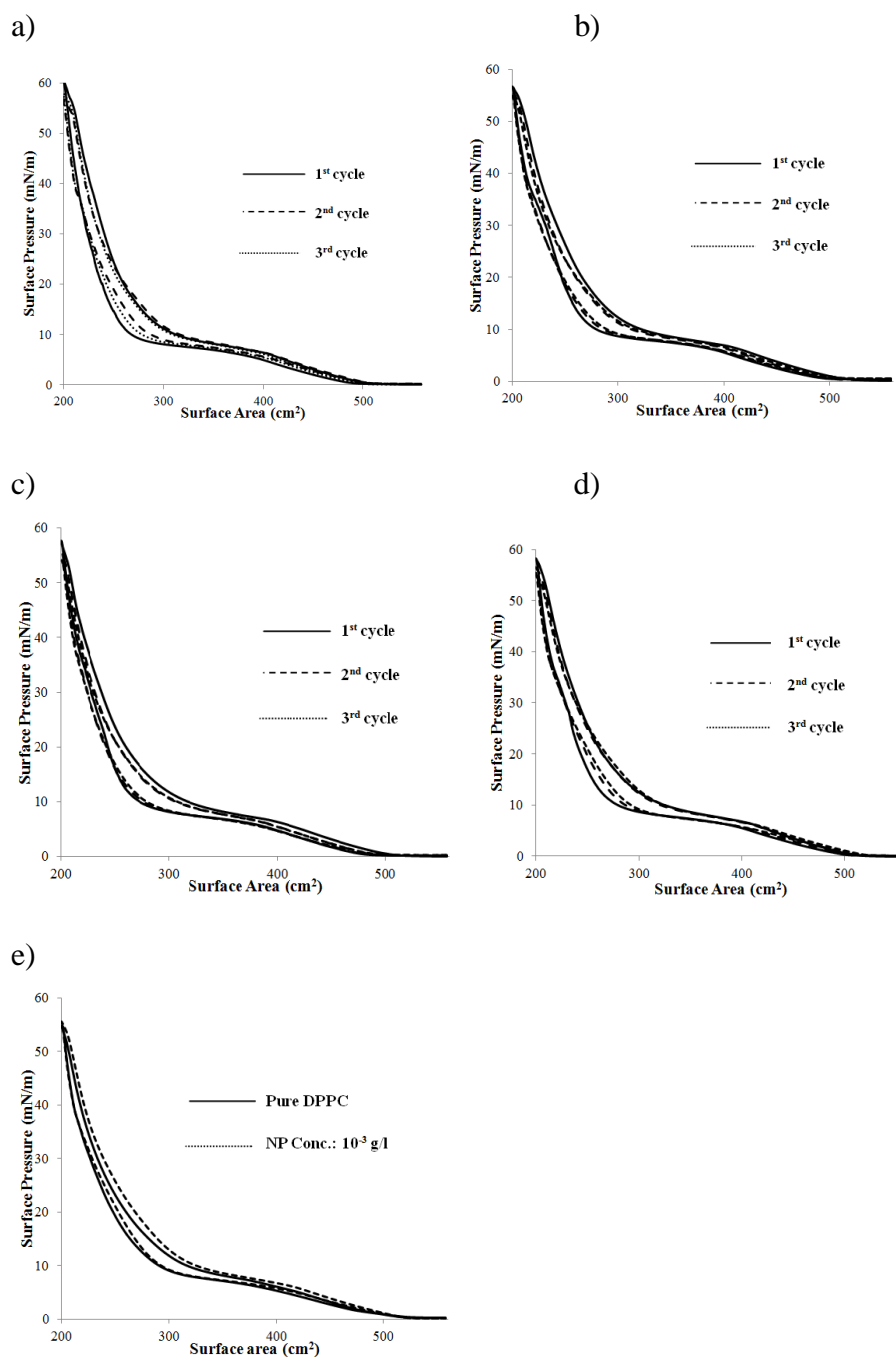
Figure 3-7. Surface pressure vs. surface area isotherms showing hysteresis behavior of DPPC films during three consecutive compression and expansion cycles performed on (a) pure subphase, or a subphase containing (b) 10^{-5} g/L, (c) 10^{-4} g/L (c) or (d) 10^{-3} g/L of 0.2 μm CML particles. An overlay of the third compression-expansion cycle for pure DPPC (bold line) and DPPC in the presence of 10^{-3} g/L of CML particles (dashed line) is shown (e). The compression-expansion cycles were performed between surface areas of 558 cm^2 and 200 cm^2.

Table 3-3. Hysteresis areas determined from surface pressure vs. surface area isotherms after sequential compression-expansion cycles of pure DPPC monolayers and DPPC monolayers after subphase injection of 10^{-5}, 10^{-4} and 10^{-3} g/L of 0.2 μm CML particles shown in Figure 3-7.

Cycle #	Hysteresis Area (mN/m·cm^2)			
	Control	10^{-5} g/L	10^{-4} g/L	10^{-3} g/L
1st cycle	943.6 ± 199.8	1022.3 ± 297.6	937.8 ± 176.3	1030.4 ± 196.3
2nd cycle	653.1 ± 83.5	661.4 ± 150.8	653.1 ± 111.1	812.4 ± 41.3[*]
3rd cycle	643.6 ± 96.1	662.5 ± 46.4	596.6 ± 118.8	802.8 ± 45.3[*]

* Significant change compared to control.

on surface pressure isotherm of DPPC has also been shown by Aroti and colleagues[71] with various concentrations of sodium iodide in the subphase. In both cases, adsorption of negative ions to the monolayer has been suggested to have an electrostatic screening effect on the dipole moments of DPPC, lowering the electrostatic repulsion between DPPC molecules which arises from oriented dipoles in the ordered phases. Consequently, the surface becomes more fluid in the LE-LC and the beginning of the LC region and surface pressure rises with an increased slope in that region. As the carboxyl modified polystyrene particles used in the current study are negatively charged, it is likely that we hypothesized that the same electrostatic screening effect was responsible for the observed changes to the surface pressure isotherms.

Changes in the surface pressure of the LE-LC and LC phases of DPPC surface pressure isotherm have also been reported in several previous studies with negatively charged nano- and sub-micron particles. Negatively charged hydrophobic poly(butyl cyanoacrylate) (PBCA) nanoparticles have improved the function of DPPC in the LE-LC and the beginning of LC region.[64] Ku and colleagues[66] have shown that the presence of gelatin particles in the subphase improved surfactant function leading to higher surface

pressures at fixed surface areas. The same effect on the LE-LC phase of DPPC isotherm has also been observed after exposure of DPPC to silica particles.[60, 63] Ku et al.[66] showed that these particles reduce the dipole moment of DPPC molecules, which resulted in lower electrostatic repulsion between ordered molecules. This would reduce the intermolecular spacing between the DPPC molecules and result in more compact solid domains. To investigate the effects of negatively-charged particles on surfactant microstructure in the present studies, the size of solid domains were examined using fluorescence microscopy techniques.

3.4 Particle Effects on Surfactant Microstructure

3.4.1 Off-line Surface Pressure Measurements

Surfactant microstructure studies were performed in a PMMA minitrough light enough to be mounted on a microscope stage. Surface pressure values were measured at various compression ratios to find the surface pressure pertaining to each fluorescent image. Different compression ratios were used for fluorescent and confocal microscopy with each ratio being identified by a mark on the PMMA trough. The values of surface pressure at different marks are presented in Tables 3-4.

As shown in Table 3-4, it was possible to perform off-line surface pressure measurements on the Langmuir-Wilhelmy setup and use them for fluorescent imaging. Naturally, the standard deviation values reported with hand compression are higher than those reported with the symmetric automatic compression by computer controlled barrier drive (Table 2-1). To ensure that manual compression did not change the behavior of the surface pressure isotherm, a complete surface pressure isotherm was performed with manual compression on Langmuir-Wilhelmy balance (Figure 3-8).

As seen in Figure 3-8, hand compression did not change the behavior of the surface pressure isotherm. This confirmed that the interfacial behavior of DPPC is not significantly affected by hand compression of the barriers and hand compression of the

Table 3-4. Surface pressure values at different compression ratios in the PMMA trough
used for fluorescent microscopy, values were measured by marking the trough
at certain surface areas, manually compressing the barriers and recording the
surface pressure at each barrier position.

Barrier Position #	Surface Pressure (mN/m) (average ± standard deviation)
1	0.9 ± 1.1
2	1.3 ± 1.6
3	2.5 ± 2.1
4	5.7 ± 1.9
5	6.6 ± 2.0
6	10.1 ± 2.2
7	12.3 ± 1.9
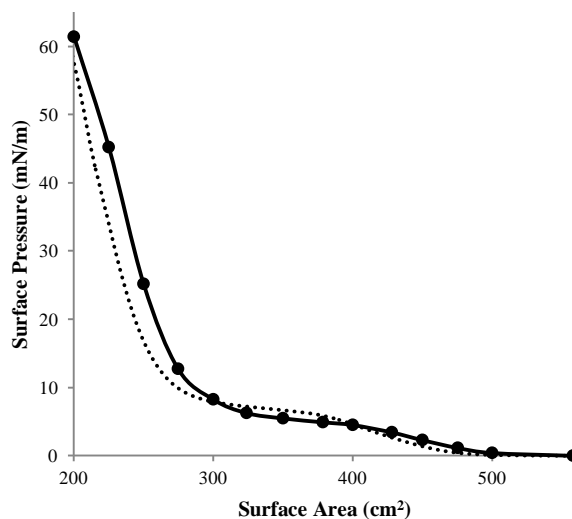
Figure 3-8. Hand compression of the barriers on the trough on the Langmuir-Wilhelmy
setup (solid marks, bold line is drawn to guide the eye) did not cause a
significant change in the surface pressure vs. surface area isotherm of DPPC
using computer-controlled symmetric compression (dashed line).

barriers could be used for fluorescent microscopy experiments.

3.4.2 Imaging with Fluorescent Microscopy

Surfactant microstructure was analyzed using fluorescent microscopy. The probe Texas-RED-DHPE was used to provide between the liquid expanded and liquid condensed phases of DPPC. Due to its size, the probe is squeezed out of the condensed phases and partitions into the fluid phase providing contrast between phases.[161, 162]

Studies of surfactant microstructure of pure DPPC in the absence of particles showed typical growth of solid lipid domains upon compression on a subphase containing salts[110, 166] (Figure 3-9-a to d). The size of the lipid domains is determined by a balance
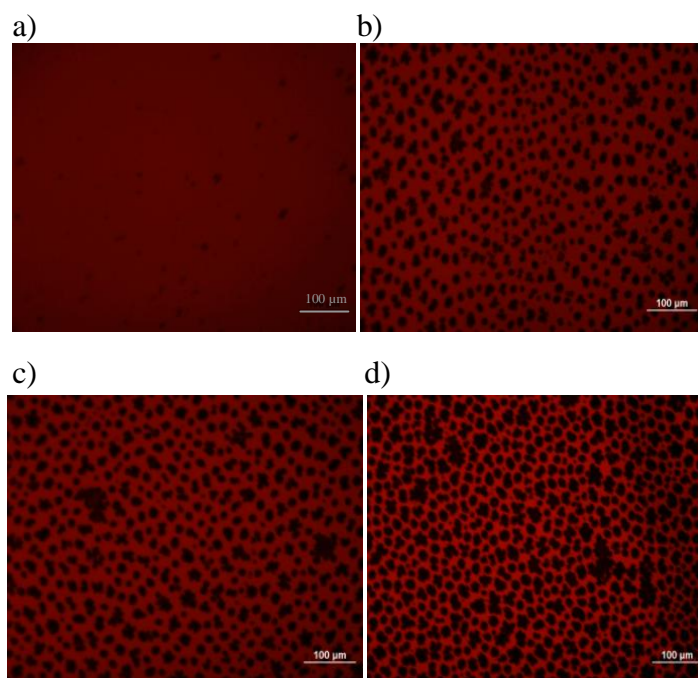
Figure 3-9. Fluorescence images of DPPC doped with Texas Red-DHPE. The lipid domains (black spots) are distinguishable from the liquid lipid (red). Images were acquired at surface pressures of 0.9 ± 1.1 mN/m (a), 5.7 ± 1.9 mN/m (b), 6.6 ± 2.0 mN/m (c) and 12.3 ± 1.9 mN/m (d). Bar = 100 μm.

between two forces: the repulsive force between the oriented dipoles of DPPC that elongates the domain and the line tension that keeps the domain in a compact shape.[89, 167]

Monolayer compression draws DPPC molecules in close proximity of each other resulting in an increase in the repulsive force of DPPC dipoles which leads to the enlargement of domain areas. This was confirmed by analyzing the surface area covered by the lipid domains. The surface coverage of condensed domains increased from $30.46 \pm 1.76\%$ at a surface pressure of 5.7 mN/m (Figure 3-9-b) to $53.10 \pm 2.62\%$ at a surface pressure of 12.3 mN/m (Figure 3-9-d). It should be noted that although DPPC domains are generally known to have a triskelion shape,[167] the presence of salts in the subphase alters the microstructure of DPPC and results in rounder solid lipid domains slightly different from those observed on pure water.[71] This phenomenon is suggested to be a result of electrostatic screening of surfactant dipoles by ions in the subphase.[71]

The addition of 10^{-3} g/L of polystyrene particles to the subphase significantly affected the microstructure of DPPC (Figure 3-10-a to d). In the presence of particles domain growth upon compression was suppressed and smaller but more numerous domains could be observed. Analysis of surface coverage of lipid domains confirmed these observations. The surface coverage of lipid domains in the presence of particles increased from $28.63 \pm 1.37\%$ at a surface pressure of 5.7 mN/m (Figure 3-10-a) to $43.58 \pm 0.98\%$ at a surface pressure of 12.3 mN/m (Figure 3-10-d) showing a 10% reduction in the surface coverage of lipid domains for pure DPPC and resulting in a more fluid surface.

The effect of particles on the growth of lipid domains was concentration dependent, with the reduction in domain size being a function of particle concentration (Figure 3-11). This effect of particles was quantified by measuring the area of lipid domains at each surface pressure and each particle concentration and creating histograms with bin sizes of 10 μm^2. These histograms followed the same trends at all surface

pressure values at which imaging was performed. The histograms at 10.1 mN/m are shown as a representative in Figure 3-12.
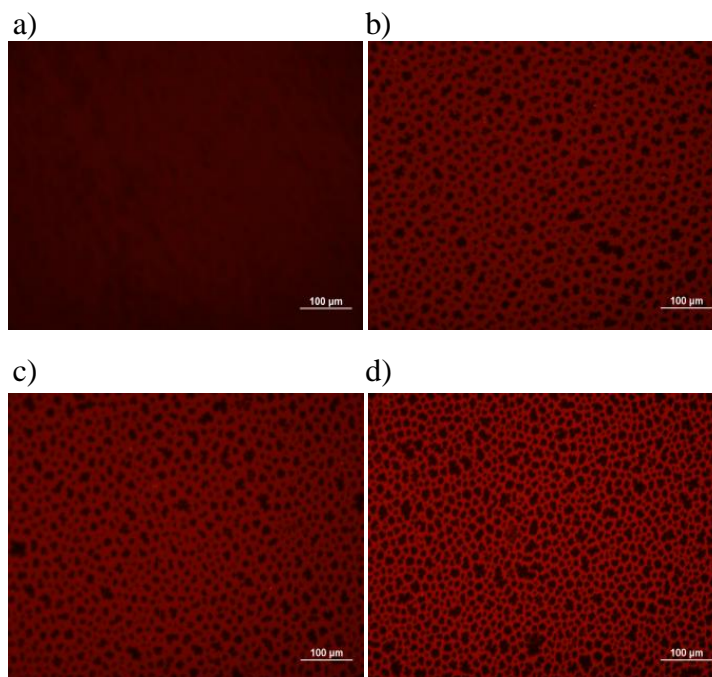
Figure 3-10. Fluorescence images of DPPC films doped with Texas Red-DHPE during surface compression on a subphase including 10^{-3} g/L of 0.2 µm CML particles. Presented images were acquired at surface pressures of 0.9 ± 1.1 mN/m (a), 5.7 ± 1.9 mN/m (b), 6.6 ± 2.0 mN/m (c) and 12.3 ± 1.9 mN/m (d). Bar = 100 µm.

The mode of the domain area reduced from 20 µm for pure DPPC to 10 µm in the presence of particles at all concentrations. In addition, the number of domains with an area less than 200 μm^2 increased with increasing particle concentration. For example, the domain count of the 10 μm^2 bin increased from 79 domains/mm^2 at a concentration of 10^{-5} g/L to 115 domains/mm^2 at a concentration of 10^{-4} g/L and 264 domains/mm^2 at a concentration of 10^{-3} g/L. This resulted in a more fluid surface, with the fraction of solid domains to the total area being reduced from $47.4 \pm 2.6\%$ for pure DPPC to $45.1 \pm 4.6\%$

at a particle concentration of 10^{-5} g/L, $39.6 \pm 1.5\%$ at a concentration of 10^{-4} g/L and 38.1

$\pm 3.4\%$ at a concentration of 10^{-3} g/L.
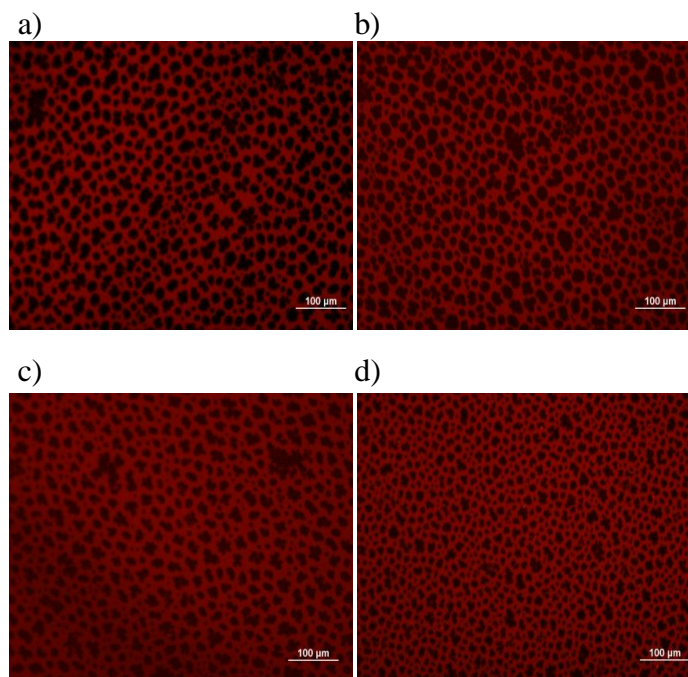
Figure 3-11. Fluorescence images of a) pure DPPC and DPPC with 0.2 µm CML at concentrations of 10^{-5} g/L (b), 10^{-4} g/L (c) and 10^{-3} g/L (d) at a surface pressure value of 10.1 ± 2.2 mN/m. The area of the lipid domains decreases as a function of particle concentration. Bar = 100 µm.

The microstructure studies suggest that the presence of particles suppressed the

growth of lipid domains leading to a more fluid surface. Similar results have been

reported in several other studies with charged hydrophilic particles including silica[60],

gelatin[75], and polyorganosiloxane.[64] Interestingly, a similar effect has also been observed

using hydrophobic alkylated gold nanoparticles. Tatur and Badia[69] have observed that

when DPPC monolayers are exposed to alkylated gold particles only a slight change is

observed in the surface pressure isotherm; however the microstructure of the DPPC

monolayer is significantly changed leading to a surface with "more numerous but smaller

domains",[69] both of these observations are in agreement with the current study.

a)

b)

c)

d)
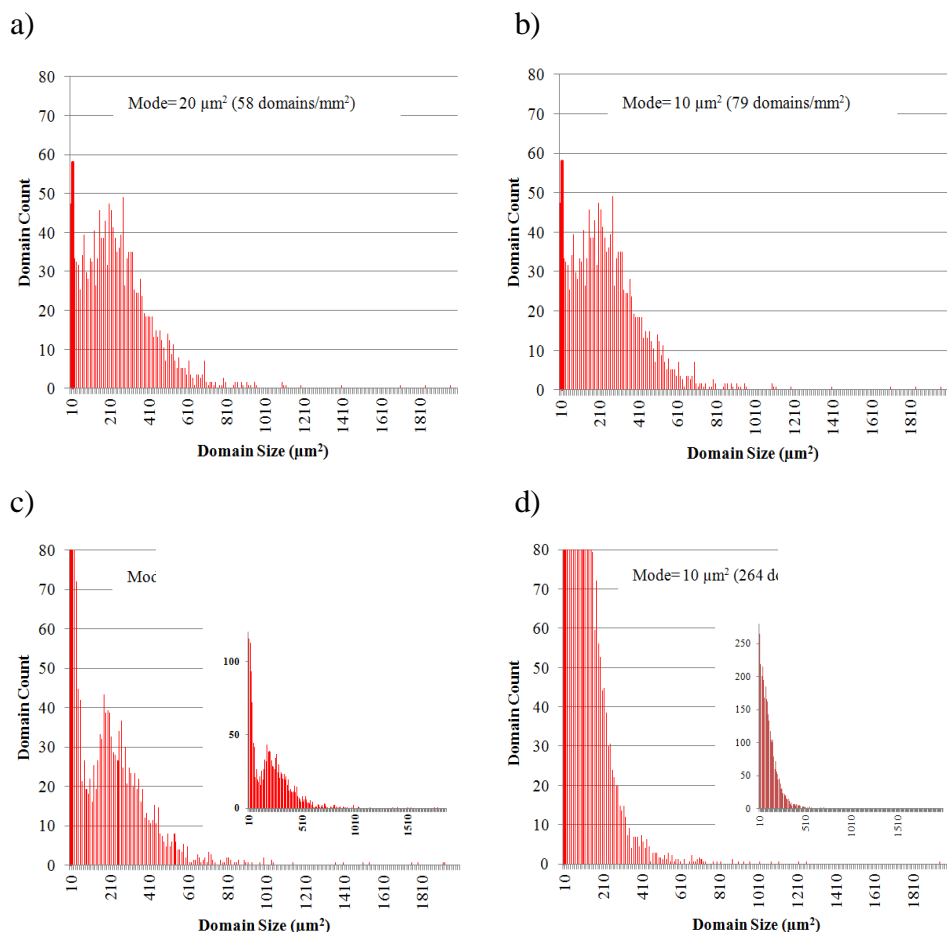
Figure 3-12. Histograms of the number of domains (domain count) as a function of domain size (μm^2) for pure DPPC (a) and DPPC after addition of 0.2 μm CML particles at concentrations of 10^{-5} g/L (b), 10^{-4} g/L (c) and 10^{-3} g/L (d). All histograms were generated from fluorescence microscopy images at a surface pressure of 10.1 ± 2.2 mN/m (shown in Figure 11. Bin size = 10 μm. Insets in c) and d) show the entire graph for those concentrations

It was mentioned earlier that the preferential adsorption of negative ions to the

surface is suggested to electrostatically screen the DPPC dipoles and result in more

compact domains.[71] Since the particles are showing a similar effect it is likely that negatively charged particles act to reduce the electrostatic force between the DPPC molecules through an electrostatic screening effect. This weakened repulsive force would change the domain force balance in lipid domains in favor of line tension and result in smaller lipid domains and a more fluid surface, as was observed in the current studies (Figures 3-11 and 3-12). These results also explain why a large hysteresis is maintained after multiple compression and expansion cycles at the highest particle concentration. As was mentioned above, some DPPC molecules are ejected to the subphase at the end of compression resulting in lower hysteresis and surface pressure for the following cycles. A fluidized surface provides less resistance for ejected molecules to readsorb to the surface compared to a crystalline surface. Thus, fewer molecules remain in the subphase after each cycle resulting in a more reproducible hysteresis. This phenomenon has been observed for binary films of DPPC and cholesterol, where the cholesterol fluidizes the monolayer[134] and results in significantly higher hysteresis compared to films of pure DPPC.[168]

3.5 Particle Placement and Effects on Surfactant Topology

Confocal imaging of the surface was performed in the PMMA minitrough with off-line surface pressure measurement similar to fluorescent microscopy imaging. Confocal imaging showed that negatively charged particles were mainly associated with the lipid domains of DPPC (Figure 3-13). A few particles (to a much lower extent) could be observed out of the domains as well. Association of particles with lipid domains has been reported in a previous study where hydrophobic particles surrounded the domains.[42] Particle placement in the current study demonstrated that particles were mainly associated with the center of the lipid domains. As the domains indicate areas of higher

dipole moments particle placement at their center suggests an electrostatic interactions between charged particles and lipids and further bolsters the likelihood of electrostatic screening. This phenomenon is similar to preferential adsorption of negative ions; however, the effect of negatively charged particles on surface pressure isotherms was not as significant as the effect of ions. The diameter of particles is several orders of magnitude higher than that of ions, likely making it difficult for them to penetrate the monolayer. Penetration of particles to the interface would result in space competition between particles and lipid molecules and inhibit surfactant function, which was not observed in the current studies. Therefore, it is logical to hypothesize that particles remain in the subphase and do not penetrate the interface. Surface topology studies were performed to examine this hypothesis.
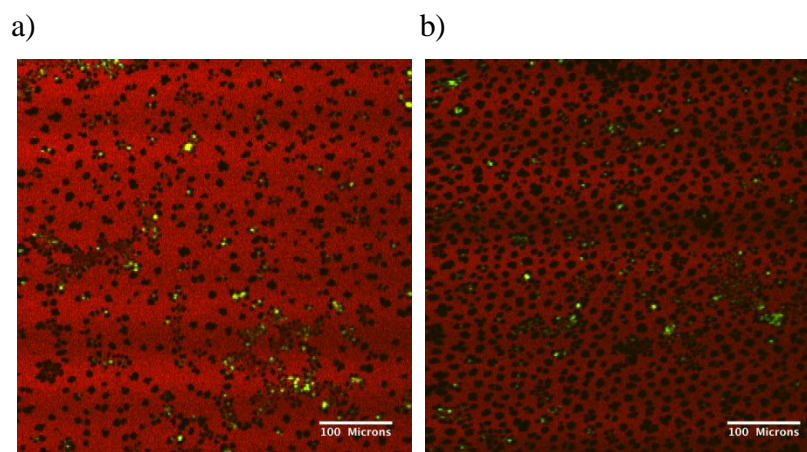
Figure 3-13. Confocal microscopy images of DPPC doped with Texas Red-DHPE and fluorescently labeled 0.2 μm CML particles at a concentration of 10^{-4} g/L at surface pressures of 5.7 mN/m (a) and 9.7 mN/m. Images were acquired after focusing on the air-water interface and the depth of field was 4 μm, Bar = 100 μm.

Surface topology of deposited monolayers after particle addition was studied using atomic force microscopy. The monolayers were deposited on hydrophilic mica after

subphase injection of the highest particle concentration (10^{-3} g/L) and at a surface pressure of 10 mN/m where significant changes in the microstructure were observed. Images were analyzed to determine the height of the lipid domains and determine whether or not particles have penetrated the air-water interface. A maximum height difference of 2.4 nm was observed between the LE and LC phases after height analysis of multiple images (Figure 3-14). This height difference is in good agreement with published values of 2.5 nm[60, 169] and 2.8 nm[170] reported for pure DPPC monolayers. This analysis confirms that no particles have penetrated the monolayer. Since the diameter of particles is two orders of magnitude higher than DPPC, it would significantly change the topology of the surface in case of penetration. This result is in agreement with the surface pressure vs. surface area isotherm studies (Figure 3-5) as particle penetration to the monolayer should significantly affect the shape of the isotherms.

a)

b)
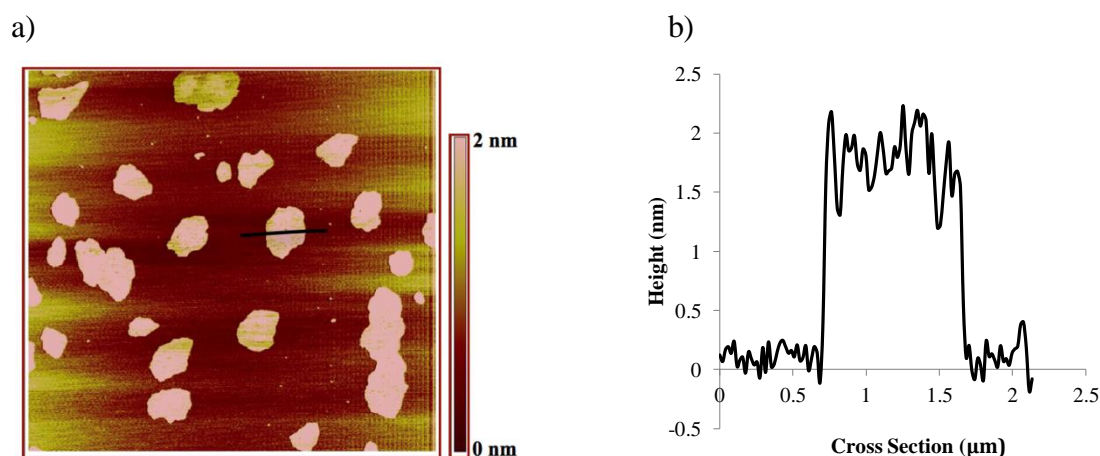
Figure 3-14. Surface topographical analysis performed using atomic force microscopy (AFM): (a) AFM image (10 μm x 10 μm) of a DPPC monolayer in the presence of 10^{-3} g/L of CML particles injected in the subphase and (b) a height analysis across the black line shown in (a). Monolayers were transferred on a mica substrate by vertical stroke at a rate of 5 mm/min at a surface pressure of 10 mN/m.

3.6. Conclusions

Interactions between DPPC monolayers and 200-nm negatively charged polystyrene particles injected in the subphase were examined. The presence of the particles in the subphase did not affect the surface pressure vs. surface area isotherms of DPPC when compressed for one cycle until monolayer collapse. However, significant changes in the hysteresis areas of the isotherms were observed at the highest particle concentration of 10^{-3} g/L. The formation of lipid domains was suppressed by the presence of particles with more numerous but smaller domains being observed. Confocal and atomic force microscopy experiments revealed that particles were mainly associated with the lipid domains but remained in the subphase and did not penetrate the monolayer. The results suggest that particles in the subphase reduced the repulsive force between DPPC headgroups, reducing the domain size of the ordered phase and leading to a more fluid surface. This same mechanism has been reported in the studies of DPPC monolayers and ions and is recently gaining attention in DPPC-particle systems. These results can be used to better understand the mechanisms of particle-surfactant interactions, which are critical in various fields such as environmental health and drug delivery.

CHAPTER 4

PARTICLE SURFACTANT INTERACTIONS FOLLOWING

SURFACTANT SPREADING ON A PARTICLE-LADEN SUBPHASE

4.1 Introduction

Studies of interfacial properties of phospholipid monolayers are of great interest for a variety of biological phenomena. Other than being the component with the highest concentration in lung surfactant, phospholipids are also the major components of biomembranes[17] and their interfacial properties play an important role in regulating the behavior of these membranes. For example, lung stability is highly dependent on the surface tension of the pulmonary surfactant that covers the alveoli. Also, interactions of biomembranes with biomolecules are controlled by properties such as surface tension and surface potential.[171-173]

With the advent of nanotechnology, studies of interactions between sub-micron particles and lung surfactant or biomembrane models have gained attention. Several studies have reported that interaction with fine particles inhibits surfactant function *in vitro*. Adverse effects on surfactant function have been observed with both environmental contaminants such as soot[45] or particle emissions from biofuel combustion[41] and therapeutically relevant particles such as gelatin[65, 66, 75] and hydroxy apatite[44] and a variety of mechanisms have been suggested to explain the interactions between the particles and surfactant models.[27, 39, 41, 44, 58, 174, 175]

Although valuable information has been gained by previous studies, several major discrepancies remain unanswered. For example, negatively charged polystyrene nanoparticles (60 nm) show only a very slight effect on surface activity of an endothelial cell membrane (ECM)[61] whereas the same particles with the same charge and almost similar (50 nm)[58] or larger size (100 nm)[59] show a significant inhibitory effect on Curosurf and Alveofact. Although difference in surfactant models could have caused the

difference in results, the difference in particle concentrations is likely to have significantly affected the results. The study on ECM[61] has used a particle concentration of 0.01 g/L whereas studies on Curosurf and Alveofact have used a maximum concentration of 0.5 g/L and 2 g/L respectively, thus observing an inhibitory effect. The difference in particle concentration between these studies is surprising and differences as large as 1000 times can be found in particle concentrations used in the literature.[41, 43, 60, 63] Moreover, in studies of pulmonary surfactant-particle interactions, it is of utmost importance to focus on realistic particle concentrations which can be determined by estimating the amount of airborne particles that deposit in the alveoli upon inhalation. Particle concentrations higher than such estimates can lead to inhibitory effects on the function of model surfactants that do not happen in real-life exposures.

Another major source of inconsistency can be observed in the studies that have used the Langmuir monolayers of phospholipids as a model to mimic pulmonary surfactant and biomembrane behavior. Three primary protocols are used for exposure of Langmuir monolayers to solid particles: surfactants and particles have been mixed beforehand and spread on the surface of the trough (mixing),[39, 42, 44, 57, 65, 75] particles have been injected into the subphase upon which a surfactant monolayer was already spread (subphase injection),[61, 62] or the monolayer has been spread on top of a subphase that already contained the particles (monolayer addition).[39, 43, 63-66] While the mixing protocol risks consequences such as surfactant adsorption to the particles before spreading, non-efficient spreading or particle dissolution in the solvent for certain particles, the last two methods seem to be equally close to the physiological situation for a biomembranes study. Although, both particle injection and monolayer addition methods result in the same system (particles in the subphase and monolayer on top), the particle-surfactant interactions may change as a result of using different protocols. Understanding whether and how different particle introduction protocols affect particle interactions with the surfactants, can help explain some of the discrepancies observed in previous studies.

In the previous chapter, the interactions between DPPC monolayer (a commonly used biomembrane and pulmonary surfactant model[42, 43, 60, 63, 64, 66, 80-82, 176]) and negatively charged polystyrene particles (200 nm) were studied (following the particle injection method). The objective of the present study was to elucidate the mechanisms of interactions in the same system using the monolayer addition method using dynamic surface tension, surface potential and fluorescent microscopy experiments. These results were compared with the subphase injection protocol to clarify how different interaction methods can affect particle-surfactant interactions. Finally, a summary of particle concentrations previously used for particle-surfactant interactions have been provided and compared to realistic concentrations to help understand some of the inconsistencies in the literature.

4.2 Materials and Methods

4.2.1 Commercial Reagents

Dipalmitoyl phosphatidylcholine (DPPC) was purchased from Genzyme Pharmaceuticals (Cambridge, MA) and used without further purification. Texas Red-dihexadecyl phosphatidyl ethanolamine (Texas Red-DHPE) was purchased from Molecular Probes (Eugene, OR). Sodium chloride, calcium chloride and HPLC-grade chloroform were purchased from Sigma-Aldrich (Sigma-Aldrich, St. Louis, MO). All water used in experiments was obtained from a Barnstead NANOpure II system from Barnstead International (Dubuque, IA) and had a resistivity of 18.2 MΩ·cm. Carboxyl modified polystyrene particles were purchased as suspensions from Invitrogen (Carlsbad, CA).

4.2.2 Surface Pressure versus Surface Area Isotherms

Tensiometric studies were conducted using a Langmuir-Wilhelmy apparatus (Minitrough System 4, KSV Instruments Ltd., Finland). The experiments were performed

similar to section 2.7 of Chapter 3. Briefly, the trough was filled with a freshly made subphase solution, which was allowed to equilibrate to room temperature (23.3 ± 0.6 °C) for 30 min, then aspirated to remove any surface impurities. Then the DPPC monolayers were obtained by spreading fifty microliters of 1.22 g/L surfactant solution using a Hamilton microsyringe and allowing 20 minutes for chloroform evaporation. The surface was compressed and expanded with a barrier speed of 10 mm/min (1.5 $Å^2$/molecule.min). For particle-surfactant interaction studies, a mixture of the subphase containing suspended particles at different concentrations from 0.001 g/L to 0.1 g/L was added to the trough, then the DPPC monolayer was spread on the surface (monolayer addition).

For dynamic compression-expansion experiments, the surface of the trough was compressed to 200 cm^2 (mean molecular area of 40 $Å^2$/molecule) and expanded to the fully expanded area of 558 cm^2 (mean molecular area of 111.5 $Å^2$/molecule) three times. The area between the compression and expansion curves (hysteresis area) was calculated using KaleidaGraph v. 3.6. For monolayer collapse experiments, the surface of the trough was compressed to 100 cm^2 (mean molecular area of 20.6 $Å^2$/molecule), with no subsequent expansion. Data in all experiments were acquired approximately every second during surface compression and expansion and were recorded using the LayerBuilder software. The dilational elasticity (C_s^{-1}) of the isotherm was calculated using Equation 1 in Chapter 2, the surface pressure and surface area values needed for this equation were recorded using the LayerBuilder software and plotted in Microsoft Excel.

4.2.3 Fluorescent Imaging

Fluorescenct microscopy experiments were performed using an Olympus BX-51 microscope (Olympus, Center Valley, PA) similar to Section 2.2.8. Briefly, a small poly (methylmethacrylate) (PMMA) minitrough (7.5 cm x 12 cm x 0.6 cm) was washed and and mounted on the microscope stage. The trough was filled with 60 mL of subphase in which 0.06 mg, 0.6 mg or 6 mg of washed and lyophilized particles were dispersed. Five

microliters of a 1.22 g/L DPPC in chloroform solution doped with about 1 mol% of the fluorescent probe Texas-Red-1,2-dihexadecanoyl-*sn*-glycero-3-phosphoethanolamine, triethylammonium salt (Texas-Red-DHPE) was added on top of the subphase for imaging. Texas-Red DHPE preferentially partitions into the fluid phases allowing for studies of structure of lipid domains which appear as black dots in the LE-LC phase of the surface pressure isotherm. A filter with an emission range of 573-648 nm was used to enable visualization of the Texas-Red probe. Twenty minutes was allowed for the evaporation of chloroform after which the surface of the trough was compressed manually using Delrin barriers and images of the microstructure were acquired at each surface pressure. To reduce the movement of lipid domains with air current a cardboard shield was placed on top of the microscope for all imaging experiments.

Off-line surface pressure measurement was performed similar to Section 3.2.8. Briefly, the PMMA trough was placed on the Wilhelmy plate setup and filled with the subphase upon which DPPC-Texas Red solution was spread. The surface pressure was changed by reducing the surface area of the trough by hand compression of Delrin barriers. The surface areas at which the desired surface pressure values were reached were marked on the side of the trough. These marks were used as guides for barrier compression on the microscope stage.

4.2.4 Surface Potential Measurements

Surface potential during monolayer compression were measured using a surface potential sensor (SPOT, KSV-NIMA, Finland), which is based on the vibrating plate (Kelvin) method.[177, 178] The sensor consists of a probe head with a plate which vibrates at 140 Hz and is connected to an electrode which is submerged in the subphase. The vibration of the plate results in an electric current due to the difference in the potential of water surface and the vibrating plate. A DC voltage in the opposite direction compensates the difference in potential and reduces the current to zero. At this point the voltage is

equal to interfacial potential and is recorded. Surface potential measurements were performed after spreading forty-five microliters of a 1.22 g/L DPPC solution on the subphase, with and without suspended particles. For measurements, the probe head was maintained 1 to 2 mm above the surface and surface potential values were recorded as the surface was being compressed from an initial surface area of 558 cm^2 (124 Å^2) to a final area of 180 cm^2 (40 Å^2) which is just above the limiting cross-sectional area of DPPC molecules (reported as 39 Å^2 by Hauser and colleagues[112]). The mean molecular of 124 Å^2 used for surface potential studies is higher compared to the mean molecular area of 111.5 Å^2/molecule used for surface pressure studies. This is due to the fact that changes in the surface potential of Langmuir monolayers usually occur at higher mean molecular areas compared to the changes in surface pressure[179], thus using a higher initial mean molecular area would allow for recording the changes that occur at high mean molecular areas. Surface potential of the monolayer during compression was measured with respect to the potential of the expanded monolayer which was taken as zero. Surface potential data upon compression were recorded approximately every second using the Layer Builder software.

Since surface potential measurements are susceptible to a drift with time,[180] the surface potential sensor was allowed to operate on a clean subphase prior to each experiment and the drift in the value of surface potential as a function of time was recorded. This drift function was then added to the surface potential experiments in the presence of surfactant to compensate for the drift effects that occurred with time. The conventional Helmholtz equation (Equation 1) was used to estimate surfactant dipole moment, $\Delta\mu$ (in units of Debye: 3.33×10^{-30} C.m), from the surface potential data:

$$\Delta\mu = \varepsilon\varepsilon_0 \Delta V a \tag{4-1}$$

where ε is the relative permittivity of the monolayer and is generally considered to be equal to one[33, 66] although values between 5 to 10 have also been suggested[181], ε_0 is the

relative permittivity of free space (8.85×10^{-12} F/m), ΔV is the surface potential (in units of Volts) and a is the mean molecular area (in units of Å^2/molecule).

4.3 Results

4.3.1 Tensiometric Studies

4.3.1.1 Particle Effects on Surface Pressure Isotherms of
Pure Subphase

Particles were examined for their surface activity in tensiometric experiments. A particle concentration of 0.1 g/L (the maximum concentration used with DPPC monolayers) in the subphase induced no significant effect on the surface pressure vs. surface area isotherm in the absence of DPPC (Figure 4-1).
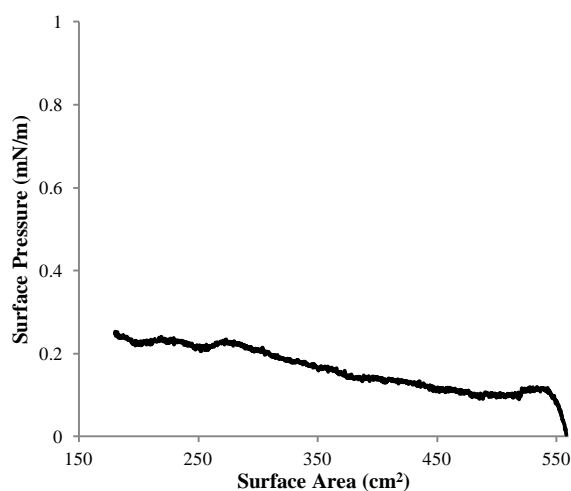
Figure 4-1. The surface pressure vs. surface area isotherm of 0.1 g/L of 0.2 μm CML particles after one compression between the surface areas of 558 cm^2 and 180 cm^2 with no DPPC added on the surface.

As depicted in Figure 4-1, the surface pressure remained below 0.2 ± 0.2 mN/m after compressing the particles from an initial area of 558 cm^2 to a final area of 180 cm^2

confirming that the particles are thoroughly washed and no surface-active component is present in particle suspensions.

4.3.1.2 Particle Effects on Surface Pressure Isotherms

During Compression to Collapse

The surface pressure vs. surface area isotherm of a DPPC monolayer on pure subphase is shown in Figure 4-2 (bold line). These isotherms showed a shape and phase behavior similar to those previously reported in the literature.[37, 113] The maximum surface pressure achievable was 72.3 ± 0.4 mN/m, demonstrating a near zero surface tension at collapse as expected for pure DPPC monolayers (Table 4-1).[37, 39] At low concentration of 0.2 μm CML particles in the subphase (0.001 g/L) no changes were observed in the surface pressure isotherm. However, in the presence of higher concentrations of particles, the isotherm shifted to the right (higher surface pressure values at fixed surface areas) (Figure 4-2). At a particle concentration of 0.01 g/L, an increase in the surface pressure of the LE-LC and the LC phases of the surface pressure isotherm was observed. The shift in the isotherm was most significant at the highest concentration of 0.1 g/L, where an increase in the surface pressure of all phases of the isotherm was observed.

In addition, a partial collapse of the monolayer at a surface pressure of 53.2 ± 5.0 mN/m in the presence of 0.1 g/L of particles (Figure 4-2, dashed line). This partial collapse of the monolayer was concentration dependent and was not observed at the lower particle concentrations. Following this partial collapse, a maximum surface pressure of ~72 mN/m could still be observed with further compression (Table 4-1).

Partial monolayer collapse has been observed with mixtures of immiscible components in a Langmuir monolayer, with the first collapse attributed to loss of one of the components from the interface.[81, 182] Thus, a partial collapse is a likely indication of particle penetration into the DPPC monolayer. Considering that this partial collapse is preceded by an increase in the surface pressure values at fixed surface areas in the surface

pressure isotherm, it is reasonable to hypothesize that the particles have penetrated to the monolayer (causing the shift to the right) and squeezed out of the monolayer (causing the partial monolayer collapse). Partial collapse was not observed at lower particle concentrations suggesting that particle penetration to the monolayer is concentration dependent. A similar concentration dependency on collapse has been noted for DPPC monolayers exposed to endohedral metallofulerene particles.[57] Final monolayer collapse was observed at a surface pressure of about 72 mN/m for all particle concentrations studied. Such high surface pressures can only be obtained with a pure DPPC monolayer[38], suggesting that the particles were squeezed out from the monolayer and entered the subphase before the end of compression. Particle squeeze-out from surface-active monolayers has previously been reported for polystyrene particles.[61]
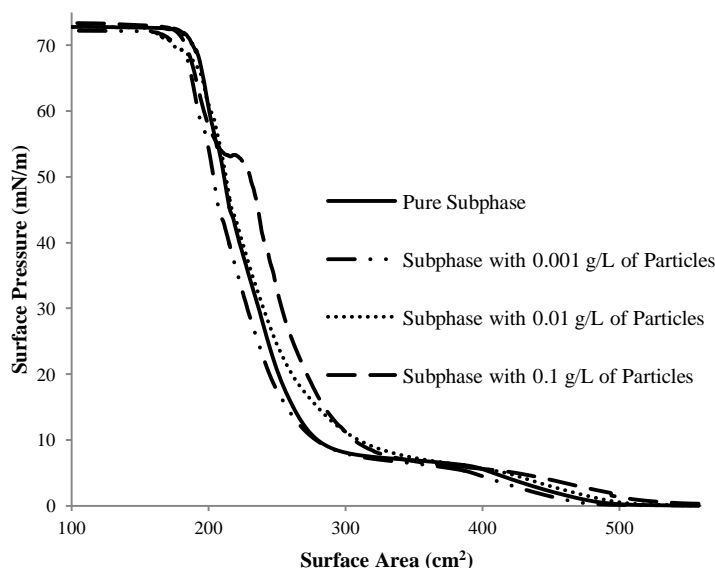
Figure 4-2. Surface pressure vs. surface area plots of DPPC on pure subphase and subphase containing various concentrations of 0.2 μm CML particles after one compression from an initial surface area of 558 cm^2 to a final area of 100 cm^2. All monolayers collapsed at a surface pressure of ~72 mN/m. A second, partial collapse is observed for the DPPC monolayer on a subphase containing 0.1 g/L of particles at a surface area of 233 $\pm$ 9 cm^2.

Table 4-1. Collapse surface pressures and surface areas determined from surface pressure vs. surface area isotherms after compressing pure DPPC films (control) and DPPC films on a subphase containing 0.2 µm CML particles at concentrations of 0.001, 0.01 and 0.1 g/L, all isotherms were generated by compressing the monolayer from an initial area of 558 cm^2 to 100 cm^2.

	Final Collapse Surface Pressure ± Standard Deviation (mN/m)	Surface Area at Final Collapse ± Standard Deviation (cm^2)	Partial Collapse Surface Pressure ± Standard Deviation (mN/m)	Surface Area at Partial Collapse ± Standard Deviation (cm^2)
Pure DPPC	72.3 ± 0.4	174 ± 3	---	---
Particle Conc.: 0.001 g/L	72.1 ± 0.4	166 ± 4	---	---
Particle Conc.: 0.01 g/L	71.7 ± 0.4	162 ± 14	---	---
Particle Conc.: 0.1 g/L	72.6 ± 0.5	173 ± 3	53.2 ± 5.0	233 ± 9

Since the penetration of particles to the DPPC monolayer is likely to affect monolayer rheological properties, the effects of particles on the dilational elasticity of the monolayer were also examined with and without 0.1 g/L of particles in the subphase. The plot of dilational elasticity of pure DPPC monolayer has been presented in Chapter 3 and was biphasic with two maxima observed at surface areas of 437 ± 21 cm^2 and 214 ± 4 cm^2 referring to the LE and the LC phase (Figure 4-3-black line) relating to the maximum elasticity of the monolayer in each phase. In the presence of 0.1 g/L of particles both maxima shift to a higher surface area (483 ± 11 cm^2 for the LE phase and 241 ± 7 cm^2 for the LC phase) (Figure 4-3-gray line). This is in agreement with the surface pressure vs. surface area isotherms and further confirms the shift in the isotherm to higher surface areas. In addition, the presence of 0.1 g/L of particles almost doubled the maximum value

of dilational elasticity (578.1 ± 165.1 mN/m compared to 239.6 ± 39.1 mN/m on pure subphase). Such a significant increase in the dilational elasticity is unlikely to refer to an actual increase in monolayer rigidity and is likely caused by the irregular shape of the surface pressure isotherm before the premature collapse. However, even if this maximum point is not considered, comparing the trends of dilational elasticity plots confirms that the presence of the particles has shifted the dilational elasticity plots to the right and has increased the values of elasticity in the LC phase denoting a more rigid monolayer in the presence of particles. The maximum point of dilational elasticity is immediately followed by a sharp drop in the elasticity of the monolayer corresponding to the premature collapse. After this drop, the elasticity values increased again followed the trend observed for the pure DPPC monolayer until the end of compression.

The dilational elasticity data are in agreement with the hypothesis that particles have penetrated the DPPC monolayer. The presence of particles shifted dilational elasticity plot to the right, suggesting the presence of a more compact film. Also, higher values of dilational elasticity were observed in the presence of particles, an indication for the presence of a more rigid monolayer. While the increase in dilational elasticity indicated a more rigid monolayer in the LC phase, the substantial drop in elasticity of the monolayer was an indication of a sudden loosening of the monolayer packing. Slight reductions in dilational elasticity are attributed to the presence of a more loosely packed monolayer.[43, 80] However, the drastic decrease observed in this case is probably a sign of monolayer destruction or desorption of molecules from the air-water interface. This is in agreement with the results from the surface pressure isotherms where a partial monolayer collapse was observed likely due to the squeeze out of particles from the monolayer.
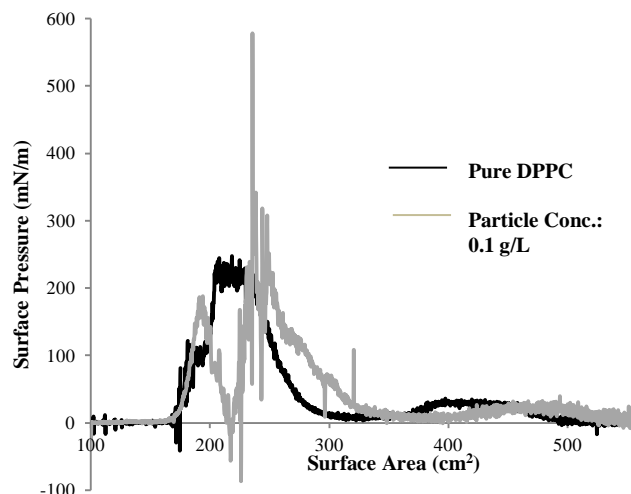
Figure 4-3. Plot of dilational elasticty versus surface area calculated from the surface pressure vs. surface area isotherms presented in Figure 4-2. Black curve= no particles. Grey curve= particle concentration of 0.1 g/L.

4.3.1.3 Particle Effects on Surface Pressure Isotherms

During Compression-Expansion Cycles

Given the significant effect of particles on the surface pressure isotherm of DPPC monolayers, it was of interest to study the potential effects of particles on monolayer respreading ability. Thus, the interfacial behavior of DPPC monolayers was studied by sequential compression and expansion after exposure to particles. In these experiments, DPPC monolayers were compressed to a surface area of 200 cm^2 so that collapse did not occur, then fully expanded, and repeated for two additional cycles. The surface pressure regimes (gas, LE, LE-LC, and LC phases) that were apparent in the collapse experiments were also observed in the compression-expansion cycles of pure DPPC monolayers (Figure 4-a). However, lower surface pressures were observed during expansion, leading to a hysteresis effect caused by non-efficient respreading of DPPC molecules at the air-water interface.[125] The effects of particles on the respreading efficiency of DPPC was

studied by monitoring the maximum surface pressure at the end of each compression

cycle.

a)

b)

c)

d)
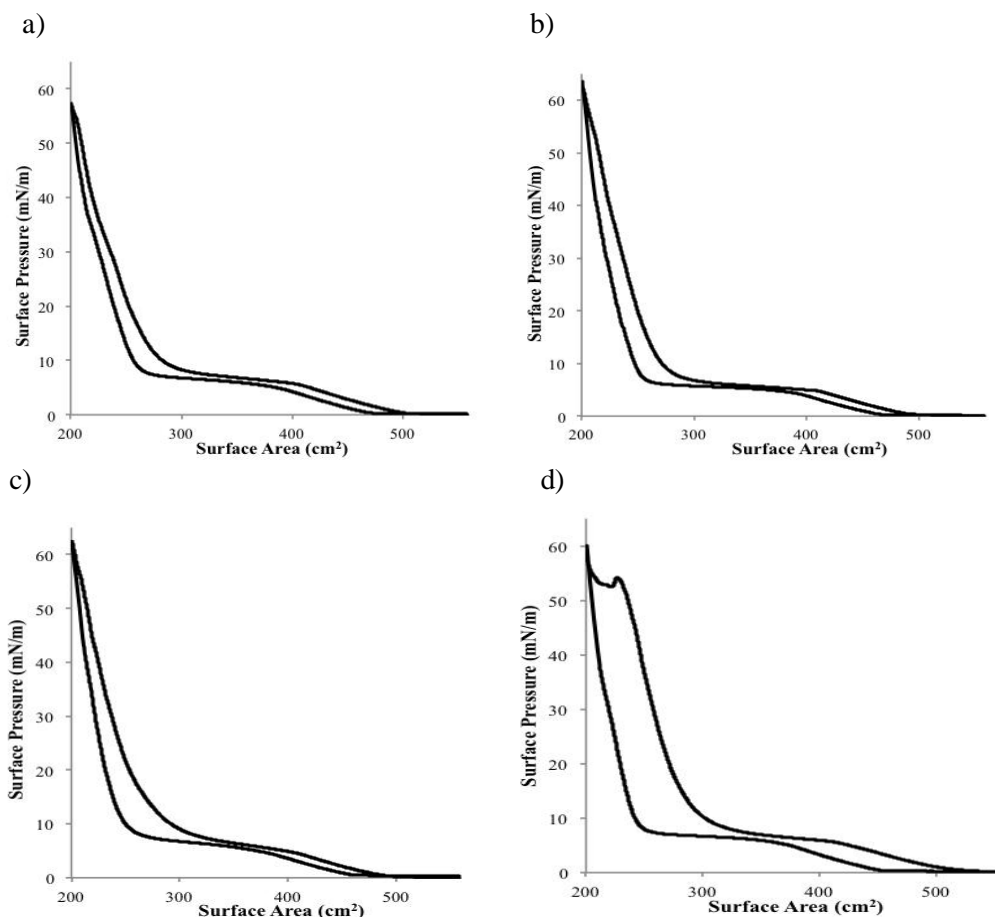
Figure 4-4. DPPC surface pressure isotherms performed with consecutive compression and expansion between surface areas of 558 cm^2 and 200 cm^2 (first cycle is shown) on the subphase containing a) no particles or, b) 0.001 g/L, c) 0.01 g/L and d) 0.1 g/L of 0.2 μm CML particles. In each figure, the upper curve represents surface compression and the lower curve represents expansion.

Addition of 0.2 μm CML particles to the subphase induced concentration–

dependent changes in the hysteresis behavior of DPPC monolayers (Figures 4-b to 4-d).

At low particles concentrations of 0.001 and 0.01 g/L, no significant changes were

observed in the hysteresis area or the maximum surface pressure obtained after sequential

compression cycles (Table 4-2). However, at the highest particle concentration of 0.1 g/L, significant changes were observed in the hysteresis area. At this particle concentration, the hysteresis area of the first cycle of the DPPC surface pressure isotherm was significantly increased from 750.2 ± 118.7 to 2109 ± 334.9 (mN/m·cm^2) (Figure 4-d). Particle effects on hysteresis area only occurred during the first cycle and other cycles were not affected by the presence of the particles.

Table 4-2. Hysteresis areas and maximum surface pressures obtained during sequential cycling of pure DPPC films (control) and DPPC films after monolayer addition of 0.2 μm CML particles at concentrations of 0.001, 0.01 and 0.1 g/L, all isotherms were generated by consecutive compression and expansion of the monolayer from an initial area of 558 cm^2 to 200 cm^2 for three cycles.

	Hysteresis Area (mN/m·cm^2)			Maximum Surface Pressure (mN/m)		
	1st Cycle	2nd Cycle	3rd Cycle	1st Cycle	2nd Cycle	3rd Cycle
Pure Subphase	750.2 ± 118.7	539.9 ± 195.9	543.1 ± 214.7	58.3 ± 2.2	56.2 ± 1.4	54.6 ± 1.7
0.001 g/L of Particles	475.6 ± 423.2	378.1 ± 154.3	331.2 ± 173.2	62.0 ± 2.1	57.0 ± 2.6	55.5 ± 1.4
0.01 g/l of Particles	986 ± 339.4	556.9 ± 40.9	519.5 ± 65.3	$63.2 \pm 2.0*$	59.5 ± 2.3	57.1 ± 2.5
0.1 g/l of Particles	$2109 \pm 334.9*$	554.0 ± 108.6	539.8 ± 112.1	58.5 ± 2.0	54.6 ± 1.6	$51.2 \pm 1.8*$

* Significantly different from control

Hysteresis is created when surfactant molecules are expelled from the surface at reduced surface areas and cannot respread at the air-water interface fast enough to participate in the following compression-expansion cycles.[97, 118, 125] The substantial increase in the hysteresis area observed in this study suggests that in the presence of

particles either more molecules are ejected from the interface upon collapse or that the ejected molecules take a longer time to readsorb from the subphase. Interestingly, the effects of 0.1 g/L of particles on the hysteresis area of the monolayer are restricted only to the first compression cycle. This is a likely indication that particles are squeezed out from the monolayer during the first cycle and do not affect DPPC respreading during the following cycles.

The presence of particles also affected the maximum surface pressure obtained at the end of each compression cycle. At the end of the first cycle, the presence of lower particle concentrations increased the maximum surface pressure and a significant change was observed at a concentration of 0.01 g/L (63.2 ± 2.0 mN/m compared to 58.3 ± 2.2 mN/m for pure subphase). Also, the presence of 0.1 g/L of particles in the subphase reduced the maximum surface pressure obtained at the end of the third compression cycle from 54.6 ± 1.7 mN/m (pure subphase) to 51.2 ± 1.8 mN/m (subphase with 0.1 g/L of particles) (Table 4-2).

Particle effects on the maximums surface pressure at the end of compression are further evidence for particle penetration into the monolayer causing the monolayer to be more packed. At the highest particle concentration of 0.1 g/L no effect on the maximum surface pressure of the first cycle was observed likely due to particle squeeze out and premature collapse of the monolayer before the compression ended. It is likely that some DPPC molecules are also ejected from the air-water interface along with the particles during this plateau region. This is further supported by the reduction in the maximum surface pressure of the third compression cycle that is observed at the highest particle concentration.

4.3.2 Surface Potential Studies

The changes induced in the surface pressure isotherm of DPPC by carboxyl modified polystyrene particles suggest that particles penetrate into the monolayer and

increase monolayer packing. Surface potential is a result of the sum of DPPC dipoles in the normal direction[180, 183, 184] and thus can be studied to provide information about the packing and alignment of DPPC monolayer in the presence of particles.

4.3.2.1 Measurement of Surface Potential Drift Over

Surface potentiometers are susceptible to a drift over time with respect to the reference (clean subphase).[180] As one compression cycle lasted approximately 25 minutes, this drift was likely to affect the data and needed to be documented. Changes in the surface potential with respect to pure subphase over 50 minutes for six experiments are presented in Figure 4-5.
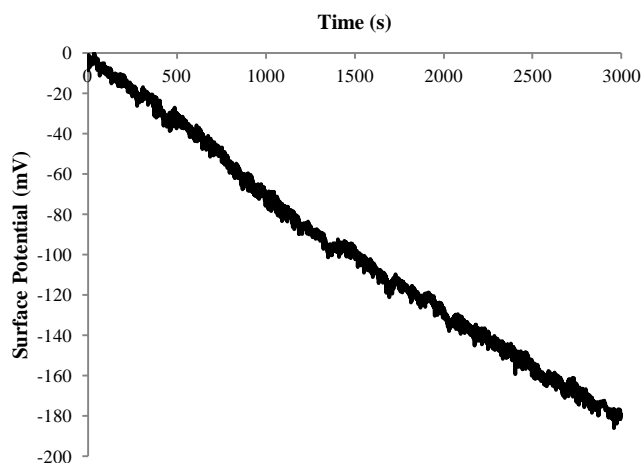
Figure 4-5. The plot of surface potential vs. time with the potentiometer held on clean subphase for 3000 seconds (50 minutes). The drift in surface potential was linear with time.

As demonstrated in Figure 4-5, the drift in surface potential was linear and negative in all experiments. After 50 minutes, the drift in potential was equal to -180 ± 42 mV showing a drift average of -0.06 mV per minute. This allowed for running a drift

experiment before each surface potential experiment and adjusting for the drift after each experiment.

4.3.2.2 Surface Potential Isotherms of Pure DPPC

The surface potential isotherm of DPPC on pure subphase was generated (Figure 4-6-a) and showed the typical shape observed in previous reports[25, 33, 166, 185] (Figure 4-6-b). Surface potential is related to the sum of DPPC dipoles in the normal direction and increases as the surface is compressed and the molecules become vertically aligned before a plateau at low mean molecular areas is observed. Due to the high standard

a)   b)
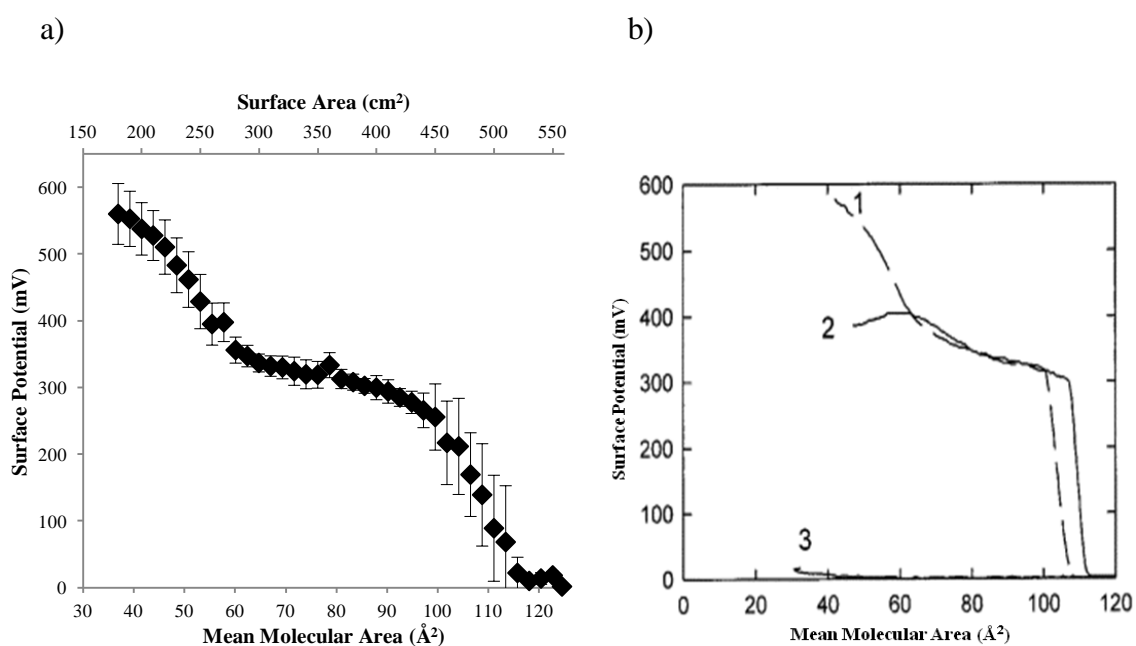
Figure 4-6. Surface potential vs. mean molecular area and surface area isotherm of DPPC during surface area reduction from 558 cm^2 to 180 cm^2 (a) was in agreement with previously published plots of surface potential vs. mean molecular area of DPPC (b). In Figure (b), Curve 1 represents the surface potential plot of DPPC, Curve 2 represents the surface potential plot of DPPC in the presence of 10^{-7} M of the peptide gramicidin and Curve 3 represents the surface potential plot of 10^{-7} M of gramicidin without DPPC. All plots in (b) are generated on a subphase of 30 mM Tris and 100 mM KCl at pH of 7.5 (b). Figure (b) was reproduced with permission.[185]

deviations at large surface areas it was difficult to find the exact mean molecular area of the initial rise in potential. However, this area was estimated to be 114 $Å^2$ and occurred at higher mean molecular areas compared to the rise in surface pressure (101.3 ± 2.4 $Å^2$) as is well known in the literature.[179, 180] Further compression resulted in a sudden increase in only a small reduction in surface area. This sudden rise in surface potential has been suggested to be the result of hydrogen bonding between DPPC headgroups and water molecules.[186] Such hydrogen bonding reduces the local permittivity as the previously free water molecules will now be bound to the monolayer and increases the surface potential for a fixed dipole moment according to Helmholtz equation (Equation 4-1). With further compression a plateau in surface potential is observed which is in good agreement with the plateau in surface pressure. Once the LC phase is reached, compression of the monolayer results in increase in increase in surface potential as the packing density of DPPC molecules at the air-water interface is increased.

The DPPC dipole moment during surface compression was estimated from the surface potential data using the Helmholtz equation assuming a relative permittivity of 1 for the monolayer and was also in agreement with previous reports that have made a similar assumption (Figure 4-7-a and b).[33, 66] Surface compression at large mean molecular areas results in a sudden rise in DPPC dipole moment which shows little change upon further compression. These estimations are in agreement with the previously published estimations of Ku and colleagues[66] who have suggested that "fairly early on upon closing the mini-trough barriersthe headgroup dipoles reorient perpendicularly and do not change during the mono-film compression".
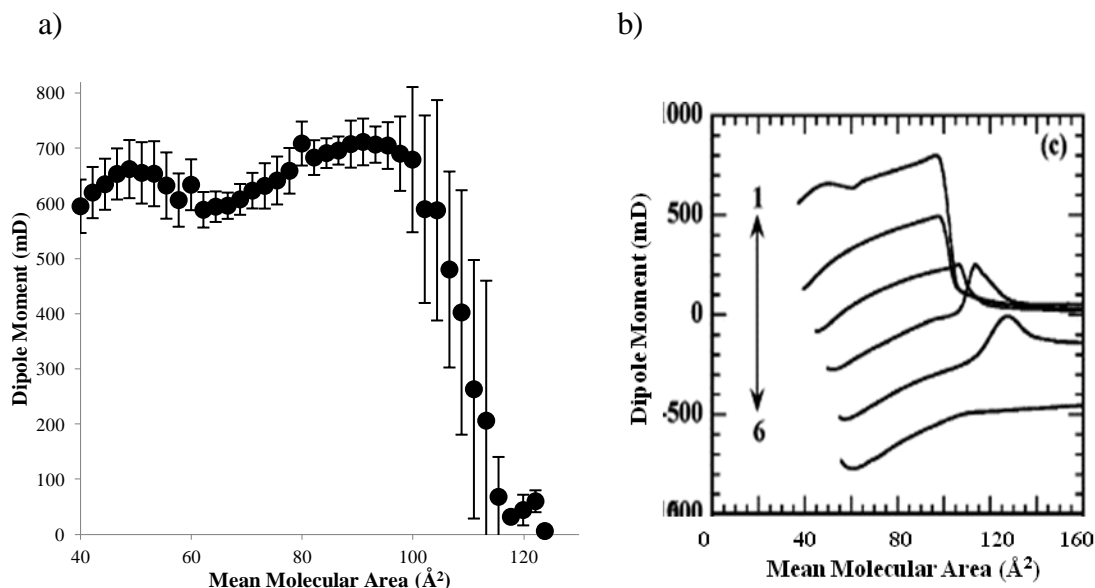
Figure 4-7. Dipole moment vs. mean molecular area plot of DPPC during mean molecular area reduction from 124 $\mathring{A}^2$ to 40 $\mathring{A}^2$ (a) was in agreement with previously published plots (b). In Figure (b) Curve 1 represents the dipole moment of DPPC, and Curves 2 to 6 represent the dipole moment of DPPC in the presence of increasing molar ratios of fluorinated amphiphilic molecule F8PH5PPhNa. All plots in (b) are generated on a subphase of 0.03 mM Tris and 0.13 mM NaCl at pH of 7.4 (b). Figure (b) modified from Hoda and colleagues[33] and reproduced with permission.

4.3.2.3 Particle Effects on Surface Pressure Isotherms of

Pure Subphase

The effects of particles dispersed in the subphase on the surface potential was examined by studying the surface potential at the highest particle concentration (0.1 g/L) used in this study. The presence of particles in the subphase reduced the surface potential by about 60 mV when the surface was compressed from an initial area of 558 cm^2 to a final area of 180 cm^2 in the absence of DPPC (Figure 4-8). When pure DPPC monolayers were compressed on a clean subphase the maximum surface potential was 560 ± 46 mV, thus the changes in surface potential observed in the presence of particles were approximately 10% of the changes observed for pure DPPC monolayers. The negative sign of surface potential for the particles suggests that some particles can reach the air-

water interface and cause an electron transfer toward the water surface where the positive

ions gather to screen the negative charge of the particles.
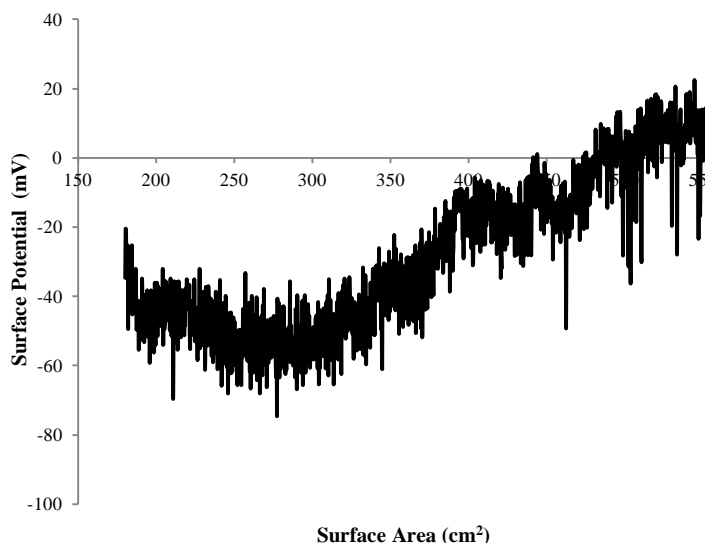
Figure 4-8. The surface potential vs. surface area plot generated by compressing the surface of the subphase including 0.1 g/L of 0.2 μm CML particles between the surface areas of 558 cm^2 and 180 cm^2 with no DPPC added on the surface.

4.3.2.4 Particle Effects on Surface Pressure Isotherms of

DPPC

The presence of 0.1 g/L of particles in the subphase induced no statistical

difference between surface potential values of DPPC monolayers compared to surface

potential values measured on pure subphase below a surface area of 500 cm^2 (Figure 4-9).

However, at surface areas higher than 500 cm^2, a significant increase in the surface

potential was observed in the presence of particles. For example, at a surface area of 530

cm^2 the surface potential was increased from 10 ± 1 mV on pure subphase to 97 ± 25 mV

in the presence of particles. The same trend was also observed in comparing the dipole

moments, providing evidence that the monolayer is either more compressed or vertically aligned in the presence of particles.
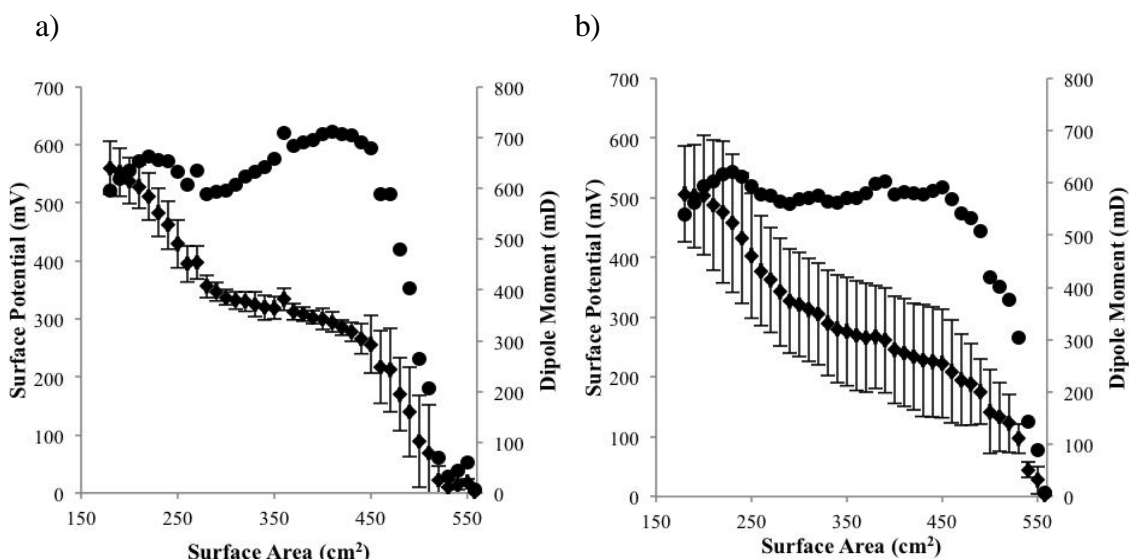
Figure 4-9. Surface potential (♦) and dipole moment (●) of DPPC monolayers as a function of surface area performed on a) pure subphase and b) subphase containing 0.1 g/L of particles. Monolayers were compressed from an initial area of 558 cm^2 to an area of 180 cm^2.

The main contributor to the surface potential of DPPC is the carbonyl group.[166] The carbonyl group is a strongly polar moiety in which the oxygen molecule is directed toward water[187] causing a positive potential in the normal direction as the molecules are compressed. Thus, more packed or vertically aligned monolayers show higher surface potentials due to higher dipole moment density in the normal direction. The increase in surface potential in the presence of 0.1 g/L particles compared to pure subphase demonstrates that the particles have increased the packing or the alignment of the monolayer. This phenomenon further supports particle penetration to the monolayer.

Particle penetration reduces the area available to DPPC molecules causing an "artificial compression" effect and increasing the packing of the monolayer and the surface potential.

Comparing Figures 4-9-a and b, it becomes clear that the presence of particles has resulted in large fluctuations in surface potential. These fluctuations are likely due to electrostatic interactions between surfactant dipoles and the particles. It has been suggested that negatively charged particles can perturb the packing of DPPC monolayers through electrostatic interactions between the charged groups on the particles and the ammonium group on DPPC.[43] Such perturbations in DPPC packing can result in changes in the alignment of dipoles and affect the measured potential. Particles might also screen DPPC dipoles as previously reported for negative ions adsorbed to DPPC monolayers[71] which will also affect the surface potential. Such perturbations are likely to modify the arrangement of DPPC molecules at the interface and potentially reduce the normal component of dipole moment. On the other hand, the presence of particles at the interface results in a more compact monolayer which increases the surface potential. The presence of these two mechanisms with opposite effects on surface potential is likely to have contributed to the fluctuations in surface potential values.

4.3.3 Studies of Surfactant Microstructure

The effects of particles on DPPC microstructure were studied using fluorescent microscopy. Since the size of the ordered DPPC phases is dependent on the distance between surfactant molecules, these studies provide further evidence on the changes in monolayer packing induced by particles. The microstructure of pure DPPC showed the typical growth of the ordered surfactant phases upon compression which were in

agreement with previous studies.[110, 166] Representative images of DPPC microstructures are presented in Section 3.3.2 and are also presented in Figure 4-10-a.

The presence of 0.2 CML particles in the subphase resulted in significant changes in the microstructure of DPPC. Particles caused an increase in the fraction of the surface covered by the ordered phases (which appear black under fluorescent microscopy) suggesting the presence of a more compact monolayer. The presence of particles appeared to facilitate the fusion of the ordered DPPC phases with connected and large blocks of ordered phases visible in the presence of particles (Figure 4-10 a to d).This effect appeared to be concentration dependent and was most significant at a particle concentration of 0.1 g/L where the surface was almost completely covered with ordered phases even at low surface pressures (Figure 10-d). Pure DPPC domains show fast movement at the air-water interface at low surface pressure values, this movement slows down as the surface pressure increases. At the surface pressures used for imaging, pure DPPC domains showed fast movement even at a surface pressure of 8.4 mN/m. However, in the presence of particles, this movement was restricted and the monolayer was almost completely still at a surface pressure of 5.2 mN/m (data not shown) which is further evidence that the monolayer is more compressed in the presence of particles.

A few previous studies have focused on the effects of sub-micron particles on DPPC microstructure.[42, 63, 69] All of these studies have shown a slight increase in the surface pressure of the LE-LC region in the presence of particles followed by a reduction in the fraction of the ordered phases.[42, 63, 69] Hindrance in domain nucleation[42, 69] or formation of lipid-particle complexes governed by elestrostatic interactions[63] have been suggested as the mechanisms for reduction in the area of ordered phases. Interestingly, an increase in the fraction of ordered phases is observed for the first time in the current study. Interestingly, an increase in the size of the ordered DPPC phases has been reported after the addition of nonoxynol-9 (a non-ionic surfactant) to the monolayer.[188] The addition of this molecule also increased the surface pressure at fixed surface areas in all

3.3 ± 1.7 mN/m   5.2 ± 1.8 mN/m   8.4 ± 3.8 mN/m
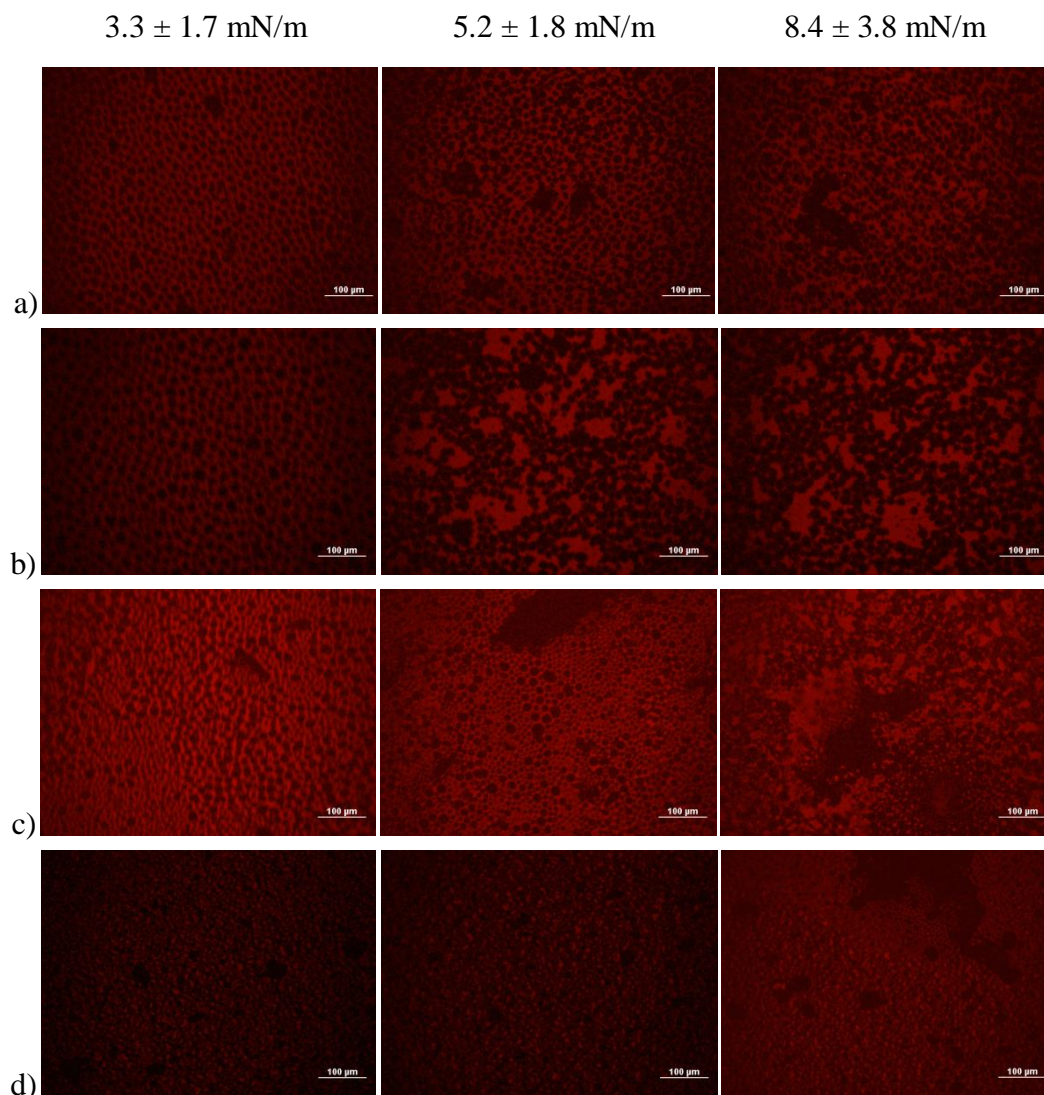
Figure 4-10. Fluorescence images of DPPC films doped with Texas Red-DHPE during surface compression on a subphase containing no particles (a), 0.001 g/L (b), 0.01 g/L and 0.1 g/L of 0.2 μm CML particles (d). Presented images were acquired at surface pressures of 3.3 ± 1.7 mN/m (left panel), 5.2 ± 1.8 mN/m (middle panel) and 8.4 ± 3.7 mN/m (right panel), bar = 100 μm.

phases of the DPPC surface pressure isotherm and the authors suggested that this molecule has an 'artificial compression' on the monolayer,[188] both the observation and the conclusion are in agreement with the current study.

It is difficult to interpret the effects of particles on the forces governing the size of lipid domains. It is known that the size of the domains is controlled by a balance between line tension (which favors larger and rounder domains) and electrostatic repulsion between DPPC dipoles (which favors smaller domains with elongated features).[89, 167, 189] It is logical to assume that the presence of negatively charged particles would reduce domain sizes due to increased electrostatic repulsive forces. This seems to be the case at least at a particle concentration of 0.1 g/L; however, a concentration dependence for this effect cannot be confirmed from microscopy images. Changes in line tension by the particles have been suggested before[69] but are unlikely to be the case here as these changes are associated with elongated domains as observed in studies of DPPC and cholesterol.[190]

4.3.4 Mechanisms of Interaction and The Role of Particle Introduction Protocols

Several potential mechanisms have been proposed to explain changes observed in the biophysical behavior of monolayers due to interactions with particles. Particle adsorption to the interface and competition for the available surface area between particles and surfactant molecules,[39, 57] release of surface-active material from the particles,[174] adsorption of surfactant molecules to the surface of particles[44, 58, 59] and formation of particle-surfactant complexes[43] are all potential mechanisms by which particles affect surfactant function.

For the system investigated in the current study, several of the above mentioned mechanisms can be ruled out. Adsorption of surfactant molecules to particles suggested by several group[44, 58, 59] or hampering surfactant adsorption at the interface suggested by Bakshi and colleagues[41] can be ruled out based on the observations in surface pressure isotherms and dilational elasticity plots. DPPC adsorption to the surface of particles is likely to cause one of two scenarios: 1. Reduction the amount of available lipids at the

air-water interface in which case the maxima of dilational elasticity should shift to lower surface areas, or 2. Disruption of monolayer packing in which case the values for dilational elasticity should decrease as observed with other materials that cause disorder in the monolayer.[60] None of these effects are observed in the dilational elasticity plots. Also, release of surface-active material from the particles did not occur as confirmed by the experiments with the particles dispersed in the subphase without surfactant addition (Figure 4-1). Formation of DPPC-particle complexes as suggested by Guzman and colleagues[43] cannot be ruled out but is unlikely to be the only mechanism of effect as it has shown only slight effects on DPPC isotherms at higher concentration studied by Guzman and colleagues.[43]

Based on the results from surface pressure, surface potential and surfactant microstructure studies, the particles penetrate into the DPPC monolayer and form a more compact monolayer before being squeezed out upon compression and leave a pure DPPC monolayer. Thus the mechanism of interaction appears to be particle adsorption to the interface and competition for the available surface area with surfactant molecules. Thus, the following explanation for the interactions between particles and DPPC monolayers can be proposed: at large surface areas, adsorption of particles to the interface results in a more compact DPPC film compared to the films on pure subphase solution. This more compact film generates a higher initial surface potential and with compression results in higher surface pressures at all surface areas (Figure 4-11-a). At lower surface areas, particles interfere with the compression of DPPC molecules and get squeezed out of the interface causing a partial collapse in the surface pressure isotherm and leaving a pure DPPC monolayer at the air-water interface (Figure 4-11-b). The remaining DPPC film undergoes further compression and collapses at a surface pressure of ~72 mN/m (Figure 4-11-c). This mechanism of interaction is in agreement with the proposed mechanisms for some of the previous studies of DPPC-particle interactions and has been suggested for

interactions between DPPC and biofuel combustion emissions[39] and endohedral metallofulerenes.[57]
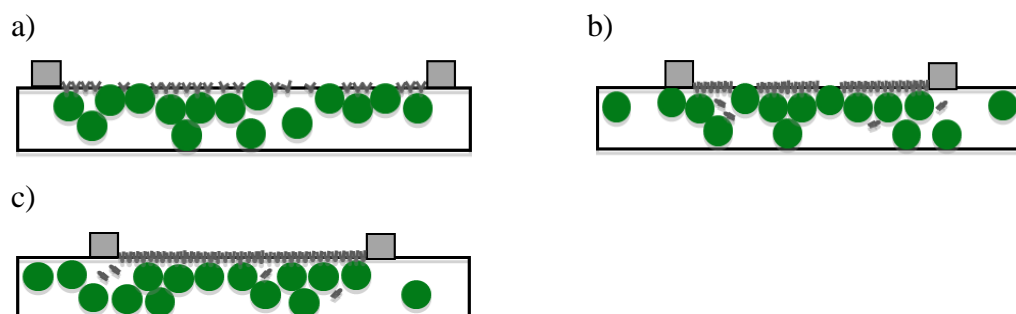
Figure 4-11. A schematic of particle-DPPC interactions during surface compression. At the start of compression, the presence of particles reduces the area between DPPC molecules resulting in higher surface potential and surface pressure (a), further compression results in ejection of particles along with some DPPC molecules from the interface reducing the slope of surface pressure increase at the end of the LC phase (b), this leaves a pure DPPC monolayer at the surface which can reach near zero surface tension at collapse (c). Figure not to scale.

The mechanisms of interaction between DPPC and particles showed a strong dependence on the particle introduction protocols. The mechanism suggested in this study in which the particles are introduced using the monolayer addition protocol (i.e. particles mixed with the subphase and surfactant spread on top) is different from the mechanism suggested in the subphase injection protocol (i.e. surfactant spread on the interface and particles injected into the subphase). When studied at the same particle concentration, the surface pressure isotherms generated following different particle introduction protocols look distinctly different (Figure 4-12).

Using the subphase injection protocol, a particle concentration of 0.1 g/L did not induce significant changes in the LC phase of the surface pressure isotherm (Figure 4-13-a). This is in agreement with the study of Peetla and Labhasetwar[61] who have used the same protocol to study the interactions polystyrene nanoparticles and surfactant

a)

b)
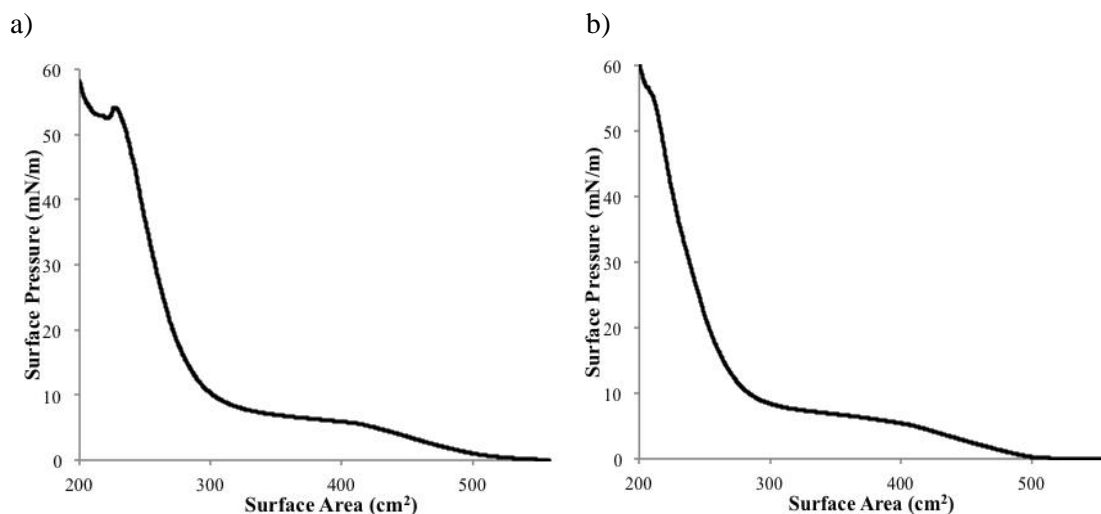
Figure 4-12. Comparison of the surface pressure vs. surface area isotherms obtained using a) addition of monolayer on top of a subphase containing the particles (monolayer addition method) and b) injection of particles in a subphase upon which the monolayer is already spread (subphase injection method). Both experiments were performed by surface compression between surface areas of 558 cm^2 and 200 cm^2.

monolayers and reported that carboxyl modified polystyrene particles "seem to squeeze out of the monolayer; hence the isotherm in their presence is almost similar to that without NPs (nanoparticles)". In comparison, the monolayer addition method resulted in particle adsorption to the interface resulting in a more packed DPPC film as corroborated by the premature, partial collapse of the monolayer (Figure 4-12-b). This method has been more commonly used in the literature and significant effects on the surface pressure isotherm by the particles have been reported.[39, 64, 65]

Interestingly, a similar effect has been observed in the binary systems of surfactant and proteins before, where the order of addition of a protein to a surfactant monolayer was switched and resulted in different interfacial behavior due to the ability of the protein to compete for space at the interface.[191] In this study, when bovine serum albumin (BSA) was injected to the subphase after spreading the surfactant monolayer,

BSA was unable penetrate the interface and the surface pressure isotherm reflected only the presence of the surfactant. However, when BSA was introduced to the subphase before the surfactant was spread on the surface, the BSA absorbed to the interface and the resulting film showed interfacial properties similar to that of a pure protein film.

A similar effect may have occurred in other particle-surfactant systems studied in literature. For example, sub-micron gelatin particles have been shown to cause a reduction in the surface pressure of DPPC monolayers in one study,[65] but induce an increase in the surface pressure of DPPC monolayers in another study by the same research group.[66] While not directly compared by the researchers, a review of the experimental details of these studies suggests that the observed differences in surface tension between the two studies are due to differences in the particle introduction protocol. These observed changes based on the particle introduction protocol are important in understanding the mechanism of interaction between surfactant monolayers and foreign particles or molecules.

4.3.5 What Particle Concentrations Are Physiologically Relevant?

The surface pressure isotherms of DPPC monolayers in the presence of particles generated in this study (Figure 4-2) revealed that the effect of particles on surfactant function is concentration dependent. However, a review of the literature suggests that there is no consensus on the particle concentrations that should be used for similar studies. Particle concentrations of 0.01 g/L,[61] 0.5 g/L[58] and 2 g/L[17] have been used in previous studies of surfactant-polystyrene particle interactions and a difference of as much as 5000 times can be found in particle concentrations between different studies (Table 4-3, second column).

Physiologically relevant particle concentrations can be estimated from two different viewpoints: therapeutic (exposure to particles for pulmonary drug delivery

purposes) and occupational health (exposure to environmental fine particles at workplaces). In either case, at the highest deposition ratio, less than half of the inhaled particles deposit in the alveolar region of the lungs.[54] For drug delivery purposes, exposure to one gram of particles can be considered an extreme case. Adverse events such as coughing have been reported after inhalation of 0.3 g of particles[159, 160] and 0.6 g over two daily doses is the highest used for delivery to cystic fibrosis patients.[160] Assuming the highest deposition after exposure to one gram of particles results in the deposition of about 0.47 g of particles in the alveolar region. This can be considered the highest physiologically relevant value for drug delivery purposes. Typical fine particle (PM 2.5) concentrations at workplaces have been reported by Pui[192] and the highest particle concentration is reported for rice harvest (1180 μg/m^3). Assuming 15 breaths per minute with 500 mL of air intake in each breath and 9 work hours per day, a worker inhales 0.0047 g of particles in a day. At maximum deposition, half of these particles (0.0024 g) will reach the alveolar region in a day. Concentrations for exposure for longer than a day have not been considered in these calculations since surfactant components are constantly replenished in the lung with the longest turn over time being about 11 hours meaning that surfactant is replenished twice per day.[128]

In an actual case of exposure to particles, the concentration of particles in the alveolar subphase does not play a role in the exposure of surfactant to particles even though particle concentrations in the subphase would be high due to the low subphase volume. In actual exposure, particles deposit on the surfactant molecules from above which is very different from particle penetration to the monolayer from the subphase as is common in studies of surfactant-particle interactions. Consequently, particle concentrations with regards to surface need to be taken into account to relate the *in vitro* studies to *in vivo* phenomena. Knowing the surface area of the alveolar region (102 m^2 according to Stone and colleagues[3]), these concentrations can be calculated for the lungs and are 0.0046 g/m^2 for drug delivery exposures (the lowest concentrations used in the

current study results in the same surface concentration in our Langmuir trough) and 2×10^{-5} g/m^2 for occupational health exposures.

Finding the particle concentrations with respect to the surface in previously published studies is not possible as the fraction of the particles that penetrate the air-water interface is not known. In contrast to actual exposures, the assumption of having all particles at the surface is not true unless for very hydrophobic particles (e.g. carbon black) which have been used in physiologically relevant concentration of 0.0036 g/m^2 before.[63] However, hydrophilic particles have been used in much higher concentrations in the literature.[44, 60, 64] Even though it is expected that hydrophilic particles do not adsorb to the air-water interface, surface adsorption of many hydrophilic particles in the presence of surfactant (mainly due to charge interactions) has been confirmed in several studies.[42, 44, 60, 61] Thus, it is likely that the surface concentration of the hydrophilic particles will be between two extreme conditions: 1. All the particles in the subphase adsorb to the air-water interface and surface concentrations much higher than the physiologically relevant values will be obtained (Table 4-3, third column) and 2. The particles are homogenously spread in the subphase and values lower than the physiologically relevant concentrations will be obtained (Table 4-3, fourth column).

In the current study the premature plateau of the monolayer happened at 233 ± 9 cm^2 while the collapse plateau of pure DPPC occurred at a surface area of 174 ± 3 cm^2. If the premature plateau is solely caused by the presence of particles at the air-liquid interface, the 59 cm^2 difference between the premature plateau and collapse should have been occupied with particles. Using the hydrodynamic diameter of particles in the subphase (236 nm) and assuming that particles have a contact angle of 90 degrees on the interface (i.e. maximum surface area at the interface), a surface area of 59 cm^2 can be occupied by 3.5 mg of particles. This amount is about 14% of the mass of particles dispersed in the subphase and is surprisingly more than what is gained by homogenous spreading of particles in the subphase (8.6×10^{-5} mg). If an equal or higher percentage of

particles reach the surface in similar studies (which can be particularly true for studies with highly charged particles) it is likely that some of the particle concentrations used in the literature do not represent physiologically relevant values. While it is not possible to obtain the surface concentration of the particles previously studied in the literature, the examples mentioned above suggest that particle dispersion in the subphase is not a good mimic for studies of lung surfactant-particle interactions as particle interactions with surfactant is dependent on their affinity to the air-water interface.

In summary, the physiologically relevant particle concentrations are estimated as 0.0046 g/m^2 for drug delivery exposures and $2x10^{-5}$ g/m^2 for occupational health exposures. These particle concentrations can also be considered physiologically relevant in *in vitro* studies using a Langmuir trough. Depending on the trough subphase volume, the concentrations with regards to volume can be calculated for each instrument. However, to ensure that a certain particle concentration is physiologically relevant, a realistic particle introduction method (i.e. aerosolization) should be used. Aerosolization can overcome the uncertainties in particle concentration and the changes observed in particle-surfactant interactions based on the particle introduction protocols.

Table 4-3. A summary of previous studies on particle-pulmonary surfactant model interactions ordered by: (a) particle concentration in the subphase (second column), (b) considering all particles suspended in the subphase come to the surface (third column) and (c) considering all particles homogenously spreading in the subphase (fourth column).

Study	Particle conc. in subphase $(g/L)^a$	Surface conc. if all particles come to the surface (g/m^2)	Surface conc. if particles homogenously spread in the subphase (g/m^2)	Particle Type
Physiologically relevant for drug delivery	22.381^b	0.0049	0.0049	NA^c
Physiologically relevant for occupational health	0.114^b	0.00002	0.00002	NA
Bakshi et al.[41]	0.002	NA	NA	Gold
Peetla and Lahasetwar[61, 62]	0.01	0.022	0.0000006	Polystyrene
Fan et al.[44]	0.05	0.300	0.0000045	Hydroxyapatite
Stuart et al.[65]	0.1	0.81	0.0000187	Gelatin
Schleh et al.[58]	0.5	NA	NA	Titanium dioxide and Polystyrene
Kondej and Sosonowski[67]	0.864	NA	NA	Dust with high metal conc.
Sosonowski et al.[45]	1	NA	NA	Soot
Ku et al.[66]	1	8.1	0.00014	Gelatin
Al-Hallak et al.[64]	1	NA	NA	PCBA
Beck-Broichsitter et al.[59]	2	NA	NA	Polystyrene, PLGA, Eudagrit-E 100
Guzman et al.[43]	10	41.1	0.0003	Silica
Santini et al.[68]	10	41.1	0.0003	Silica
Guzman et al.[60]	10	41.1	0.0003	Silica

Table 4-3. Continued

Study	Particle conc. in subphase $(g/L)^a$	Surface conc. if all particles come to the surface (g/m^2)	Surface conc. if particles homogenously spread in the subphase (g/m^2)	Particle Type
Guzman et al.[63]	10	41.1	0.0003	Silica and carbon black
Guzman et al.[70]	10	41.1	0.0003	Silica

[a] Calculations performed based on an alveolar subphase volume of 21 mL.[193]
[b] NA: Not applicable
[c] Concentrations could not be found, either Langmuir trough was not used or trough dimensions were not given. in cases where multiple concentrations have been used the maximum concentration has been reported

4.4 Conclusions

Interactions between DPPC monolayers and 200-nm negatively charged polystyrene particles following the monolayer addition protocol were examined. DPPC function was altered at a particle concentration of 0.1 g/L, as marked by a shift in the isotherm to the right, a premature plateau in surface pressure and significant changes in hysteresis area. This result together with an early rise in surface potential suggested the adsorption of particles to the air-water interface causing an artificial compression of DPPC molecules shifting the surface pressure isotherm to the right. Further compression of the DPPC monolayer resulted in particle squeeze out from the monolayer causing a premature plateau in the surface pressure. Particle ejection from the monolayer was confirmed by monolayer collapse at a surface pressure of ~72 mN/m, a value that can be achieved only with pure DPPC monolayers. These alterations in surfactant behavior did not occur when the monolayer was exposed to particles using the particle injection method at a particle concentration of 0.1 g/L. Finally, a summary of particle concentrations used in the literature and a comparison between those concentrations and

physiologically relevant concentrations was provided. These results suggest that particle interaction with the monolayer is highly dependent on the particle introduction method and particle concentrations. These results are important in understanding particle interactions with Langmuir monolayers and can help interpret the results of the growing literature in the field of particle-monolayer interactions.

CHAPTER 5

PARTICLE SURFACTANT INTERACTIONS FOLLOWING

PARTICLE AEROSOLIZATION ON SURFACTANT

5.1 Introduction

Despite the existence of a few recent studies on the effects of inhaled particles on lung surfactant function, finding the underlying mechanisms of interaction remains a challenge. This is in part due to the methods used for exposure of surfactant molecules to the particles. Previously used methods for exposure of surfactants to particles in a Langmuir trough have been explained in Chapter 1. These methods include: mixing the particles with the surfactant and spreading the mixed film on top of an aqueous subphase,[39, 65, 66, 75] spreading the surfactant on top of the subphase and injecting the particles into the subphase[61, 62] (studied in Chapter 3) and dispersing the particles in the subphase and spreading the surfactant material on top[39, 42, 43, 60, 63, 64] (Studied in Chapter 4). While these methods have been useful in providing information on particle interactions with lung surfactant films, none of these methods truly mimic particle-surfactant interactions following inhalation.

During inhalation, particles deposit on top of surfactant molecules as aerosols. Surfactant interactions with deposited aerosols and hydrated particles dispersed in the subphase are likely to be very different. Surfactant molecules are mainly made of phospholipids, which are composed of hydrophilic headgroups and hydrophobic tails. Aerosolized particles interact with the hydrophobic tails of phospholipids, whereas particles dispersed in the subphase come into contact with the hydrophilic headgroups and thus are likely to induce different effects (Figure 5-1). Also, the dry aerosolized particles interact with the surfactant molecules as large agglomerates, which are likely to induce different effects in comparison to particles dispersed in the subphase that are more probable to stay separate as a result of electrostatic repulsion. Finally, interactions

between particles dispersed in the subphase and surfactant molecules is a function of particle affinity to the air-water interface; consequently, the actual 'dose' of particles interacting with surfactant molecules is not known (refer to the discussion in section 3.4 of Chapter 3). In contrast, all aerosolized particles will come in contact with surfactant molecules although finding the exact dose of aerosolized particles that deposit in the Langmuir trough can be a challenge. Despite all the advantages brought forth by particle aerosolization, this method for surfactant exposure to particles has not been studied in the literature perhaps due to the technical difficulties and the uncertainties in estimating the concentration of the aerosolized particles in the subphase.
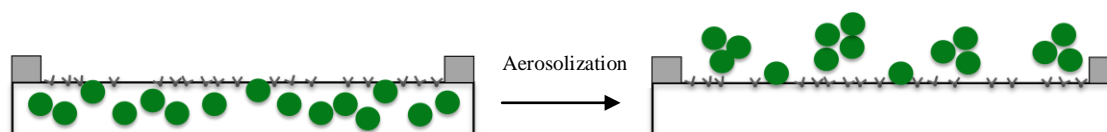
Figure 5-1. Differences between particles dispersed in the subphase (left) and aerosolized particles (right): 1. Particles dispersed in the subphase will come in contact with the hydrophilic headgroups of surfactant molecules, whereas aerosolized particles (right) will be in contact with the hydrophobic tails, 2. Interaction between surfactant molecules and particles dispersed in the subphase depends on particle surface affinity whereas all aerosolized particles will reach the air-water interface and interact with surfactant molecules and 3. Particles dispersed in the subphase are less likely to form agglomerates in comparison with dry aerosolized particles.

In the previous chapters, the interactions between 200-nm negatively charged polystyrene (0.2 μm CML) particles and surfactant molecules following particle injection into the subphase after spreading the surfactant layer (subphase injection) and spreading the surfactant after dispersing the particles in the subphase (monolayer addition) were investigated. In this chapter, a more realistic system for mimicking particle-surfactant interactions following inhalation is studied by aerosolizing the particles on top of surfactant molecules. A simple procedure was used to estimate the concentration of

aerosolized particles in the subphase. Finally, a better mimic of the physiologically relevant surfactant surface is provided by using Infasurf (calf lung surfactant extract) as the surfactant model. Dipalmitoyl phosphatidylcholine (DPPC) was also used as a simple surfactant model to provide more mechanistic information and allow comparison to our previous studies.

5.2 Materials and Methods

5.2.1 Commercial Reagents

Dipalmitoyl phosphatidylcholine (DPPC) was purchased from Genzyme Pharmaceuticals (Cambridge, MA) and used without further purification. Infasurf was a generous gift from ONY Inc. (Amherst, NY). Sodium chloride, calcium chloride and HPLC-grade chloroform were purchased from Sigma-Aldrich (Sigma-Aldrich, St. Louis, MO). Methanol was 99.9% pure and purchased from Research Product International (Mount Prospect, IL). All water used in experiments was obtained from a Barnstead NANOpure II system from Barnstead International (Dubuque, IA) and had a resistivity of 18.2 MΩ·cm. Carboxyl modified polystyrene particles were purchased as suspensions from Invitrogen (Carlsbad, CA). Dry Powder Insufflator™ model DP-4 was purchased from PennCentury (Wyndmoor, PA).

5.2.2 Particle Aerosolization Using Dry Powder Insufflator™

A Dry Powder Insufflator™ (PennCentury, Wyndmoor, PA) was used for aerosolization experiments. The insufflator held up to 5 mg of powder (up to 100 mg with an extension chamber) and was designed to use for intratracheal delivery in rats (Figure 5-2). The device was made of two parts: an air intake and a delivery tube. The air intake had an air intake port which was connected to a 3 mL plastic air syringe to create air puffs. Inside this part there was a cone structure where the dry particles were added. The

delivery tube part is connected to the air intake part and leads to a two-inch long delivery tube following a 120º bend. This bend is provided so that the user's hand does not block the line of sight during aerosol delivery to animals. The device is made of polyether ether ketone (PEEK) while the delivery tube is made of stainless steel.
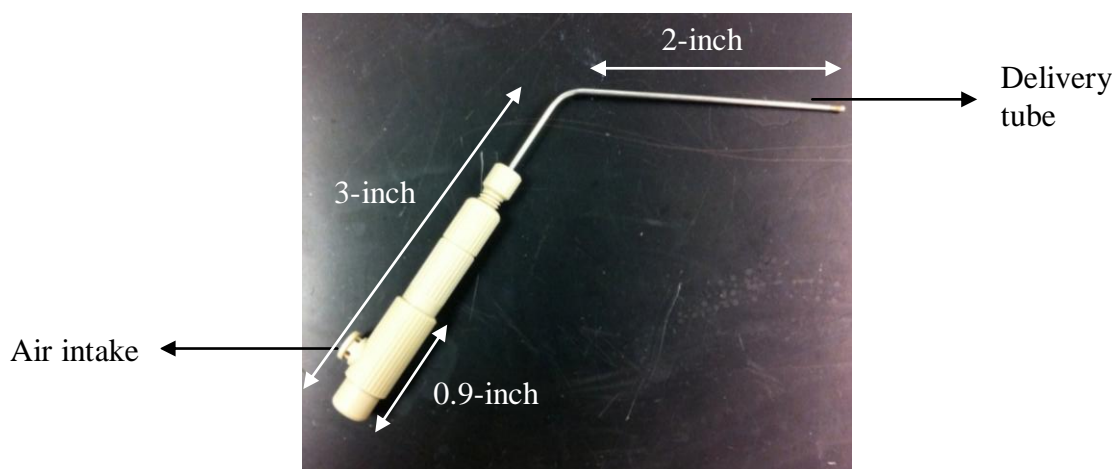
Figure 5-2. The Dry Powder Insufflator^{TM} is made of an air intake part which is connected to a delivery tube via a 120º bend.

Prior to each experiment, the cone structure of the air intake part (Figure 5-3-a) was filled with the desired amount (typically 4.1 mg) of dry particles. Then, the delivery tube was attached and the syringe was filled with air and pushed in to create air current needed to aerosolize the powders. The syringe was filled with air and pushed completely for three times for each aerosolization experiment although most of the powders were aerosolized with the first puff of air. Following each aerosolization, the insufflator was cleaned with the valve cleaning device (Figure 5-3-b) provided by the manufacturer which could be used to clear any potential clogged particles from inside the device. This

step was followed by pushing high-pressure air through the device to remove any remaining powder.

a)   b)
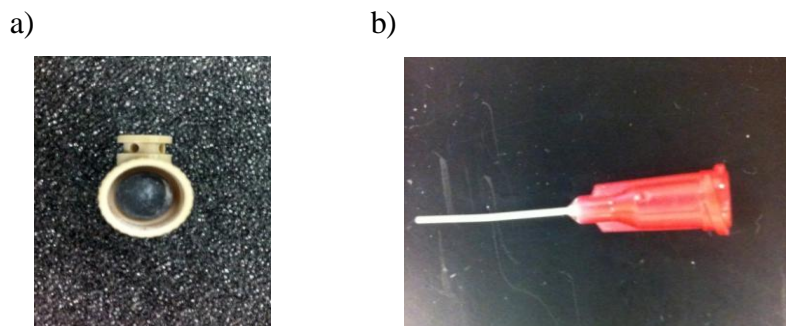
Figure 5-3. Top-view of the air intake part of the insufflator (a), which has a cone structure used to fill the device with lyophilized particles. A valve cleaning device (b) was used to clean the valves and the tube of the insufflator.

5.2.3 Particle Quantification Following Aerosolization on
The Langmuir Trough

Absorbance of particle suspensions at different concentrations was used to quantify particle deposition following aerosolization on the Langmuir trough. This idea was inspired by a study by Irache and colleagues[194] who showed that for a certain wavelength, specific turbidity is linearly related to particle size. According to Beer-Lambert law (Equation 5-1), absorbance, A, has a linear relationship with particle concentration up to an approximate absorbance value of one.

$$A = \log_{10} I_0/I = \varepsilon CL \tag{5-1}$$

In Equation 5-1, I_0 is the intensity of the incident light at a given wavelength, I is the transmitted intensity, L is the path length through the sample, c is the concentration of the absorbing species and ε is the molar absorptivity (also known as extinction coefficient) which is constant for each species at a certain wavelength, temperature and pressure and has units of 1/M·cm.

For measuring the absorbance, initially a calibration curve of absorbance vs. particle concentration was created by making particle suspensions at concentrations of 0.001 g/L, 0.01 g/L and 0.1 g/L. These suspensions were placed on vortex for 90 seconds and sonicated for 10 minutes a total of three times to ensure that particles did not form agglomerates and were homogenously suspended. Then the suspensions were transferred to disposable polystyrene cuvettes (Sarstedt AG&Co., Germany) and their absorbance at various wavelengths (from 300 nm to 950 nm with 50 nm steps) was determined using a Spectramax Plus 384 Spectrophotometer (Molecular Devices, Sunnyvale, CA). For each sample, the absorbance was measured by subtracting the absorbance of the blank sample (sample with no particles) from the absorbance of the sample with particles to obtain the final absorbance value. Based on the obtained absorbance curves, a laser wavelength of 350 nm was chosen to generate particle concentration vs. absorbance calibration curves. This wavelength was chosen as it provided a relatively large absorbance (0.19) for the lowest particle concentration without having a large absorbance from the blank sample. Then, an absorbance vs. concentration curve was developed at the chosen wavelength by measuring the absorbance of various particle suspensions with concentrations from 0.0001 g/L to 0.1 g/L at a laser wavelength of 350 nm. The resulting absorbance vs. concentration curve was linear as expected from the Beer-Lambert law. Since Beer-Lambert law is valid for absorbance values of less than 1, samples that exhibited absorbance values of higher than 1 were diluted and their obtained absorbance values were multiplied by the dilution factor.

The calibration curve generated with fixed-particle concentrations was used to measure the concentration of aerosolized particles in the subphase solution following aerosolization. For this step, the subphase of the trough (with a volume of 250 mL) was carefully transferred to a beaker using a pipette. Then the trough and the pipette were washed with an extra 50 mL of the subphase solution to remove any remaining particles

in the trough or inside the pipette leading to a final volume of 300 mL. The beaker was left in a bath sonicator for 15 minutes to ensure that the particles were dispersed homogenously in the subphase. Then, the suspension in the beaker was transferred to test tubes and the test tubes were placed on vortex for 90 seconds and sonicated for 10 minutes for three times to break apart particle agglomerates. The suspensions in the test tubes were then transferred to disposable cuvettes and their absorbance at 350 nm was determined. The concentration of particles was determined by comparing the absorbance reading from each sample and using the relationship between particle concentration and absorbance acquired from the calibration curve. Finally, this concentration was multiplied by 6/5 to compensate for the extra 50 mL of the subphase solution that was added to the 250 mL of subphase volume during the washing steps.

5.2.4 Surface Pressure versus Surface Area Isotherms

Tensiometric studies were conducted using a Langmuir-Wilhelmy apparatus (Minitrough System 4, KSV Instruments Ltd., Finland). Full trough compression experiments with DPPC were performed similar to Section 2.2.7. Briefly, the trough was filled with a freshly made subphase solution and was allowed to equilibrate to room temperature (23.3 ± 0.6 ºC) for 30 min, then aspirated to remove any surface impurities. Then the DPPC monolayers were obtained by spreading fifty microliters of 1.22 g/L surfactant solution using a Hamilton microsyringe and allowing 20 minutes for chloroform evaporation. The surface was compressed with a barrier speed of 10 mm/min (1.5 $Å^2$/molecule.min). For particle-surfactant interaction studies, 4.1 mg of particles were aerosolized on the surface of the trough using the insufflator before the trough compression was initiated.

Lung-relevant experiments were performed by compressing and expanding the surfactant films in the lung-relevant surface pressure range. This range was found from previously published reports as explained in Section 2.3.6.4. Briefly, the graphs of

surface tension vs. lung volume in excised animal lungs from four published studies were used as reference.[143-145, 147] Surface tension values at lung volumes equal to 50% and 58% of total lung capacity (i.e. one normal breathing cycle) were estimated. The surface tension range of 3-24 mN/m which was the widest range observed in these studies was used as the lung-relevant surface tension range and converted to surface pressure for lung-relevant surface pressure experiments. Lung-relevant experiments with DPPC monolayers were performed by dynamic compression-expansion of the barriers between the surface areas of 210 cm^2 and 185 cm^2 with a barrier speed of 150 mm/min (22.5 $Å^2$/molecule·min) for 10 cycles. The surface areas were chosen so that a lung-relevant surface pressure range of 48 mN/m to 69 mN/m was acquired. The chosen barrier speed (150 mm/min) was the highest barrier speed available on the instrument and was chosen to mimic the fast compression and expansion in the lungs. For particle-surfactant interaction studies, the surface of the trough was compressed to 185 cm^2, then 4.1 mg of particles were aerosolized on the surface during surface expansion from 185 cm^2 to 210 cm^2. The rest of the compression and expansion cycles were followed similar to pure DPPC experiments. All control experiments were performed under similar conditions but with puffing air (with no particles) through the Dry Powder Insufflator[TM].

Experiments with Infasurf films were performed similar to section 2.2.7. Briefly, Infasurf solutions were made by dissolving 174 μL of the surfactant in 5 mL of chloroform/methanol (2/1 volume ratio) to obtain a final phospholipid concentration of 1.22 g/L, equal to the concentration of phospholipids in DPPC solutions. An initial amount of 70 μL out of this solution was added to the surface of the trough using a Hamilton syringe leading to an initial surface pressure of 11.9 ± 0.6 mN/m allowing for all different phases of Infasurf isotherm to be observed in one compression cycle. The surface of the trough was compressed with a barrier speed of 10 mm/min (1.5 $Å^2$/molecule·min) from an initial surface area of 558 cm^2 to a final area of 100 cm^2 or 60 cm^2 depending on the experiment. For particle-surfactant interaction studies, 4.1 mg of

particles were aerosolized on the surface of the trough using the Dry Powder Insufflator[TM] before the trough compression was initiated. Similar to DPPC experiments, all control experiments without particles were performed under similar conditions but with puffing air through the Dry Powder Insufflator[TM]. Aerosolization experiments in each phase of the Infasurf isotherm were performed by aerosolizing particles at surface pressures of 25 mN/m and 43 mN/m. Finally, experiments with longer interaction times between particles and surfactant were performed by waiting for 3 or 6 hours after particle aerosolization on the surface of the trough before initiating surface compression. Similarly, control experiments were performed by puffing air with no particles on the surface of the trough and waiting for 3 or 6 hours before initiating surface compression. Data in all experiments were acquired approximately every second during surface compression and expansion and were recorded using the LayerBuilder software.

5.2.5 Fluorescent Imaging

Fluorescent microscopy experiments were performed using an Olympus BX-51 microscope (Olympus, Center Valley, PA) similar to Section 2.2.8. Briefly, a small poly (methylmethacrylate) (PMMA) minitrough (7.5 cm x 12 cm x 0.6 cm) was washed and filled with 60 mL of subphase and mounted on the microscope stage. Five microliters of a 1.22 g/L DPPC solution doped with about 1 mol% of the fluorescent probe Texas-Red-1,2-dihexadecanoyl-*sn*-glycero-3-phosphoethanolamine, triethylammonium salt (Texas-Red-DHPE) was added on top of the subphase for imaging. Texas-Red DHPE preferentially partitions into the fluid phases allowing for studies of structure of lipid domains which appear as black dots in the LE-LC phase of the surface pressure isotherm.[161, 162] A filter with an emission range of 573-648 nm was used to enable visualization of the Texas-Red probe.

The insufflator with one milligram of 0.2 μm CML particles and particle aerosolization was performed 20 minutes after DPPC was added to the surface to allow

chloroform to evaporate. The surface of the trough was compressed manually using Delrin barriers and images of the microstructure were acquired at each surface pressure. To reduce the movement of lipid domains with air current a cardboard shield was placed on top of the microscope for all imaging experiments. When the imaging was finished, the subphase was carefully transferred to a beaker and the concentration of the aerosolized particles was determined using turbidimetry as explained in Section 5.2.3. Off-line surface pressure measurement was performed similar to Section 3.2.8. Briefly, the PMMA trough was placed on the Wilhelmy plate setup and filled with the subphase upon which DPPC-Texas Red solution was spread. The surface pressure was changed by reducing the surface area of the trough by hand compression of Delrin barriers. The surface areas at which the desired surface pressure values were reached were marked on the side of the trough. These marks were used as guides for barrier compression on the microscope stage.

5.2.6 Aerosol Size Characterization Using Laser
Diffraction

The particles used for aerosolization experiments had already been characterized for their size distribution, charge, surface area and surface chemical composition (Section 3.3.1). However, the size distribution of dry particles after aerosolization is different from the hydrodynamic particle size distribution with large agglomerates likely to form in the dry state. Laser diffraction was used for initial characterization of the size distribution of aerosolized particles. A Helium Neon Laser Optical System (HELOS)/BF laser diffraction particle size analysis instrument (Sympatec GmbH, Germany) was used for laser diffraction experiments. The instrument was equipped with helium-neon laser with a wavelength of 632.8 nm and could measure particle sizes ranging from 0.1 μm to 875 μm. WINDOX software was used for evaluation of particle size distributions using

Fraunhofer theory (applicable without knowledge of optical parameters of particles) and recording the particle size data.

The optical concentration, a measure of the amount of laser light blocked by the sample, was used as an indicator of the relative concentration of the aerosolized particles. In order to avoid erroneous data produced at low optical concentrations, all experiments were performed by setting a precondition to record data only when optical concentration is equal to or higher than 1%. In all experiments, aerosolization was started right after starting the experiment. Experiments were performed for 5 seconds with data being recorded every 5 milliseconds. Data were recorded as volume distributions using the WINDOX software and converted to number distribution assuming spherical particles.

5.2.7 Aerosol Size Characterization Using Scanning
Electron Microscopy (SEM)

Size distribution and morphology of aerosolized particles were determined using a Hitachi 4800 Scanning Electron Microscope (SEM). For these experiments, a double-sided black carbon tape was attached to a SEM stub. Particles were aerosolized on top of the carbon tape and then sputter coated with Au-Pl at 10 mA and at a pressure of $7x10^{-2}$ mBar for 3 minutes using an Emitech Sputter Coater K550 (Quorum Technologies, United Kingdom). After imaging, particle sizing was performed by measuring the projected surface area of 90 particle agglomerates in ImageJ. The diameter of agglomerates was estimated by assuming spheres. The frequency distribution of particles was determined by categorizing the estimated diameters in 0.1 µm bins and counting the number of particles in each bin. Particle counts in each bin were divided by the total number of counted particles to generate normalized particle frequency distributions. Particle cumulative distribution was generated by adding the normalized frequency in each bin with the normalized frequencies of all the previous bins and plotting them against particle diameter.

5.3. Results

5.3.1 Particle Dose Measurement Following Aerosolization

Particle dose quantification after insufflation was performed by measuring the absorbance of particle suspensions in the subphase solution and finding the particle concentration based on absorbance. For this approach, it was required to find a laser wavelength that resulted in detectable absorbance even at low particle concentrations. To this aim, the absorbance of particle suspensions at different concentrations (0.001 g/L, 0.01 g/L and 0.1 g/L) along with a blank sample with no particles were measured at different laser wavelengths using a spectrophotometer (Figure 5-4).

Based on the plots shown in Figure 5-4, a laser wavelength of 350 nm was chosen for the rest of the experiments. At this wavelength, the lowest particle concentration of 0.001 g/L exhibited an absorbance value of 0.19, this value was high enough to allow for the quantification of lower particle concentrations. Also, the blank sample did not generate a very high absorbance value at this wavelength. This wavelength was also close to the wavelength of 300 nm chosen by Irache and colleagues[194] for characterizing the diameter of small particles (between 114 nm to 530 nm). After choosing the wavelength, nine particle concentrations (from 0.0001 g/L to 0.1 g/L) were chosen for further experiments to find the relationship between the particle concentration and absorbance (Figure 5-5).

As shown in Figure 5-5, absorbance (y) showed a linear relationship with particle concentration (x) with a function of y=14.57x + 0.01 and an R squared of 0.99 showing that the linear regression is appropriate for fitting the absorbance vs. particle concentration data. This function was used to find particle concentrations based on the measured absorbance values following aerosolization.

Getting a consistent output of aerosols out of the insufflator required a good and reproducible aerosolization technique. Initial experiments with the insufflator led to
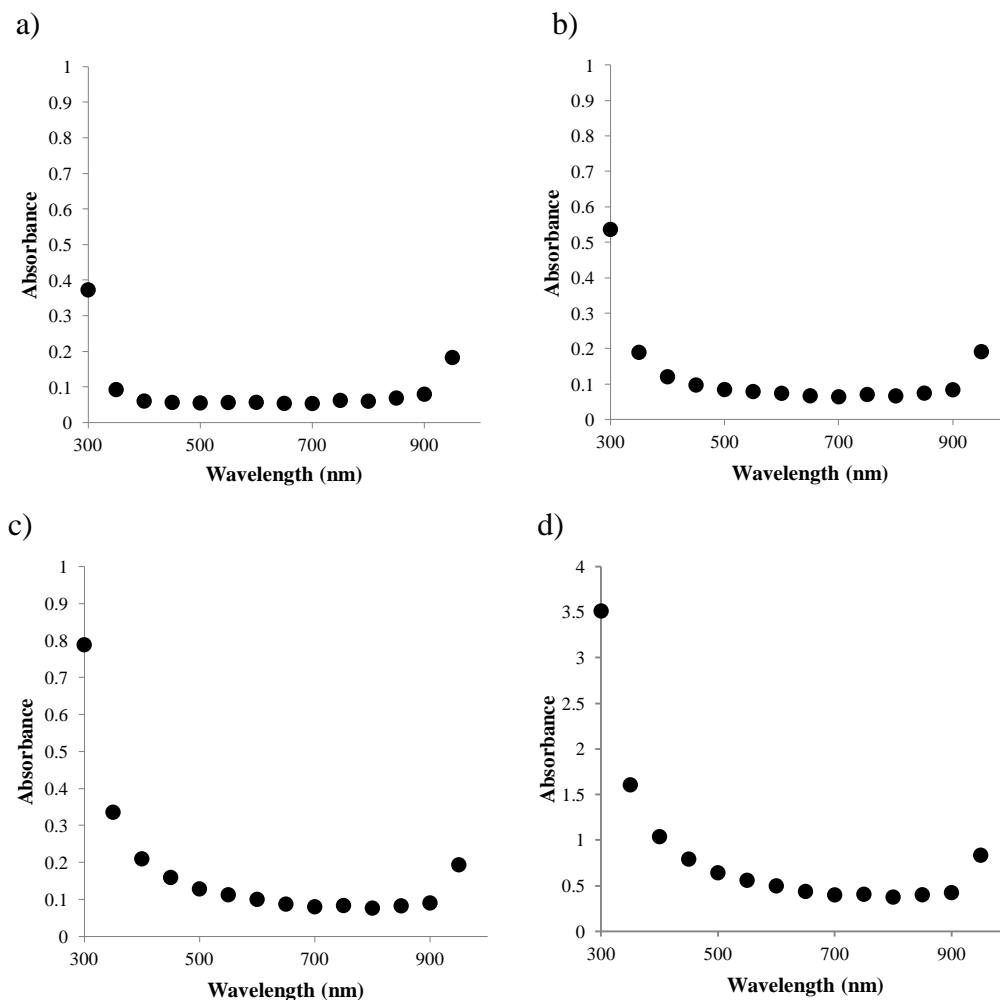
Figure 5-4. Absorbance vs. wavelength plots for (a) pure water (blank sample), (b) suspension of 0.001 g/L of 0.2 µm CML particles in water, (c) suspension of 0.01 g/L of particles in water and (d) suspension of 0.1 g/L of particles in water. Absorbance of all particle suspensions were measured following vortex and sonication, laser wavelength was changed with 50 nm intervals for all experiments.

inconsistent amount of aerosol output (data not shown), but more consistent values were achieved with considerable practice. Initial experiments to ensure proper aerosolization were performed in a small PMMA trough (described in section 3.2.8) to save material and time. A summary of aerosolization experiments with an initial powder mass of 3 mg is presented in Table 5-1. These experiments were performed both with and without

DPPC to ensure that the presence of the small amount of surfactant does not interfere

with absorbance readings.
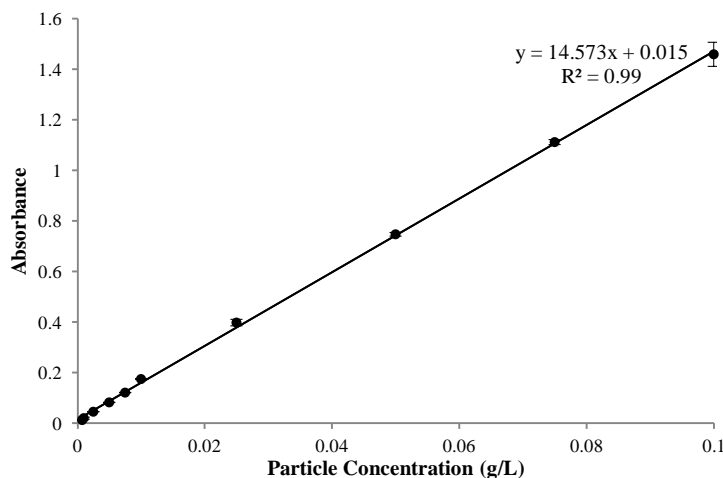
Figure 5-5. Different concentrations of 0.2 µm CML particles (from 0.00075 g/L to 0.1 g/L) showed a linear correlation with absorbance at a laser wavelength of 350 nm. Absorbance of all particle suspensions were measured following vortex and sonication.

Table 5-1. Sample aerosolization experiments on the PMMA trough with and without surfactant, the presence of surfactant did not significantly affect the resulting particle concentrations; all trials were performed after filling the insufflator with 3 mg of 0.2 μm CML particles, subphase volume= 60 mL.

	Trial #	1	2	3	4	5	6	Ave.	Std. Dev.
No Surfactant	Abs.	0.517	0.484	0.370	0.543	0.372	0.429	0.452	0.074
	Conc. (g/L)	0.035	0.032	0.025	0.036	0.025	0.029	0.030	0.004
With Surfactant	Abs.	0.314	0.520	0.452	0.552	0.377	-	0.443	0.098
	Conc. (g/L)	0.021	0.035	0.030	0.037	0.025	-	0.030	0.007

As shown in Table 5-1, dry powder insufflations led to a consistent particle concentration in the subphase with an average and standard deviation of 0.030 ± 0.004 g/L. Considering that the subphase volume in these experiments was 60 mL, the calculated concentration was equal to a mass of 1.8 mg of particles in the subphase or 60% of the mass of particles loaded in the insufflator. The presence of a DPPC monolayer did not significantly affect the measured absorbance and particle concentration in the subphase with an average and standard deviation of 0.030 ± 0.007 g/L being obtained after five experiments.

The same method used for aerosolization and dose measurement on the PMMA trough was used for aerosolization experiments on the large trough. Since sixty percent of the initial powder was shown to deposit in the trough, it was possible to estimate the amount of powder needed to feed to the insufflator for a desired particle concentration. For example, for a particle concentration of 0.01 g/L (i.e. 2.50 mg of particles in the trough) an initial weight of powder of 4.14 mg was used. Using this initial concentration, a particle concentration of 0.012 ± 0.002 g/L in the subphase was achieved after 23 trials (Table 5-2) which confirmed that the method was reproducible and experiments could be performed at desired particle concentrations.

Table 5-2. Sample aerosolization experiments on the PMMA trough with and without surfactant, the presence of surfactant did not significantly affect the resulting particle concentrations; all trials were performed after filling the insufflator with 3 mg of 0.2 μm CML particles, subphase volume= 60 mL.

Trial #	1	2	3	4	5	6	7	8	9	10	11
Abs.	0.183	0.109	0.220	0.224	0.244	0.148	0.234	0.220	0.214	0.203	0.209
Conc. (g/L)	0.012	0.007	0.014	0.015	0.016	0.009	0.015	0.012	0.014	0.014	0.013
Trial #	12	13	14	15	16	17	18	19	20	21	22
Abs.	0.216	0.112	0.172	0.161	0.193	0.144	0.169	0.178	0.140	0.151	0.145
Conc. (g/L)	0.014	0.007	0.011	0.010	0.011	0.009	0.011	0.011	0.009	0.010	0.009
Trial #	23	Ave.	Std. Dev.								
Abs.	0.179	0.184	0.035								
Conc. (g/L)	0.011	0.012	0.002								

5.3.2 Particle Size Distribution Characterization Following

Aerosolization

5.3.2.1 Laser Diffraction Experiments

Particle characterization using laser diffraction was performed by aerosolizing the particles in the path of the laser in the sample chamber of the instrument. To avoid averaging of erroneous data that could be generated at low optical concentrations, conditions were set so that measurements were performed only for samples with an optical concentration of 1% or higher. The results from aerosolization of four different

samples through the sample chamber are presented in Figure 5-6 with the number distribution plots shown on the left and volume distribution plots on the right. In each plot, an intensity distribution (particle count vs. particle diameter) and a cumulative distribution (percent of total particles vs. particle diameter) are shown.

As shown in Figure 5-6, the number distribution graphs were mostly populated with smaller particles with a peak that was slightly lower than 200 nm. However, this peak showed a broad shoulder to the right covering the particle size of 200 nm. The mass distribution graphs show several peaks at sizes much larger than 200 nm with a peak around 30 μm being visible in all experiments. This implies that aerosolization leads to the formation of large agglomerates, which is expected from dry particles. The trends for number and volume distributions were in agreement with what is expected for fine (<1 μm) particles. In fine particles, the number distribution graphs are generally dominated by peaks at small particles, whereas the volume distribution graphs are dominated by peaks from large particles.[195] This is due to the dependence of particle volume on particle diameter to the third power which increases the weight of large particles in volume distributions. Despite the agreement of trends with that expected from fine particles, several drawbacks were associated with using laser diffraction for particle size analysis. The presence of a peak at 140 nm did not seem logical since TEM imaging had confirmed that the size of dry particles was 218 ± 16 nm. This was most likely due to the use of Fraunhofer theory for measuring particle size by the WINDOX software. This theory does not consider the absorption of light by the particles and assumes that the particle diameter is larger than laser wavelength. The instrument used in this research used a laser with the wavelength of 632.8 nm, meaning that particles with a diameter smaller than this wavelength might not have been measured with the accuracy of larger particles. Finally, laser diffraction measures the size of airborne particles; however, it is the deposited and not the airborne particles that come into contact with the surfactant in the Langmuir trough. Thus, a method for measuring the size of the deposited particles is

a)

b)

c)
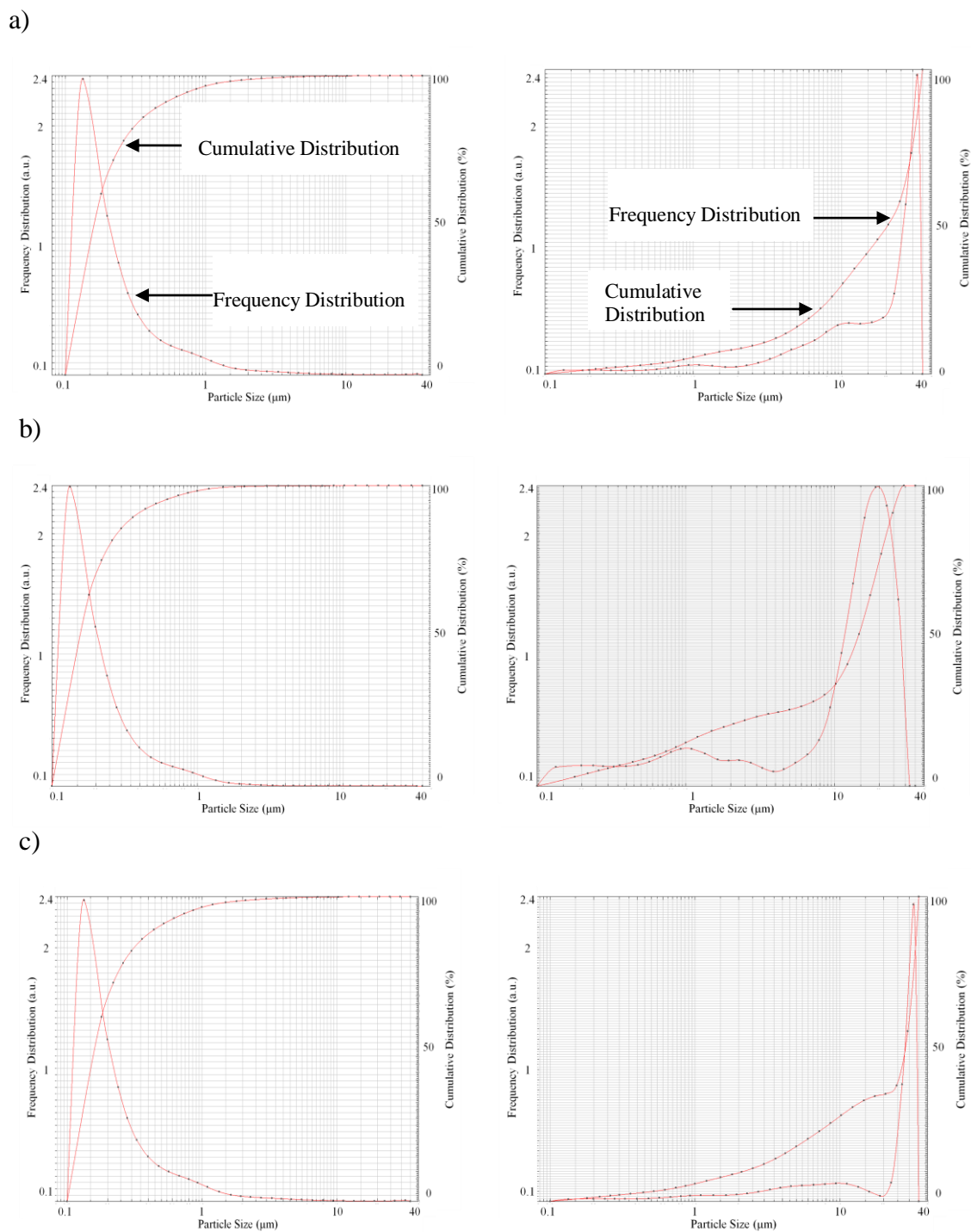
Figure 5-6. Laser diffraction results for aerosolized 0.2 μm CML particles obtained from four different experiments (a to d). The left column shows number distribution (with a peak at ~140 nm) and the right column shows volume distribution (with various peaks mostly located around 30 μm). Both frequency and cumulative distribution are shown in each graph (arrows).

d)
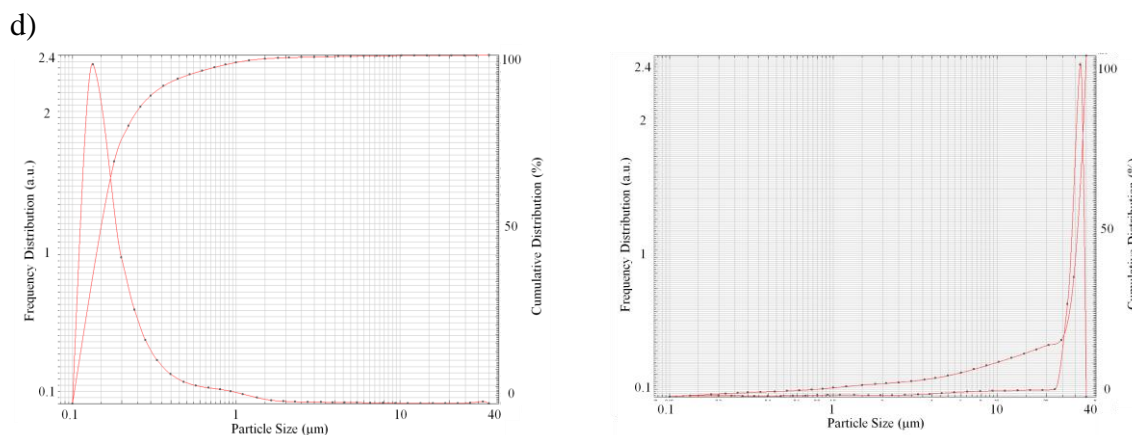
Figure 5-6. Continued.

needed to provide information about the particles that come into contact with the surfactant.

5.3.2.2 SEM Imaging

SEM imaging was used to provide information on the size of the particles that deposit onto SEM stubs following aerosolization. Measurement of the surface area of these particles would help determine the size distribution of the deposited particles based on their surface area. These experiments were performed following particle aerosolization on SEM stubs covered with a carbon tape and acquiring images of the deposited particles. SEM images showed the presence of agglomerates after particle aerosolization as expected for dry particles (Figure 5-7). However, a large number of individual, non-agglomerated particles could also be observed. To quantify the size distribution of particles, particle diameters were estimated by measuring their projected surface area in SEM images and assuming that the agglomerates were spherical. The estimated particle diameters were separated into 0.1 μm bins and the number of particles in each bin was counted. Then, the number of particles in each bin was divided by the total particle count and plotted vs. bin size. This resulted in normalized frequency

distribution plots similar to those obtained using laser diffraction (Figure 5-8-black curve). Cumulative distribution plots were generated by adding the normalized frequencies and plotting them vs. particle diameter (Figure 5-8-red curve).

a)   b)
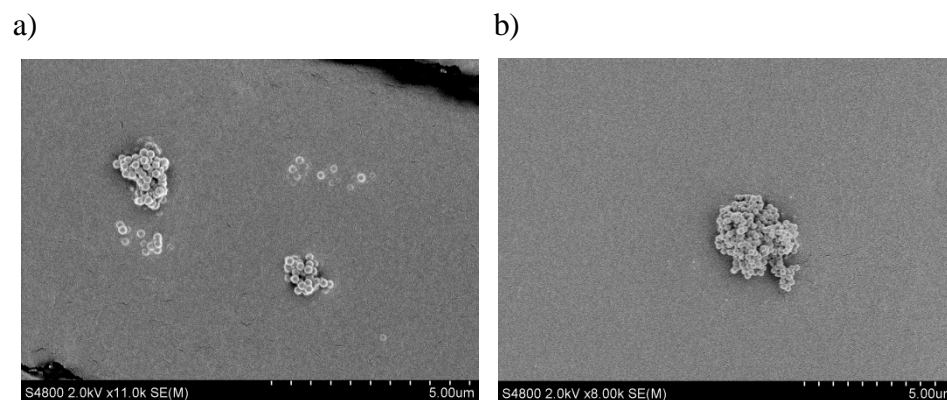
Figure 5-7. Representative SEM images of particles aerosolized on SEM stubs covered with carbon tape. Both images were acquired at 11000 magnification.

As shown in Figure 5-8, a large fraction of particles (53%) showed a diameter of 0.3 μm or less, suggesting the presence of many single particles after aerosolization. After a peak at particle diameters of less than 0.3 μm, there was a steep reduction in the frequency of particles with larger diameters. These results were qualitatively similar to the number distribution plots observed from laser diffraction with small particles dominating the number distribution plots (Figure 5-6). The largest estimated particle diameter was 10.4 μm with only one of the 90 particles counted from SEM images at this diameter. The cumulative particle distribution reached 100% at this diameter confirming that all particles had an estimated diameter of 10.4 μm or lower. Unlike laser diffraction studies, no particles with a diameter of around 30 μm were observed in the SEM images. This observation could be due to the impaction of particles on SEM stubs following aerosolization, which could potentially break the large agglomerates. Also, only a few

particles with a diameter of around 30 μm were detected using laser diffraction (as evidenced by the number distribution graphs in Figure 5-6). The small number of these particles can explain why they were not observed under the point of view of the microscope during the SEM imaging.
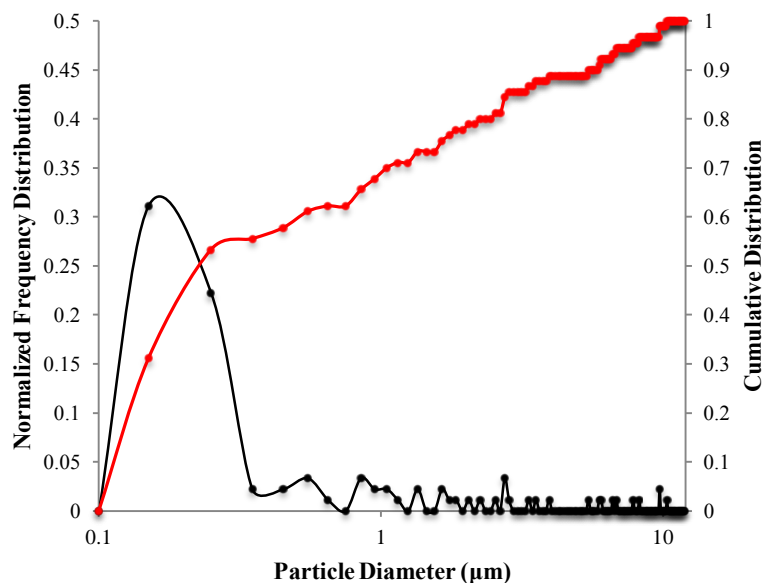
Figure 5-8. Normalized frequency (left y-axis, black curve) and cumulative distribution (right y-axis, red curve) vs. particle diameter plots generated for particles aerosolized on SEM stubs. Particle diameter values used for graphs were estimated from the projected surface area of 90 particles from SEM images and classified into bins. The lines between data points are drawn to guide the eye.

It should be emphasized that the data presented in Figures 5-7 and 5-8 pertain to dry particles. When the particles reach the subphase in the Langmuir trough, the electrostatic repulsive forces between the charged carboxyl groups on particle surfaces are likely to overcome the attractive van der Waals forces between the particles and promote further particle separation. However, the presence of Infasurf on top of the subphase and its potential adsorption on particle surfaces is likely to affect these delicate

interparticle forces. Particle aggregation due to adsorption of surfactant proteins or lipids on particle surfaces as has been suggested before.[72, 196] Adsorption of surfactant lipids or proteins can change the attractive or repulsive forces between the particles, potentially reduce the energy barrier toward particle aggregation and result in larger particles.

5.3.2.3 Modeling Particle Interaction Energy

To understand the effect of adsorption of surfactant components on interparticle forces the classical Darjeuin, Landau, Verwey and Overbeek (DLVO) theory was utilized. This theory has been widely used to model the interaction energy between colloids for a variety of applications.[197-199] In this theory, the interparticle forces are described by the interplay between attractive van der Waals forces promoting particle aggregation (Equation 5-2) and electrostatic repulsive forces upon close approach and overlap of particle double layers promoting particle stability (Equation 5-3).[100] The sum of interparticle forces is estimated by calculating the sum of two forces (Equation 5-4).

$$\phi_{vdw} = -\frac{A_{212}}{12} f(x,y) = -\frac{A_{212}}{12} \left(\frac{y}{x^2+xy+x} + \frac{y}{x^2+xy+x+y} + 2\ln\left(\frac{x^2+xy+x}{x^2+xy+x+y}\right) \right) \tag{5-2}$$

$$\phi_{elec} = \frac{64\pi R C k_B T}{\kappa^2} \tanh^2\left(\frac{ze\psi}{4k_B T}\right) \exp(-\kappa S_0) \tag{5-3}$$

$$\phi_{net} = \phi_{vdw} + \phi_{elec} \tag{5-4}$$

In the above equations, Φ_{vdw}, Φ_{elect} and Φ_{net} are the attractive force, repulsive and net interparticle forces (in units of Joules) respectively. The attractive forces are a function of x and y, where $x = S_0/2R_1$ and $y = R_2/R_1$ with S_0 being the distance between particle surfaces and R_1 and R_2 being particle radii in meters (shown as R when particles have the same diameter). A_{212} is the Hamaker constant of particles of material 2 (polystyrene) in medium 1(water) in Joules, z is ion valence, C is the salt concentration in the medium in mol/m^3, k_B is Boltzmann constant (equal to 1.38×10^{23} J/K), e is the elementary charge (equal to 1.6×10^{-19} C), ψ is the zeta potential of particles in units of

Volt, T is temperature in units of Kelvin and κ is the inverse of Debye length (in m^{-1}) calculated using Equation 5-5 and 5-6.

$$\kappa=\left[\frac{e^2N_A(2I)}{\varepsilon_r\varepsilon_0k_BT}\right]^{0.5} \tag{5-5}$$

$$I=\frac{1}{2}\sum z_i^2C_i \tag{5-6}$$

In the above equations, N_A is the Avogadro constant (equal to 6.02×10^{23} #/mol), ε_r is the relative dielectric constant of the liquid (80.1 for water), ε_0 is the permittivity of vacuum (equal to 8.85×10^{-12} C^2/J.m) and z_i and C_i are ion valence and concentration of all ions in the medium, respectively. The Hamaker constant required for calculation of attractive forces (Equation 5-2) depends on the atom density of the particles and the polarizability of the atoms.[100] The values of this constant in various media are available in the literature, unknown values of Hamaker constant can be calculated from known values of the constant in vacuum using the geometric mean rule (Equation 5-7).

$$A_{212}=\left(\sqrt{A_{22}}-\sqrt{A_{11}}\right)^2 \tag{5-7}$$

where A_{212} is the Hamaker constant of two particles of composition 1 when suspended in a medium 2. A_{11} and A_{22} are Hamaker constants of particles in vacuum. Finally, it should be mentioned that equations 5-2 to 5-4 explain the classical or non-extended DLVO theory. The extended DLVO model considers the steric interaction between solvent molecules and coatings on particle surfaces and elastic forces arising from energy loss due to compression of coating layers on particles and requires knowledge of additional parameters.[199, 200]

To ensure the accuracy of DLVO calculations performed in this study, Equations 5-2 to 5-6 were first used to reproduce previously published data on the interparticle forces between silver nanoparticles (11.6 nm in diameter) with known Hamaker constants (Figure 5-9).[199] The interaction energy between two silver particles as a function of interparticle distance is illustrated in Figure 5-9. The height of the interaction energy is

the primary determinant of colloid stability. An interaction energy higher than the energy of Brownian motion (considered to be around 1.5 kT)[199, 201] is needed to keep the particles separate. As demonstrated in Figure 5-9, using Equations 5-2 to 5-6 it was possible to closely match previously published calculations confirming the accuracy of calculations.

The DLVO model was applied to the suspension of 0.2 μm CML particles in the subphase solution to provide information about the stability of the particles. The Hamaker constants needed for these calculations were found for each component in vacuum (3.7×10^{-20} J for water and 6.5×10^{-20} J for polystyrene)[100] and the Hamaker

a)　　　　　　　　　　　　　　　b)
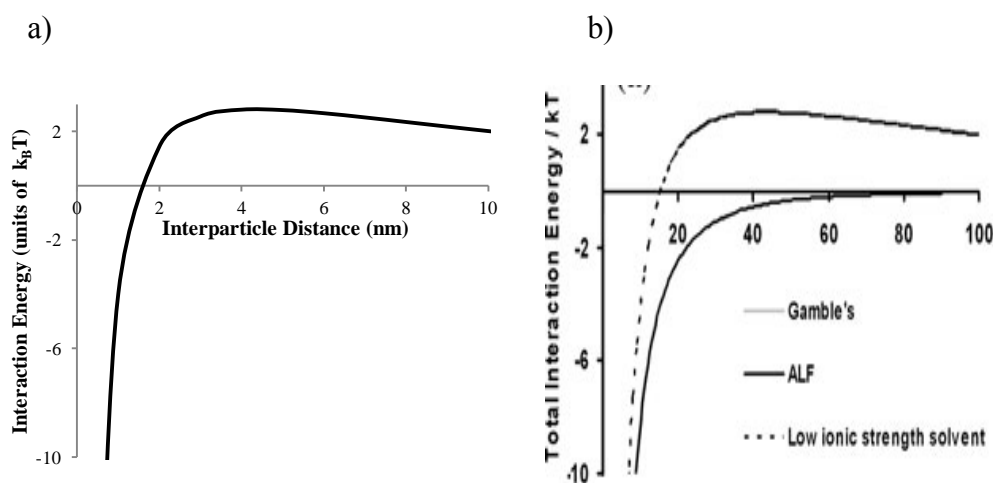
Figure 5-9. Using the DLVO theory, it was possible to calculate the interaction energy between silver nanoparticles (diameter=11.6 nm) in a low ionic strength medium (1 mol/m^3) with known Hamaker constant of 0.159×10^{-20} J at 311 K. The results of calculations closely resembled previously published values: (a) calculations performed in this study, x-axis in nanometers, (b) calculations from Stebounova et al.[199] reprinted with permission (x-axis in angstroms). In (b) the curve at the top represents interparticle potential in a low ionic strength medium (1 mol/m^3), two identical curves at the bottom represent interparticle forces in Gamble's medium and artificial lysosomal fluid (ALF).

constant of particles in water was calculated using Equation 5-7. Also, it was assumed that all particles are 200 nm in diameter and that the zeta potential remains unchanged. Finally, the small amount of calcium chloride in the subphase solution was ignored for the sake of simplicity. Applying the DLVO model to the system of 0.2 μm CML particles in the subphase solution resulted in a plot with a high maximum interaction energy of 36 kT (Figure 5-10).

The large, positive interaction energy observed in Figure 5-10 showed that repulsive forces are larger than attractive forces for 0.2 μm CML particles in the subphase solution. Thus, a large energy barrier avoids particle aggregation leading to colloid stability. However, the presence of surfactant can substantially affect the inter-particleforces and especially the van der Waals forces due to adsorption of lipids or proteins. Although Equations 5-2 to 5-6 are useful for finding the forces between bare particles in a medium, they cannot be used to calculate the effects of adsorbed layers on van der Waals forces.
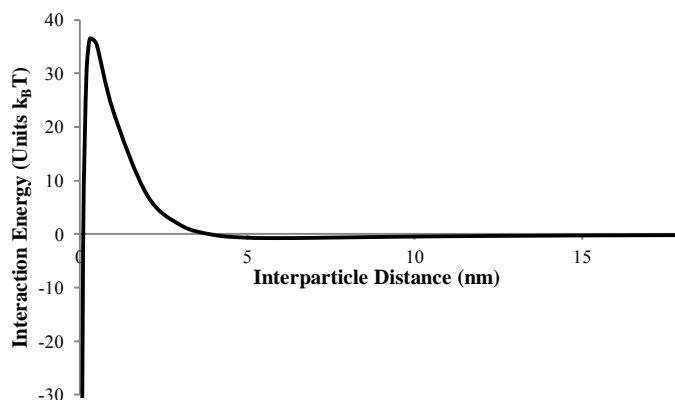
Figure 5-10. The interaction energy between 0.2 μm CML particles in the subphase solution at room temperature (296 K) as predicted using the classical DLVO model (equations 5-2 to 5-6).

To study the interparticle behavior in the presence of surfactant, the model proposed by Vold[202] was used. This model considers interactions between two particles with adsorbed layers with two "phantom" particles of the medium. Interaction energy for each particle with an adsorbed layer is calculated by assuming the particles are made entirely of the adsorbate material with the radius of the particle plus the adsorbate (or R+∂ which is original radius + adsorbed layer), then subtracting this energy from the energy of the particles with their original radii but made of adsorbate and finally adding the energy for particles with its original radii and original material. Thus, Equation 5-2 can be modified to include the effects of adsorbed layers (Equation 5-8).

$$-12\phi_{vdw}=\left(A_M^{0.5}-A_A^{0.5}\right)^2 f_A(x,y)+\left(A_A^{0.5}-A_P^{0.5}\right)^2 f_P(x,y)+2\left(A_M^{0.5}-A_A^{0.5}\right)\left(A_A^{0.5}-A_P^{0.5}\right)f_{PA}(x,y) \quad (5\text{-}8)$$

In Equation 5-8, A_M, A_A and A_P are respective Hamaker constants of the medium, the adsorbate and the particles, f_A is the f function (see Equation 5-2) for two spheres of radius R+∂ which are separated by a distance of S_0, f_P is the function for two spheres of radius R and a separation of $S_0+2\partial$ and finally f_{PA} corresponds to two spheres one with a radius of R and one with a radius of R+∂ which are separated by a distance of of $S_0+\partial$. This model was applied to the mixture of particles and surfactant, for the sake of simplicity it was assumed that the surfactant is made entirely of DPPC and that the surface of the particles are completely covered with one layer of surfactant. Also, it was assumed that the Hamaker constant of the subphase did not change by the presence of surfactant components. The value for Hamaker constant of DPPC in vacuum was found using the geometric mean rule.[203] The thickness of the adsorbed DPPC layer was assumed to be the same as the length of a DPPC molecule (3.4 nm).[170] The result of the modification of DLVO theory using Equation 5-8 is presented in Figure 5-11.
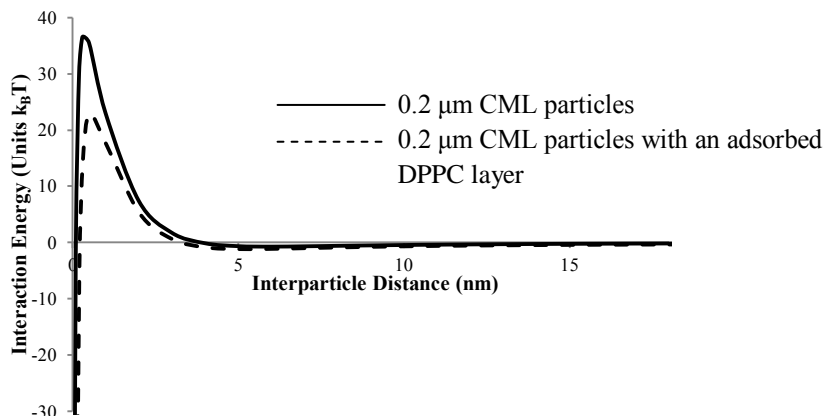
Figure 5-11. The interaction energy between 0.2 μm CML particles in the subphase
solution at room temperature using the classical DLVO theory (bold line) and
the same particles with an adsorbed layer of DPPC after changing the
attractive forces of the DLVO theory according to Equation 5-8 (dashed line).

Figure 5-11 reveals interesting information about interparticle energy following

surfactant adsorption. An adsorbed layer of DPPC affects the interaction energy between

the particles, reducing the energy barrier by about 14 k_BT. However, there is still a large

energy barrier (22 k_BT) for particle aggregation. This large energy barrier suggests that

the single particles are less likely to aggregate following aerosolization on the subphase

on which Infasurf is spread due to the large energy barrier at close approach. However,

this energy barrier rapidly reduces at interparticle distances less than 0.3 nm implying

that agglomerates that have already formed in the dry state will remain aggregated even

in the subphase solution. Finally, it should be mentioned that the lower curve in Figure 5-

11 has been generated assuming one adsorbed layer of DPPC on particle surfaces. The

presence of multiple layers of DPPC or additional lipids or proteins from Infasurf can

reduce the energy barrier even further and promote particle aggregation.

5.3.3 Particle Aerosolization on DPPC Monolayers

<u>5.3.3.1 Particle Effects on DPPC Surface Pressure Isotherm</u>

Initial particle aerosolization experiments on DPPC monolayers were performed at a target particle concentration of 0.001 g/L. Although this exact particle concentration was not achieved in the aerosolization experiment, a higher concentration of 0.004 g/L did not show any changes in the surface pressure isotherm of DPPC (Figure 5-12), making it difficult to study mechanisms of interaction. Thus, the particle concentration was increased by an order of magnitude and a particle concentration of 0.01 g/L in the subphase was studied. This concentration was still lower than most particle concentrations used in the literature (see Table 4-3). Particle aerosolization at this concentration led to changes in the surface pressure isotherm of DPPC (Figure 5-13). After particle aerosolization, a reduction in the rate of surface pressure increase between
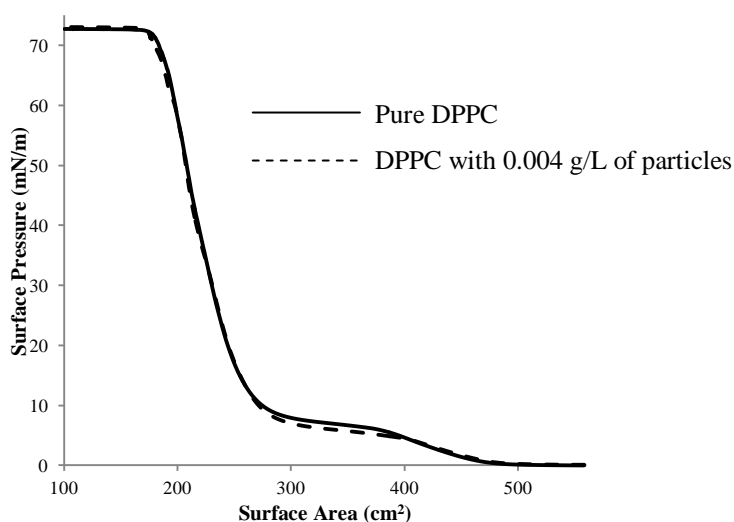
Figure 5-12. Surface pressure vs. surface area isotherms of pure DPPC and DPPC after aerosolization of 0.004 g/L of 0.2 μm CML particles. DPPC monolayers were compressed from an initial surface area of 558 cm^2 to a target area of 100 cm^2 in both experiments.
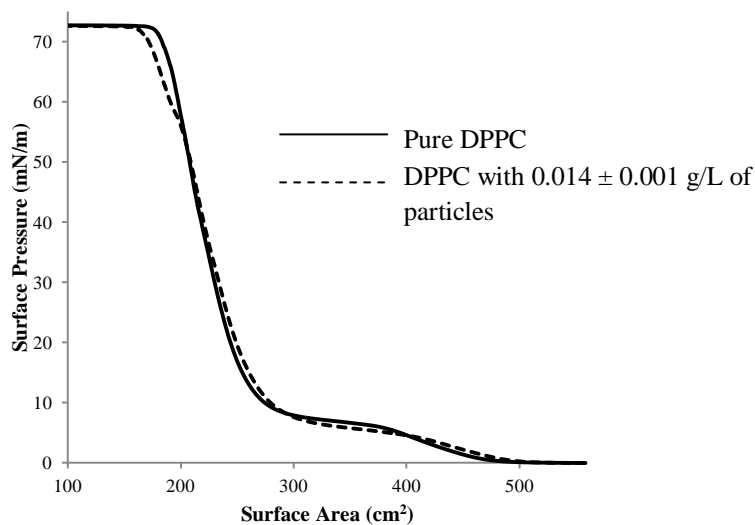
Figure 5-13. Surface pressure vs. surface area isotherms of pure DPPC and DPPC after aerosolization of 0.014 ± 0.001 g/L of 0.2 µm CML particles. DPPC monolayers were compressed from an initial surface area of 558 cm^2 to a target area of 100 cm^2 in both experiments.

approximately 55 mN/m and monolayer collapse was observed. The monolayer collapse occurred at a surface pressure of ~72 mN/m similar to pure DPPC monolayers; however the collapse point was shifted to a surface area of 162 ± 3 cm^2 compared to an area of 174 ± 3 cm^2 for pure DPPC monolayers.

Interpreting the changes observed in the DPPC monolayer after particle aerosolization is a difficult task as there are no previously published work on the effects of aerosolized particles on surfactant monolayers. Considering that the monolayer in the presence of particles collapses at a surface pressure of ~72 mN/m, it can be concluded that no particles remain at the air-water interface during monolayer collapse, as such high collapse surface pressures can only be obtained with pure DPPC monolayers.[38] However, the shift in collapse surface area demonstrates that DPPC molecules need further compression to reach a pure monolayer at the air-water interface in the presence of particles. Given that the particle surface area is much larger than the mean molecular area of DPPC molecules even at the start of compression (31400 nm^2 vs. 1.11 nm^2) particles

cannot land on a surface that is not covered with DPPC molecules. Thus, only two possible mechanisms are likely: 1. Particles land on DPPC monolayers, adsorbing phospholipids on particle surfaces and reducing the amount of DPPC molecules at the air-water interface and 2. Particles submerge into the subphase and get adsorbed to the air-water interface through the subphase. The first mechanism has not been reported in the previous Langmuir trough studies of particle-DPPC interactions where particles are dispersed in the subphase and interact with the hydrophilic headgroup of DPPC. However, interaction of particles with the hydrophobic tails of DPPC following aerosolization might lead to surfactant adsorption on particle surfaces. Phospholipid adsorption on the surface of fine urban particles has been suggested after incubating the particles with bronchoalveolar lavage (BAL) fluid[72, 204] and could be the mechanism in this case. The second mechanism seems less likely as subphase injection studies with the particles being added after the monolayer did not suggest the presence of particles at the air-water interface.

Comparison of two particle introduction methods, monolayer addition and aerosolization at a particle concentration of 0.01 g/L revealed that particles shift the monolayer collapse to lower surface areas in both methods. Although the difference in collapse surface area was not significantly different between the two methods (162 ± 3 cm^2 vs. 162 ± 14 cm^2 for monolayer addition) (Figure 5-14). Higher surface pressure values were observed in the LE-LC phase and the beginning of the LC phase with the monolayer addition method. Since the shift in the surface pressure of the monolayer is a likely sign of particle penetration to the monolayer, the larger shift with the monolayer addition method suggests that more particles penetrate the monolayer in the monolayer addition method compared to aerosolization.
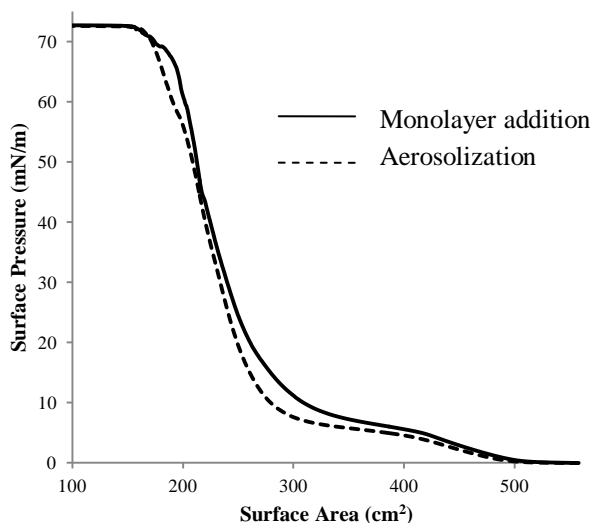
Figure 5-14. Surface pressure vs. surface area isotherms of DPPC after exposure to 0.01 g/L of 0.2 μm CML particles using the monolayer addition protocol (solid line) and 0.014 ± 0.001 g/L of particles using particle aerosolization (dashed line). DPPC monolayers were compressed from an initial surface area of 558 cm^2 to a target area of 100 cm^2 in both experiments.

5.3.3.2 Particle Effects on DPPC Microstructure

The effects of particle aerosolization on DPPC microstructure were studied using fluorescent microscopy. The microstructure of pure DPPC has been presented in Section 3.3.3.2 and Section 4.3.3 and is presented in Figure 5-15-a. The presence of particles induced a slight increase in the fluid phases of DPPC (which appeared red in fluorescent images). In some images, streaks of bright red could be observed in the microstructure (Figure 5-15-b, arrow) which were likely to be clusters of particles at the air-water interface. Such streaks of particles have been previously shown in the surfactant microstructure in the studies of DPPC microstructure after the addition of alkylated gold nanoparticles.[69]

3.3 ± 1.7 mN/m   5.2 ± 1.8 mN/m   8.4 ± 3.8 mN/m
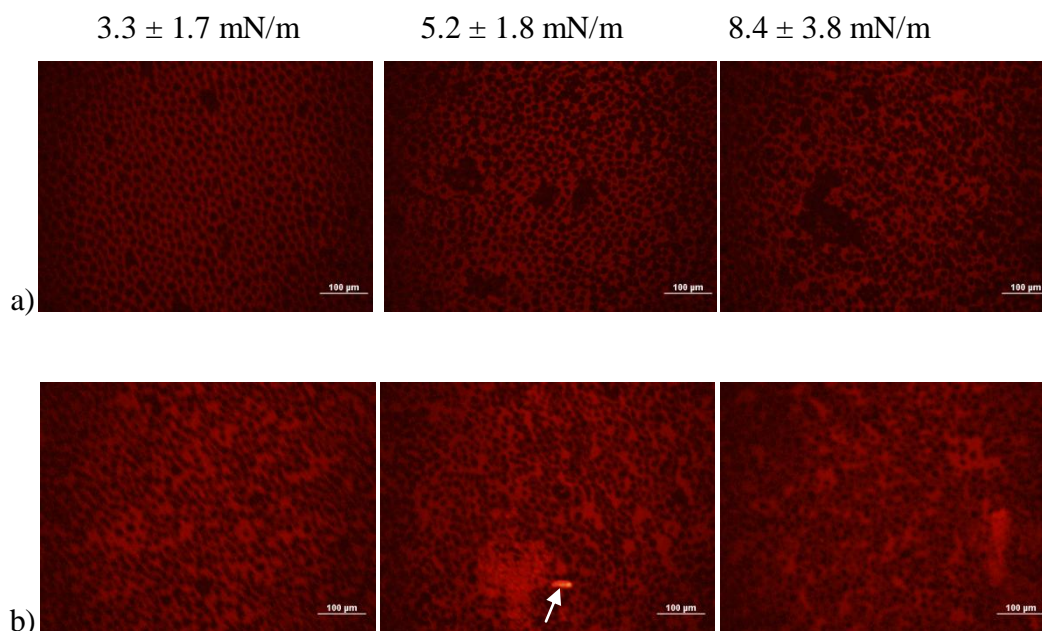
Figure 5-15. Fluorescence images of DPPC films doped with Texas Red-DHPE during surface compression on (a) subphase containing no particles and (b) subphase containing 0.011 g/L of 0.2 µm CML particles. Presented images were acquired at surface pressures of 3.3 ± 1.7 mN/m (left panel), 5.2 ± 1.8 mN/m (middle panel) and 8.4 ± 3.7 mN/m (right panel), bar = 100 μm. Arrow shows one of the streaks of bright red which was likely a particle agglomerate.

The changes observed in the microstructure of DPPC after particle aerosolization were in agreement with the subphase injection studies of particles (Section 3.3.2). In both cases, an increased amount of fluid phase were observed in the microstructure whereas little effect was observed in the LE-LC region of the DPPC surface pressure isotherm. These changes were also in agreement with previously published reports which reported a decrease in the size of DPPC domains but only slight changes in the surface pressure of the LE-LC region of the surface pressure isotherm.[42, 63, 69] Given that the size of the ordered domains is inversely related to electrostatic repulsive forces between the domains,[189] this reduction in the size of the domains is likely a result of increased repulsive forces caused by negatively charged particles. An interesting observation was the presence of streaks of particles at the interface. Interestingly, these streaks were only observed with aerosolized particles and did not appear in cases where particles were

dispersed in the subphase (Chapters 3 and 4). The presence of these streaks could be evidence that a fraction of particles remain at the air-water interface following aerosolization.

5.3.3.3 Lung-relevant DPPC

A better mimic of pulmonary surfactant function can be achieved by performing the experiments in the lung-relevant surface pressure range (estimated in Section 2.3.6.4). A summary of the effects of particles on the maximum surface pressure at the end of each cycle is presented in Table 5-2 and depicted in Figure 5-16. As seen in Table 5-2, the surface pressure at the end of the first compression cycle and before the start of aerosolization is similar for both experiments. However, following particle aerosolization (during surface expansion in the first cycle) a significant drop in the maximum surface pressure of each cycle can be observed. Although aerosolization was performed only once, this effect persisted through different cycles with the maximum surface pressure showing a significant difference even at the end of the last cycle (62.1 ± 2.2 mN/m vs. 52.2 ± 2.4 mN/m).

As shown in Table 5-2 and Figure 5-16, particle effect on the surface pressure isotherm of DPPC were more significant when the monolayer was compressed in the lung-relevant range compared to full monolayer compression experiments. This was not surprising as the changes in surfactant function during full monolayer compression were observed only at high surface pressure values (above 55 mN/m) which were lung-relevant. Similar to the complete monolayer compression experiments, phospholipid adsorption on particle surfaces is likely to have played a role in the reduction of the maximum surface pressure. This mechanism is likely as the surface concentration of DPPC molecules is much higher in the lung-relevant surface pressure range compared to an expanded state facilitating potential adsorption on particle surfaces. However, it is also likely that the particles have pushed surfactant molecules into the subphase and the fast

Table 5-3. Maximum surface pressure obtained during surface area cycling (between surface areas of 210 cm^2 and 185 cm^2) of pure DPPC monolayers and DPPC monolayers after aerosolization of 0.013 ± 0.001 g/L of 0.2 μm CML particles before the start of the second cycle.

Cycle #	Maximum surface pressure at the end of each cycle (mN/m)	
	Pure DPPC	DPPC with 0.01 g/L of particles
1st	71.0 ± 1.7	70.2 ± 1.2
2nd	70.2 ± 1.3	51.0 ± 2.8
3rd	69.2 ± 1.7	51.8 ± 2.0
4th	67.9 ± 1.9	52.0 ± 2.0
5th	66.4 ± 2.0	52.0 ± 2.1
6th	65.1 ± 1.9	52.1 ± 2.1
7th	64.8 ± 2.4	51.6 ± 2.2
8th	63.9 ± 2.3	51.4 ± 2.4
9th	63.0 ± 2.3	51.2 ± 2.3
10th	62.1 ± 2.2	52.2 ± 2.4
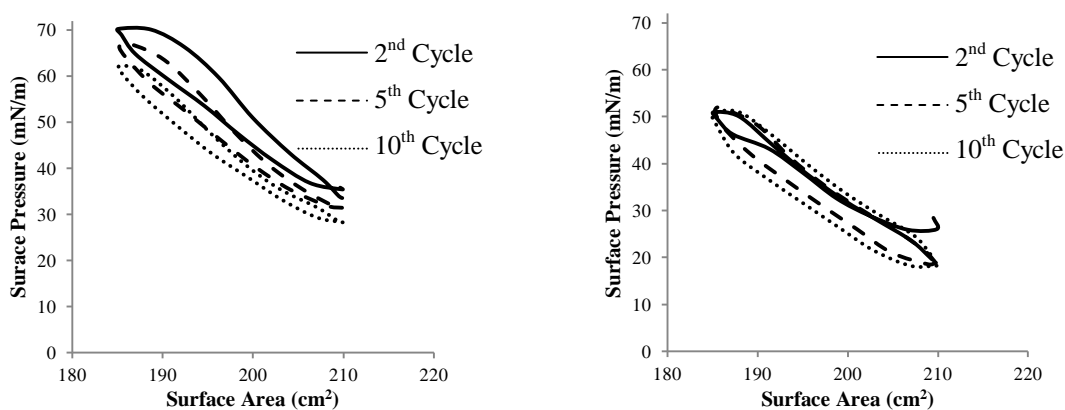
Figure 5-16. Surface pressure vs. surface area isotherms pure DPPC monolayers (a) and DPPC monolayers after aerosolization of 0.013 ± 0.001 g/L of 0.2 μm CML particles (b) in the lung-relevant range. Particle aerosolization was performed at the end of the first cycle. Both monolayers were compressed at a speed of 150 mm/min between surface areas of 210 cm^2 and 185 cm^2.

compression and expansion of the surface combined with the crystalline surface at such high surface pressure values has not allowed for the readsorption of the ejected molecules. All control experiments presented in Table 5-2 and Figure 5-16 were performed with puffing air on DPPC monolayers using the insufflator to account for the potential loss of DPPC molecules to the subphase after aerosolization. However, this mechanism cannot be completely ruled out.

<div align="center">5.4.3 Particle Aerosolization on Infasurf Films</div>

5.4.3.1 Particle Effects on Infasurf Surface Pressure

Isotherms

The surface pressure isotherms of Infasurf have been previously presented in Section 2.3.5 and were in good agreement with previously reported isotherm.[44, 86, 87] Further controls were performed by puffing air on Infasurf films using the insufflator, this did not affect the surface pressure isotherm of Infasurf and the controls were very similar to those performed without air puffing. (Figure 5-17, bold line). Particle aerosolization on Infasurf resulted in changes at high surface pressure values (Figure 5-17). A reduction in the maximum surface pressure (65.6 ± 1.3 mN/m vs. 68.3 ± 0.3 mN/m for pure Infasurf) was observed in the presence of 0.012 ± 0.002 g/L of particles. Pure Infasurf films showed a steady collapse plateau starting at 149.2 ± 4.2 cm^2, this plateau started at 129.0 ± 2.0 cm^2 in the presence of particles.

A shift in the surface area of the collapse plateau is a sign of reduction in the pool of surface-active material. Given that the changes caused by particles are observed only at surface pressure values higher than 50 mN/m where the surfactant film is highly compressed, it was likely that particles were being squeezed out of the film at low surface areas resulting in the ejection of some surfactant molecules. Since Infasurf films change from monolayer to bilayer structure at a surface pressure of approximately 40 mN/m,[46, 87] if particle squeeze out is occurring after aerosolization, it is possible that some particles
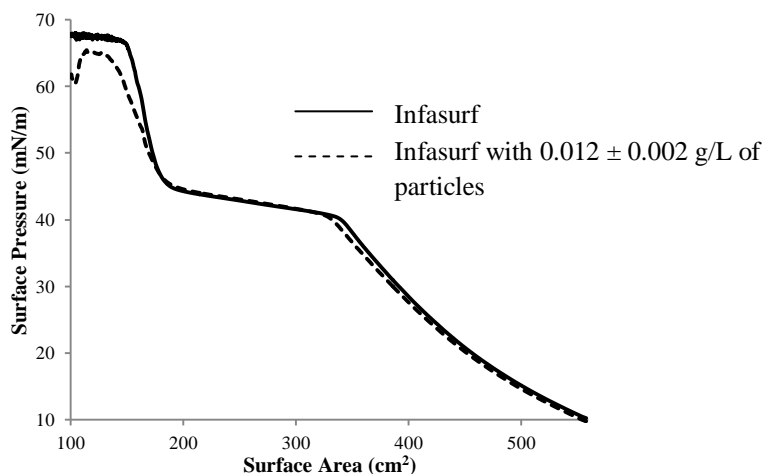
Figure 5-17. Surface pressure vs. surface area isotherms pure Infasurf film (bold line) and Infasurf film after aerosolization of 0.012 ± 0.002 g/L of 0.2 μm CML particles (dashed line). Both films were compressed from an initial surface area of 558 cm^2 and 100 cm^2.

are being ejected from the film during this change of structure. To test this hypothesis, particles were aerosolized on Infasurf films at surface pressure values of 25 mN/m and 43 mN/m to investigate whether the particles are being squeezed out during multilayer formation (Figure 5-18).

Aerosolization of particles resulted in a slight dip in surface pressure at the point of aerosolization; however, the rest of the surface pressure isotherm remained unaffected. Interestingly, the effects of particles at high surface pressure values vanished when the particles were introduced at different regions of surface pressure increase. These observations suggest that particle effects on the surface pressure isotherm of Infasurf are less likely to be caused by particle ejection from the film. This is supported by the fact that even when the particles were aerosolized before surfactant compression, no significant effects at surface pressures lower than 50 mN/m (Figure 5-17). If the particles were incorporated into the surfactant film an increase in the surface pressure at low

surface pressure values would be expected due to the artificial compression caused by the particles.

The effects observed in Figure 5-18 could be due to particle adsorption of surfactant components. When the particles were introduced to the surfactant before the start of film compression (Figure 5-17), the interaction time between the particles and surfactant was 30 minutes. This time was reduced to 22 minutes for particle aerosolization at a surface pressure of 25 mN/m (Figure 5-18-a) and 13.5 minutes for

a)

b)
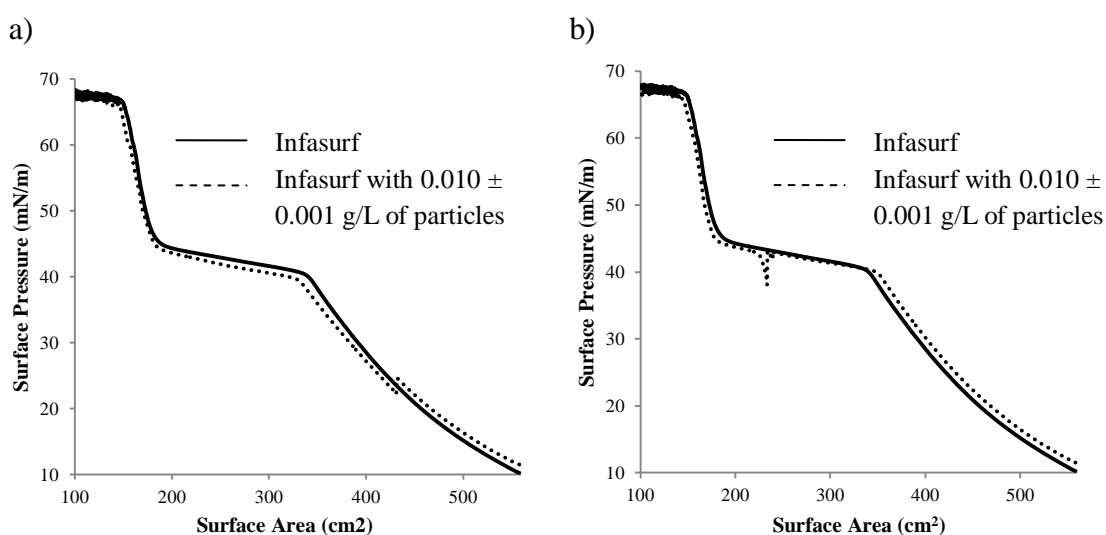
Figure 5-18. Surface pressure vs. surface area isotherms of pure Infasurf film (bold line) and Infasurf film after aerosolization of 0.010 ± 0.001 g/L of 0.2 μm CML particles (dashed line) at surface pressures of 25 mN/m (a) and (b).

particle aerosolization at a surface pressure of 43 mN/m (Figure 5-18-b). These observations suggest that particle effects on the surface pressure isotherm of Infasurf could be related to the interaction time between particles and surfactant films and potential adsorption of surfactant components on particle surfaces. This hypothesis was tested by probing the effect of interaction time between particles and Infasurf films on the surface pressure isotherm of Infasurf.

5.4.3.2 Effects of Particle Interaction Time on Infasurf

Surface Pressure Isotherms

Interaction times of 3 and 6 hours were chosen to investigate the effects of particles on Infasurf surface pressure isotherm. Replenishment of pulmonary surfactant components in the lungs between takes between 4 to 11 hours.[128] Thus, the chosen interaction times were within the time scale during which surfactant replenishment occurs. Control experiments were performed to probe the effect of time on the surface pressure isotherm of Infasurf (Figure 5-19).
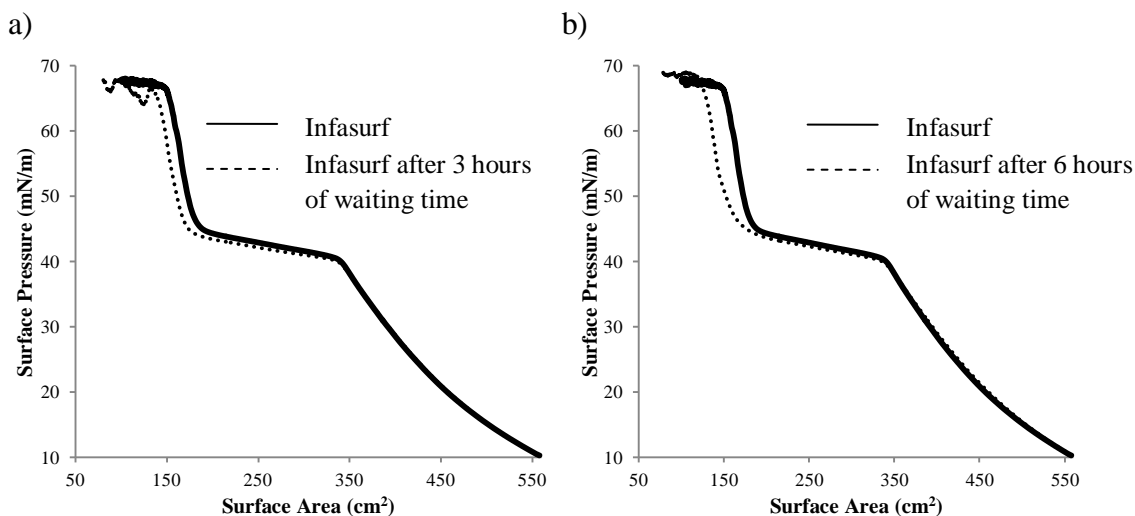
Figure 5-19. Surface pressure vs. surface area isotherms of pure Infasurf film (bold line) and Infasurf film after (a) three and (b) six hours of waiting time (dashed lines). Controls after increased waiting times were compressed to a final surface area of 80 cm^2.

As demonstrated in Figure 5-19, three hours of waiting time induced a slight reduction in the surface pressure values of the surface pressure vs. surface area isotherm of Infasurf. The same shift with a larger extent was observed in the surface pressure vs. surface area isotherm of Infasurf after six hours of waiting time. The changes observed

after six hours of waiting time were more significant with a reduction in the rate of surface pressure increase between ~45 mN/m and collapse. These resulted in a slight shift in the onset of surfactant collapse, Infasurf collapsed at a surface area of 131.8 ± 9.1 cm^2 after three hours and a surface area of 118.0 ± 1.1 cm^2 after six hours of waiting time (compared to 149.2 ± 4.2 cm^2 with no waiting time). Both waiting times also led to instabilities in the collapse plateau of Infasurf, slightly changing it compared to the stable collapse plateau of Infasurf. These changes are likely due to the deposition of dust or other airborne contaminants on the surface of the trough during the waiting time.

Aerosolization of particles at both interaction times shifted the collapse surface area of the films further to the left (Figure 5-20). Infasurf films collapsed at a surface area of 103.0 ± 7.8 cm^2 (compared to 131.8 ± 9.1 cm^2 with no particles) after three hours of interaction time and a surface area of 105.4 ± 0.6 cm^2 (compared to 118.0 ± 1.1 cm^2 with no particles) after six hours of interaction time with the particles. Instable collapse
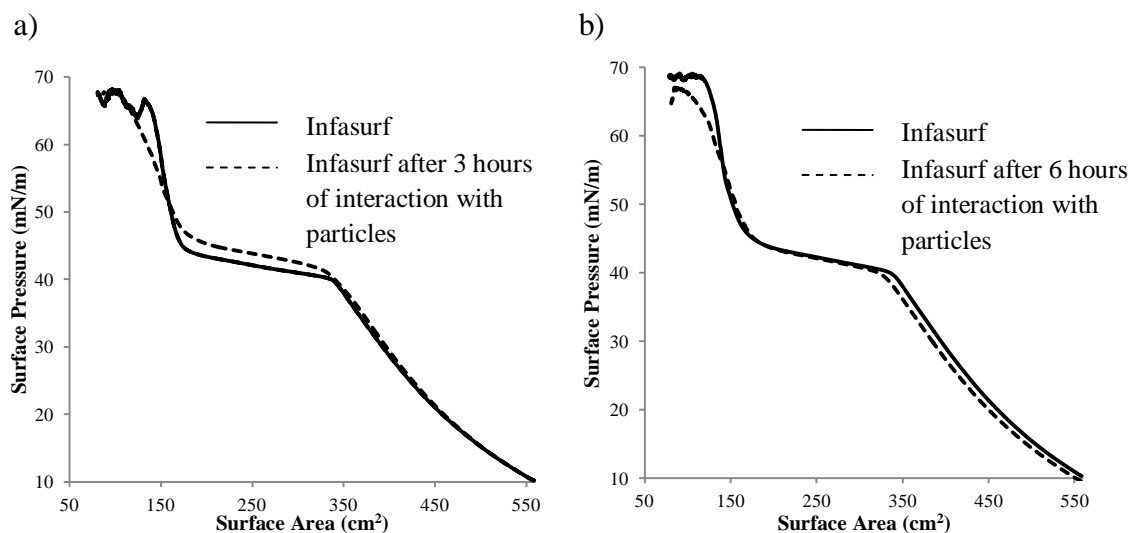
Figure 5-20. Surface pressure vs. surface area isotherms of Infasurf films after interaction with 0.2µm CML particles for (a) 3 hours, particle concentration: 0.009 ± 0.002 g/L, (b) 6 hours, particle concentration 0.010 ± 0.001 g/L.

plateau was observed in the presence of particles; however, the maximum surface pressure achieved by Infasurf films was not significantly affected.

A shift to the left in the collapse surface area means that less surfactant molecules are present at the surface in the presence of particles. Considering that these shifts were not observed when the particles were in contact with the surfactant for smaller times (Figure 5-18), particle effects on the surfactant is likely to be due to adsorption of surfactant components on particle surfaces. This mechanism has been suggested in the systems of particles and complex surfactant films before.[41, 42, 58] Fan and colleagues[44] reported a similar but more emphasized effect than the current study following increased interaction time between Infasurf films and hydroxyapatite particles.

Unsteady collapse surface pressures in the presence of particles have not been reported before and deserve further investigation. Although the setup used in this study was in a closed system, waiting time induced instabilities on the collapse plateau even for control Infasurf experiments. These instabilities were observed only once in four control experiments conducted with three hours of waiting time and three control experiments conducted with six hours of waiting time. However, unstable plateaus were observed in all experiments with the particles making it likely that the particles can also induce instabilities in Infasurf collapse. It is known that Infasurf is a multilayer even prior to collapse with the height of the multilayers increasing from ~6 nm to ~10 nm during collapse.[47] Thus, particle effects on collapse plateau could potentially be due to particle effects on the multilayer structure of the surfactant which could be a focus for future studies.

5.4 Conclusion

Particle aerosolization as a realistic route of exposure has been tried for the first time to investigate the interactions between aerosolized 200-nm negatively charged polystyrene particles and two surfactant models (DPPC and Infasurf). A simple method

for particle dose measurement following aerosolization was successfully developed based on turbidimetry and reproducible doses of particles in the Langmuir trough were achieved using a Dry Powder Insufflator^{TM}. Aerosolization of particles on DPPC monolayers resulted in a shift in the surface area of surfactant collapse and a slight reduction in the maximum surface pressure. However, significant reductions in the maximum surface pressure of DPPC was observed when the particles were aerosolized on top of DPPC monolayers in lung-relevant surface pressure range. A shift in the surface area of surfactant collapse and a slight reduction in the maximum surface pressure was also observed when particles were aerosolized on Infasurf. However, particle effects on Infasurf seemed to be a function of time with larger interaction times resulting in a reduction of the maximum surface pressure and an unsteady collapse surface pressure likely due to adsorption of surfactant components.

CHAPTER 6

CONCLUSIONS AND FUTURE PERSPECTIVES

6.1 Conclusions

This research investigated the interactions between negatively charged sub-micron polymeric particles and surfactant interfaces. Surfactant models were spread on an air-water interface to study the interfacial behavior of surfactant films when exposed to solid particles. This system can be used to provide mechanistic information on particle-surfactant interactions, which are important for a variety of fields most prominent among them pulmonary drug delivery and occupational and environmental health.

In Chapter 2, the behavior of two surfactant models, dipalmitoyl phosphatidylcholine (DPPC) and Infasurf, commonly used for mimicking biomembranes and pulmonary surfactant behavior was characterized at air-water interface using a Langmuir-Wilhelmy balance instrument. Also, common metrics for characterization of surfactant biophysical function such as phase behavior, maximum surface pressure, compression modulus and especially hysteresis area were discussed in detail. Finally, the range of physiologically relevant surface pressure values was determined and DPPC and Infasurf were compared for their hysteresis behavior in that range.

In Chapter 3, the effects of negatively charged sub-micron (200 nm) polystyrene particles on DPPC surfactant function following particle injection into the subphase (particle injection method) was examined using tensiometric experiments, studies of surfactant microstructure and surface topology. It was found that while particles induce small changes in the surface pressure isotherm of DPPC during monolayer collapse, DPPC respreading behavior is significantly affected by the particles. Also, particles significantly affect DPPC microstructure by shrinking the size of ordered phases likely through increased electrostatic repulsion effects. Finally, atomic force microscopy studies revealed that particles do not penetrate the air-water interface in this particle introduction

method and the surface topology remains unaffected. These resuls enhance the understanding of the interfacial behavior of DPPC in the presence of particle and provide insight on particle interactions with biomembranes and lung surfactant.

In Chapter 4, the effect of a different particle introduction method on surfactant biophysical behavior was investigated. Particle dispersion in the subphase before surfactant addition (monolayer addition method) resulted in more pronounced effects on surfactant function marked by an increase in surface pressure at high surface areas, premature collapse and increased hysteresis areas. Particles also increased DPPC dipoles at high mean molecular areas suggesting that particles penetrated into the monolayer and occupied some of the surface area at the air-water interface, causing the monolayer to become more compressed. Therefore, the choice of particle introduction method, (subphase injections vs. monolayer addition) altered the mechanism by which particles interacted with surfactant monolayers. Electrostatic interactions dominated particle-surfactant interactions in the particle injection method whereas particle adsorption to the interface dominated the interactions in the monolayer addition method. Such findings are important in understanding the role of the exposure method on the mechanisms of particle interactions with surfactant and explain some of the inconsistencies observed in previous studies in this field.

In Chapter 5, the biophysical behavior of DPPC and Infasurf following particle aerosolization on surfactant films was performed for the first time to investigate the effect of a realistic exposure route on particle-surfactant interactions. In this set-up, particles were aerosolized onto the surfactant interface using dry powder insufflations. A simple method to quantify the concentration of aerosolized particles deposited on the surface based on turbidimetry was successfully developed. Particles affected DPPC function by shifting the surface area of monolayer collapse. However, particle effects on surfactant function were more significant in the lung-relevant surface pressure range. Particles affected the maximum surface pressure and collapse area of Infasurf with the effects

being a function of the interaction time between the particles and surfactant suggesting that the effects are likely due to adsorption of surfactant components on particles surfaces. Mimicking the physiologically relevant route of exposure is critical to better determine the mechanisms of particle-surfactant interactions following inhalation and can be used for further studies on the effects of particle physicochemical properties on surfactant function.

<div align="center">6.2 Future Perspectives</div>

The studies of particle aerosolization on surfactant films performed in this research are a large step forward toward better understanding of particle-surfactant interactions and provide a good basis for future studies. However, this system can be further improved for better understanding of the interactions that occur following inhalation. Since particle deposition in the alveolar region of the lung is governed by diffusion and gravitational settling, devising a setup that ensures particle deposition on the surfactant film is governed by these mechanisms, rather than impaction to the surface would be a step forward for better mimicking inhalation and making the studies more physiologically relevant. Also, studying surfactant films at physiologically relevant temperature, humidity and surface pressure range can greatly improve current understanding of particle-surfactant interactions in the lungs.

Particle effects on the interfacial behavior of complex surfactants such as Infasurf could be affected by the adsorption of surfactant components on particle surfaces. Characterizing surfactant components following interaction with particles would provide a better understanding of the components adsorbed on particle surfaces and their role on surfactant biophysical behavior. Thus, incorporating experiments focused on surfactant lipid and protein quantification along with tensiometric experiments can be valuable in providing insight on particle-surfactant interactions. A more challenging but more useful approach is *in situ* detection of adsorbed species on particles surfaces, for example by

spectroscopy techniques, which can directly link particle-induced surfactant dysfunction with particle surface properties. Also, knowledge of particle placement at the air-water interface can be very useful in interpreting the effects of particles on surfactant function. A non-invasive microscopy technique that can provide this information, such as Brewster angle microscopy can significantly increase our understanding of the system. This technique is also beneficial in studies of surfactant microstructure as it does not require the use of fluorescent probes and avoids potential contaminations caused by such probes. Thus, further examination of particle-surfactant interactions using Brewster angle microscopy should be considered in the future.

Finally, studies of various particle sizes and surface chemistries are needed to improve the understanding of particle effects on surfactant behavior. Adsorption of surfactant components, particle incorporation into the monolayer and electrostatic interactions between particles and surfactant are dependent on particle physicochemical properties. Thus, a better understanding of potential adverse effects of particles on pulmonary surfactant following inhalation can be provided when various particles formulations with different sizes, charges and surface chemistries are studied. Such understanding is crucial for the design of biocompatible particles for pulmonary drug delivery. These studies can also help understand potential physiological dysfunction caused by exposure to ultrafine environmental pollutants by relating the adverse physiological effects of certain particles to particle physicochemical properties.

REFERENCES

1. Weibel, E. R.; Gomez, D. M. Architecture of the human lung. Use of quantitative methods establishes fundamental relations between size and number of lung structures. *Science* **1962,** *137*, 577-585.

2. Ochs, M.; Nyengaard, J. R.; Jung, A.; Knudsen, L.; Voigt, M.; Wahlers, T.; Richter, J.; Gundersen, H. J. G. The number of alveoli in the human lung. *American Journal of Respiratory and Critical Care Medicine* **2004,** *169* (1), 120-124.

3. Stone, K. C.; Mercer, R. R.; Gehr, P.; Stockstill, B.; Crapo, J. D. Allometric relationships of cell numbers and size in the mammalian lung. *American Journal of Respiratory Cell and Molecular Biology* **1992,** *6* (2), 235-243.

4. Gehr, P. Annexe A. Anatomy and morphology of the respiratory tract. *Annals of the ICRP* **1994,** *24* (1), 121-166.

5. Levitzky, M. G., *Pulmonary physiology : Lange physiology series*. 5th ed.; McGraw-Hill: New York, 1995.

6. Nag, K.; Munro, J. G.; Hearn, S. A.; Rasmusson, J.; Petersen, N. O.; Possmayer, F. Correlated atomic force and transmission electron microscopy of nanotubular structures in pulmonary surfactant. *Journal of Structural Biology* **1999,** *126* (1), 1-15.

7. Williams, M. C. Conversion of lamellar body membranes into tubular myelin in alveoli of fetal rat lungs. *The Journal of Cell Biology* **1977,** *72* (2), 260-277.

8. Griese, M. Pulmonary surfactant in health and human lung diseases: state of the art. *European Respiratory Journal* **1999,** *13* (6), 1455-1476.

9. Chander, A.; Claypool, W.; Strauss, J.; Fisher, A. Uptake of liposomal phosphatidylcholine by granular pneumocytes in primary culture. *American Journal of Physiology-Cell Physiology* **1983,** *245* (5), C397-C404.

10. Gurel, O.; Ikegami, M.; Chroneos, Z. C.; Jobe, A. H. Macrophage and type II cell catabolism of SP-A and saturated phosphatidylcholine in mouse lungs. *American Journal of Physiology-Lung Cellular and Molecular Physiology* **2001,** *280* (6), L1266-L1272.

11. Wright, J. R.; Dobbs, L. G. Regulation of pulmonary surfactant secretion and clearance. *Annual Review of Physiology* **1991,** *53* (1), 395-414.

12. Miles, P.; Ma, J.; Bowman, L. Degradation of pulmonary surfactant disaturated phosphatidylcholines by alveolar macrophages. *Journal of Applied Physiology* **1988,** *64* (6), 2474-2481.

13. Rodríguez-Capote, K.; Manzanares, D.; Haines, T.; Possmayer, F. Reactive oxygen species inactivation of surfactant involves structural and functional alterations to surfactant proteins SP-B and SP-C. *Biophysical Journal* **2006,** *90* (8), 2808-2821.

14.   Perez-Gil, J.; Weaver, T. E. Pulmonary surfactant pathophysiology: current models and open questions. *Physiology* **2010,** *25* (3), 132-141.

15.   Whitsett, J. A.; Wert, S. E.; Weaver, T. E. Alveolar surfactant homeostasis and the pathogenesis of pulmonary disease. *Annual Review of Medicine* **2010,** *61*, 105-119.

16.   Postle, A. D. A comparison of the molecular species compositions of mammalian lung surfactant phospholipids. *Comparative Biochemistry and Physiology. Part A, Molecular Integrative Physiology* **2001,** *129* (1), 65-73.

17.   Zuo, Y. Y.; Veldhuizen, R. A. W.; Neumann, A. W.; Petersen, N. O.; Possmayer, F. Current perspectives in pulmonary surfactant--inhibition, enhancement and evaluation. *Biochimica et Biophysica Acta-Biomembranes* **2008,** *1778* (10), 1947-1977.

18.   Yu, S. H., P. Smith, N. Possmayer F. . Bovine pulmonary surfactant: chemical composition and physical properties. *Lipids* **1983,** *18* (8), 522-529.

19.   Daniels, C. B.; Orgeig, S. Pulmonary surfactant: the key to the evolution of air breathing. *Physiology* **2003,** *18* (4), 151-157.

20.   Possmayer, F.; Nag, K.; Rodriguez, K.; Qanbar, R.; Schurch, S. Surface activity in vitro: role of surfactant proteins. *Comparative Biochemistry and Physiology. Part. A, Toxicology and Pharmacology* **2001,** *129* (1), 209-220.

21.   Coonrod, J. Role of surfactant free fatty acids in antimicrobial defenses. *European Journal of Respiratory Diseases* **1987,** *71* (153), 209-214.

22.   Wu, H.; Kuzmenko, A.; Wan, S.; Schaffer, L.; Weiss, A.; Fisher, J. H.; Kim, K. S.; McCormack, F. X. Surfactant proteins A and D inhibit the growth of Gram-negative bacteria by increasing membrane permeability. *Journal of Clinical Investigation* **2003,** *111* (10), 1589-1602.

23.   Bilek, A. M.; Dee, K. C.; Gaver, D. P. Mechanisms of surface-tension-induced epithelial cell damage in a model of pulmonary airway reopening. *Journal of Applied Physiology* **2003,** *94* (2), 770-783.

24.   Nakamura, T.; Malloy, J.; McCaig, L.; Yao, L.-J.; Joseph, M.; Lewis, J.; Veldhuizen, R. Mechanical ventilation of isolated septic rat lungs: effects on surfactant and inflammatory cytokines. *Journal of Applied Physiology* **2001,** *91* (2), 811-820.

25.   Nakahara, H.; Lee, S.; Shibata, O. Pulmonary surfactant model systems catch the specific interaction of an amphiphilic peptide with anionic phospholipid. *Biophysical Journal* **2009,** *96* (4), 1415-1429.

26.   Rhoades, R. A.; Bell, D. R., *Medical Physiology: Principles for Clinical Medicine*. Lippincott Williams & Wilkins: Baltimore, MD, 2012.

27.   Holm, B. A.; Notter, R.; Finkelstein, J. N. Surface property changes from interactions of albumin with natural lung surfactant and extracted lung lipids. *Chemistry and Physics of Lipids* **1985,** *38* (3), 287-298.

28. Wert, S. E.; Whitsett, J. A.; Nogee, L. M. Genetic disorders of surfactant dysfunction. *Pediatric and Developmental Pathology* **2009,** *12* (4), 253-274.

29. Kurashima, K.; Fujimura, M.; Matsuda, T.; Kobayashi, T. Surface activity of sputum from acute asthmatic patients. *American Journal of Respiratory and Critical Care Medicine* **1997,** *155* (4), 1254-1259.

30. Günther, A.; Siebert, C.; Schmidt, R.; Ziegler, S.; Grimminger, F.; Yabut, M.; Temmesfeld, B.; Walmrath, D.; Morr, H.; Seeger, W. Surfactant alterations in severe pneumonia, acute respiratory distress syndrome, and cardiogenic lung edema. *American Journal of Respiratory and Critical Care Medicine* **1996,** *153* (1), 176-184.

31. Avery, M. E.; Mead, J. Surface properties in relation to atelectasis and hyaline membrane disease. *Archives of Pediatrics & Adolescent Medicine* **1959,** *97*, 517-523.

32. Kanno, S.; Furuyama, A.; Hirano, S. Effects of eicosane, a component of nanoparticles in diesel exhaust, on surface activity of pulmonary surfactant monolayers. *Archives of Toxicology* **2008,** *82* (11), 841-850.

33. Hoda, K.; Kawasaki, H.; Yoshino, N.; Chang, C.; Morikawa, Y.; Sugihara, G.; Shibata, O. Mode of interaction of two fluorinated-hydrogenated hybrid amphiphiles with dipalmitoylphosphatidylcholine (DPPC) at the air−water interface. *Colloids and Surfaces B, Biointerfaces* **2006,** *53* (1), 37-50.

34. Chimote, G.; Banerjee, R. Effect of antitubercular drugs on dipalmitoylphosphatidylcholine monolayers: Implications for drug loaded surfactants. *Respiratory Physiology & Neurobiology* **2005,** *145* (1), 65-77.

35. Wallace, W. E.; Keane, M. J.; Murray, D. K.; Chisholm, W. P.; Maynard, A. D.; Ong, T. Phospholipid lung surfactant and nanoparticle surface toxicity: Lessons from diesel soots and silicate dusts. *Nanotechnology and Occupational Health* **2007**, 23-38.

36. Crane, J. M.; Putz, G.; Hall, S. B. Persistence of phase coexistence in disaturated phosphatidylcholine monolayers at high surface pressures. *Biophysical Journal* **1999,** *77* (6), 3134-3143.

37. Wustneck, R. Interfacial properties of pulmonary surfactant layers. *Advances in Colloid and Interface Science* **2005,** *117* (1-3), 33-58.

38. Watkins, J. C. The surface properties of pure phospholipids in relation to those of lung extracts. *Biochimica et Biophysica Acta-Lipids and Lipid Metabolism* **1968,** *152* (2), 293-306.

39. Kanishtha, T.; Banerjee, R.; Venkataraman, C. Effect of particle emissions from biofuel combustion on surface activity of model and therapeutic pulmonary surfactants. *Environmental Toxicology and Pharmacology* **2006,** *22* (3), 325-333.

40. Notter, R. H. Dynamic surface properties of phosphatidylglycerol-dipalmitoylphosphatidylcholine mixed films. *Chemistry and Physics of Lipids* **1980,** *27* (4), 305-319.

41. Bakshi, M. S.; Zhao, L.; Smith, R.; Possmayer, F.; Petersen, N. O. Metal nanoparticle pollutants interfere with pulmonary surfactant function in vitro. *Biophysical Journal* **2008,** *94* (3), 855-868.

42. Harishchandra, R. K.; Saleem, M.; Galla, H. J. Nanoparticle interaction with model lung surfactant monolayers. *Journal of The Royal Society Interface* **2010,** *7*, 15-26.

43. Guzman, E.; Liggieri, L.; Santini, E.; Ferrari, M.; Ravera, F. DPPC-DOPC Langmuir monolayers modified by hydrophilic silica nanoparticles: phase behaviour, structure and rheology. *Colloids and Surfaces A, Physicochemical and Engineering Aspects* **2011**, 174-183.

44. Fan, Q.; Wang, Y. E.; Zhao, X.; Loo, J. S. C.; Zuo, Y. Y. Adverse biophysical effects of hydroxyapatite nanoparticles on natural pulmonary surfactant. *ACS Nano* **2011,** *5* (8), 6410-6416.

45. Sosnowski, T. R.; Gradon, L.; Podgorski, A. Influence of insoluble aerosol deposits on the surface activity of the pulmonary surfactant: a possible mechanism of alveolar clearance retardation? *Aerosol Science and Technology* **2000,** *32* (1), 52-60.

46. Zhang, H.; Wang, Y. E.; Fan, Q.; Zuo, Y. Y. On the low surface tension of lung surfactant. *Langmuir* **2011,** *27* (13), 8351-8358.

47. Zhang, H.; Fan, Q.; Wang, Y. E.; Neal, C. R.; Zuo, Y. Y. Comparative study of clinical pulmonary surfactants using atomic force microscopy. *Biochimica et Biophysica Acta-Biomembranes* **2011,** *1808* (7), 1832-1842.

48. Stenger, P. C.; Alonso, C.; Zasadzinski, J. A.; Waring, A. J.; Jung, C.-L.; Pinkerton, K. E. Environmental tobacco smoke effects on lung surfactant film organization. *Biochimica et Biophysica Acta - Biomembranes* **2009,** *1788* (2), 358-370.

49. Girard-Egrot, A. P.; Godoy, S.; Blum, L. J. Enzyme association with lipidic Langmuir–Blodgett films: interests and applications in nanobioscience. *Advances in Colloid and Interface Science* **2005,** *116* (1), 205-225.

50. Schoel, W. M.; Schürch, S.; Goerke, J. The captive bubble method for the evaluation of pulmonary surfactant: surface tension, area, and volume calculations. *Biochimica et Biophysica Acta-General Subjects* **1994,** *1200* (3), 281-290.

51. Schürch, S. Surface tension at low lung volumes: dependence on time and alveolar size. *Respiration Physiology* **1982,** *48* (3), 339-355.

52. Enhorning, G. Pulsating bubble technique for evaluating pulmonary surfactant. *Journal of Applied Physiology* **1977,** *43* (2), 198-203.

53. Enhorning, G. Pulmonary surfactant function studied with the pulsating bubble surfactometer (PBS) and the capillary surfactometer (CS). *Comparative Biochemistry and Physiology-Part A: Molecular & Integrative Physiology* **2001,** *129* (1), 221-226.

54.   Lippmann, M., Regional deposition of particles in the human respiratory tract. In *Handbook of Physiology, Section 9: Reactions to Environmental Agents*, American Physiology Society: Bethesda, Md., 1977; pp 213-232.

55.   Seaton, A.; Tran, L.; Aitken, R.; Donaldson, K. Nanoparticles, human health hazard and regulation. *Journal of The Royal Society Interface* **2010,** *7*, 119-129.

56.   Clements, J. A.; Hustead, R. F.; Johnson, R. P.; Gribetz, I. Pulmonary surface tension and alveolar stability. *Journal of Applied Physiology* **1961,** *16* (3), 444-450.

57.   Wang, Z.; Li, X.; Yang, S. Studies of dipalmitoylphosphatidylcholine (DPPC) monolayers embedded with endohedral metallofullerene (Dy@ C82). *Langmuir* **2009,** *25* (22), 12968-12973.

58.   Schleh, C.; Muhlfeld, C.; Pulskamp, K.; Schmiedl, A.; Nassimi, M.; Lauenstein, H. D.; Braun, A.; Krug, N.; Erpenbeck, V. J.; Hohlfeld, J. M. The effect of titanium dioxide nanoparticles on pulmonary surfactant function and ultrastructure. *Respiratory Research* **2009,** *10* (1), 90-101.

59.   Beck Broichsitter, M.; Ruppert, C.; Schmehl, T.; Guenther, A.; Betz, T.; Bakowsky, U.; Seeger, W.; Kissel, T.; Gessler, T. Biophysical investigation of pulmonary surfactant surface properties upon contact with polymeric nanoparticles *in vitro*. *Nanomedicine: Nanotechnology, Biology and Medicine* **2010**.

60.   Guzmán, E.; Liggieri, L.; Santini, E.; Ferrari, M.; Ravera, F. Influence of silica nanoparticles on phase behavior and structural properties of DPPC–palmitic acid Langmuir monolayers. *Colloids and Surfaces A, Physicochemical and Engineering Aspects* **2011,** *413*, 280-287.

61.   Peetla, C.; Labhasetwar, V. Biophysical characterization of nanoparticle-endothelial model cell membrane interactions. *Molecular Pharmaceutics* **2008,** *5* (3), 418-429.

62.   Peetla, C.; Labhasetwar, V. Effect of molecular structure of cationic surfactants on biophysical interactions of surfactant-modified nanoparticles with a model membrane and cellular uptake. *Langmuir* **2009,** *25* (4), 2369-2377.

63.   Guzman, E.; Liggieri, L.; Santini, E.; Ferrari, M.; Ravera, F. Effect of hydrophilic and hydrophobic nanoparticles on the surface pressure response of DPPC monolayers. *The Journal of Physical Chemistry.C* **2011,** *115* (44), 21715-21722.

64.   Al-Hallak, M. H. D. K.; Azarmi, S.; Sun, C.; Lai, P.; Prenner, E. J.; Roa, W.; Lobenberg, R. Pulmonary toxicity of polysorbate-80-coated inhalable nanoparticles *in vitro* and *in vivo* evaluation. *The AAPS Journal* **2010,** *12* (3), 294-299.

65.   Stuart, D.; Lobenberg, R.; Ku, T.; Azarmi, S.; Ely, L.; Roa, W.; Prenner, E. J. Biophysical investigation of nanoparticle interactions with lung surfactant model systems. *Journal of Biomedical Nanotechnology* **2006,** *2* (3), 245-252.

66.   Ku, T.; Gill, S.; Lobenberg, R.; Azarmi, S.; Roa, W.; Prenner, E. J. Size dependent interactions of nanoparticles with lung surfactant model systems and the significant impact on surface potential. *Journal of Nanoscience and Nanotechnology* **2008,** *8* (6), 2971-2978.

67.   Kondej, D.; Sosonowski, T. R. The influence of metal-containing occupational dust on pulmonary surfactant activity. *Chemical Engineering Transactions* **2010,** *19* (3), 315-320.

68.   Santini, E.; Guzmán, E.; Ravera, F.; Ferrari, M.; Liggieri, L. Properties and structure of interfacial layers formed by hydrophilic silica dispersions and palmitic acid. *Physical Chemistry Chemical Physics* **2012,** *14* (2), 607-615.

69.   Tatur, S.; Badia, A. Influence of hydrophobic alkylated gold nanoparticles on the phase behavior of monolayers of DPPC and clinical lung surfactant. *Langmuir* **2012,** *28* (1), 628-639.

70.   Guzmán, E.; Liggieri, L.; Santini, E.; Ferrari, M.; Ravera, F. Mixed DPPC–cholesterol Langmuir monolayers in presence of hydrophilic silica nanoparticles. *Colloids and Surfaces B: Biointerfaces* **2013,** *105*, 284-293.

71.   Aroti, A.; Leontidis, E.; Maltseva, E.; Brezesinski, G. Effects of Hofmeister anions on DPPC Langmuir monolayers at the air-water interface. *The Journal of Physical Chemistry B* **2004,** *108* (39), 15238-15245.

72.   Kendall, M. Fine airborne urban particles (PM 2.5) sequester lung surfactant and amino acids from human lung lavage. *American Journal of Physiology-Lung Cellular and Molecular Physiology* **2007,** *293* (4), 1053-1058.

73.   Salvador-Morales, C.; Townsend, P.; Flahaut, E.; Vénien-Bryan, C.; Vlandas, A.; Green, M. L. H.; Sim, R. B. Binding of pulmonary surfactant proteins to carbon nanotubes; potential for damage to lung immune defense mechanisms. *Carbon* **2007,** *45* (3), 607-617.

74.   Panyam, J.; Labhasetwar, V. Biodegradable nanoparticles for drug and gene delivery to cells and tissue. *Advanced Drug Delivery Reviews* **2012,** *64*, 61-71.

75.   Lai, P.; Nathoo, S.; Ku, T.; Gill, S.; Azarmi, S.; Roa, W.; Lobenberg, R.; Prenner, E. J. Real-time imaging of interactions between dipalmitoylphosphatidylcholine monolayers and gelatin based nanoparticles using Brewster angle microscopy. *Journal of Biomedical Nanotechnology* **2010,** *6* (2), 145-152.

76.   Langmuir, I. The constitution and fundamental properties of solids and liquids. II. Liquids. 1. *Journal of the American Chemical Society* **1917,** *39* (9), 1848-1906.

77.   Graham, D. E.; Phillips, M. C. Proteins at liquid interfaces: I. Kinetics of adsorption and surface denaturation. *Journal of Colloid and Interface Science* **1979,** *70* (3), 403-414.

78.   Hardy, N. J.; Richardson, T. H.; Grunfeld, F. Minimising monolayer collapse on Langmuir troughs. *Colloids and Surfaces A, Physicochemical and Engineering Aspects* **2006,** *284-285*, 202-206.

79. Duncan, S. L.; Larson, R. G. Comparing experimental and simulated pressure-area isotherms for DPPC. *Biophysical Journal* **2008,** *94* (8), 2965-2986.

80. Montanha, E. A.; Caseli, L.; Kaczmarek, O.; Liebscher, J.; Huster, D.; Oliveira Jr, O. N. Comparative study of liponucleosides in Langmuir monolayers as cell membrane models. *Biophysical Chemistry* **2011,** *153* (2-3), 154-158.

81. Więcek, A.; Dyranowicz-Latka, P.; Vila-Romeu, N.; Nieto-Suarez, M.; Flasinski, M. Interactions between an anticancer drug–edelfosine–and DPPC in Langmuir monolayers. *Colloids and Surfaces A, Physicochemical and Engineering Aspects* **2008,** *321* (1-3), 201-205.

82. Salay, L. C.; Ferreira, M.; Oliveira Jr, O. N.; Nakaie, C. R.; Schreier, S. Headgroup specificity for the interaction of the antimicrobial peptide tritrpticin with phospholipid Langmuir monolayers. *Colloids and Surfaces B, Biointerfaces* **2012,** *100*, 95-102.

83. Willson, D. F.; Zaritsky, A.; Bauman, L. A.; Dockery, K.; James, R. L.; Conrad, D.; Craft, H.; Novotny, W.; Egan, E.; Dalton, H. Instillation of calf lung surfactant extract (calfactant) is beneficial in pediatric acute hypoxemic respiratory failure. *Critical Care Medicine* **1999,** *27* (1), 188-195.

84. Bissinger, R. L.; Carlson, C. A. Surfactant. *Newborn and Infant Nursing Reviews* **2006,** *6* (2), 87-93.

85. Notter, R. H.; Wang, Z.; Egan, E. A.; Holm, B. A. Component-specific surface and physiological activity in bovine-derived lung surfactants. *Chemistry and Physics of Lipids* **2002,** *114* (1), 21-34.

86. Alonso, C.; Bringezu, F.; Brezesinski, G.; Waring, A. J.; Zasadzinski, J. A. Modifying calf lung surfactant by hexadecanol. *Langmuir* **2005,** *21* (3), 1028-1035.

87. Wang, Y. E.; Zhang, H.; Fan, Q.; Neal, C. R.; Zuo, Y. Y. Biophysical interaction between corticosteroids and natural surfactant preparation: implications for pulmonary drug delivery using surfactant as a carrier. *Soft Matter* **2012,** *8* (2), 504-511.

88. Baoukina, S.; Monticelli, L.; Risselada, H. J.; Marrink, S. J.; Tieleman, D. P. The molecular mechanism of lipid monolayer collapse. *Proceedings of the National Academy of Sciences of the United States of America* **2008,** *105* (31), 10803-10808.

89. McConlogue, C. W.; Vanderlick, T. K. Molecular determinants of lipid domain shape. *Langmuir* **1999,** *15* (1), 234-237.

90. McConlogue, C. W.; Vanderlick, T. K. A close look at domain formation in DPPC monolayers. *Langmuir* **1997,** *13* (26), 7158-7164.

91. Krägel, J.; Kretzschmar, G.; Li, J. B.; Loglio, G.; Miller, R.; Mohwald, H. Surface rheology of monolayers. *Thin Solid Films* **1996,** *284-285*, 361-364.

92. Kaganer, V. M.; Möhwald, H.; Dutta, P. Structure and phase transitions in Langmuir monolayers. *Reviews of Modern Physics* **1999,** *71* (3), 779-819.

93.	Harbottle, R. R.; Nag, K.; McIntyre, N. S.; Possmayer, F.; Petersen, N. O. Molecular organization revealed by time-of-flight secondary ion mass spectrometry of a clinically used extracted pulmonary surfactant. *Langmuir* **2003,** *19* (9), 3698-3704.

94.	Lee, K. Y. C. Collapse mechanisms of Langmuir monolayers. *Annual Review of Physical Chemistry* **2008,** *59* (1), 771-791.

95.	Rugonyi, S.; Smith, E. C.; Hall, S. B. Transformation diagrams for the collapse of a phospholipid monolayer. *Langmuir* **2004,** *20* (23), 10100-10106.

96.	Tchoreloff, P.; Gulik, A.; Denizot, B.; Proust, J. E.; Puisieux, F. A structural study of interfacial phospholipid and lung surfactant layers by transmission electron microscopy after Blodgett sampling: influence of surface pressure and temperature. *Chemistry and Physics of Lipids* **1991,** *59* (2), 151-165.

97.	Notter, R. H.; Tabak, S. A.; Mavis, R. D. Surface properties of binary mixtures of some pulmonary surfactant components. *Journal of Lipid Research* **1980,** *21* (1), 10-22.

98.	Holm, B. A.; Wang, Z.; Egan, E. A.; Notter, R. H. Content of dipalmitoyl phosphatidylcholine in lung surfactant: ramifications for surface activity. *Pediatric Research* **1996,** *39* (5), 805-811.

99.	Arriaga, L. R.; Lopez-Montero, I.; Ignes-Mullol, J.; Monroy, F. Domain-growth kinetic origin of nonhorizontal phase coexistence plateaux in Langmuir monolayers: compression rigidity of a raft-like lipid distribution. *The Journal of Physical Chemistry B* **2010,** *114* (13), 4509-4520.

100.	Berg, J. C., *Introduction to Interfaces and Colloids*. World Scientific: Hackensack, NJ, 2009.

101.	Jabłonowska, E.; Bilewicz, R. Interactions of ibuprofen with Langmuir monolayers of membrane lipids. *Thin Solid Films* **2007,** *515* (7-8), 3962-3966.

102.	Banerjee, R.; Bellare, J. R. Scoring of surface parameters of physiological relevance to surfactant therapy in respiratory distress syndrome. *Journal of Applied Physiology* **2001,** *90* (4), 1447-1454.

103.	Schürch, S.; Bachofen, H.; Goerke, J.; Green, F. Surface properties of rat pulmonary surfactant studied with the captive bubble method: adsorption, hysteresis, stability. *Biochimica et Biophysica Acta (BBA)-Biomembranes* **1992,** *1103* (1), 127-136.

104.	Pison, U.; Seeger, W.; Buchhorn, R.; Joka, T.; Brand, M.; Obertacke, U.; Neuhof, H.; Schmit-Neuerberg, K. Surfactant abnormalities in patients with respiratory failure after multiple trauma. *American Journal of Respiratory and Critical Care Medicine* **1989,** *140* (4), 1033-1039.

105.	Notter, R.; Morrow, P. Pulmonary surfactant: a surface chemistry viewpoint. *Annals of Biomedical Engineering* **1975,** *3* (2), 119-159.

106.	Nielson, D. W. Electrolyte composition of pulmonary alveolar subphase in anesthetized rabbits. *Journal of Applied Physiology* **1986,** *60* (3), 972-979.

107. Schurch, S.; Possmayer, F.; Cheng, S.; Cockshutt, A. M. Pulmonary SP-A enhances adsorption and appears to induce surface sorting of lipid extract surfactant. *American Journal of Physiology-Lung Cellular and Molecular Physiology* **1992,** *263* (2), 210-218.

108. Schief, W. R.; Dennis, S. R.; Frey, W.; Vogel, V. Light scattering microscopy from monolayers and nanoparticles at the air/water interface. *Colloids and Surfaces A: Physicochemical and Engineering Aspects* **2000,** *171* (1), 75-86.

109. Worthman, L.; Nag, K.; Davis, P. J.; Keough, K. Cholesterol in condensed and fluid phosphatidylcholine monolayers studied by epifluorescence microscopy. *Biophysical Journal* **1997,** *72* (6), 2569-2580.

110. Nag, K.; Taneva, S. G.; Perez-Gil, A.; Cruz, A.; Keough, K. Combinations of fluorescently labeled pulmonary surfactant proteins SP-B and SP-C in phospholipid films. *Biophysical Journal* **1997,** *72* (6), 2638-2650.

111. Jyoti, A.; Prokop, R. M.; Li, J.; Vollhardt, D.; Kwok, D. Y.; Miller, R.; Mohwald, H.; Neumann, A. W. An investigation of the compression rate dependence on the surface pressure-surface area isotherm for a dipalmitoyl phosphatidylcholine monolayer at the air/water interface. *Colloids and Surfaces A, Physicochemical and Engineering Aspects* **1996,** *116* (1-2), 173-180.

112. Hauser, H.; Pascher, I.; Pearson, R. H.; Sundell, S. Preferred conformation and molecular packing of phosphatidylethanolamine and phosphatidylcholine. *Biochimica et Biophysica Acta* **1981,** *650* (1), 21-51.

113. Tamm, L. K.; Mc Connell, H. Supported phospholipid bilayers. *Biophysical Journal* **1985,** *47* (1), 105-113.

114. Hsiao, F. W.; Lee, Y. L.; Chang, C. H. On the characteristics of mixed Langmuir monolayer templates containing dipalmitoyl phosphatidylcholine for gold nanoparticle formation. *Colloids and Surfaces B, Biointerfaces* **2009,** *73* (1), 110-115.

115. Yuan, C.; Johnston, L. J. Phase evolution in cholesterol/DPPC monolayers: atomic force microscopy and near field scanning optical microscopy studies. *Journal of Microscopy* **2002,** *205* (2), 136-146.

116. Chang, C. H.; Yu, S. D.; Chuang, T. K.; Liang, C. N. Roles of γ-globulin in the dynamic interfacial behavior of mixed dipalmitoyl phosphatidylcholine/γ-globulin monolayers at air/liquid interfaces. *Journal of Colloid and Interface Science* **2000,** *227* (2), 461-468.

117. Putz, G.; Goerke, J.; Schurch, S.; Clements, J. A. Evaluation of pressure-driven captive bubble surfactometer. *Journal of Applied Physiology* **1994,** *76* (4), 1417-1424.

118. Tabak, S.; Notter, R.; Ultman, J.; Dinh, S. Relaxation effects in the surface pressure behavior of dipalmitoyl lecithin. *Journal of Colloid and Interface Science* **1977,** *60* (1), 117-125.

119. Hildebran, J. N.; Goerke, J.; Clements, J. A. Pulmonary surface film stability and composition. *Journal of Applied Physiology: Respiratory, Environmental and Exercise Physiology* **1979,** *47* (3), 604-611.

120. Cavagna, G.; Brandi, G.; Saibene, F.; Torelli, G. Pulmonary hysteresis. *Journal of Applied Physiology* **1962,** *17* (1), 51-53.

121. Mead, J.; Whittenberger, J. L.; Radford Jr., E. P. Surface tension as a factor in pulmonary volume-pressure hysteresis. *Journal of Applied Physiology* **1957,** *10* (2), 191-196.

122. Glaister, D. H.; Schroter, R. C.; Sudlow, M. F.; Milic-Emili, J. Bulk elastic properties of excised lungs and the effect of a transpulmonary pressure gradient. *Respiration physiology* **1973,** *17* (3), 347-364.

123. Bachofen, H.; Hildebrandt, J.; Bachofen, M. Pressure-volume curves of air-and liquid-filled excised lungs-surface tension in situ. *Journal of Applied Physiology* **1970,** *29* (4), 422-431.

124. Gil, J.; Bachofen, H.; Gehr, P.; Weibel, E. R. Alveolar volume-surface area relation in air-and saline-filled lungs fixed by vascular perfusion. *Journal of Applied Physiology: Respiratory, Environmental and Exercise Physiology* **1979,** *47* (5), 990-1001.

125. Notter, R. H.; Taubold, R.; Mavis, R. D. Hysteresis in saturated phospholipid films and its potential relevance for lung surfactant function *in vivo*. *Experimental Lung Research* **1982,** *3* (2), 109-127.

126. Frazer, D. G.; Weber, K. C.; Franz, G. N. Evidence of sequential opening and closing of lung units during inflation-deflation of excised rat lungs. *Respiration Physiology* **1985,** *61* (3), 277-288.

127. Cook, C.; Sutherland, J.; Segal, S.; Cherry, R.; Mead, J.; McIlroy, M.; Smith, C. Studies of respiratory physiology in the newborn infant. III. Measurements of mechanics of respiration. *Journal of Clinical Investigation* **1957,** *36* (3), 440-448.

128. Baritussio, A. G.; Magoon, M. W.; Goerke, J.; Clements, J. A. Precursor-product relationship between rabbit type II cell lamellar bodies and alveolar surface-active material: surfactant turnover time. *Biochimica et Biophysica Acta (BBA)-Lipids and Lipid Metabolism* **1981,** *666* (3), 382-393.

129. Snik, A. F. M.; Kruger, A. J.; Joos, P. Dynamical behavior of monolayers of dipalmitoyl lecithin and cholesterol. *Journal of Colloid and Interface Science* **1978,** *66* (3), 435-439.

130. Notter, R. H., *Lung Surfactants: Basic Science and Clinical Applications*. Marcel Dekker Inc.: New York, NY, 2000.

131. Ladbrooke, B. D.; Williams, R. M.; Chapman, D. Studies on lecithin-cholesterol-water interactions by differential scanning calorimetry and X-ray diffraction. *Biochimica et Biophysica Acta-Biomembranes* **1968,** *150* (3), 333-340.

132. Estep, T. N.; Mountcastle, E. B.; Bitonen, R. L.; Thompson, T. E. Studies on the anomalous thermotropic behavior of aqueous dispersions of dipalmitoylphosphatidylcholine-cholesterol mixtures. *Biochemistry* **1978,** *17* (10), 1984-1989.

133. Mabrey, S.; Mateo, P. L.; Sturtevant, J. M. High-sensitivity scanning calorimetric study of mixtures of cholesterol with dimyristoyl-and dipalmitoylphosphatidylcholines. *Biochemistry* **1978,** *17* (12), 2464-2468.

134. Shah, D. O.; Shulman, J. H. Influence of calcium, cholesterol, and unsaturation on lecithin monolayers. *Journal of Lipid Research* **1967,** *8* (3), 215-226.

135. Yu, S. H.; Possmayer, F. Interaction of pulmonary surfactant protein A with dipalmitoylphosphatidylcholine and cholesterol at the air/water interface. *Journal of Lipid Research* **1998,** *39* (3), 555-568.

136. Morrow, M. R.; Perez-Gil, A.; Simatos, G.; Boland, C.; Stuart, J.; Absolom, D.; Sarin, V.; Keough, K. Pulmonary surfactant-associated protein SP-B has little effect on acyl chains in dipalmitoylphosphatidylcholine dispersions. *Biochemistry* **1993,** *32* (16), 4397-4402.

137. Shiffer, K.; Hawgood, S.; Haagsman, H. P.; Benson, B.; Clements, J. A.; Goerke, J. Lung surfactant proteins, SP-B and SP-C, alter the thermodynamic properties of phospholipid membranes: a differential calorimetry study. *Biochemistry* **1993,** *32* (2), 590-597.

138. Keating, E.; Rahman, L.; Francis, J.; Petersen, A.; Possmayer, F.; Veldhuisen, R.; Petersen, N. O. Effect of cholesterol on the biophysical and physiological properties of a clinical pulmonary surfactant. *Biophysical Journal* **2007,** *93* (4), 1391-1401.

139. Gunasekara, L.; Schurch, S.; Schoel, W. M.; Nag, K.; Leonenko, Z.; Haufs, M.; Amrein, M. Pulmonary surfactant function is abolished by an elevated proportion of cholesterol. *Biochimica and Biophysica Acta-Molecular and Cell Biology of Lipids* **2005,** *1737* (1), 27-35.

140. Taeusch, H. W.; Lu, K.; Ramierez-Schrempp, D. Improving pulmonary surfactants. *Acta Pharmacologica Sinica* **2002,** *23*, 11-15.

141. Taneva, S. G.; Keough, K. Dynamic surface properties of pulmonary surfactant proteins SP-B and SP-C and their mixtures with dipalmitoylphosphatidylcholine. *Biochemistry* **1994,** *33* (49), 14660-14670.

142. Qanbar, R.; Cheng, S.; Possmayer, F.; Schurch, S. Role of the palmitoylation of surfactant-associated protein C in surfactant film formation and stability. *American Journal of Physiology-Lung Cellular and Molecular Physiology* **1996,** *271* (4), 572-580.

143. Horie, T.; Ardila, R.; Hildebrandt, J. Static and dynamic properties of excised cat lung in relation to temperature. *Journal of Applied Physiology* **1974,** *36*, 317-322.

144. Smith, J. C.; Stamenovic, D. Surface forces in lungs. I. Alveolar surface tension-lung volume relationships. *Journal of Applied Physiology* **1986,** *60* (4), 1341-1350.

145. Schurch, S.; Bachofen, H.; Weibel, E. R. Alveolar surface tensions in excised rabbit lungs: effect of temperature. *Respiration Physiology* **1985,** *62* (1), 31-45.

146. Malcolm, J. D.; Elliott, C. D. Interfacial tension from height and diameter of a single sessile drop or captive bubble. *The Canadian Journal of Chemical Engineering* **1980,** *58* (2), 151-153.

147. Bachofen, H.; Schurch, S.; Urbinelli, M.; Weibel, E. Relations among alveolar surface tension, surface area, volume, and recoil pressure. *Journal of Applied Physiology* **1987,** *62* (5), 1878-1887.

148. Caro, A. L.; Rodriguez Nino, M. R.; Rodriguez Patino, J. M. Dynamics of penetration of dipalmitoyl-phosphatidyl-choline (DPPC) monolayers by [beta]-casein. *Colloids and Surfaces A, Physicochemical and Engineering Aspects* **2009,** *341* (1-3), 134-141.

149. Flasiński, M.; Broniatowski, M.; Majewski, J.; Dyranowicz-Latka, P. X-ray grazing incidence diffraction and Langmuir monolayer studies of the interaction of β-cyclodextrin with model lipid membranes. *Journal of Colloid and Interface Science* **2010,** *348* (2), 511-521.

150. Britt, D. W.; Buijs, J.; Hlady, V. Tobacco mosaic virus adsorption on self-assembled and Langmuir–Blodgett monolayers studied by TIRF and SFM. *Thin Solid Films* **1998,** *327*, 824-828.

151. Lee, K. Y. C.; Gopal, A.; von Nahmen, A.; Zasadzinski, J. A.; Majewski, J.; Smith, G. S.; Howes, P. B.; Kjaer, K. Influence of palmitic acid and hexadecanol on the phase transition temperature and molecular packing of dipalmitoylphosphatidyl-choline monolayers at the air–water interface. *The Journal of Chemical Physics* **2002,** *116* (2), 774-783.

152. Dickinson, E. Use of nanoparticles and microparticles in the formation and stabilization of food emulsions. *Trends in Food Science Technology* **2012,** *24* (1), 4-12.

153. Eskandar, N. G.; Simovic, S.; Prestidge, C. A. Chemical stability and phase distribution of all- trans-retinol in nanoparticle-coated emulsions. *International Journal of Pharmaceutics* **2009,** *376* (1-2), 186-194.

154. Moxon, N.; Keast-Jones, R. The effect of collector emulsification using non-ionic surfactants on the flotation of coarse coal particles. *International Journal of Mineral Processing* **1986,** *18* (1), 21-32.

155. Singh, A.; Wang, H.; Silva, L. C.; Na, C.; Prieto, M.; Futerman, A. H.; Luberto, C.; Del Poeta, M. Methylation of glycosylated sphingolipid modulates membrane lipid topography and pathogenicity of Cryptococcus neoformans. *Cellular Microbiology* **2011,** *14* (4), 500-516.

156. Engelmann, B.; Streich, S.; Schönthier, U. M.; Richter, W. O.; Duhm, J. Changes of membrane phospholipid composition of human erythrocytes in hyperlipidemias. I. Increased phosphatidylcholine and reduced sphingomyelin in patients with elevated levels of triacylglycerol-rich lipoproteins. *Biochimica et Biophysica Acta (BBA)-Lipids and Lipid Metabolism* **1992,** *1165* (1), 32-37.

157. Abràmoff, M. D.; Magalhães, P. J.; Ram, S. J. Image processing with ImageJ. *Biophotonics International* **2004,** *11* (7), 36-42.

158. Baltrusaitis, J. Experimental and theoretical studies of the adsorption of atmospherically relevant gases on metal oxide and carbonate surfaces. Ph.D. Dissertation, The University of Iowa, Iowa City, Iowa, 2007.

159. Iacono, A. T.; Smaldone, G. C.; Keenan, R. J.; Diot, P.; Dauber, J. H.; Zeevi, A.; Burckart, G. J.; Griffith, B. P. Dose-related reversal of acute lung rejection by aerosolized cyclosporine. *American Journal of Respiratory and Critical Care Medicine* **1997,** *155* (5), 1690-1698.

160. Konstan, M. W.; Flume, P. A.; Kappler, M.; Chiron, R.; Higgins, M.; Brockhaus, F.; Zhang, J.; Angyalosi, G.; He, E.; Geller, D. E. Safety, efficacy and convenience of tobramycin inhalation powder in cystic fibrosis patients: The EAGER trial. *Journal of Cystic Fibrosis* **2011,** *10* (1), 54-61.

161. Dietrich, C.; Bagatolli, L.; Volovyk, Z.; Thompson, N.; Levi, M.; Jacobson, K.; Gratton, E. Lipid rafts reconstituted in model membranes. *Biophysical Journal* **2001,** *80* (3), 1417-1428.

162. Stottrup, B. L.; Keller, S. L. Phase behavior of lipid monolayers containing DPPC and cholesterol analogs. *Biophysical Journal* **2006,** *90* (9), 3176-3183.

163. Weiner, B. B., Particle characterization using photon correlation spectroscopy. In *Modern Methods of Particle Size Analyis*, Barth, H. G., Ed. Wiley-Interscience: New York, 1984; pp 93-116.

164. Browne, M. M.; Lubarsky, G. V.; Davidson, M. R.; Bradley, R. H. Protein adsorption onto polystyrene surfaces studied by XPS and AFM. *Surface Science* **2004,** *553* (1-3), 155-167.

165. Zhang, D.; Dougal, S. M.; Yeganeh, M. S. Effects of UV irradiation and plasma treatment on a polystyrene surface studied by IR-visible sum frequency generation spectroscopy. *Langmuir* **2000,** *16* (10), 4528-4532.

166. Nakahara, H.; Nakamura, S.; Kawasaki, H.; Shibata, O. Properties of two-component Langmuir monolayer of single chain perfluorinated carboxylic acids with dipalmitoylphosphatidylcholine (DPPC). *Colloids and Surfaces B, Biointerfaces* **2005,** *41* (4), 285-298.

167. McConnell, H. M. Structures and transitions in lipid monolayers at the air-water interface. *Annual Review of Physical Chemistry* **1991,** *42* (1), 171-195.

168. Lusted, D. Wilhelmy surface tension data in mixed-lipid cyclic film compression. *Journal of Colloid and Interface Science* **1973,** *44* (1), 72-78.

169. Mikrut, J.; Dutta, P.; Ketterson, J.; MacDonald, R. Atomic-force and fluorescence microscopy of Langmuir-Blodgett monolayers of L-α-dimyristoylphosphatidic acid. *Physical Review B* **1993,** *48* (19), 14479-14487.

170. Yang, X. M.; Xiao, D.; Lu, Z. H.; Wei, Y. Structural investigation of Langmuir-Blodgett monolayers of L-α-dipalmitoylphosphatidylcholine by atomic force microscopy. *Applied Surface Science* **1995,** *90* (2), 175-183.

171. de Kroon, A. I. P. M.; de Gier, J.; de Kruijff, B. The effect of a membrane potential on the interaction of mastoparan X, a mitochondrial presequence, and several regulatory peptides with phospholipid vesicles. *Biochimica et Biophysica Acta (BBA)-Biomembranes* **1991,** *1068* (2), 111-124.

172. Ege, C.; Lee, K. Y. C. Insertion of Alzheimer's Aß 40 peptide into lipid monolayers. *Biophysical Journal* **2004,** *87* (3), 1732-1740.

173. Koppenol, S.; Tsao, F. H. C.; Yu, H.; Zografi, G. The interaction of lung annexin I with phospholipid monolayers at the air/water interface. *Biochimica et Biophysica Acta-Biomembranes* **1998,** *1369* (2), 221-232.

174. Hall, S. B.; Lu, R. Z.; Venkitaraman, A. R.; Hyde, R. W.; Notter, R. H. Inhibition of pulmonary surfactant by oleic acid: mechanisms and characteristics. *Journal of Applied Physiology* **1992,** *72* (5), 1708-1716.

175. Nieman, G. F.; Clark, W. R. Effects of wood and cotton smoke on the surface properties of pulmonary surfactant. *Respiration Physiology* **1994,** *97* (1), 1-12.

176. Nobre, T. M.; Pavinatto, F. J.; Cominetti, M. R.; Selistre-de Araujo, H. S.; Zaniquelli, M. E. D.; Beltramini, L. M. The specificity of frutalin lectin using biomembrane models. *Biochimica et Biophysica Acta-Biomembranes* **2010,** *1798* (8), 1547-1555.

177. Brockman, H. Dipole potential of lipid membranes. *Chemistry and Physics of Lipids* **1994,** *73* (1-2), 57-79.

178. Taylor, D. M.; De Oliveira Jr., O. N.; Morgan, H. Models for interpreting surface potential measurements and their application to phospholipid monolayers. *Journal of Colloid and Interface Science* **1990,** *139* (2), 508-518.

179. Oliveira Jr, O. N.; Bonardi, C. The surface potential of Langmuir monolayers revisited. *Langmuir* **1997,** *13* (22), 5920-5924.

180. Dynarowicz-Łątka, P.; Dhanabalan, A.; Oliveira Jr, O. N. Modern physicochemical research on Langmuir monolayers. *Advances in Colloid and Interface Science* **2001,** *91* (2), 221-293.

181. Adam, N.; Danielli, J.; Harding, J. The structure of surface films. XXI. Surface potentials of dibasic esters, alcohols, aldoximes, and ketones. *Proceedings of the Royal Society of London. Series A-Mathematical and Physical Sciences* **1934,** *147* (862), 491-499.

182. Dynarowicz Łątka, P.; Kita, K. Molecular interaction in mixed monolayers at the air/water interface. *Advances in Colloid and Interface Science* **1999,** *79* (1), 1-17.

183. Heckl, W. M.; Baumgärtner, H.; Möhwald, H. Lateral surface potential distribution of a phospholipid monolayer. *Thin Solid Films* **1989,** *173* (2), 269-278.

184. Oliveira, O. N.; Taylor, D. M.; Lewis, T. J.; Salvagno, S.; Stirling, C. J. Estimation of group dipole moments from surface potential measurements on Langmuir monolayers. *Journal of Chemical Society, Faraday Transactions 1: Physical Chemistry in Condensed Phases* **1989,** *85* (4), 1009-1018.

185.   Shapovalov, V. L.; Kotova, E. A.; Rokitskaya, T. I.; Antonenko, Y. N. Effect of gramicidin A on the dipole potential of phospholipid membranes. *Biophysical Journal* **1999,** *77* (1), 299-305.

186.   Morgan, H.; Martin Taylor, D.; Oliveira, O. N. Proton transport at the monolayer-water interface. *Biochimica et Biophysica Acta (BBA)-Biomembranes* **1991,** *1062* (2), 149-156.

187.   Miller, A.; Helm, C. A.; Mohwald, H. The colloidal nature of phospholipid monolayers. *Journal de Physique* **1987,** *48* (4), 693-701.

188.   McConlogue, C. W.; Malamud, D.; Vanderlick, T. K. Interaction of DPPC monolayers with soluble surfactants: electrostatic effects of membrane perturbants. *Biochimica et Biophysica Acta (BBA)-Biomembranes* **1998,** *1372* (1), 124-134.

189.   Keller, D. J.; Korb, J. P.; Mc Connell, H. M. Theory of shape transitions in two-dimensional phospholipid domains. *Journal of Physical Chemistry* **1987,** *91* (25), 6417-6422.

190.   Weis, R. M. Fluorescence microscopy of phospholipid monolayer phase transitions. *Chemistry and Physics of Lipids* **1991,** *57* (2), 227-239.

191.   Glomm, W. R.; Wolden, S.; Halskau Jr, O.; Ese, M. G. Same system−different results: The importance of protein-introduction protocols in Langmuir-monolayer studies of lipid-protein interactions. *Analytical Chemistry* **2009,** *81* (8), 3042-3050.

192.   Pui, D. Y. H. Direct-reading instrumentation for workplace aerosol measurements. A review. *Analyst* **1996,** *121* (9), 1215-1224.

193.   Macklin, C. Pulmonary sumps, dust accumulations, alveolar fluid and lymph vessels. *Acta anatomica* **1955,** *23* (1), 1-33.

194.   Irache, J.; Durrer, C.; Ponchel, G.; Duchene, D. Determination of particle concentration in latexes by turbidimetry. *International Journal of Pharmaceutics* **1993,** *90* (3), 9-12.

195.   Hinds, W. C., *Aerosol Technology*, 2nd Ed. John Wiley & Sons: New York, NY 1999.

196.   Salvador-Morales, C.; Townsend, P.; Flahaut, E.; Vénien-Bryan, C.; Vlandas, A.; Green, M. L.; Sim, R. B. Binding of pulmonary surfactant proteins to carbon nanotubes; potential for damage to lung immune defense mechanisms. *Carbon* **2007,** *45* (3), 607-617.

197.   Hermansson, M. The DLVO theory in microbial adhesion. *Colloids and Surfaces B: Biointerfaces* **1999,** *14* (1), 105-119.

198.   Missana, T.; Adell, A. On the applicability of DLVO theory to the prediction of clay colloids stability. *Journal of Colloid and Interface Science* **2000,** *230* (1), 150-156.

199. Stebounova, L. V.; Guio, E.; Grassian, V. H. Silver nanoparticles in simulated biological media: a study of aggregation, sedimentation, and dissolution. *Journal of Nanoparticle Research* **2011,** *13* (1), 233-244.

200. Shah, P. S.; Holmes, J. D.; Johnston, K. P.; Korgel, B. A. Size-selective dispersion of dodecanethiol-coated nanocrystals in liquid and supercritical ethane by density tuning. *The Journal of Physical Chemistry B* **2002,** *106* (10), 2545-2551.

201. Van Oss, C.; Giese, R.; Costanzo, P. M. DLVO and non-DLVO interactions in hectorite. *Clays Clay Miner* **1990,** *38* (2), 151-159.

202. Vold, M. J. The effect of adsorption on the van der Waals interaction of spherical colloidal particles. *Journal of colloid science* **1961,** *16* (1), 1.

203. Israelachvili, J. Strength of van der Waals attraction between lipid bilayers. *Langmuir* **1994,** *10* (9), 3369-3370.

204. Mornet, S.; Lambert, O.; Duguet, E.; Brisson, A. The formation of supported lipid bilayers on silica nanoparticles revealed by cryoelectron microscopy. *Nano Letters* **2005,** *5* (2), 281-285.